HOLOGRAPHIC STUDIES OF THERMAL GAUGE THEORIES WITH FLAVOUR

by

Rowan F. M. Thomson

A thesis
presented to the University of Waterloo
in fulfillment of the
thesis requirement for the degree of
Doctor of Philosophy
in
Physics

Waterloo, Ontario, Canada, 2007

AUTHOR'S DECLARATION FOR ELECTRONIC SUBMISSION OF A THESIS

I hereby declare that I am the sole author of this thesis. This is a true copy of the thesis, including any required final revisions, as accepted by my examiners.

I understand that my thesis may be made electronically available to the public.

Abstract

The AdS/CFT correspondence and its extensions to more general gauge/gravity dualities have provided a powerful framework for the study of strongly coupled gauge theories. This thesis explores properties of a large class of thermal strongly coupled gauge theories using the gravity dual. In order to bring the holographic framework closer to Quantum Chromodynamics (QCD), we study theories with matter in the fundamental representation. In particular, we focus on the holographic dual of $SU(N_{\rm c})$ supersymmetric Yang-Mills theory coupled to $N_{\rm f} \ll N_{\rm c}$ flavours of fundamental matter at finite temperature, which is realised as $N_{\rm f}$ Dq-brane probes in the near horizon (black hole) geometry of $N_{\rm c}$ black Dp-branes.

We explore many aspects of these Dp/Dq brane systems, often focussing on the D3/D7 brane system which is dual to a four dimensional gauge theory. We study the thermodynamics of the Dq-brane probes in the black hole geometry. At low temperature, the branes sit outside the black hole and the meson spectrum is discrete and possesses a mass gap. As the temperature increases, the branes approach a critical solution. Eventually, they fall into the horizon and a phase transition occurs. At large $N_{\rm c}$ and large 't Hooft coupling, we show that this phase transition is always first order. We calculate the free energy, entropy and energy densities, as well as the speed of sound in these systems. We compute the meson spectrum for brane embeddings outside the horizon and find that tachyonic modes appear where this phase is expected to be unstable from thermodynamic considerations. We study the system at non-zero baryon density $n_{\rm b}$ and find that there is a line of phase transitions for small $n_{\rm b}$, terminating at a critical point with finite $n_{\rm b}$. We demonstrate that, to leading order in $N_{\rm f}/N_{\rm c}$, the viscosity to entropy density ratio in these theories saturates the conjectured universal bound $\eta/S \geq 1/4\pi$. Finally, we compute spectral functions and diffusion constants for fundamental matter in the high temperature phase of the D3/D7 theory.

Acknowledgements

It is a pleasure to thank my advisor, Rob Myers, for his support and encouragement, and for sharing his ideas, insights, and knowledge with me.

I would like to thank Jaume Gomis, Shimpei Kobayashi, David Mateos, Shunji Matsuura, Rob Myers, and Andrei Starinets for excellent collaborations, interesting conversations, and humourous *Sightspeed* conferences.

I have been privileged to be a resident at the Perimeter Institute for Theoretical Physics (PI) through the course of my PhD studies. Apart from a desk with a computer and a window, PI has offered a stimulating environment in which to study. Research at the Perimeter Institute is supported in part by the Government of Canada through the Natural Sciences and Engineering Research Council (NSERC) and by the Province of Ontario through MRI. I am also grateful for support from NSERC (through Canada Graduate Scholarships), the Canadian Institute for Advanced Research, and the University of Waterloo.

From my earliest days, my family instilled in me a love of learning by providing opportunities to learn and grow in all areas of life. I appreciate their support from the very beginning.

Finally, I would like to thank Kevin for his constant encouragement and inspiration: "Go confidently in the direction of your dreams! Live the life you've imagined. As you simplify your life, the laws of the universe will be simpler." $\sim$ Henry David Thoreau

Dedication

To my family, for all the opportunities from the very beginning, and to Kevin, for encouraging and helping me to follow my dreams.

Contents

1 Introduction **1**

2 Thermodynamics of the brane **13**

2.1 Black Dp-branes 16

2.1.1 Supergravity Background 16

2.1.2 Thermodynamics 18

2.2 Criticality, scaling, and phase transitions in Dp/Dq systems 20

2.2.1 Dp/Dq brane intersections 20

2.2.2 Critical behaviour 21

2.2.3 Phase Transitions 24

2.3 The D3/D7 system 27

2.3.1 D7-brane embeddings 28

2.3.2 D7-brane thermodynamics 31

2.3.3 Meson spectrum 41

2.4 The D4/D6 system 52

2.4.1 D6-brane embeddings 53

2.4.2 D6-brane thermodynamics 56

2.4.3 Meson spectrum for Minkowski embeddings 60

2.5 Discussion 62

2.6 Supplementary material for Chapter 2 73

2.6.1 Embeddings for high and low temperatures for D3/D7 73

2.6.2 Computation of the D7-brane entropy 75

2.6.3 Positivity of the entropy 78

2.6.4 Constituent quark mass in the D3/D7 system 80

2.6.5 Holographic Renormalisation of the D4-brane 81

3 Holographic phase transitions at finite baryon density 87
3.1 Holographic framework 89
3.1.1 Black D3-branes 89
3.1.2 D7-brane embeddings 90
3.1.3 Near-horizon embeddings 93
3.1.4 Strings from branes 99
3.1.5 Numerical embeddings 102
3.2 D7-brane thermodynamics: Free energy, entropy and stability 106
3.3 Discussion 114

4 Holographic viscosity of fundamental matter 119
4.1 Holographic Framework 121
4.2 Viscous Branes 122
4.3 Discussion 126

5 Holographic spectral functions and diffusion constants 129
5.1 Prelude: spectral functions and holography 132
5.1.1 Field theory picture 133
5.1.2 Gravity picture 135
5.1.3 A simple example: spectral function of R currents in $\mathcal{N} = 4$ SYM . 135
5.2 Adding flavour: D7-brane embedding and thermodynamics 139
5.2.1 Thermodynamics of the brane 140
5.3 Spectral functions for excitations of fundamental fields 142
5.3.1 Vector 142
5.3.2 Scalars 155
5.4 Diffusion constant for 'light' quarks 163
5.4.1 Membrane paradigm method 163
5.4.2 Green-Kubo formula 165
5.4.3 Lowest quasinormal frequency (in the diffusion channel) 168
5.5 Discussion 168
5.6 Supplementary material for chapter 5 178
5.6.1 Spectral function for scalar meson at $T = 0$ 178

5.6.2 Spectral function high frequency asymptotics 180
5.6.3 Effective potentials and quasinormal modes 182
5.6.4 Diffusion constants for Dp/Dq systems 189

6 Conclusion **193**

A Holographic dictionary for fundamental fields in an $\mathcal{N} = 2$ theory **198**
A.1 Scalar 200
A.2 Vector 202
A.3 Pseudoscalar 204
A.4 Operators with $\ell > 0$ 206

List of Figures

2.1 Dq-brane configurations in a black Dp-brane background 14
2.2 Profiles of D7-brane embeddings in the black D3-brane background 30
2.3 Quark mass and condensate versus $R_0 - 1$ (D3/D7) 31
2.4 Quark condensate versus temperature (D3/D7) 32
2.5 Free-energy, entropy and energy densities versus temperature (D3/D7) . . 35
2.6 Deviation of the speed of sound from the conformal value (D3/D7) 40
2.7 Pseudoscalar mass spectrum for low temperature phase (D3/D7) 45
2.8 Scalar mass spectrum for low temperature phase (D3/D7) 46
2.9 Vector mass spectrum for low temperature phase (D3/D7) 48
2.10 Dispersion relation in low temperature phase (D3/D7) 50
2.11 Scalar meson radial profiles (D3/D7) 51
2.12 Quark condensate versus temperature (D4/D6) 56
2.13 Free-energy, entropy and energy densities versus temperature (D4/D6) . . 59
2.14 Pseudoscalar mass spectrum for low temperature phase (D4/D6) 63
2.15 Scalar mass spectrum for low temperature phase (D4/D6) 64
2.16 Interpolation between weak and strong coupling regimes 69
2.17 Constituent quark mass as a function of temperature (D3/D7) 82

3.1 Phase diagram: Baryon number n_b versus temperature T 89
3.2 D7-brane embeddings in the D3-brane background at finite baryon density 102
3.3 Quark mass m versus boundary condition χ_0 on the horizon 103
3.4 Quark condensate versus temperature at small baryon density 104
3.5 Quark condensate versus temperature near the critical point 105
3.6 Quark condensate versus temperature at large baryon density 106
3.7 Chemical potential versus temperature 107

3.8 Legendre transform of the action for small baryon density 110
3.9 Legendre transform of the action for large baryon density 111
3.10 Phase diagram 111
3.11 Entropy versus temperature for small baryon density 113
3.12 Entropy versus temperature for large baryon density 113

5.1 Sketch of typical spectral functions 130
5.2 R-current spectral function for $\mathcal{N} = 4$ SYM 138
5.3 Free energy for temperatures near $T_{\rm fun}$ (D3/D7) 141
5.4 Vector spectral function 147
5.5 Vector spectral function for $\ell = 1$ and for massless quarks 152
5.6 Vector spectral function for $\ell = 1$ 154
5.7 Pseudoscalar spectral function 158
5.8 Scalar spectral function for $T > T_{\rm fun}$ 161
5.9 Scalar spectral function for T near $T_{\rm fun}$ 162
5.10 Scalar spectral function for $\ell = 1$ 164
5.11 Diffusion constant versus temperature (D3/D7) 166
5.12 Diffusion constant versus T for T near $T_{\rm fun}$ (D3/D7) 167
5.13 Diffusion constant versus the 't Hooft coupling λ (D3/D7) 175
5.14 Effective potential for the pseudoscalar 184
5.15 Effective potential for the scalar 187
5.16 WKB approximation: $\bar{n}/\pi + 1/2$ versus χ_0 188
5.17 Diffusion constant versus temperature (D4/D6) 191

Chapter 1

Introduction

The last century has seen remarkable advances in our understanding of nature. Just over a hundred years ago, Einstein's special theory of relavity unified the separate notions of space and time into the spacetime continuum, thereby recognising the arena in which physical processes occur. A short time later, quantum mechanics was discovered and quantum theory was shown to be the correct framework for the description of microscopic phenomena. These developments represented significant changes in paradigm which shaped the subsequent evolution of physical theories, requiring that they be formulated in a relativistic quantum framework.

With the recognition of four fundamental interactions in nature – gravitational, weak, strong, and electromagnetic – physicists attempted to develop quantum theories describing all interactions. To date, quantum field theories exist for the latter three while a full quantum theory of gravity remains a challenge. Electroweak theory (describing weak and electromagnetic interactions) together with Quantum Chromodynamics (QCD) (describing the strong interaction) form the Standard Model of Particle Physics. Along with twelve bosonic force carriers mediating interactions, the model contains two types of fundamental particles, leptons and quarks, both fermionic. The Standard Model is the culmination of decades of progress in physics and has proven to be very powerful in describing nature, even though it does not include gravity.

Of the gauge theories which make up the Standard Model, QCD is the least well understood. Despite being around for several decades, this theory describing the interaction of quarks and gluons, usually within nucleons, remains mysterious. The reason is the

running of the QCD effective coupling and the resulting property of asymptotic freedom [1, 2]. At first sight, the Lagrangians for Quantum Electrodynamics (QED), the quantum theory of the electromagnetic interaction, and QCD look very similar. While QED describes interactions between electrically charged particles mediated by photons, QCD describes interactions between colour-charged particles mediated by gluons. The great difference between these theories occurs at the level of the effective coupling: In QED, the interaction strength decreases with distance between particles or with energy. By contrast, the QCD interaction strength increases as the interparticle distance increases (energy decreases) and decreases as the interparticle distance decreases (energy increases). This property of QCD is the basis of asymptotic freedom [1, 2] and is, of course, why in the world around us, at everyday energy scales, we see hadrons rather than quarks and gluons.

Shortly after the discovery and acceptance of QCD, it was realised that at extremely high energy densities there might be a new phase of matter [3, 4]. With the QCD coupling small at high energy density, quarks and gluons are weakly interacting and one might expect to see a deconfined phase of quarks and gluons [5–8], called the quark gluon plasma (QGP) [9–13]. Such a phase of quarks and gluons may have existed in the very early universe. Accepted models of cosmology suggest that the universe underwent a violent beginning with extreme energies, densities, and gravitational fields. In the first $10 - 20\mu$s of the universe, it is expected that the energy and particle densities would have been sufficiently high for quarks and gluons to exist in a deconfined phase. As the universe expanded and cooled, the primordial quark gluon plasma would have undergone a confining phase transition in which the plasma constituents became confined in hadrons. Interestingly, there may be signs of the transition from primordial quark gluon plasma to hadronic gas imprinted on the universe (see, *e.g.,* [14–17]).

Hoping to create a quark gluon plasma experimentally, the Relativistic Heavy Ion Collider (RHIC) at Brookhaven National Laboratory in New York was constructed [18]. The goal of RHIC was to study the properties of matter at high energy densities. Through the collision of heavy ions, a QGP has been produced at RHIC, however, unlike the relatively 'simple' phase in which the quarks and gluons are deconfined and weakly interacting, the QGP at RHIC seems to be strongly coupled [19].[1] One indication of strong coupling is the small ratio between the shear viscosity η and the entropy density S [19] which is

[1] Recent accounts of the results from RHIC are summarised in [20]; for earlier accounts, see, *e.g.,* [21–24].

characteristic of a liquid, rather than a gas (for which the ratio η/S is large).

Of course, one would like to be able to 'apply' QCD, as the accepted theory of nuclear interactions, to the RHIC results to understand the state of matter formed when two relativistic heavy ions are collided. The barrier to the simple application of QCD to the RHIC results is part of the great challenge of theoretical studies of the physics of strongly interacting systems. At strong coupling, perturbation theory is inapplicable. Lattice techniques have been used with some success to understand strong coupling physics, however, their application is generally limited to equilibrium (static) studies and modelling dynamics remains a challenge. Hence new approaches for studying the physics of strongly coupled gauge theories such as QCD are needed.

One might hope that string theory, as a leading candidate for a unified theory of all interactions, would provide insights into such questions. String theory originates from attempts to understand the strong interactions, prior to the discovery of quarks or advent of QCD. In the 1960s, particle collider experiments produced a plethora of hadrons and it was suggested that the hadrons and mesons might be regarded as different oscillation modes of a string [25–27]. However, asymptotic freedom was discovered [1, 2] and with experimental results suggesting that hadrons are made up of quarks [28–33], *i.e.,* that hadrons have point-like constituents, the quantum field theory of quarks, QCD, supplanted string theory as a theory of the strong interactions.

String theory was later revisited as a possible theory of gravity. String theory contains both open and closed strings, the latter of which have massless spin-two excitations. These massless high-spin particles, which were an embarrassment for a theory of hadrons, are natural candidates for the quanta of gravity, gravitons. The existence of these higher spin particles led to the consideration of string theory as a candidate for a unified theory of all interactions [34]. String theory unifies all forces and particles by postulating that all particles in the Standard Model are actually different vibrational modes of a string. At first, formulating string theory as a unified theory of all interactions proved to be a challenge until the recognition of the importance of supersymmetry in the theory in the early 1980s [35–38] (for a review, see [39]). String theory's subsequent formulation in a consistent and anomaly-free way marked the birth of superstring theory.

It was later realised that string theory is not just a theory of strings but also contains extended objects called D-branes [40–42] (for reviews, see, *e.g.,* [43–45]). Dirichlet p-branes are hypersurfaces extended in p spatial directions on which open strings can end.

The coordinates of strings attached to a Dp-brane satisfy Dirichlet boundary conditions in the directions transverse to the brane and Neumann conditions in longitudinal directions. Though D-branes were discovered in 1989 [40, 41], they were largely ignored until the mid-1990s when, following the work of Witten [46], Strominger [47], and Hull and Townsend [48], Polchinski [42] identified Dp-branes with supergravity solitons carrying nonzero Ramond-Ramond (RR) charge which had been known to exist for some time [49].

Polchinski's discovery that Dp-branes carry an elementary unit of charge with respect to the RR sector of type II superstring theory revolutionised string theory. As D-branes are endowed with tension, bringing many D-branes together can result in the formation of an event horizon. One breakthrough came with the reproduction of the Bekenstein-Hawking entropy (computed in the strongly-coupled supergravity regime) via a calculation of the statistical entropy of a weakly interacting system of D-branes [50]. Polchinski's seminal work [42] also led to the realisation that the five ten-dimensional superstring theories, known to exist since the mid 1980s, and eleven-dimensional M-theory are all different limits of a single unique theory [46, 48, 51]. Though this theory remains mysterious today, it is promising that all known superstring theories are facets of a single theory.

A major development occurred in 1997 with Juan Maldacena's now famous conjecture concerning the equivalence of 10-dimensional superstring theory on anti-de Sitter (AdS) spaces and supersymmetric Yang-Mills theories [52]. The AdS/CFT correspondence relates type IIB string theory on $AdS_5 \times S^5$ (where the five-form flux through the S^5 is an integer N_c and the radii of AdS_5 and S^5 are both L) to a conformal field theory, $SU(N_\mathrm{c})$ $\mathcal{N} = 4$ super-Yang-Mills (SYM) theory in four dimensions. The parameters of both theories are related via

$$g^2_{\mathrm{YM}} = 2\pi g_\mathrm{s}\,, \quad L^4 = 4\pi g_\mathrm{s} N_\mathrm{c} \ell_\mathrm{s}^4\,, \tag{1.1}$$

where g_s and ℓ_s are the string coupling constant and length scale respectively, L is the AdS radius, and g_{YM} is the Yang-Mills coupling constant.

The strongest form of the equivalence holds for all values of N_c and $g^2_{\mathrm{YM}} = 2\pi g_\mathrm{s}$. Unfortunately, the quantization of string theory on arbitrary curved manifolds (including $AdS^5 \times S^5$) with Ramond-Ramond flux remains a challenge and thus use of the strongest form of the duality is limited. There are limits, however, in which Maldacena's duality is tractable and non-trivial [52] (for reviews, see [53, 54]). The 't Hooft limit [55] consists of holding the 't Hooft coupling $\lambda = g^2_{\mathrm{YM}} N_\mathrm{c}$ fixed while taking $N_\mathrm{c} \to \infty$. In the Yang-Mills

theory, at least in perturbation theory, this is a well-defined limit corresponding to the topological expansion of the field theory's Feynman diagrams. On the string theory side, $g_{\rm s} \sim \lambda/N_{\rm c}$ and thus the 't Hooft limit corresponds to weak coupling. The conjecture remains powerful, relating perturbative string theory to the strong coupling regime of large $N_{\rm c}$ gauge theories. Futher, taking the limit of large 't Hooft coupling ($\lambda \to \infty$) renders the radius $L^4 \sim \lambda \ell_{\rm s}^4$ of the AdS space large in relation to the string length scale $\ell_{\rm s}$. In this limit, massive string modes with energies $\sim 1/\ell_{\rm s}$ become very heavy and can be decoupled. With only massless string excitations remaining, string theory reduces to type IIB supergravity in ten dimensions. Hence the large 't Hooft coupling, large-$N_{\rm c}$ limit of field theory corresponds to gravity or string theory in the regime $g_{\rm s} \ll 1$ and $L \gg \ell_{\rm s}$ which can be approximated as classical supergravity.

The equivalence is manifested by mappings of global symmetries, of fields ϕ in string theory to operators $\mathcal{O}$ in the field theory, of correlation functions, and so on. An exact statement of the correspondence is that the partition function of string theory on $AdS_5 \times S^5$ coincides with that of $\mathcal{N} = 4$ super-Yang-Mills theory (on Minkowski space) [56, 57]. This can be written succinctly as

$$\mathcal{Z}_{\rm CFT} = \langle e^{\int \phi_0 \mathcal{O} d^4x} \rangle_{\rm CFT} = \mathcal{Z}_{\rm AdS}\left[\phi|_{\partial AdS} = \phi_0\right] , \tag{1.2}$$

where $\mathcal{Z}_{\rm CFT}$, $\mathcal{Z}_{\rm AdS}$ are the theories' partition functions. Note that the string partition function on the right hand side is evaluated by specifying the fields on the boundary of the AdS space. In the large-$N_{\rm c}$, large-λ limit, the string theory partition function can be approximated as $e^{-I_{\rm AdS}}$ where $I_{\rm AdS}$ is the supergravity action evaluated on AdS. This results in a recipe to compute 'field theory' correlation functions on the gravity side, originally proposed in [56, 57] and subsequently developed in many different contexts (for reviews, see [53, 54]).

It should be emphasised that the correspondence is a conjecture and, to date, no rigorous proof has be found. Tests of the conjecture via comparisons of quantities on both sides of the correspondence represent a challenge because the equivalence relates the strong coupling regime of one theory to the weak coupling regime of the other. However, there are properties of the theory which are independent of coupling and these can be compared. These include the global symmetries, the spectrum of chiral primary operators, some correlation functions, and so on – for a review, see [53]. Many tests of the correspondence have been performed, all supporting the conjecture.

The AdS/CFT correspondence has been extended to encompass a large number of more general gauge/gravity dualities, relating string theory on various backgrounds to (possibly non-conformal) field theories. The duality central to this thesis was proposed in [58]. Itzhaki *et al* [58] studied the general case of a stack of N_c coincident Dp-branes ($p < 5$) in the limit in which the brane modes decouple from the bulk. They argued that the SYM $SU(N_c)$ gauge theory on the $(p+1)$-dimensional worldvolume of the Dp-branes is dual to the closed string theory on the 'near-horizon' background induced by these branes.

These dualities follow from a straightforward extension of the usual decoupling limit for D3-branes [53] now applied to Dp-branes [58]. For general p ($\neq 3$), the gauge theory is distinguished from the conformal case by the fact that the Yang-Mills coupling g_{YM} is dimensionful. Hence there is a power-law running of the effective coupling with the energy scale U: $g^2_{\rm eff} = g^2_{YM} N_c U^{p-3}$. The duality relates the energy scale and the radial coordinate u transverse to the Dp-brane worldvolume in the usual way, $U = u/\ell_s^2$. In the dual background, the absence of conformal invariance in the general case is manifest in the radial variation of both the string coupling (or dilaton) and the spacetime curvature – see section 2.1 for details. As the supergravity background is only trustworthy for weak string coupling and small curvatures, it provides a dual description of the theory which is reliable for an intermediate regime of energies. In this regime, the dual gauge theory is always strongly coupled.

In all the dualities above, the gauge theories are at zero temperature. Temperature may be introduced into the correspondence by considering black Dp-branes [59]. Starting from the general black Dp-brane solution (see, *e.g.,* [45] and references therein) and taking the decoupling limit [58], one obtains the gravity dual of thermal $SU(N_c)$ SYM at temperature T. This gravity dual contains a black hole and the temperature of the Hawking radiation is identified with the temperature in the field theory. For the case $p = 3$, corresponding to a four-dimensional thermal gauge theory, the background is AdS space with a black hole, often referred to as the AdS-Schwarzschild geometry.

All matter in these gauge theories is in the adjoint representation of the gauge group. Of course, to approach QCD with this holographic framework, matter in the fundamental representation must be included. Karch and Katz [60] demonstrated that probe D7-branes can be used to introduce fundamental matter fields into the standard AdS/CFT correspondence from D3-branes. Inserting N_f D7-branes into the $AdS_5 \times S^5$ background corresponds to coupling N_f flavours of 'dynamical' quarks, (*i.e.,* N_f hypermultiplets in the

fundamental representation) to the original four-dimensional SYM theory. Adding these extra branes/fields also reduces the number of conserved supercharges from sixteen to eight. The hypermultiplets arise from the lightest modes of strings stretching between the D7- and D3-branes and their mass is set by the coordinate distance between the two sets of branes. The resulting gauge theory containing quarks has a rich spectrum of quark-antiquark bound states, which we henceforth refer to as 'mesons' [61]. In the decoupling limit, the duals are open strings attached to the D7-branes and the calculation of the meson spectrum in the field theory becomes an exercise in studying the fluctuation of probe branes. These ideas have been further developed in a number of directions towards the goal of constructing gauge/gravity duals for QCD-like theories [62–90] with the meson spectrum studied in a number of different contexts [61, 91–100].

In general, one can consider the addition of $N_{\rm f}$ Dq-brane probes to the Dp-brane geometry. The dual gauge theory is thermal $SU(N_{\rm c})$ SYM in $p+1$ dimensions coupled to a hypermultiplet in the fundamental representation. Depending on the choice of p and q and orientation of branes, the fundamental fields may be confined to a lower-dimensional defect in the full gauge theory. The discussion above for the D3/D7 brane system now generalises to one for Dp/Dq brane systems: The quarks in these theories arise as the lightest modes of the (q, p) and (p, q) strings stretching between the two sets of branes. In the decoupling limit, the meson string duals are open strings with both ends on the Dq-brane probes. At zero temperature, the spectrum of mesons in these theories has been explored in detail [101, 102].

The dualities between gauge and gravity theories are remarkable in that they relate the physics of gravitational degrees of freedom to those of non-gravitational degrees of freedom, all with spin ≤ 1. The gauge/gravity duality is a concrete realisation of the idea of holography, with the physics in one region of space being represented in terms of a theory living on the boundary of that region. Hence the word 'holographic' is frequently used to describe the dual theories.

The power of the correspondence lies in its nature as a duality, relating the strong coupling regime of one theory to the perturbative regime in the other. As noted above, string theory in the weak coupling regime, where supergravity is often a suitable approximation, can be used to study strongly coupled gauge theories. Conversely, gauge theories may provide clues about quantum gravity. Computations which were previously thought to be intractable may now be possible using the dual description. Hence the duality opens new

avenues for tackling outstanding questions in theoretical physics.

The description of non-perturbative physics in gauge theories such as QCD is one such issue. As mentioned above, the duality relates the large-N_c, strong 't Hooft coupling limit of gauge theories with classical supergravity. This makes the study of a large class of theories sharing some features, for example, confinement (see, *e.g.,* [59, 103–105]), chiral symmetry breaking (see, *e.g.,* [62, 93, 106–110]), and thermal phase transitions (see, *e.g.,* [106, 111–116]), of QCD possible. Unfortunately, the asymptotic freedom of QCD means that it is not in this class so that a full holographic study of QCD would require going beyond the supergravity approximation. However, it is hoped that certain properties of QCD may be studied in this approximation and that universal results may also apply to QCD.

An encouraging recent example comes from the computation of transport coefficients in the hydrodynamic regime of strongly-coupled finite-temperature field theories. Hydrodynamics is an effective theory describing the long-wavelength, low energy relaxation of a system to thermal equilibrium [117]. It is characterised by a number of 'transport coefficients' such as the shear and bulk viscosities, diffusion constants, conductivity, and the speed of sound. As noted above, the gravity dual to a thermal field theory contains a black hole and the equilibrium temperature in the field theory is the temperature of the Hawking radiation [59]. Deviations from thermal equilibrium in the field theory, *i.e.,* the existence of hydrodynamic modes, correspond to gravitational perturbations of the black hole background, *i.e.,* low-lying quasinormal modes of the black-brane metric [118]. Thus, the gauge/gravity correspondence makes possible calculations of transport coefficients in thermal field theories, which are otherwise currently intractable, using the gravity dual [119–122] (for a review, see [118]). The framework for these calculations comes from [123,124] where the real-time (rather than Euclidean time), finite-temperature gauge/gravity correspondence was developed. Calculations of diffusion constants of conserved charges (*e.g.,* [119,121,125,126], chapter 5), the speed of sound (*e.g.,* [112,120,122,127–132], chapter 2) and the rate of energy loss of a quark in the fundamental representation moving in a finite temperature plasma (*e.g.,* [133–136]) have all appeared.

The most celebrated example of hydrodynamic calculations using gravity duals is the computation of the shear viscosity. Calculations of the shear viscosity using the gravity dual first appeared in [137]. Subsequent computations [138–140] suggest that the shear viscosity to entropy density ratio is universal in a large class of large-N_c, large-λ field

theories:[2] $\eta/S = 1/4\pi$. This ratio has been shown to hold for all gauge theories with a known gravity dual, including black Dp-branes [125], M-branes [121], Klebanov-Tseytlin and Maldacena-Nunez backgrounds [138], $\mathcal{N} = 2^*$ SYM theory [141], systems at nonzero chemical potential [142–146], and systems containing fundamental matter [147] (see chapter 4). The ratio of η/S has been computed in $\mathcal{N} = 4$ SYM to the next order in the inverse 't Hooft coupling expansion and the correction raises the ratio above $\eta/S = 1/4\pi$ [148]. From all the holographic results, it has been argued that for all relativistic quantum field theories, the ratio of the shear viscosity to entropy density satisfies [125, 140]

$$\frac{\eta}{S} \geq \frac{1}{4\pi}\,. \tag{1.3}$$

Interestingly, the value of η/S inferred from experiments at RHIC suggest that for QCD just above the deconfinement phase transition this bound is nearly saturated [149, 150].

The universality of the shear viscosity to entropy density ratio and the success at applying this result to the value of η/S inferred from RHIC experiments [149, 150] suggest that holographic studies of gauge theories may yield insights into QCD, despite the fact that the holographic dual for QCD remains unknown. This thesis presents studies of the physics of strongly coupled thermal gauge theories with flavour performed in the framework of the gauge/gravity duality. In particular, we investigate properties of the class of thermal field theories dual to Dp/Dq brane systems, namely $SU(N_\mathrm{c})$ $\mathcal{N} = 4$ SYM coupled to N_f $\mathcal{N} = 2$ fundamental hypermultiplets (in the language of four-dimensional supersymmetry) in various dimensions.

We begin in chapter 2 by studying the thermodynamics of these systems [111, 112]. We review the throat geometries for black Dp-branes which are dual to $(p + 1)$-dimensional SYM at finite-temperature. As mentioned above, at finite temperature this geometry contains a black hole. Fundamental matter is introduced by inserting N_f Dq-brane probes into the black hole background. At low temperatures the Dq-branes sit outside the black hole and the meson spectrum is discrete and possesses a mass gap. As the temperature increases the branes approach a critical solution. Eventually they fall into the horizon and a phase transition occurs [111, 112]. In the new phase the meson spectrum is continuous and gapless. At large N_c and large 't Hooft coupling, this phase transition is always first order, and in confining theories with heavy quarks it occurs at a temperature higher than the

[2] Restoring $\hbar$, c and the Boltzmann constant k_B, this ratio is $\eta/S = \hbar/4\pi k_\mathrm{B}$.

deconfinement temperature for the glue. We compute the free energy, entropy and energy densities in these theories, as well as the speed of sound. For the D3/D7 and D4/D6 brane systems, we compute the meson spectrum for brane embeddings outside the horizon (corresponding to the low temperature phase of the dual gauge theory) and find that tachyonic modes appear where this phase is expected to be unstable from thermodynamic considerations.

Chapter 3 generalises the results of chapter 2 to the case of nonvanishing baryon density [151]. We focus on the D3/D7 brane system for which the dual gauge theory is four-dimensional, but our results apply in other dimensions as well [152]. A non-zero chemical potential $\mu_{\rm b}$ or baryon number density $n_{\rm b}$ is introduced via a nonvanishing worldvolume gauge field on the D7-branes. The first order phase transition described in chapter 2 [111, 112] extends to a line of phase transitions for small $n_{\rm b}$ which terminates at a critical point at finite $n_{\rm b}$ [151]. Investigation of the D7-branes' thermodynamics reveals that $(\partial\mu_{\rm b}/\partial n_{\rm b})_T < 0$ in a small region of the phase diagram, indicating an instability. We comment on a new phase which may appear in this region.

In chapter 4 we compute the shear viscosity in theories with fundamental matter [147]. As mentioned above, the holographic dual of a finite-temperature $SU(N_{\rm c})$ gauge theory with a small number of flavours $N_{\rm f} \ll N_{\rm c}$ typically contains Dq-branes in a black hole background. By considering the backreaction of the Dq-branes, we demonstrate that to leading order in $N_{\rm f}/N_{\rm c}$ the viscosity to entropy ratio in these theories saturates the universal bound $\eta/S \geq 1/4\pi$ [125, 140]. With the entropy density results from chapter 2, we find that the contribution of fundamental matter $\eta_{\rm fun}$ is enhanced at strong 't Hooft coupling λ; for example, in four dimensions, $\eta_{\rm fun} \sim \lambda N_{\rm c} N_{\rm f} T^3$ [112]. These results hold with or without baryon number chemical potential.

In chapter 5 we compute the spectral functions and diffusion constants for fundamental matter [126], focussing on the case of four dimensions for which the supergravity dual is the D3/D7 brane system. We study the high temperature phase of the system in which the D7-branes fall through the black hole horizon. We compute the spectral function for vector, scalar, and pseudoscalar modes on the D7-brane probes. The scalar spectral function reveals that tachyonic modes appear where thermodynamics indicate that this phase should be unstable. We also compute the diffusion constant for flavour currents, finding that at high temperatures the result matches the R-charge diffusion constant for $\mathcal{N} = 4$ SYM theory [125]. We extend the calculation of the diffusion constant to theories

in various dimensions.

We conclude in chapter 6 with a summary of results and discussion of possible future directions.

Appendix A contains a holographic dictionary for fundamental fields in the $\mathcal{N} = 2$ four-dimensional gauge theory dual to the D3/D7 brane system.

Previously published material

The research presented in this thesis has either been published in or submitted to scientific journals. While these papers were collaborative efforts, the author of this thesis was involved in all aspects of research and publication, *i.e.,* performing calculations, interpreting results, drafting papers, and editing manuscripts. In the following, the articles on which each chapter is based are listed and the author's contributions are highlighted:

Chapter 2:

- D. Mateos, R. C. Myers and R. M. Thomson, "Holographic phase transitions with fundamental matter," Phys. Rev. Lett. **97**, 091601 (2006) [arXiv:hep-th/0605046],
- D. Mateos, R. C. Myers and R. M. Thomson, "Thermodynamics of the brane," JHEP **0705**, 067 (2007) [arXiv:hep-th/0701132].

The first paper provides a brief summary of the results described in more detail in the second paper. The author was the first to perform most of the calculations (*e.g.,* brane embeddings, thermodynamics quantities, meson spectra, constituent quark mass) and also verified all of the calculations in the papers, drafted the second paper, and edited both papers. The vector meson spectrum for the D3/D7 brane system appearing in section 2.3.3 (fig. 2.9) is not included in either of the papers.

Chapter 3:

- S. Kobayashi, D. Mateos, S. Matsuura, R. C. Myers and R. M. Thomson, "Holographic phase transitions at finite baryon density," JHEP **0702**, 016 (2007) [arXiv:hep-th/0611099].

The author performed most of the calculations (D7-brane embeddings, thermodynamic quantities) and drafted and edited the paper. Details from the appendix of this paper also appear in appendix A of this thesis.

Chapter 4:

- D. Mateos, R. C. Myers and R. M. Thomson, "Holographic viscosity of fundamental matter," Phys. Rev. Lett. **98**, 101601 (2007) [arXiv:hep-th/0610184].

The author performed preliminary calculations to determine the viscosity, was involved in discussions to argue why the universal result $\eta/S = 1/4\pi$ should hold, and edited the paper.

Chapter 5:

- R. C. Myers, A. O. Starinets and R. M. Thomson, "Holographic spectral functions and diffusion constants for fundamental matter," arXiv:0706.0162 [hep-th].

The author performed most of the calculations (spectral functions, effective potentials, and diffusion constants, all for fundamental matter) and drafted and edited the paper. Details from appendix A of this paper also appear in appendix A of this thesis.

The author's (Ph.D.) research also appeared in the following publication:

- R. C. Myers and R. M. Thomson, "Holographic mesons in various dimensions," JHEP **0609**, 066 (2006) [arXiv:hep-th/0605017].

The author performed all calculations and drafted and edited the paper. While the material in this paper does not explicitly appear in this thesis, it sets up the framework for the calculations of meson spectra and spectral functions appearing in chapters 2 and 5.

Chapter 2

Thermodynamics of the brane

As discussed in the introduction, in a broad class of large-N_c, strongly coupled gauge theories with a holographic dual, a small number of flavours of fundamental matter, $N_f \ll N_c$, may be described by N_f probe Dq-branes in the gravitational background of N_c black Dp-branes [60, 153]. At a sufficiently high temperature T, the background geometry contains a black hole [59]. Working with $N_f \ll N_c$ flavours ensures that the matter branes only make a small perturbation to this background. Then much of the physics can be studied in the probe approximation where the gravitational backreaction of these branes is neglected.[1] We will see in this chapter that these systems generally undergo a universal first order phase transition characterised by a change in the behaviour of the fundamental matter [111, 112].[2]

From the viewpoint of the holographic description, the basic physics behind this transition is easily understood. Increasing the temperature increases both the radial position and the energy density of the event horizon in the Dp-brane throat. For a sufficiently small temperature or a sufficiently large separation for the Dq-branes, the probe branes are gravitationally attracted towards the horizon but their tension is sufficient to balance this attractive force. The probe branes then lie entirely outside of the black hole in what we call a 'Minkowski' embedding (see fig. 2.1). However, above a critical temperature $T_{\rm fun}$, the

[1] The backreaction cannot be ignored in calculating the effect of the fundamental matter on hydrodynamic transport coefficients such as the shear viscosity [147] – see chapter 4.

[2] Specific examples of this transition were originally seen in [62, 93, 106] and aspects of these transitions in the D3/D7 system were independently studied in [113–116]. Recently, similar holographic transitions have also appeared in a slightly different framework [107–110].

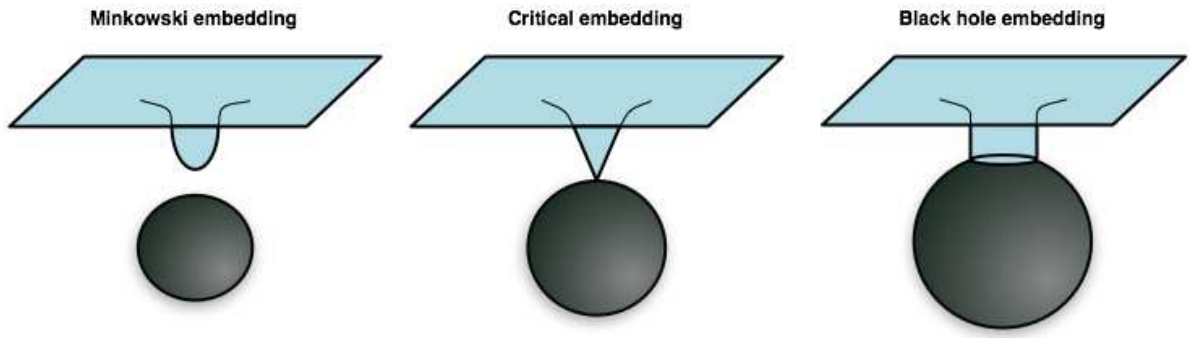

Figure 2.1: Various Dq-brane configurations in a black Dp-brane background with increasing temperature from left to right. For low temperatures, the probe branes close off smoothly above the horizon. For high temperatures, the branes fall through the event horizon. In between, a critical solution exists in which the branes just 'touch' the horizon at a point.

gravitational force overcomes the tension and the branes are pulled into the horizon. We refer to such configurations where the branes fall through the horizon as 'black hole' embeddings. In between these two phases there exists a critical solution which just 'touches' the horizon. In section 2.2 [111], we show that in the vicinity of this critical solution the embeddings show a self-similar behaviour. As a result, multiple solutions of the embedding equations exist for given temperature in a regime close to $T_{\rm fun}$. Using thermodynamic considerations to select the true ground state then reveals a first order phase transition at $T_{\rm fun}$, where the probe branes jump discontinuously from a Minkowski to a black hole embedding.

In the dual field theory,[3] this phase transition is exemplified by discontinuities in, *e.g.,* the quark condensate $\langle\bar{\psi}\psi\rangle$ or the contribution of the fundamental matter to the energy density. However, the most striking feature of this phase transition is found in the spectrum of the mesons, *i.e.,* the quark-antiquark bound states. As discussed in the introduction, the latter correspond to excitations supported on the probe branes – see, *e.g.,* [61,101,102,154]. In the low-temperature or Minkowski phase, the mesons are stable (to leading order within

[3]Recall for these supersymmetric field theories, the fundamental matter includes both fermions and scalars, which we will refer to collectively as 'quarks'.

the approximations of large N_c and strong coupling) and the spectrum is discrete with a finite mass gap. In the high-temperature or black hole phase, stable mesons cease to exist. Rather one finds a continuous and gapless spectrum of excitations [126, 155]. Hence the first order phase transition is characterised by the dissociation or 'melting' of the mesons.

This physics is particularly interesting in theories with a confinement/deconfinement phase transition. The dual description of the confining, low-temperature phase involves a horizon-free background. At a temperature $T_{\rm deconf}$ the theory undergoes a phase transition at which the gluons and the adjoint matter become deconfined, at which point the dual background develops a black hole horizon [59]. However, if the mass of the fundamental matter is large enough, the branes remain outside the horizon and therefore mesonic bound states survive for temperatures $T_{\rm deconf} < T < T_{\rm fun}$. At $T = T_{\rm fun}$ the branes finally fall into the horizon, *i.e.,* the mesons melt. This physics is in qualitative agreement with that observed in QCD for heavy-quark mesonic bound states. For example, lattice calculations suggest that charmonium states such as the J/ψ meson melt at temperatures between $1.65T_{\rm deconf}$ [156–158] and $2.1T_{\rm deconf}$ [159,160], while lattice results for the QCD deconfinement temperature are in the range: $T_{\rm deconf} \simeq 151$ to 192 MeV [161–163]. Although the holographic description may provide some useful geometric intuition for this phenomenon, there are also some caveats that we will discuss in due course.

An overview of this chapter is as follows: In section 2.1 we review the throat geometries for black Dp-branes which are dual to $(p+1)$-dimensional super-Yang-Mills (SYM) at finite temperature [58]. Section 2.2 reviews and expands on the self-similar behaviour of the embeddings near the critical solution for general Dp/Dq systems, as originally presented in [111]. In the subsequent detailed discussion of the thermodynamics, we focus our attention on the D3/D7 [93, 106] and D4/D6 [62] cases for concreteness. In section 2.3, we compute the free energy, entropy and energy densities, as well as the speed of sound for the D3/D7 system. We also study the meson spectrum on the Minkowski embeddings in this section. This spectrum is related to the dynamical stability, or lack thereof, of this phase, as we find that tachyonic modes appear where thermodynamic considerations indicate that these embeddings are unstable. Section 2.4 repeats the salient calculations for the D4/D6 system. A discussion of the results from this chapter appears in section 2.5. Finally, section 2.6 contains various technical details: Section 2.6.1 provides an analytic description of the D7-brane embeddings at very high and very low temperatures. Then section 2.6.2 presents some of the details of the calculation of the entropy density contributed by the D7-branes.

Section 2.6.3 discusses the appearance of the 'swallow tail' form in the plots of the free energy, *e.g.,* fig. 2.5. Section 2.6.4 provides a calculation of the constituent quark mass in the low temperature phase of the fundamental matter. Finally, section 2.6.5 discusses the holographic renormalisation of the D4-brane background.

2.1 Black Dp-branes

In this section we briefly review the relevant aspects of the throat geometries and thermodynamics of black Dp-branes. This will be of use in subsequent chapters and in subsequent sections in this chapter, in particular, in sections 2.3 and 2.4, where we specialise to black D3- and D4-brane backgrounds, respectively.

2.1.1 Supergravity Background

The supergravity solution corresponding to the decoupling limit of $N_{\rm c}$ coincident black Dp-branes is, in the string frame (see, *e.g.,* [45] and references therein),[4]

$$\begin{aligned} ds^2 &= H^{-\frac{1}{2}}\left(-f dt^2 + dx_p^2\right) + H^{\frac{1}{2}}\left(\frac{du^2}{f} + u^2 d\Omega_{8-p}^2\right) , \\ e^{\Phi} &= H^{\frac{3-p}{4}} , \qquad C_{01\ldots p} = H^{-1} , \end{aligned} \tag{2.1}$$

where $H(u) = (L/u)^{7-p}$ and $f(u) = 1-(u_0/u)^{7-p}$. The horizon lies at $u = u_0$. The length scale L is defined in terms of the string coupling constant $g_{\rm s}$ and the string length ℓ_s:

$$L^{7-p} = g_{\rm s} N_{\rm c} \left(4\pi\ell_s^2\right)^{\frac{7-p}{2}} \Gamma\left(\tfrac{7-p}{2}\right)/4\pi \ . \tag{2.2}$$

For the special case $p = 3$, L is the radius of curvature for the $\mathrm{AdS}_5\times S^5$ geometry appearing in eq. (2.1).

According to the general gauge/gravity duality of [58], type II string theory in these backgrounds is dual to the super-Yang-Mills $SU(N_{\rm c})$ gauge theory on the $(p{+}1)$-dimensional worldvolume of the Dp-branes. For general p ($\neq 3$), the gauge theory is distinguished from

[4]The decoupling limit consists of holding $g_{\rm YM}^2 = 2\pi g_{\rm s}(2\pi\ell_{\rm s})^{p-3}$ fixed while taking $\alpha' = \ell_{\rm s}^2 \to 0$. In this limit, energy scales $U = u/\ell_{\rm s}^2$ are also held constant as the limit $\alpha' \to 0$ is taken [58].

the conformal case ($p = 3$) by the fact that the Yang-Mills coupling $g_{\rm YM}$ is dimensionful. The holographic dictionary provides

$$g_{\rm YM}^2 = 2\pi g_{\rm s}(2\pi\ell_{\rm s})^{p-3}\,. \tag{2.3}$$

Hence there is a power-law running of the dimensionless effective coupling with the energy scale U:

$$g_{\rm eff}^2 = g_{\rm YM}^2 N_{\rm c}\, U^{p-3}\,, \tag{2.4}$$

where $U = u/\alpha'$ by virtue of the usual energy/radius correspondence. The absence of conformal invariance for the general case is manifested in the dual geometry by the radial variation of both the string coupling and the spacetime curvature. The supergravity solution (2.1) is a trustworthy background provided that both the curvatures and string coupling are small. Hence in these general dualities, the supergravity description is limited to an intermediate regime of energies in the field theory or of radial distances in the background. This restriction is succinctly expressed in terms of the effective coupling (2.4) as [58]:

$$1 \ll g_{\rm eff} \ll N_{\rm c}^{\frac{4}{7-p}}\,. \tag{2.5}$$

Hence the field theory is always strongly coupled where the dual supergravity description is valid.

With the event horizon at $u = u_0$, Hawking radiation appears in the background with a temperature fixed by the surface gravity $T = \kappa/2\pi$. This temperature is identified with that of the dual $(p+1)$-dimensional gauge theory. In the geometry (2.1), the temperature can also be determined by demanding regularity of the Euclidean section obtained through the Wick rotation $t \to it_{\rm E}$. Then $t_{\rm E}$ must be periodically identified with a period β where

$$\frac{1}{\beta} = T = \frac{7-p}{4\pi L}\left(\frac{u_0}{L}\right)^{\frac{5-p}{2}}\,. \tag{2.6}$$

In some cases, one periodically identifies some of the Poincaré directions x_p in order to render the theory effectively lower-dimensional at low energies; a prototypical example is that of a D4-brane with one compact space direction – see, *e.g.,* [59, 62]. Under these circumstances a different background with no black hole may describe the low-temperature physics, and a phase transition at $T = T_{\rm deconf}$ may occur [59]. In the gauge theory this is typically a confinement/deconfinement phase transition for the gluonic (or adjoint) degrees of freedom. Throughout this chapter we assume that $T > T_{\rm deconf}$, in which case the appropriate gravitational background has an event horizon, as in eq. (2.1).

2.1.2 Thermodynamics

As alluded to above, with the Wick rotation $t \to it_{\rm E}$, the Euclidean path integral yields a thermal partition function. Further the Euclidean black hole is interpreted as a saddle-point in this path integral and so the gravity action evaluated for this classical solution is interpreted as the leading contribution to the free energy, *i.e.,* $I_{\rm E} = \beta F$ – see, *e.g.,* [164]. Hence to study the gauge theory thermodynamics holographically, one needs to evaluate the supergravity action $I_{\rm E}$ for the Euclidean version of the above backgrounds (2.1). This suffers from IR (large radius) divergences, but these may be regulated by adding appropriate boundary terms to the action. These boundary terms were originally found for asymptotically AdS backgrounds, such as the black D3-brane, in [165–170]. As we discuss in section 2.6.5, similar surface terms should exist in the general gauge/gravity dualities to complete the holographic description. Here we simply comment that for the black D4-brane, which is the relevant background in section 2.4, we are guided in the construction of these counterterms by considering the M5-brane counterpart in M-theory. In any event, after including the appropriate boundary terms, the Euclidean action is finite.[5] Then with $F = TI_{\rm E}$ and standard thermodynamic relations, various thermal quantities can be determined. For example, the entropy S and the energy E are computed as:

$$S = -\frac{\partial F}{\partial T}\,, \qquad E = F + TS\,. \tag{2.7}$$

For the black D3-brane background, the length scale (2.2) is given by $L^4 = 4\pi g_s N_{\rm c} \ell_s^4$, and the free energy is

$$F = -\frac{\pi^6 L^8}{16G}\, T^4 = -\frac{\pi^2}{8} N_{\rm c}^2\, T^4\,, \tag{2.8}$$

where G is the ten-dimensional Newton's constant. In terms of the string length and coupling, the latter is given by:

$$16\pi G = (2\pi)^7 \ell_{\rm s}^8\, g_s^2\,. \tag{2.9}$$

[5]For the above backgrounds (2.1) describing the gauge theory on flat p-dimensional space, the action still contains an IR divergence, namely a factor of the spatial volume $\widetilde{V}_x = \int d^p x$. In the following, we divide all extensive thermodynamic quantities by $\widetilde{V}_x$ so that we are really looking at densities, *e.g.,* eq. (2.11) really gives the free energy per unit p-volume. When we refer to contributions from the brane probes, the relevant volume factor is instead that of the defect on which the fundamental matter lives, $V_x = \int d^d x$.

For the black D4-brane geometry we have $L^3 = \pi g_s N_{\rm c} \ell_s^3$ and

$$F = -\frac{2^{10}\pi^7 L^9}{3^7 G}\, T^6 = -\frac{2^5\pi^2}{3^7}\, \lambda\, N_{\rm c}^2\, T^6\,, \tag{2.10}$$

where as usual $\lambda = g_{\rm YM}^2 N_{\rm c}$ denotes the 't Hooft coupling. (The reader is referred to section 2.6.5 for further discussion of this case.) In general, the free energy for a general black Dp-brane geometry can be written as [58, 171]

$$F \sim N_{\rm c}^2 T^{p+1} g_{\rm eff}(T)^{\frac{2(p-3)}{5-p}}\,, \tag{2.11}$$

where

$$g_{\rm eff}^2(T) = \lambda T^{p-3} = g_{\rm YM}^2 N_{\rm c} T^{p-3} \tag{2.12}$$

is the effective coupling (2.4) evaluated at the temperature scale $U = T$. In eq. (2.11), $N_{\rm c}^2$ reflects the number of degrees of freedom in the $SU(N_{\rm c})$ gauge theory while T^{p+1} is the expected temperature dependence for a $(p+1)$-dimensional theory. However, the dependence on $g_{\rm eff}$ is a prediction of the holographic framework for the strongly coupled gauge theory. Note that for the conformal case ($p = 3$), but only for this case, this factor is simply unity and so the thermodynamic results can compared to those calculated at weak coupling [172].

Another quantity that is often studied in the context of the gauge/gravity duality is the speed of sound, *e.g.,* [120, 122, 127–132]. While this quantity can be inferred from the pole structure of certain correlators [120, 122, 127], it can also be derived from the thermal quantities discussed above, with

$$v_s^2 = \frac{\partial P}{\partial E} = \frac{\partial P}{\partial T}\left(\frac{\partial E}{\partial T}\right)^{-1} = \frac{S}{c_{\rm V}}\,. \tag{2.13}$$

Here we have used the fact that for a system without a chemical potential, the pressure and free energy density are identical up to a sign, *i.e.,* $P = -F$. Hence $\partial P/\partial T = -\partial F/\partial T = S$. Also we use $c_{\rm V}$ to denote the heat capacity (density), *i.e.,* $c_{\rm V} \equiv \partial E/\partial T$. From eqs. (2.11) and (2.12), one finds the simple result that for the strongly coupled gauge theory in $(p+1)$ dimensions

$$v_s^2 = \frac{5-p}{9-p} = \begin{cases} 1/3 & \text{for } p = 3\,, \\ 1/5 & \text{for } p = 4\,. \end{cases} \tag{2.14}$$

We see above that the conformal result $v_s^2 = 1/p$ is only achieved for $p = 3$ [120, 122, 127], as expected. We note, however, that the $p = 1$ and 4 backgrounds are related through a simple

chain of dualities to the AdS_4 and AdS_7 throats of M2- and M5-branes, respectively. Hence for these specific cases with $v_s^2 = 1/2$ and $1/5$, the speed of sound reflects the conformal nature of the holographic theories dual to these M-theory backgrounds [122].

2.2 Criticality, scaling, and phase transitions in Dp/Dq systems

We now turn to the systems of interest in this thesis: Configurations of probe Dq-branes in the background geometry induced by black Dp-branes. The addition of the probes in the gravitational description is dual to the addition of matter in the fundamental representation in the gauge theory [60, 153]. In this section, we describe the embedding of the Dq-branes, study the critical behaviour and analyse the nature of the phase transition for general p and q. The latter involves extending the Euclidean techniques of the previous section to the worldvolume action of the Dq-brane, to study the thermal properties of the fundamental matter. This discussion naturally leads to sections 2.3 and 2.4, where we provide a detailed analysis of the D3/D7 and D4/D6 brane systems.

2.2.1 Dp/Dq brane intersections

Consider a configuration of N_c coincident black Dp-branes intersecting N_f coincident Dq-branes along d spacelike directions. In the limit $N_f \ll N_c$ the Dq-branes may be treated as a probe in the Dp-brane geometry (2.1), wrapping an S^n inside the S^{8-p}. We will assume that the Dq-brane also extends along the radial direction, so that $q = d + n + 1$. The corresponding gauge theory now contains fundamental matter propagating along a $(d+1)$-dimensional defect. To ensure stability, we will consider Dp/Dq intersections which are supersymmetric at zero temperature. Generally this means that we are interested in $q = p + 4$, $p + 2$ or p, as studied in [101, 102, 154]. In this case, the Ramond-Ramond field sourced by the Dp-branes does not couple to the Dq-brane. For the two cases of special interest here, the D3/D7 and the D4/D6 systems, one has $n = 3$ and $n = 2$ respectively. If the appropriate direction along the D4-brane is compactified, then both cases can effectively be thought of as describing the dynamics of a four-dimensional gauge theory with fundamental matter.

2.2.2 Critical behaviour

To uncover the critical behaviour of the Dp/Dq brane system, we study the behaviour of the probe brane near the horizon, following [173] closely – see also [174, 175]. First it is useful to adapt the S^{8-p} metric in (2.1) to the probe brane embedding, and so we write

$$d\Omega_{8-p}^2 = d\theta^2 + \sin^2\theta\, d\Omega_n^2 + \cos^2\theta\, d\Omega_{7-p-n}^2 \,. \tag{2.15}$$

As described above, the Dq-brane wraps the internal S^n with radius $\sin\theta$ in this line element. Now we zoom in on the near horizon geometry with the coordinates

$$u = u_0 + \pi T z^2 \,, \quad \theta = \frac{y}{L}\left(\frac{L}{u_0}\right)^{\frac{p-3}{4}} \,, \quad \tilde{x} = \left(\frac{u_0}{L}\right)^{\frac{7-p}{4}} x \,, \tag{2.16}$$

with T the temperature defined in (2.6). With these coordinates, the event horizon is at $z = 0$. Further $y = 0$ denotes the axis running orthogonally to the Dq-brane from the Dp-branes. Expanding the metric (2.1) to lowest order in z and y gives Rindler space together with some spectator directions:

$$ds^2 = -(2\pi T)^2 z^2 dt^2 + dz^2 + dy^2 + y^2 d\Omega_n^2 + d\tilde{x}_d^2 + \cdots \,. \tag{2.17}$$

The Dq-brane lies at constant values of the omitted coordinates, so these play no role in the following. The Dq-brane embedding is specified by a curve $(z(\sigma), y(\sigma))$ in the (z, y)-plane. Since the dilaton approaches a constant near the horizon, up to an overall constant the Dq-brane (Euclidean) action is simply the volume of the brane, namely

$$I_{\text{bulk}} \propto \int d\sigma \sqrt{\dot{z}^2 + \dot{y}^2}\, z y^n \,, \tag{2.18}$$

where the dot denotes differentiation with respect to σ and the reason for the subscript 'bulk' will become clear shortly. This is precisely the action considered in ref. [173]. In the gauge $z = \sigma$ the equation of motion takes the form

$$zy\ddot{y} + (y\dot{y} - nz)(1 + \dot{y}^2) = 0 \,, \tag{2.19}$$

while the gauge choice $y = \sigma$ yields

$$yz\ddot{z} + (nz\dot{z} - y)(1 + \dot{z}^2) = 0 \,. \tag{2.20}$$

The two types of embeddings described in the introduction for the full background extend to this near-horizon geometry (2.17). Hence the solutions again fall into two classes: 'black hole' and 'Minkowski' embeddings – see fig. 2.1. Black hole embeddings are those for which the brane falls into the horizon, and may be characterised by y_0, the size of the S^n there, which is also the size of the induced horizon on the Dq-brane worldvolume. The appropriate boundary condition is $\dot{y} = 0, y = y_0$ at $z = 0$. Minkowski embeddings are those for which the brane closes off smoothly above the horizon. These are characterised by the distance of closest approach to the horizon, z_0, and satisfy the boundary condition $\dot{z} = 0, z = z_0$ at $y = 0$. There is a simple limiting solution for the equations of motion (2.19): $y = \sqrt{n}\, z$. This critical solution just touches the horizon at the point $y = z = 0$, and so it lies between the above two classes. Note that this point is a singularity in the induced metric of the Dq-brane.

The equation of motion (2.19) enjoys a scaling symmetry: If $y = f(z)$ is a solution, then so is $y = f(\mu z)/\mu$ for any real positive μ. This transformation rescales $z_0 \to z_0/\mu$ for Minkowski embeddings, or $y_0 \to y_0/\mu$ for black hole embeddings, which implies that all solutions of a given type can be generated from any other one by this scaling transformation.

Consider now a solution very close to the critical one, $y(z) = \sqrt{n}\, z + \xi(z)$. Linearising the equation of motion (2.19), one finds that for large z the solutions are of the form $\xi(z) = z^{\nu_\pm}$, with

$$\nu_\pm = -\frac{n}{2} \pm \frac{\sqrt{n^2 - 4(n+1)}}{2}\,. \tag{2.21}$$

If $n \leq 4$, these exponents have non-vanishing imaginary parts, which leads to oscillatory behaviour. It appears that one can also get real exponents with $n \geq 5$. However, we will show below that no such systems are realised in superstring theory. Hence we will only work with $n \leq 4$ in the following. In this case it is convenient to write the general solution as

$$y = \sqrt{n}\, z + \frac{T^{-1}}{(Tz)^{\frac{n}{2}}}\Big[a \sin(\alpha \log Tz) + b \cos(\alpha \log Tz)\Big]\,, \tag{2.22}$$

where $\alpha = \sqrt{4(n+1) - n^2}/2$ and a, b are dimensionless constants determined by z_0 or y_0. It is easy to show that under the rescaling discussed above, these constants transform as

$$\begin{pmatrix} a \\ b \end{pmatrix} \to \frac{1}{\mu^{\frac{n}{2}+1}} \begin{pmatrix} \cos(\alpha \log \mu) & \sin(\alpha \log \mu) \\ -\sin(\alpha \log \mu) & \cos(\alpha \log \mu) \end{pmatrix} \begin{pmatrix} a \\ b \end{pmatrix}\,. \tag{2.23}$$

This result implies that the solutions exhibit discrete self-similarity and yields critical exponents that characterise the near-critical behaviour. We refer the reader to [173–175] for details but emphasise that this behaviour depends only on the dimension of the sphere. Hence it is universal for all Dp/Dq systems (with $n \leq 4$).

Each near-horizon solution gives rise to a global solution when extended over the full spacetime (2.1). Each of these embeddings is characterised by two constants, which can be read off from its asymptotic behaviour and which can be interpreted as the quark mass $M_{\rm q}$ and (roughly) the quark condensate $\langle\bar{\psi}\psi\rangle$ in the dual field theory – see below. Both of these quantities are fixed by z_0 or y_0. As we will see, the values corresponding to the critical solution, $M_{\rm q}^*$ and $\langle\bar{\psi}\psi\rangle^*$, give a rough estimate of the point at which a phase transition occurs.

Real scaling exponents?

From eq. (2.21), we see that the exponents will be real if the dimension of the internal sphere wrapped by the Dq-brane is sufficiently large, *i.e.,* if $n \geq 5$. This would be interesting because, whereas the oscillatory behaviour for $n \leq 4$ leads to a first order phase transition, as we show below, real exponents would seem to lead to a second order phase transition. However, we will now argue that (under the same assumption to guarantee stability as above) no such analysis can be applied for the Dp/Dq systems that actually arise in superstring theory.

Choosing a value of n, the dimension of the internal sphere, places restrictions on the allowed values of both p and q. The internal S^n is a subspace of the spherical part of the geometry (2.1) and hence we must have $p < 8 - n$. We have taken a strict inequality here, *i.e.,* we do not consider $p = 8 - n$, because the size of the n-sphere must vary to have nontrivial embeddings and so it can not fill the entire internal $(8-p)$-sphere. Given that $p \geq 0$,[6] we need only consider $n = 5, 6, 7$.

Next, we note that by T-dualising along the p directions common to both sets of branes, the brane configuration is reduced to a D0/Dq' intersection, where $q' = n + 1 + (p - d)$. Given the previous restriction on n, we must have $q' \geq 6$. Now, if we require as above that the intersection be supersymmetric at zero temperature (for stability), then we must have $q' = 8$. Hence the only brane configurations of interest are T-dual to the D0/D8

[6]No black brane geometry exists for a Euclidean D(–1)-brane.

system. However, these configurations are those in which string creation arises through the Hanany-Witten effect [176]. In particular, as discussed in [177], the background Ramond-Ramond field of the Dp-branes will induce a nontrivial worldvolume gauge field on the Dq-brane. While this does not rule out the possibility of interesting embeddings and a possible (second order) phase transition, it certainly indicates that the present analysis (with no worldvolume gauge fields) does not apply to these systems. For this reason, in the remainder of this chapter we will concentrate on Dp/Dq systems with $n \leq 4$.

2.2.3 Phase Transitions

In order to study the global solutions corresponding to the near horizon solutions of the previous subsection it is convenient to introduce an isotropic, dimensionless radial coordinate ρ through

$$(u_0\rho)^{\frac{7-p}{2}} = u^{\frac{7-p}{2}} + \sqrt{u^{7-p} - u_0^{7-p}}\,. \tag{2.24}$$

Note that the horizon is at $\rho = 1$. Following the discussion in the previous subsection,[7] we assume that the Dp/Dq system under consideration is T-dual to the D3/D7 one, in which case $(p-d)+(n+1)=4$. Then the Euclidean Dq-brane action density of $N_{\rm f}$ coincident Dq-branes in the black Dp-brane background is

$$\frac{I_{\rm bulk}}{\mathcal{N}} = \int_{\rho_{\rm min}}^{\infty} d\rho \left(\frac{u}{u_0\rho}\right)^{d-3} \left(1 - \frac{1}{\rho^{2(7-p)}}\right) \rho^n (1-\chi^2)^{\frac{n-1}{2}} \sqrt{1-\chi^2+\rho^2\dot{\chi}^2}\,, \tag{2.25}$$

where $\chi = \cos\theta$, $\dot{\chi} = d\chi/d\rho$ and we have introduced the normalisation constant

$$\mathcal{N} = \frac{N_{\rm f} T_{\rm Dq} u_0^{n+1} \Omega_n}{4T}\,. \tag{2.26}$$

Here, $T_{\rm Dq} = 1/(2\pi\ell_s)^q g_s \ell_s$ is the Dq-brane tension and Ω_n is the volume of a unit n-sphere. Up to a numerical constant of $O(1)$, the normalisation factor is found to be

$$\mathcal{N} \sim N_{\rm f} N_{\rm c} T^d g_{\rm eff}(T)^{\frac{2(d-1)}{5-p}}\,, \tag{2.27}$$

where $g_{\rm eff}(T)$ is the effective coupling (2.12) and we have used the standard gauge/gravity relations (2.2) and (2.3).

[7] Above, we pointed out that our present analysis does not apply to Dp/Dq systems T-dual to D0/D8-branes. Systems T-dual to D0/D0 systems would be trivial for the present purposes as $n = 0$. Hence those T-dual to the D0/D4 or D3/D7 system are the only other possibility with a supersymmetric limit.

The equation of motion that follows from (2.25) leads to the large-ρ behaviour[8]

$$\chi = \frac{m}{\rho} + \frac{c}{\rho^n} + \cdots . \tag{2.28}$$

Holography relates the dimensionless constants m, c to the quark mass and condensate by[9,10]

$$M_{\rm q} = \frac{u_0 m}{2^{\frac{9-p}{7-p}}\pi\ell_s^2} \sim g_{\rm eff}(T)^{\frac{2}{5-p}}\, T\, m\,, \tag{2.29}$$

$$\langle \mathcal{O}_m \rangle = -\frac{2\pi\ell_s^2(n-1)\Omega_n N_{\rm f} T_{\rm Dq} u_0^n c}{4^{\frac{n}{7-p}}} \sim -N_{\rm f}\, N_{\rm c}\, g_{\rm eff}^{\frac{2(d-2)}{5-p}}\, T^d\, c\,. \tag{2.30}$$

Here $M_{\rm q}$ is the mass of the fields in the fundamental hypermultiplets, both the fermions ψ and the scalars q. The operator $\mathcal{O}_m$ is a supersymmetric version of the quark bilinear, and it takes the schematic form

$$\mathcal{O}_m = \bar\psi\psi + q^\dagger \Phi q + M_{\rm q} q^\dagger q\,, \tag{2.31}$$

where Φ is one of the adjoint scalars. We will loosely refer to its expectation value as the 'quark condensate'. A detailed discussion of this operator, including a precise definition, can be found in appendix A [126, 151].

Eq. (2.29) implies the relation $m^{(5-p)/2} = \bar{M}/T$ between the dimensionless quantity m, the temperature T and the mass scale

$$\bar{M} = \frac{7-p}{2^{\frac{9-p}{7-p}}\pi L}\left(\frac{2\pi\ell_s^2 M_{\rm q}}{L}\right)^{\frac{5-p}{2}} \sim \frac{M_{\rm q}}{g_{\rm eff}(M_{\rm q})}\,. \tag{2.32}$$

Up to numerical factors, this scale is the mass gap in the discrete meson spectrum at temperatures well below the phase transition [61, 62, 101, 102, 154]. We shall see below that it is also the scale of the temperature of the phase transition for the fundamental degrees of freedom, $T_{\rm fun} \sim \bar{M}$, since the latter takes place at $m \sim 1$.

The key observation [174, 175] is that the values (m, c) of a near-critical solution are linearly related to the integration constants fixing the corresponding embedding in the near-horizon region. Combining this with the transformation rule (2.23) for the near-horizon

[8] Here we assume $n > 1$. Otherwise the term multiplied by c is $\log\rho/\rho$.

[9] Note that the factor of $N_{\rm f}$ in the second equation was missing in refs. [111, 147].

[10] A derivation of these relations for the D3/D7 brane system appears in appendix A. The derivation for Dp/Dq systems is analogous.

constants (a, b) and eliminating μ, we deduce that $(m - m^*)/z_0^{\frac{n}{2}+1}$ and $(c - c^*)/z_0^{\frac{n}{2}+1}$ are periodic functions of $(\alpha/2\pi)\log z_0$ with unit period for Minkowski embeddings, and similarly with z_0 replaced by y_0 for black hole embeddings. This is confirmed by our numerical results, which will be discussed in the next sections and are illustrated for the D3/D7 brane system in figure 2.3.

The oscillatory behaviour of m and c as functions of z_0 or y_0 implies that for a fixed value of m near the critical value, several consistent Dq-brane embeddings are possible with different values of c. Alternatively, one finds the quark condensate is not a single-valued function of the quark mass. Physically, the preferred solution will be the one that minimises the free energy density of the Dq-branes, $F = TI_{\rm E}$. As with the bulk action, the Dq-action (2.25) contains large-radius divergences, as can be seen by substituting the asymptotic behaviour (2.28) in eq. (2.25). It therefore needs to be regularised and renormalised. We can achieve the former by replacing the upper limit of integration by a finite ultraviolet cut-off $\rho_{\rm max}$. Then in analogy to the holographic renormalisation of the supergravity action [165–170], boundary 'counter-terms' $I_{\rm bound}$ are added to the brane action $I_{\rm bulk}$, such that the renormalised brane energy $I_{\rm E} = I_{\rm bulk} + I_{\rm bound}$ is then finite as the cut-off is removed, $\rho_{\rm max} \to \infty$ [178]. The latter method applies directly to asymptotic AdS geometries, but it can be easily extended to the D4/D6 system, as discussed below. We expect that a similar procedure can be developed for any Dp/Dq system for which there is a consistent gauge/gravity duality. (In any event, the brane action can also be regulated by subtracting the free energy of a fiducial embedding.) The details for the D3/D7 and D4/D6 cases are discussed in the following sections and the results are presented in figures 2.5 and 2.13, respectively. In both cases, we see that as the temperature is increased, a first order phase transition occurs by discontinuously jumping from a Minkowski embedding (point A) to a black hole embedding (point B). We emphasise again that this first order transition is a direct consequence of the multi-valued nature of the physical quantities brought on by the critical behaviour described in the previous section. It may be possible to access this self-similar region by supercooling the system (although most of the other solutions in this region are dynamically unstable – see below).

It is interesting to ask if the strong coupling results obtained here could in principle be compared with a weak coupling calculation. It follows from our analysis that the free energy density takes the form $F = \mathcal{N}Tf(m^2)$, where the function f can only depend on even powers of m because of the reflection symmetry $\chi \to -\chi$. The limit $m \to 0$ may

be equivalently regarded as a zero quark mass limit or as a high-temperature limit. In this limit the brane lies near the equatorial embedding $\chi = 0$, which slices the horizon in two equal parts. In general $f(0)$ is a non-zero numerical constant; in the D3/D7 case, for example, a straightforward calculation yields $f(0) = -1/2$. Given eq. (2.27), we have that at strong coupling the free energy density scales as

$$F \sim N_{\rm f}\, N_{\rm c}\, T^{d+1}\, g_{\rm eff}(T)^{\frac{2(d-1)}{5-p}} \,. \tag{2.33}$$

The temperature dependence is that expected on dimensional grounds for a d-dimensional defect, and the $N_{\rm f}N_{\rm c}$ dependence follows from large-N counting rules. However, the dependence on the effective 't Hooft coupling indicates that this contribution comes as a strong coupling effect, without direct comparison to any weak coupling result. The same is true for other thermodynamic quantities such as, for example, the entropy density $S = -\partial F/\partial T$. We remind the reader that the background geometry makes the leading contribution to the free energy density (2.11), which corresponds to that coming from the gluons and adjoint matter. Recall that only for $p = 3$ is the effective coupling factor absent in eq. (2.11). Only in this case the string coupling result differs from that at weak coupling by a mere numerical factor of 3/4 [172]. For the fundamental matter, a similar circumstance arises for $d = 1$, as would be realised with the D1/D5, D2/D4 or D3/D3 systems. In these special cases, the strong and weak coupling calculations for the fundamental matter could in principle be compared. Hence the D3/D3 system is singled out since such a comparison can be made for both the adjoint and fundamental sectors.

2.3 The D3/D7 system

Here we will specialise the above discussion to the D3/D7 system. This intersection is summarised by the array

	0	1	2	3	4	5	6	7	8	9
D3:	×	×	×	×						
D7:	×	×	×	×	×	×	×	×		

(2.34)

Of course, this is an interesting system because both the gluons and the fundamental fields in the gauge theory propagate in $3 + 1$ dimensions.

2.3.1 D7-brane embeddings

In the D3/D7 brane system with the radial coordinate defined in (2.24),

$$(u_0\rho)^2 = u^2 + \sqrt{u^4 - u_0^4}\,, \tag{2.35}$$

the background metric (2.1) becomes

$$ds^2 = \frac{1}{2}\left(\frac{u_0\rho}{L}\right)^2\left[-\frac{f^2}{\tilde{f}}dt^2 + \tilde{f}dx_3^2\right] + \frac{L^2}{\rho^2}\left[d\rho^2 + \rho^2 d\Omega_5^2\right]\,, \tag{2.36}$$

where

$$f(\rho) = 1 - \frac{1}{\rho^4}\,, \quad \tilde{f}(\rho) = 1 + \frac{1}{\rho^4}\,. \tag{2.37}$$

The coordinates $\{t, x^i\}$ parametrise the intersection, while $\{\rho, \Omega_5\}$ are spherical coordinates on the 456789-directions transverse to the D3-branes. As in eq. (2.15), it is useful to adapt the metric on the five-sphere to the D7-brane embedding. Since the D7-brane spans the 4567-directions, we introduce spherical coordinates $\{r, \Omega_3\}$ in this space and $\{R, \phi\}$ in the 89-directions. Denoting by θ the angle between these two spaces we then have:

$$\rho^2 = r^2 + R^2\,, \quad r = \rho\sin\theta\,, \quad R = \rho\cos\theta\,, \tag{2.38}$$

and

$$\begin{aligned} d\rho^2 + \rho^2 d\Omega_5^2 &= d\rho^2 + \rho^2\left(d\theta^2 + \sin^2\theta\, d\Omega_3^2 + \cos^2\theta\, d\phi^2\right) &(2.39)\\ &= dr^2 + r^2 d\Omega_3^2 + dR^2 + R^2 d\phi^2\,. &(2.40)\end{aligned}$$

Describing the profile in terms of $\chi(\rho) = \cos\theta(\rho)$ simplifies the analysis – note that $\chi = R/\rho$. With this coordinate choice, the induced metric on the D7-brane becomes

$$ds^2 = \frac{1}{2}\left(\frac{u_0\rho}{L}\right)^2\left[-\frac{f^2}{\tilde{f}}dt^2 + \tilde{f}dx_3^2\right] + \left(\frac{L^2}{\rho^2} + \frac{L^2\dot{\chi}^2}{1-\chi^2}\right)d\rho^2 + L^2(1-\chi^2)\,d\Omega_3^2\,, \tag{2.41}$$

where, as above, $\dot{\chi} = d\chi/d\rho$. Since we are studying static embeddings of the probe brane, the equation of motion for $\chi(\rho)$ can be derived equally well from the Lorentzian or Euclidean action. Here we proceed directly to the latter because it is relevant for the thermodynamic calculations in the following. The Euclidean D7-brane action density is

$$\frac{I_{\rm bulk}}{\mathcal{N}} = \int d\rho\left(1 - \frac{1}{\rho^8}\right)\rho^3(1-\chi^2)\sqrt{1-\chi^2+\rho^2\dot{\chi}^2}\,, \tag{2.42}$$

where

$$\mathcal{N} = \frac{2\pi^2 N_{\rm f} T_{\rm D7} u_0^4}{4T} = \frac{\lambda N_{\rm f} N_{\rm c}}{32}\, T^3 \tag{2.43}$$

is the normalisation constant defined in (2.26). Recall from footnote 5 that $I_{\rm bulk}$ denotes a density because we have divided out the volume V_x. The equation of motion for $\chi(\rho)$ is then

$$\partial_\rho \left[\left(1 - \frac{1}{\rho^8}\right) \frac{\rho^5 (1-\chi^2)\dot{\chi}}{\sqrt{1-\chi^2+\rho^2\dot{\chi}^2}} \right] + \rho^3 \left(1 - \frac{1}{\rho^8}\right) \frac{3\chi(1-\chi^2) + 2\rho^2 \chi \dot{\chi}^2}{\sqrt{1-\chi^2+\rho^2\dot{\chi}^2}} = 0\,, \tag{2.44}$$

which implies that the field χ asymptotically approaches zero as

$$\chi = \frac{m}{\rho} + \frac{c}{\rho^3} + \cdots\,. \tag{2.45}$$

The holographic dictionary (see appendix A) relates the dimensionless constants m and c to the quark mass and condensate through eqs. (2.29) and (2.30) with $p = 3$ and $n = 3$:

$$M_{\rm q} = \frac{u_0 m}{2^{3/2}\pi \ell_s^2} = \frac{1}{2}\sqrt{\lambda}\, T\, m\,, \tag{2.46}$$

$$\langle \mathcal{O}_m \rangle = -2^{3/2}\pi^3 \ell_s^2 N_{\rm f} T_{\rm D7} u_0^3\, c = -\frac{1}{8}\sqrt{\lambda}\, N_{\rm f}\, N_{\rm c}\, T^3\, c\,. \tag{2.47}$$

In this case $m = \bar{M}/T$ and eq. (2.32) takes the form

$$\bar{M} = \frac{\sqrt{2}(2\pi \ell_s^2 M_{\rm q})}{\pi L^2} = \frac{2M_{\rm q}}{\sqrt{\lambda}} = \frac{M_{\rm gap}}{2\pi}\,, \tag{2.48}$$

where $\lambda = g_{\rm YM}^2 N_{\rm c} = 2\pi g_s N_{\rm c}$ is the 't Hooft coupling. In the last equality, we are relating $\bar{M}$ to the meson mass gap in the D3/D7 theory at zero temperature [61].

The equation of motion (2.44) can be recast in terms of the R and r coordinates, related to the ρ and θ coordinates via (2.38):

$$\partial_r \left[r^3 \left(1 - \frac{1}{(r^2+R^2)^4}\right) \frac{\partial_r R}{\sqrt{1+(\partial_r R)^2}} \right] = 8 \frac{r^3 R}{(r^2+R^2)^5} \sqrt{1+(\partial_r R)^2}\,, \tag{2.49}$$

where the embedding of the D7-brane is now specified by $R = R(r)$. Asymptotically,

$$R(r) = m + \frac{c}{r^2} + \cdots\,. \tag{2.50}$$

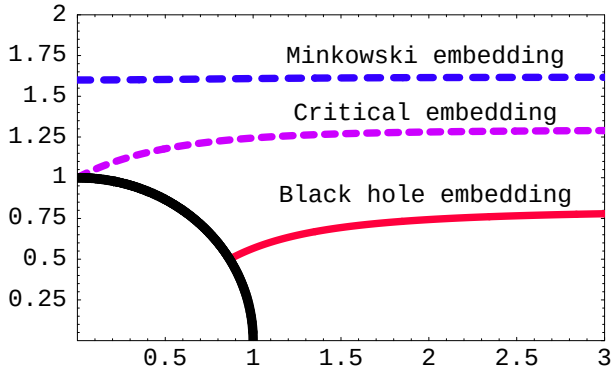

Figure 2.2: Profiles of various D7-brane embeddings in a D3-brane background in the (R, r)-plane. The circle represents the horizon at $\rho = 1$.

In the limits of large and small m we were able to find approximate analytic solutions for the embeddings – see discussion below and section 2.6.1. However, for arbitrary m we were unable to find an analytic solution of eq. (2.44) or (2.49) and so we resorted to solving these equations numerically. It was simplest to solve for Minkowski embeddings using the (R, r) coordinates with equation of motion (2.49) while the (χ, ρ) coordinates were best suited to the black hole embeddings. Our approach was to specify the boundary conditions at a minimum radius and then numerically integrate outward. For the black hole embeddings, the following boundary conditions were specified at the horizon $\rho_{\rm min} = 1$: $\chi = \chi_0$ and $d\chi/d\rho = 0$ for $0 \leq \chi_0 < 1$. For Minkowski embeddings, the following boundary conditions were specified at $r_{min} = 0$ (*i.e.,* at the axis $\chi = 1$): $R = R_0$ and $\partial_r R = 0$ for $R_0 > 1$. In order to compute the constants m, c corresponding to each choice of boundary conditions at the horizon, we fitted the solutions to the asymptotic form (2.45) for $\chi(\rho)$ or (2.50) for $R(r)$. A few characteristic profiles are shown in fig. 2.2.

Recall that, as elucidated in section 2.2.2, the black hole and Minkowski embeddings are separated by a critical solution which just touches the horizon. This critical embedding is characterised by certain critical values of the integration constants, m^* and c^*. For Minkowski embeddings near the critical solution, fig. 2.3 shows plots of $(m-m^*)/(R_0-1)^{5/2}$ and $(c-c^*)/(R_0-1)^{5/2}$ versus $\sqrt{7}\log(R_0-1)/4\pi$. In this regime, we may relate the boundary value to that in the near horizon analysis with $R_0 - 1 \simeq z_0$. Here our numerical results confirm that, near the critical solution, $(m - m^*)/z_0^{5/2}$ and $(c - c^*)/z_0^{5/2}$ are both periodic

functions of $\sqrt{7}\log(z_0)/4\pi$ with unit period, as discussed above in section 2.2.2. This oscillatory behaviour of m and c as functions of z_0 (or y_0) implies that the quark condensate is not a single-valued function of the quark mass and this is clearly visible in our plots of c versus $T/\bar{M} = 1/m$, displayed in figure 2.4. By increasing the resolution in these plots, we are able to follow the two families of embeddings spiralling in on the critical solution, the behaviour predicted by the near-horizon analysis. Thermodynamic considerations will resolve the observed multi-valuedness by determining the physical solution as that which minimises the free energy density of the D7-branes. As discussed in section 2.2.3, since the physical parameters are multi-valued, we can anticipate that there will be a first order phase transition when the physical embedding moves from the Minkowski branch to the black hole branch. We will proceed to computing the free energy density in the next subsection. The position of the resulting phase transition is indicated in the second plot of fig. 2.4.

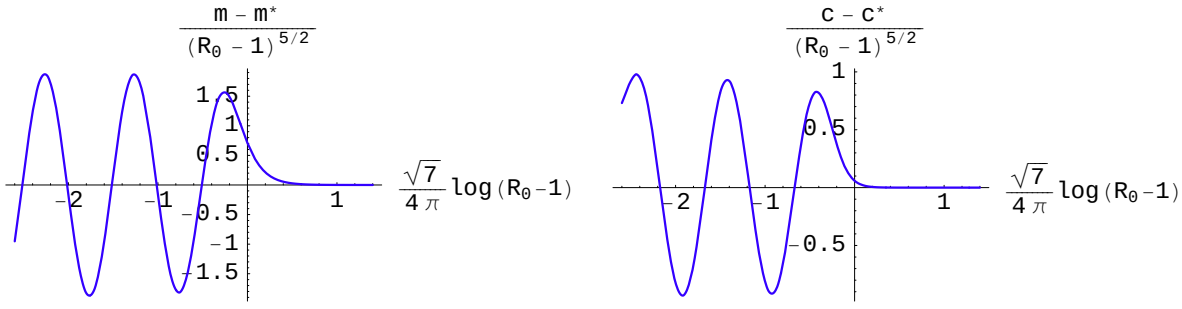

(a) (b)

Figure 2.3: Quark mass (a) and condensate (b) as a function of the distance to the horizon $R_0 - 1$ for D7-brane Minkowski embeddings in a D3-brane background. Note that near the horizon $R_0 - 1 \sim z_0$.

2.3.2 D7-brane thermodynamics

Having discussed the embeddings of the D7-brane in the black D3-brane geometry, we proceed to compute the free energy, entropy and energy densities associated with the D7-brane, or equivalently, the fundamental fields. We start with the Euclidean D7-brane

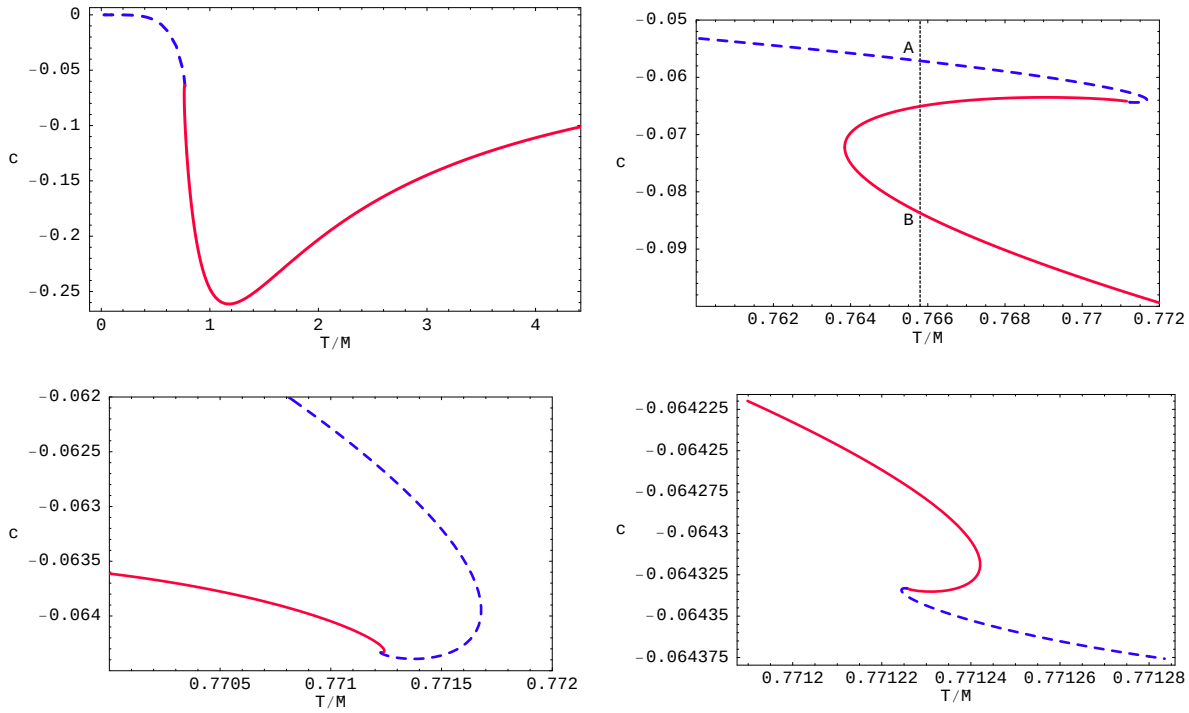

Figure 2.4: Quark condensate c for a D7 in a D3 background versus $T/\bar{M}$. The blue dashed (red continuous) curves correspond to the Minkowski (black hole) embeddings. The dotted vertical line indicates the precise temperature of the phase transition.

action (2.42). Using the asymptotic behaviour (2.45), we see that the action contains a UV divergence, since

$$\frac{I_{\rm bulk}}{\mathcal{N}} \simeq \int_{\rho_{\rm min}}^{\rho_{\rm max}} d\rho\, \rho^3 \simeq \frac{1}{4}\rho_{\rm max}^4 \tag{2.51}$$

diverges as the regulator is removed, *i.e.*, $\rho_{\rm max} \to \infty$.

This kind of problem is well-known in the context of the AdS/CFT correspondence and was first resolved for the gravity action by introducing boundary counter-terms, which depend only on the intrinsic geometry of the boundary metric [165–170]. These ideas can be generalised to other fields in an AdS background, such as a scalar [179] – for a review, see [180]. The latter formed the basis for the renormalisation of probe brane actions in [178], where the brane position or profile is treated as a scalar field in an asymptotically AdS geometry. That is, one implicitly performs a Kaluza-Klein reduction of the D7 action

to five dimensions so that it appears to be a complicated nonlinear action for a scalar field χ propagating in a five-dimensional (asymptotically) AdS geometry. One then introduces boundary counter-terms which are local functionals (polynomials) of the scalar field (and boundary geometry) on an asymptotic regulator surface. These terms are designed to remove the bulk action divergences that arise as the regulator surface is taken off to infinity, as in eq. (2.51). The D3/D7 system is explicitly considered in ref. [178], which also introduces a finite counterterm that ensures that the brane action vanishes for the supersymmetric embedding of a D7-brane in an extremal D3-background, *i.e.,* eq. (2.1) with $u_0 = 0$ and $p = 3$. In the calculation of [178] the D7-brane embedding is specified as $\theta(\rho)$, but this is easily converted to a counter-term action for $\chi(\rho)$ using the obvious coordinate/field redefinition: $\frac{\pi}{2} - \theta = \arcsin\chi \simeq \chi + 1/6\,\chi^3 + \cdots$. The final result is

$$\frac{I_{\rm bound}}{\mathcal{N}} = -\frac{L^4 T}{u_0^4}\int dt_{\rm E} d^3x \sqrt{\det\gamma}\left(1 - 2\chi^2 + \chi^4\right)\,, \tag{2.52}$$

where this boundary action is evaluated on the asymptotic regulator surface $\rho = \rho_{\rm max}$ introduced above. The boundary metric γ at $\rho = \rho_{\rm max}$ in the (effective) five-dimensional geometry is given by

$$ds^2(\gamma) = \frac{1}{2}\left(\frac{u_0\rho_{\rm max}}{L}\right)^2\left(\frac{f(\rho_{\rm max})^2}{\tilde f(\rho_{\rm max})}\,dt_{\rm E}^2 + \tilde f(\rho_{\rm max})dx_3^2\right) \tag{2.53}$$

and so $\sqrt{\gamma} = u_0^4\rho_{\rm max}^4 f(\rho_{\rm max})\tilde f(\rho_{\rm max})/4L^4$. Evaluating the counter-term action (2.52) with an asymptotic profile as in eq. (2.28), one finds

$$\frac{I_{\rm bound}}{\mathcal{N}} = -\frac{1}{4}\left[(\rho_{\rm max}^2 - m^2)^2 - 4mc\right]. \tag{2.54}$$

Here we have divided out the volume factor V_x – see footnote 5. Comparing eqs. (2.51) and (2.54), one sees that the leading divergence proportional to $\rho_{\rm max}^4$ cancels in the sum of $I_{\rm E} = I_{\rm bulk} + I_{\rm bound}$. As a further check, one can consider the supersymmetric limit $u_0 \to 0$, in which one must work with a rescaled coordinate $\varrho = u_0\rho$, since the change of variables (2.35) is not well defined at $u_0 = 0$. In this limit $\chi = u_0 m/\varrho = \sqrt{2}\,2\pi\ell_s^2 M_{\rm q}/\varrho$ is an exact solution, and one can easily verify that for this configuration $I_{\rm E} = I_{\rm bulk} + I_{\rm bound} = 0$.

In order to produce a finite integral which is more easily evaluated numerically, it is useful to incorporate the divergent terms in the boundary action (2.54) into the integral

in eq. (2.42) using

$$\begin{aligned} \rho_{\rm max}^4 &= \int_{\rho_{\rm min}}^{\rho_{\rm max}} d\rho\, 4\rho^3 + {\rho_{\rm min}}^4 \,, \\ \rho_{\rm max}^2 &= \int_{\rho_{\rm min}}^{\rho_{\rm max}} d\rho\, 2\rho + {\rho_{\rm min}}^2 \,. \end{aligned} \tag{2.55}$$

Then the total action may be written as

$$\frac{I_{\rm E}}{\mathcal{N}} = G(m) - \frac{1}{4}\left[({\rho_{\rm min}}^2 - m^2)^2 - 4mc\right] \,, \tag{2.56}$$

where $G(m)$ is defined as

$$G(m) = \int_{\rho_{\rm min}}^{\infty} d\rho\, \left[\rho^3\left(1-\frac{1}{\rho^8}\right)\left(1-\chi^2\right)\left(1-\chi^2+\rho^2\,\dot{\chi}^2\right)^{1/2} - \rho^3 + m^2\rho\right]. \tag{2.57}$$

Note that the upper bound for the range of integration has been set to infinity, since the integral above is finite.

From these expressions, the free energy density is given by $F = TI_{\rm E}$. Now using our numerical results, the free energy density is shown as a function of the temperature in the first two plots in fig. 2.5. The second of these shows the classic 'swallow tail' form, typically associated with a first order phase transition. To our best numerical accuracy, the phase transition takes place at $T_{\rm fun}/\bar{M} = 0.7658$ (or $m = 1.306$), where the free energy curves for the Minkowski and black hole phases cross. The fact that the transition is first order is illustrated by fig. 2.4, which shows that the quark condensate makes a finite jump at this temperature between the points labelled A and B. Similar discontinuities also appear in other physical quantities, like the entropy and energy density, as we now calculate.

Given the free energy density, a standard identity (2.7) yields the entropy density as

$$S = -\frac{\partial F}{\partial T} = -\pi L^2 \frac{\partial F}{\partial u_0} \,, \tag{2.58}$$

where we have used the expression $u_0 = \pi L^2 T$ from eq. (2.6). Evaluating this expression requires a straightforward but somewhat lengthy calculation, which we have relegated to section 2.6.2. The final result is

$$\frac{S}{\mathcal{N}} = -4G(m) + ({\rho_{\rm min}}^2 - m^2)^2 - 6mc \,. \tag{2.59}$$

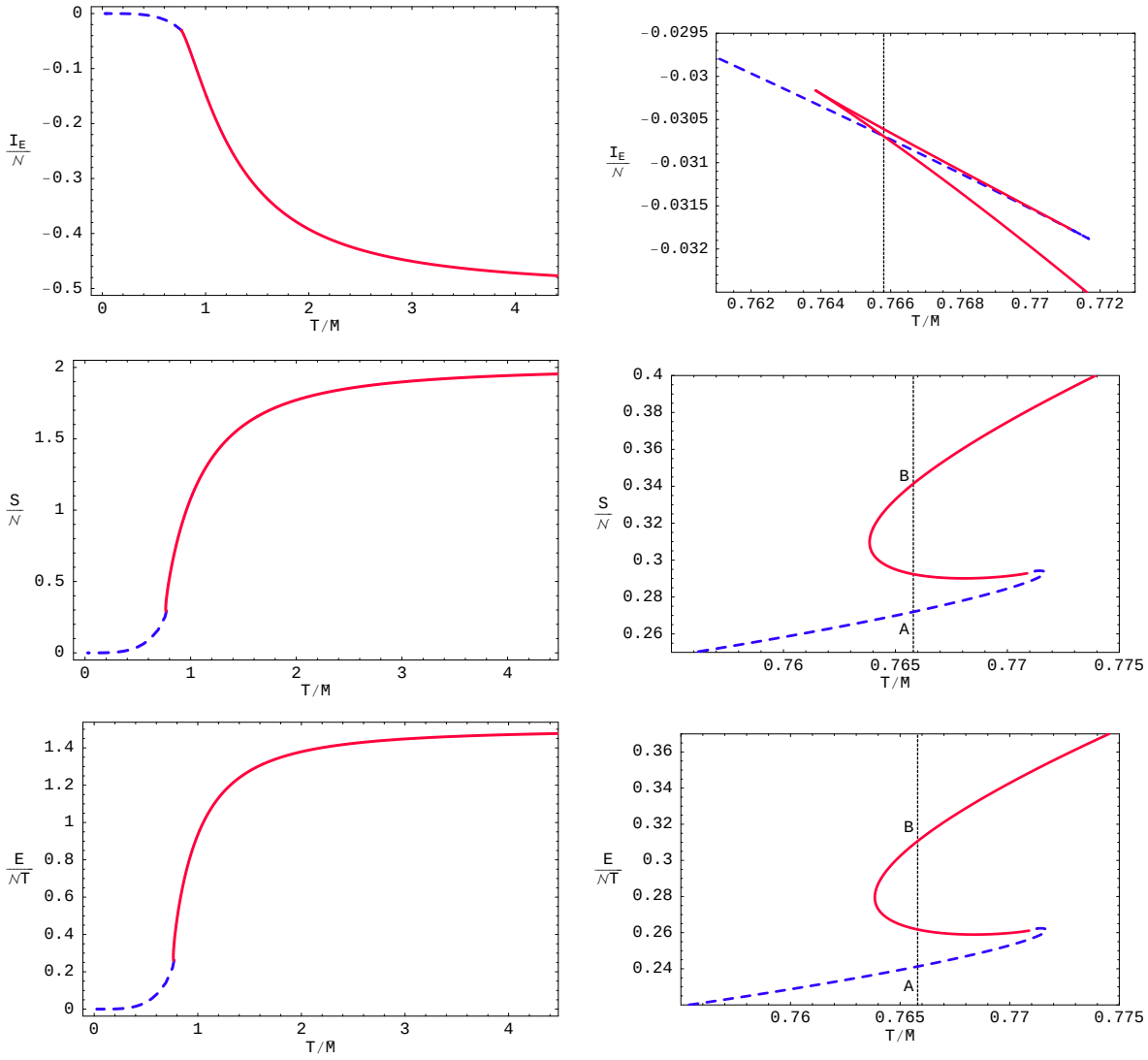

Figure 2.5: Free-energy, entropy and energy densities for a D7-brane in a D3-brane background; note that $\mathcal{N} \propto T^3$. The blue dashed (red continuous) curves correspond to the Minkowski (black hole) embeddings. The dotted vertical line indicates the precise temperature of the phase transition.

Comparing eqs. (2.56) and (2.59), we see that the entropy and free energy densities are simply related as

$$S = -\frac{4F}{T}\left(1 + \frac{2\mathcal{N}\,mc}{4F/T}\right) . \tag{2.60}$$

The first term above can be recognized as the behaviour expected for a conformal system, *i.e.,* a system for which $F \propto T^4$. Hence the second term can be interpreted as summarising the deviation from conformal behaviour. We note that, as illustrated in fig. 2.4, c vanishes in both the limits $T \to 0$ and $T \to \infty$ and so the deviation from conformality is reduced there. More precisely, using the results from section 2.6.1 we see that $c \sim m$ at high temperature and $c \sim 1/m^5$ at low temperature. Together with (2.43) this implies that the deviation from conformality scales as $\bar{M}^2/T^2$ at high temperature. Conformality is also restored at low temperatures but only because both S and F/T approach zero more quickly than T^3. That is, $S \sim T^7/\bar{M}^4$ as $T \to 0$.

Finally, the thermodynamic identity $E = F + TS = T(I_{\rm E} + S)$ gives the contribution of the D7-brane to the energy density:

$$\frac{E}{\mathcal{N}T} = -3G(m) + \frac{3}{4}\left[({\rho_{\rm min}}^2 - m^2)^2 - \frac{20}{3}mc\right] . \tag{2.61}$$

We evaluated both the expressions (2.59) and (2.61) numerically and plotted S and E in fig. 2.5. In both cases, the phase transition is characterised by a finite jump in these quantities, as illustrated by the second plot in each case. However, these plots also show that there is a large rise in, say, the entropy density in the vicinity of $T_{\rm fun}$ and that the jump associated with the phase transition only accounts for roughly 3% of this total increase.

We close with a few observations about these results. First, recall from (2.43) that $\mathcal{N} \sim \lambda N_{\rm c} N_{\rm f} T^3$ so that the leading contribution of the D7-branes to all the various thermodynamic quantities will be order $\lambda N_{\rm c} N_{\rm f}$, in comparison to $N_{\rm c}^2$ for the usual bulk gravitational contributions. As noted in [111, 147], the factor of λ represents a strong coupling enhancement over the contribution over a simple free-field estimate for the $N_{\rm c}N_{\rm f}$ fundamental degrees of freedom. We return to this point below in section 2.5.

Next, note that in order for the entropy $S = -\partial F/\partial T$ to be positive, the free energy F, or equivalently the action $I_{\rm E}$, must always be a decreasing function of the temperature. This means that the apparent 'kinks' in the plot of these quantities versus the temperature are true mathematical kinks and not just very rapid turn overs. An analytic proof of this fact is given in section 2.6.3.

Finally, from the plots of the energy density one can immediately read off the qualitative behaviour of the specific heat $c_V = \partial E/\partial T$. In particular, note that this slope must become negative as the curves spiral around near the critical solution. Hence the corresponding embeddings are thermodynamically unstable. Examining the fluctuation spectrum of the branes, we will show that a corresponding dynamical instability sets in at precisely the same points. One may have thought that these phases near the critical point could be accessed by 'supercooling' the system but this instability severely limits the embeddings which can be reached with such a process.

Thermodynamic expressions for large $T/\bar{M}$

With precisely $m = 0$, $\chi(\rho) = 0$ is an exact solution. We denote this solution as the equatorial embedding, since the D7-brane remains at the maximal S^3 for all values of ρ. This embedding describes the infinite-temperature limit for massive quarks (or massless quarks for any temperature), *i.e.,* $T/\bar{M} \to \infty$. For $T/\bar{M} \gg 1$ or $m \ll 1$, approximate analytic solutions for the D7-brane profile can be found by perturbing around the equatorial embedding, as discussed in section 2.6.1. The final result is given in eq. (2.133). In the notation of that section, the integral (2.57) can be expressed as

$$\begin{aligned} G(m) &= \int_1^\infty \frac{dx}{2}\left[x\left(1-\frac{1}{x^4}\right)\left(1-\frac{3}{2}m^2\tilde{\chi}^2+2x^2\left(\partial_x m\tilde{\chi}\right)^2\right)-x+m^2\right] \\ &= -\frac{1}{4}+m^2 G_2 \end{aligned}$$

where we have introduced

$$G_2 \equiv \int_1^\infty \frac{dx}{2}\left[x\left(1-\frac{1}{x^4}\right)\left(-\frac{3}{2}\tilde{\chi}^2+2x^2\left(\partial_x\tilde{\chi}\right)^2\right)+1\right] \simeq 0.413893\,. \tag{2.62}$$

We were only able to evaluate this integral numerically.

We are now in a position to evaluate the various thermal quantities given by eqs. (2.56), (2.59) and (2.61) in this limit. We find

$$\begin{aligned} \frac{I_{\rm E}}{\mathcal{N}} &\simeq -\frac{1}{2}+\left(G_2+\tilde{c}+\frac{1}{2}\right)\left(\frac{\bar{M}}{T}\right)^2-\frac{1}{4}\left(\frac{\bar{M}}{T}\right)^4+\cdots, \\ \frac{S}{\mathcal{N}} &\simeq 2+\left(-4G_2-6\tilde{c}-2\right)\left(\frac{\bar{M}}{T}\right)^2+\left(\frac{\bar{M}}{T}\right)^4+\cdots, \\ \frac{E}{\mathcal{N}T} &\simeq \frac{3}{2}+\left(-3G_2-5\tilde{c}-\frac{3}{2}\right)\left(\frac{\bar{M}}{T}\right)^2+\frac{3}{4}\left(\frac{\bar{M}}{T}\right)^4+\cdots, \end{aligned}$$

using $\rho_{\rm min} = 1$ for black hole embeddings and $\tilde{c} \simeq -0.456947$ from eq. (2.136). In this high temperature limit, the quark mass is negligible and so the first term in these expressions could be characterised as conformal behaviour. The remaining contributions are small corrections indicating a deviation from this simple behaviour generated by the finite quark mass. This is essentially the form expected in the high T limit in finite temperature field theory – for example, see [181] and the references therein.

Thermodynamic expressions for small $T/\bar{M}$

Turning to the opposite, low-temperature limit, *i.e.,* $T/\bar{M} \ll 1$, the D7-branes lie on flat embeddings far from the event horizon, *i.e.,* $\chi \simeq R_0/\rho$ to leading order. One can calculate perturbative improvements to this simple embedding – see section 2.6.1 – but it suffices to determine the leading thermodynamic behaviour. We find that

$$G(m) = \int_0^\infty dr \left[r^3 \left(1 - \frac{1}{\rho^8}\right) \sqrt{1 + (\partial_r R)^2} + (r + R\,\partial_r R)(m^2 - \rho^2) \right] \simeq \frac{1}{12}\frac{1}{m^4}\,. \quad (2.63)$$

Then using $R_0 \simeq m$ and $c \simeq -1/6m^5$, the thermal densities become

$$\frac{I_{\rm E}}{\mathcal{N}} \simeq -\frac{1}{12}\left(\frac{T}{\bar{M}}\right)^4, \qquad \frac{S}{\mathcal{N}} \simeq \frac{2}{3}\left(\frac{T}{\bar{M}}\right)^4, \qquad \frac{E}{\mathcal{N}T} \simeq \frac{7}{12}\left(\frac{T}{\bar{M}}\right)^4. \quad (2.64)$$

Hence these contributions are going rapidly to zero. Note that they still contain the same normalisation constant (2.43) and so these densities are still proportional to $\lambda N_{\rm f} N_{\rm c}$. At low temperature, one might have expected that the thermodynamics of the fundamental matter is dominated by the low lying-mesons, *i.e.,* the lowest energy excitations in the fundamental sector, and so that the leading contributions are proportional to $N_{\rm f}^2$, reflecting the number of mesonic degrees of freedom. Such contributions to the thermal densities will arise in the gravity path integral in evaluating the fluctuation determinant on the D7-brane around the classical saddle-point. As indicated by the $N_{\rm c}$ and λ factors, the leading low-temperature contributions above come from the interaction of the (deconfined) adjoint fields and the fundamental matter.

Speed of sound

As mentioned in section 2.1.2, the speed of sound is another interesting probe of the deconfined phase of the strongly coupled gauge theories. In this section, we calculate the

effect of fundamental matter on the speed of sound. From eq. (2.13), we must evaluate the D7-branes contribution to the total entropy density and the specific heat. The first is already given by eq. (2.59) and we denote this contribution as S_7 in the following. From eq. (2.61), the energy density can be written as $E = -3F - 2\mathcal{N}Tmc$. Then recalling $\mathcal{N} \propto T^3$ from eq. (2.43), the D7-brane contribution to the specific heat can be written as

$$c_{\rm V7} = \frac{\partial E}{\partial T} = 3S_7 - \alpha \, \frac{\partial}{\partial T} \left(T^4 \, mc\right), \tag{2.65}$$

where we have introduced the dimensionless constant $\alpha \equiv \lambda N_{\rm f} N_{\rm c}/16$. From the black D3 background, the free energy of the adjoint fields is given in eq. (2.8). It follows then that the adjoint contributions to the entropy and specific heat are:

$$S_3 = -\frac{\pi^2}{2} N_{\rm c}^2 \, T^3 \,, \qquad c_{\rm V3} = 3 \, S_3 \,. \tag{2.66}$$

Combining all of these results, we can now calculate the speed of sound

$$\begin{aligned} v_s^2 &= \frac{S}{c_{\rm V}} = \frac{S_3 + S_7}{c_{\rm V3} + c_{\rm V7}} \\ &= \frac{S_3 + S_7}{3S_3 + 3S_7 - \alpha \, \partial_T (T^4 \, mc)} \\ &\simeq \frac{1}{3} \left[1 + \frac{\alpha}{3 \, S_3} \, \partial_T \big(T^4 \, mc \big) \right] . \end{aligned} \tag{2.67}$$

Note all of our brane calculations are to first order in an expansion in $N_{\rm f}/N_{\rm c}$ and hence we have applied the Taylor expansion in the last line above, reflecting this perturbative framework *e.g.*, $c_{\rm V7}/c_{\rm V3} \ll 1$. Now using various expressions above, as well as $m = 2M_q/\sqrt{\lambda}T$ and $\varepsilon \equiv \frac{\lambda}{2\pi}\frac{N_{\rm f}}{N_{\rm c}}$, we may write the final result as

$$\delta v_s^2 \equiv v_s^2 - \frac{1}{3} \simeq \frac{\varepsilon}{12\pi} \left(mc + \frac{1}{3} mT \frac{\partial c}{\partial T} \right) . \tag{2.68}$$

This expression indicates that the D7-brane produces a small deviation away from the conformal result, $v_s^2 = \frac{1}{3}$.

The result of numerically evaluating δv_s^2 as a function of the temperature is given in fig. 2.6. We see that δv_s^2 is negative. That is, the fundamental matter reduces the speed of sound. Following the discussion below eq. (2.60) one finds that $\delta v_s^2 \sim T^4/\bar{M}^4$ at low temperature and $\delta v_s^2 \sim \bar{M}^2/T^2$ at high temperature. Thus we see again that the

deviation from conformal behaviour vanishes for large and small T. We also note that δv_s^2 is largest near the phase transition, where it makes a discrete jump. Since we are working in a perturbative framework, eq. (2.68) is only valid when this deviation is a small perturbation. By assumption $\varepsilon \propto N_{\rm f}/N_{\rm c} \ll 1$ and so this is guaranteed provided the last factor in (2.68) is not large. This is indeed satisfied for the thermodynamically favoured embeddings, as illustrated in fig. 2.6. Similar deviations have been investigated in [129,130] for other gauge/gravity dualities.

In fig. 2.6, we have also continued δv_s^2 on the disfavoured embeddings beyond the phase transition and we see that it diverges (towards $-\infty$) at precisely the points where, *e.g.*, the energy density curve turns around – see fig. 2.5. That is, $c_{\rm V7}$ diverges at these points, so that the perturbative derivation of eq. (2.68) breaks down. Hence our perturbative framework does not allow us to investigate interesting effects, as seen in [131, 132].

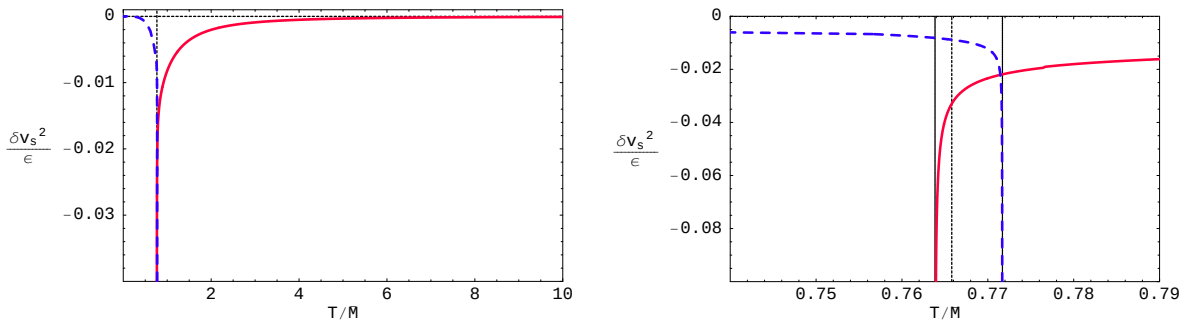

(a) (b)

Figure 2.6: The deviation of the speed of sound from the conformal value. (a) In the limits $T \to 0$ and $T \to \infty$, $\delta v_s^2 \to 0$. (b) The temperature of the phase transition is marked by the dashed vertical line. Note there is a finite discontinuity in the speed of sound at the phase transition. If we follow the black hole branch (red line) or the Minkowski branch (dotted blue line) past the phase transition, we find that δv_s^2 diverges.

We see from eq. (2.68) that, for massive quarks, the deviation from the conformal result is of proportional to $N_{\rm f}/N_{\rm c}$, as expected from large-$N_{\rm c}$ counting rules. However, if $M_{\rm q} = 0$ then the result above vanishes, and so $\delta v_s^2 = O(N_{\rm f}^2/N_{\rm c}^2)$ at least. Presumably, this additional suppression is due to the fact that for massive quarks conformal invariance

is broken explicitly at the classical level, whereas if $M_{\rm q} = 0$ it is broken only at the quantum mechanical level by the non-vanishing beta function of the theory in the presence of fundamental matter. This is proportional to $N_{\rm f}/N_{\rm c}$, leading to an additional suppression. In the gravitational description this is most easily understood at zero temperature. In this case the D3-brane background is exactly $AdS_5 \times S^5$, and the isometries of the first factor correspond to the conformal group in four dimensions. Adding D7-brane probes with non-zero quark mass breaks the conformal isometries, and hence this effect is visible at order $N_{\rm f}/N_{\rm c}$. Instead, if $M_{\rm q} = 0$ then the branes' worldvolume is $AdS_5 \times S^3$, which preserves all the AdS isometries. Hence in this case one must go beyond the probe approximation to see the breaking of conformal invariance, *i.e.,* beyond $O(N_{\rm f}/N_{\rm c})$.

2.3.3 Meson spectrum

As discussed earlier, introducing the D7-brane probes into the black D3-brane geometry corresponds to adding dynamical quarks into the gauge theory. The resulting theory has a rich spectrum of mesons, *i.e.,* quark-antiquark bound states. Since the mesons are dual to open strings with both ends on the D7-brane, the mesonic spectrum can be found by computing the spectrum of D7-brane fluctuations. For temperatures below the phase transition, $T < T_{\rm fun}$, corresponding to Minkowski embeddings of the D7-branes, we expect the spectrum to exhibit a mass gap and be discrete, as found at $T = 0$ [61, 101, 102, 154]. This is confirmed by our calculations below – similar calculations have also appeared recently in [155]. For temperatures above the phase transition, corresponding to black hole embeddings, the spectrum will be continuous and gapless. Excitations of the fundamental fields in this phase are however characterised by a discrete spectrum of quasinormal modes, in analogy with [182–184]. Investigations of the black hole phase appear in chapter 5 [126] and in ref. [155].

Mesons on Minkowski embeddings

In this section we compute the spectrum of low-lying mesons corresponding to fluctuations of the D7-brane in the black D3-brane geometry (2.36). The full meson spectrum would include scalar, vector and spinor modes. For simplicity, we will focus on vector and scalar mesons which correspond to small vector and scalar fluctuations of the probe D7-branes about the embeddings determined in section 2.3.1. We will work with the (R, r) coordinates

introduced in eq. (2.38), in which case the background embedding is given by $R = R_v(r)$, $\phi = 0$, where the subscript v now indicates that this is the 'vacuum' solution.

We focus first on the scalar mesons which correspond to geometric fluctuations of the probe branes. Explicitly, we consider small fluctuations $\delta R, \delta\phi$ about the background embedding:

$$R = R_v(r) + \delta R\,, \quad \phi = 0 + \delta\phi. \tag{2.69}$$

The pullback of the bulk metric (2.36) to this embedding is

$$\begin{aligned} ds^2 &= \frac{1}{2}\left(\frac{u_0\rho}{L}\right)^2\left[-\frac{f^2}{\tilde{f}}dt^2 + \tilde{f}dx_3^2\right] + \frac{L^2}{\rho^2}\left[(1+\dot{R}_v^2)dr^2 + r^2 d\Omega_3^2 + 2(\partial_a\delta R)\dot{R}_v dx^a dr\right] \\ &\quad + \frac{L^2}{\rho^2}\left[(\partial_a\delta R)(\partial_b\delta R)dx^a dx^b + (R_v+\delta R)^2(\partial_a\delta\phi)(\partial_b\delta\phi)dx^a dx^b\right]\,, \end{aligned}$$

where the indices a, b run over all D7 worldvolume directions and the dot denotes differentiation with respect to r, *i.e.,* $\dot{R}_v = \partial_r R_v$. Using the DBI action,

$$I_{\rm DBI} = -N_{\rm f}\,T_{\rm D7}\int d^8\sigma\sqrt{-\det\left(P[G]_{ab} + 2\pi\ell_{\rm s}^2 F_{ab}\right)}\,, \tag{2.70}$$

where, as usual, P denotes the pullback of a bulk field to the probe brane's worldvolume [185], we find that, to quadratic order in fluctuations, the Lagrangian density for the scalar $\delta\phi$, δR modes decouples from that for the gauge field modes:

$$\begin{aligned} \mathcal{L} &= \mathcal{L}_0 - N_{\rm f}\,T_{\rm D7}\frac{u_0^4}{4}r^3\sqrt{h}\sqrt{1+\dot{R}_v^2}\left\{\frac{1}{2}\frac{L^2}{\rho_v^2}\left(1-\frac{1}{\rho_v^8}\right)\sum_a g^{aa}\left(\frac{(\partial_a\delta R)^2}{1+\dot{R}_v^2} + R_v^2(\partial_a\delta\phi)^2\right)\right. \\ &\quad \left. + \frac{4R_v\dot{R}_v\partial_r(\delta R)^2}{\rho_v^{10}(1+\dot{R}_v^2)} + \frac{4(\delta R)^2}{\rho_v^{10}} - \frac{40R_v^2(\delta R)^2}{\rho_v^{12}}\right\}\,, \end{aligned} \tag{2.71}$$

where $\mathcal{L}_0$ is the Lagrangian density for the vacuum embedding:

$$\mathcal{L}_0 = -N_{\rm f}\,T_{\rm D7}\frac{u_0^4}{4}r^3\sqrt{h}\sqrt{1+\dot{R}_v^2}\left(1-\frac{1}{\rho_v^8}\right). \tag{2.72}$$

Here $\rho_v^2 = r^2 + R_v^2$ and h is the determinant of the metric on the S^3 of unit radius. The metric g_{ab} in the first line of (2.71) is the induced metric on the D7-brane with the fluctuations set to zero:

$$ds^2(g) = \frac{1}{2}\left(\frac{u_0\rho_v}{L}\right)^2\left[-\frac{f^2}{\tilde{f}}dt^2 + \tilde{f}dx_3^2\right] + \frac{L^2}{\rho_v^2}\left[(1+\dot{R}_v^2)dr^2 + r^2 d\Omega_3^2\right]\,. \tag{2.73}$$

Note that integration by parts and the equation of motion for R_v allowed terms linear in δR to be eliminated from the Lagrangian density. The linearised equation of motion is

$$\partial_a\left[\frac{L^2r^3f\tilde{f}\sqrt{h}}{\rho_v^2\sqrt{1+\dot{R}_v^2}}g^{aa}\partial_a(\delta R)\right]=8\sqrt{h}\left[\frac{r^3}{\rho_v^{10}}\sqrt{1+\dot{R}_v^2}\left(1-\frac{10R_v^2}{\rho_v^2}\right)-\partial_r\left(\frac{r^3R_v\dot{R}_v}{\rho_v^{10}\sqrt{1+\dot{R}_v^2}}\right)\right]\delta R$$

for δR and

$$\partial_a\left[r^3f\tilde{f}\sqrt{h}R_v^2\sqrt{1+\dot{R}_v^2}\frac{L^2}{\rho_v^2}g^{aa}\partial_a(\delta\phi)\right]=0 \tag{2.74}$$

for $\delta\phi$. Summation over the repeated index a is implied.

We proceed by separation of variables, taking

$$\delta\phi=\mathcal{P}(r)\,\mathcal{Y}^\ell(S^3)\,e^{-i\omega t+iqx}\,,\quad \delta R=\mathcal{R}(r)\,\mathcal{Y}^\ell(S^3)\,e^{-i\omega t+iqx}\,, \tag{2.75}$$

where $\mathcal{Y}^\ell(S^3)$ are spherical harmonics on the S^3,[11] satisfying

$$\nabla^2_{[3]}\mathcal{Y}^\ell=-\ell(\ell+2)\,\mathcal{Y}^\ell \tag{2.76}$$

where $\nabla^2_{[3]}$ is the Laplacian on the unit three-sphere. In (2.75) we've assumed that the $x^1=x$ axis is aligned with the spatial momentum, *i.e.*, $k=(-\omega,q,0,0)$. The equation of motion for the angular fluctuations becomes

$$\partial_r\left[\frac{r^3f\tilde{f}R_v^2}{\sqrt{1+\dot{R}_v^2}}\partial_r\mathcal{P}\right]+r^3fR_v^2\sqrt{1+\dot{R}_v^2}\left[\frac{2}{\rho_v^4}\left(\frac{\tilde{f}^2}{f^2}\tilde{\omega}^2-\tilde{q}^2\right)-\frac{\ell(\ell+2)}{r^2}\tilde{f}\right]\mathcal{P}=0\,, \tag{2.77}$$

while for the radial fluctuations we have:

$$\begin{aligned}\partial_r\left[\frac{r^3f\tilde{f}}{(1+\dot{R}_v^2)^{3/2}}\partial_r\mathcal{R}\right]+\frac{r^3f}{\sqrt{1+\dot{R}_v^2}}\left[\frac{2}{\rho_v^4}\left(\frac{\tilde{f}^2}{f^2}\tilde{\omega}^2-\tilde{q}^2\right)-\frac{\ell(\ell+2)}{r^2}\tilde{f}\right]\mathcal{R}\\ =8\left[\frac{r^3}{\rho_v^{10}}\sqrt{1+\dot{R}_v^2}\left(1-\frac{10R_v^2}{\rho_v^2}\right)-\partial_r\left(\frac{r^3R_v\dot{R}_v}{\rho_v^{10}\sqrt{1+\dot{R}_v^2}}\right)\right]\mathcal{R}.\end{aligned}$$

In these equations, $\tilde{\omega}$ and $\tilde{q}$ are dimensionless and are related to their dimensionful counterparts via

$$\omega^2=\tilde{\omega}^2\frac{u_0^2}{L^4}=\tilde{\omega}^2\pi^2T^2=\tilde{\omega}^2\frac{\pi^2\bar{M}^2}{m^2}\,, \tag{2.78}$$

[11] Of course, the spherical harmonics for a given ℓ are also labeled by two further $SU(2)$ quantum numbers, but we drop these as they are irrelevant in the following.

and analogously for q.

We solve these equations using the shooting method. For each choice of three-momentum $\tilde{q}$, angular momentum ℓ, and embedding $R_v(r)$ (corresponding to one value of quark mass and chiral condensate) we solve these equations numerically, requiring that with $r_{min} \to 0$, $\mathcal{P}(r_{min}) = r_{min}^{\ell}$ and $\partial_r \mathcal{P}(r_{min}) = \ell r_{min}^{\ell-1}$ for the $\delta\phi$ fluctuations and $\mathcal{R}(r_{min}) = r_{min}^{\ell}$ and $\partial_r \mathcal{R}(r_{min}) = \ell r_{min}^{\ell-1}$ for δR. Then, as $\mathcal{P}(r) \sim Ar^{\ell} + Br^{-\ell-2}$ and $\mathcal{R}(r) \sim Cr^{\ell} + Dr^{-\ell-2}$ for some constants A, B, C, D as $r \to \infty$, we tune $\tilde{\omega}^2$ to find solutions which behave as $r^{-\ell-2}$ asymptotically.

At finite temperature, the system is no longer Lorentz invariant and so one must consider the precise definition for the meson masses. We define the 'rest mass' of the mesons as the energy ω with vanishing three-momentum q in the rest-frame of the plasma.[12] Thus, solving the equations of motion (2.77) and (2.78) with $\tilde{q} = 0$ yields the dimensionless constants $\tilde{\omega}^2$, which then give the rest masses through (2.78). Plots of the mass spectrum for these modes are given in figs. 2.7 and 2.8.

We now turn to the vector mesons which correspond to fluctuations of the gauge fields on the D7-branes. The full action for gauge fields on a D7-brane contains the DBI action plus a Wess-Zumino term (see *e.g.,* [45] and references therein),

$$I_{\rm D7} = I_{\rm DBI} - N_{\rm f}\, T_{\rm D7} \frac{(2\pi\ell_{\rm s}^2)^2}{2} \int P[C_{0123}] \wedge F \wedge F \,, \tag{2.79}$$

where the RR 4-form was given in (2.1). To quadratic order in the fluctuations of the gauge fields, the equations of motion are

$$\partial_a \left(\sqrt{-g} F^{ab}\right) - \frac{u_0^4}{L^4}\, \rho_v^3\, f \tilde{f}\, \epsilon^{bij} \nabla_{[3]i} A_j = 0 \tag{2.80}$$

where ϵ^{bij} is an antisymmetric tensor density on the three-sphere, taking values ± 1 while $\nabla_{[3]i}$ is the covariant derivative on the S^3 of unit radius. The indices a, b run over all worldvolume directions of the probe D7-branes and angular coordinate indices are denoted by i, j, k. The first term comes from the Wess-Zumino portion of the action while the second is from the Wess-Zumino term and is only present if b is an S^3 index.

[12] Note that this definition differs from [93,106,113–115] which choose $M^2 = -q^2$ with $\omega = 0$. The latter might better be interpreted as the low-lying masses of a confining theory in 2+1 dimensions, in analogy to, *e.g.,* [59,186,187].

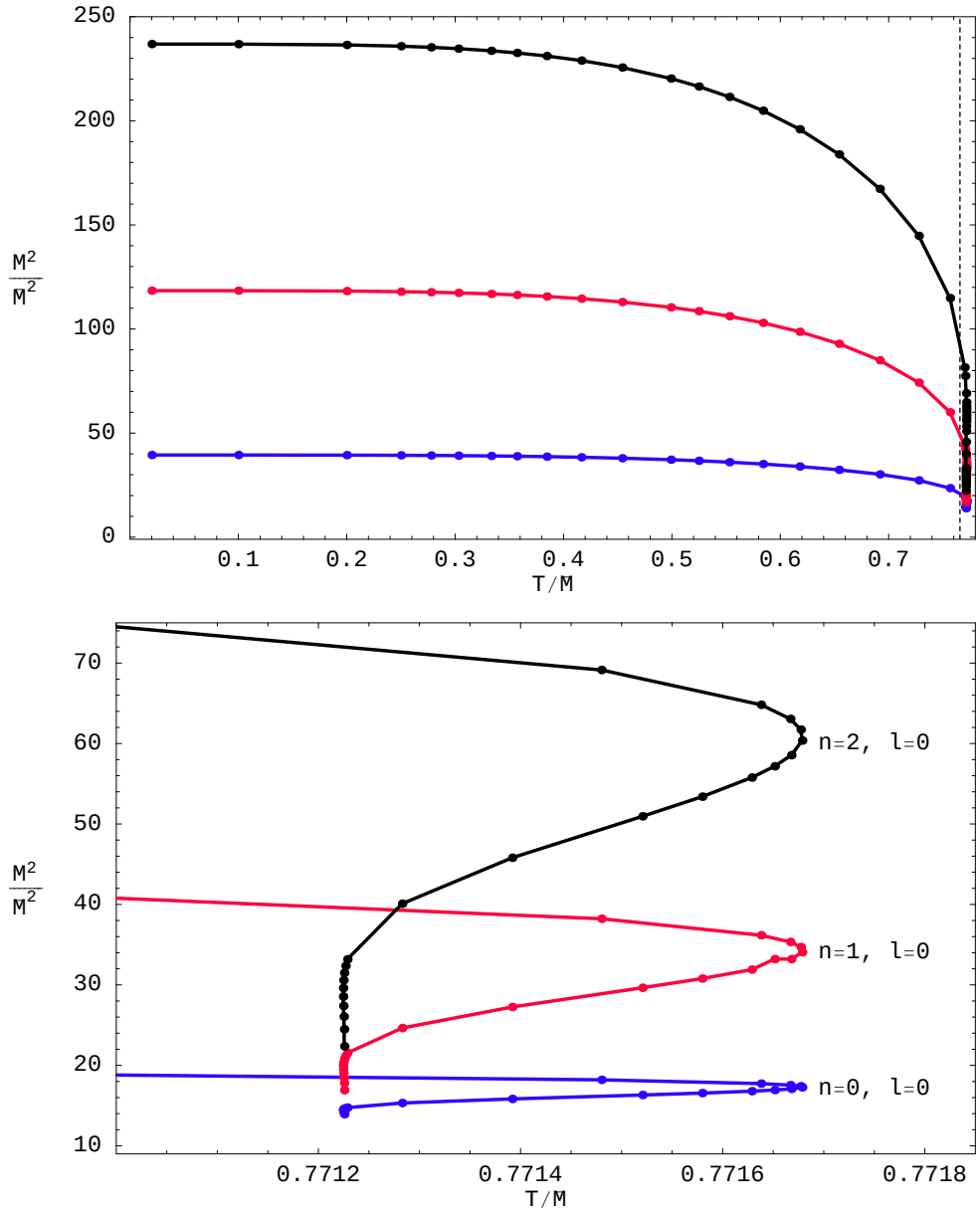

Figure 2.7: Mass spectrum $M^2 = \omega^2|_{q=0}$ for the $\delta\phi$ fluctuations for Minkowski embeddings in the D3/D7 system.

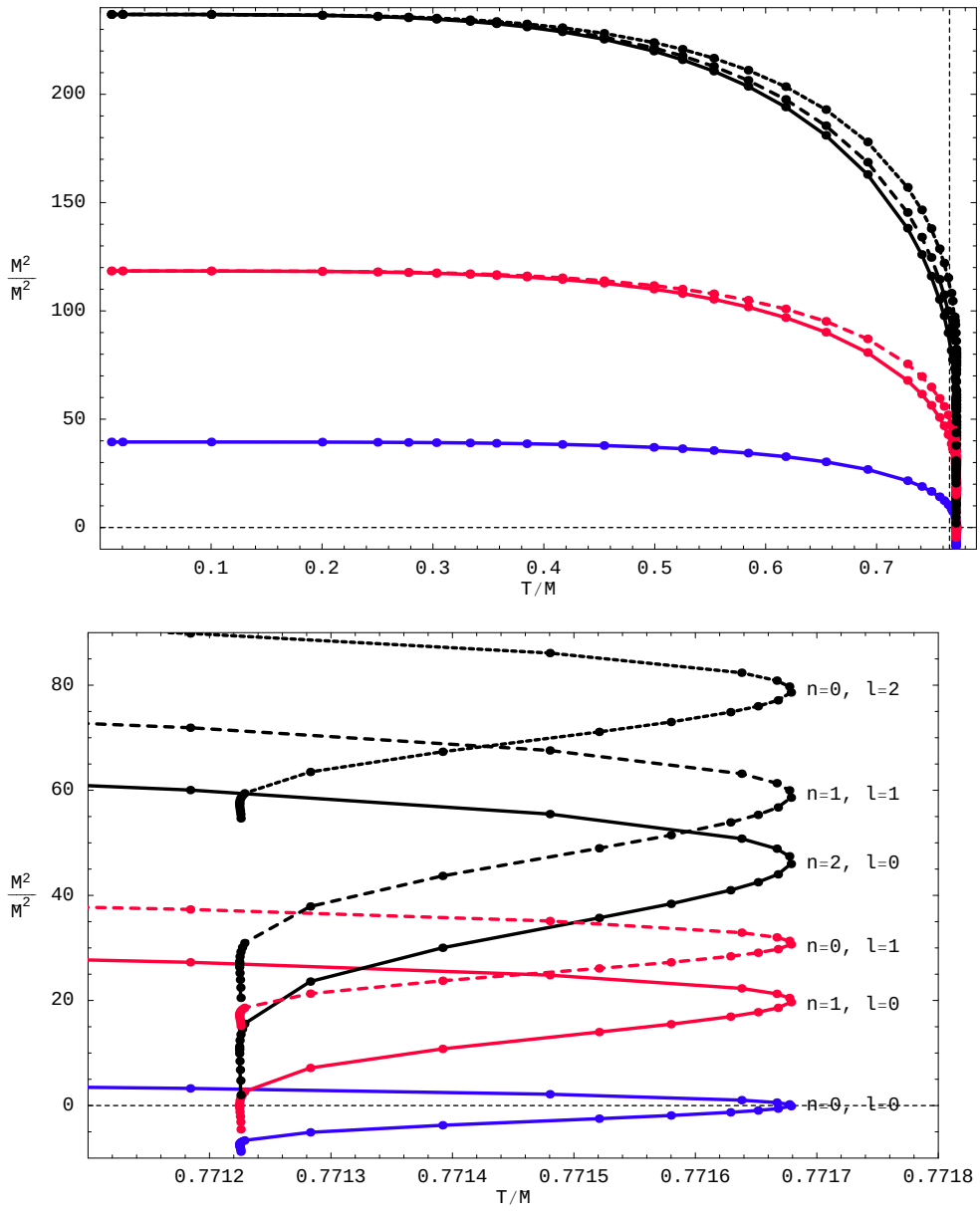

Figure 2.8: Mass spectrum $M^2 = \omega^2|_{q=0}$ for the δR fluctuations for Minkowski embeddings in the D3/D7 system. Note that some of the modes are tachyonic.

Eq. (2.80) can be solved by expanding the gauge fields in terms of Fourier modes and spherical harmonics [101]. As we wish to determine the mass spectrum, we assume that the three-momentum is zero: $q = 0$. In this case, the equations for A_x, A_y, A_z are identical and decouple from all others:

$$\partial_r \left(\sqrt{-g} g^{rr} g^{xx} \partial_r A_x\right) + \partial_i \left(\sqrt{-g} g^{ij} g^{xx} \partial_j A_x\right) - \omega^2 \sqrt{-g} g^{xx} g^{tt} A_x = 0\,. \tag{2.81}$$

Hence, we focus on gauge field modes with $A_{x,y,z}$ nonzero and $A_t = A_r = A_{S^3} = 0$ which correspond to vector mesons in the dual field theory.

Taking

$$A_x = \mathcal{A}(r)\, \mathcal{Y}^\ell(S^3)\, e^{-i\omega t}\,, \tag{2.82}$$

eq. (2.81) becomes

$$\partial_r^2 \mathcal{A} + \frac{\sqrt{1+\dot{R}_v^2}}{r^3 f} \partial_r \left(\frac{r^3 f}{\sqrt{1+\dot{R}_v^2}}\right) \partial_r \mathcal{A} + (1+\dot{R}_v^2) \left[\frac{2\tilde{\omega}^2 \tilde{f}}{\rho_v^4 f^2} - \frac{\ell(\ell+2)}{r^2}\right] \mathcal{A} = 0\,. \tag{2.83}$$

We solve this equation using the shooting method, as described above for the scalar modes, imposing $\mathcal{A}(r_{\rm min}) = r_{\rm min}^\ell$ and $\partial_r \mathcal{A}(r_{\rm min}) = \ell\, r_{\rm min}^{\ell-1}$ as $r_{\rm min} \to 0$ and tuning $\tilde{\omega}^2$ to find solutions behaving as $r^{-\ell-2}$ asymptotically. Plots of the vector meson spectrum for $\ell = 0$ are given in fig. 2.9.

Note that in the zero-temperature limit, the scalar δR, pseudoscalar $\delta\phi$, and vector spectra coincide with those previously calculated for the supersymmetric D3 background [61, 101, 102, 154]. In particular, using (2.48), the lightest meson in all three spectra has a mass squared matching $M_{\rm gap}^2 = 4\pi^2 \bar{M}^2 \simeq 39.5\, \bar{M}^2$. The degeneracy between the three different modes arises because supersymmetry is restored at $T = 0$ and all three types of fluctuations are part of the same supermultiplet [61, 101, 102, 154]. At finite T, this degeneracy between δR, $\delta\phi$, and vector modes is broken. For example, at the phase transition, the mass of the lightest meson is roughly 25% and 50% of its zero-temperature value in the δR and $\delta\phi$ spectra, respectively. The supersymmetric spectrum also showed an unexpected degeneracy in that it only depended on the combination $n + \ell$, where n and ℓ are the radial and angular quantum numbers characterising the individual excitations [61]. Fig. 2.8 illustrates that this degeneracy is broken at finite temperature, where the masses are shown for all the modes with $n + \ell = 1$ and 2. However, this breaking is not large except near the phase transition.

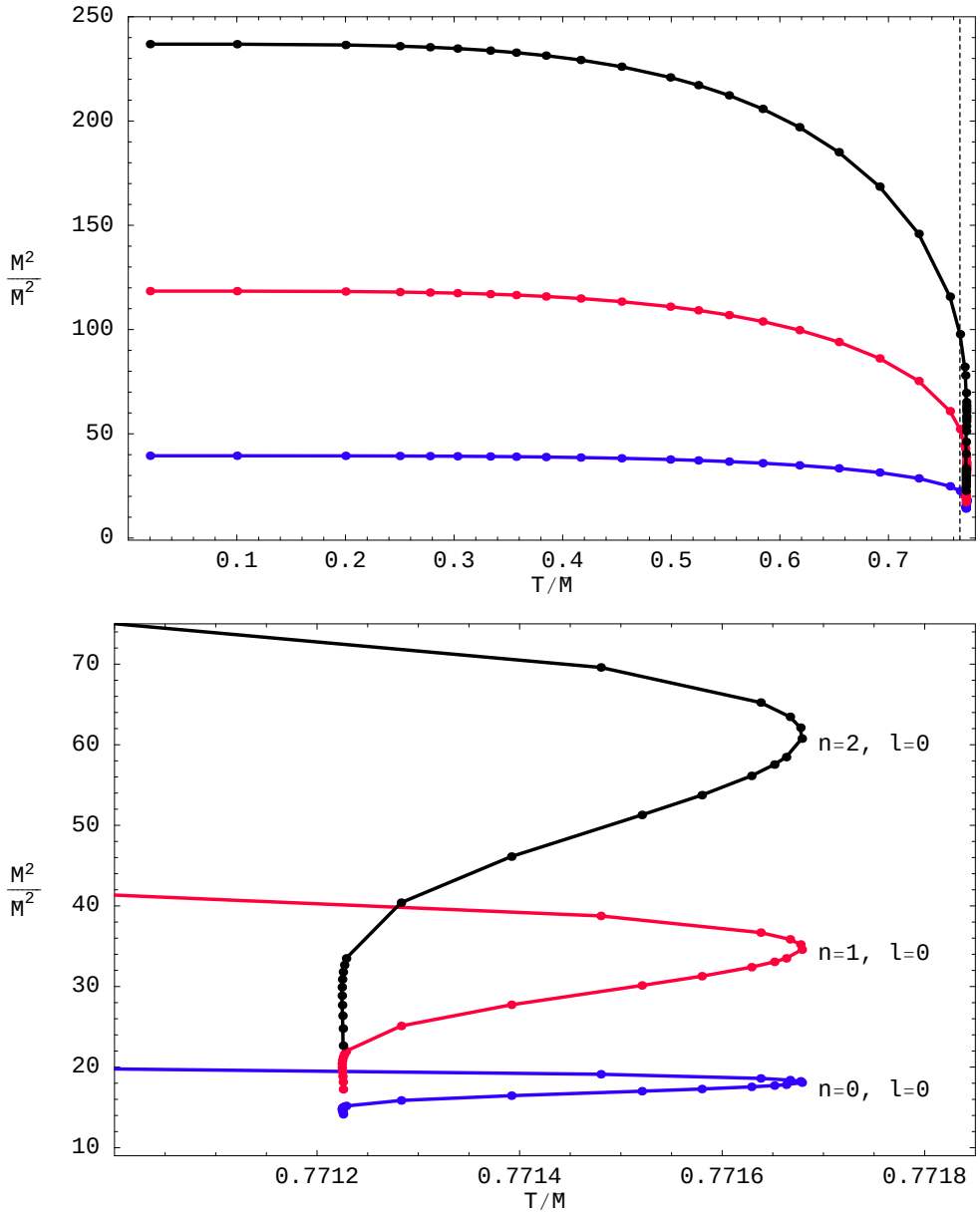

Figure 2.9: Mass spectrum $M^2 = \omega^2|_{q=0}$ for the vector field on Minkowski embeddings in the D3/D7 system.

All three figures show that in general the meson masses decrease as the temperature increases. As noted above, the thermal shift of the meson rest mass may be of the order of 25 to 50 percent at the phase transition. This reduction must reflect in part the decrease in the constituent quark mass, discussed in section 2.6.4. However, the lowering of the meson masses is actually small relative to that seen for the constituent quark mass. As seen in figure 2.17, at the phase transition, the latter has fallen to only 2% of its $T = 0$ value. However, the thermal shift of the mesons becomes even more dramatic near the critical solution. In particular, embeddings with $R_0 \in (1, 1.07)$ possess tachyonic δR fluctuations. Note that $R_0 = 1$ corresponds to the critical solutions and the phase transition occurs at $R_0 \simeq 1.15$, *i.e.,* this is the minimum value of R_0 for which the thermodynamically preferred embedding is of Minkowski type. As discussed above, the embeddings are not unique in the vicinity of the critical solution and so physical quantities spiral in on their critical values. As observed at the end of section 2.3.2, the spiralling of the energy density leads to a negative specific heat and indicates an instability. It is satisfying to note in the second plot of fig. 2.8 that the lowest-lying δR-mode becomes tachyonic at precisely the point where the first turn-around in the spiral occurs (with T). Hence a dynamical instability is appearing in the Minkowski embeddings, in precise agreement with the thermodynamic considerations. In fact the second lowest-lying δR-mode becomes tachyonic at the second turn-around and it seems to suggest that at the i'th turn of the spiral, the δR-mode with $n = i - 1, \ell = 0$ becomes tachyonic. We found no other evidence of instabilities in other modes. In particular, neither the vector nor pseudoscalar $\delta\phi$ modes, which have very similar spectra, exhibit an instability. It is not surprising that a dynamical instability manifests itself in the δR-modes, since in the region near the critical solution, the nonuniqueness that brings about the phase transition arises precisely because the branes have slightly different radial profiles $R(r)$.

While a dynamical instability set in for the Minkowski embeddings, in agreement with the thermodynamic analysis, it is interesting that this point is away from the phase transition. In particular, the Minkowski embeddings with $R_0 \in [1.07, 1.15]$, namely those between the point at which the phase transition takes place and the first turn-around, do not exhibit any tachyonic modes. Thus these embeddings are presumably meta-stable and might be reached through supercooling.

We have also made some preliminary investigations of the low-lying scalar mesons moving through the thermal plasma and numerical results are shown in figure 2.10. For

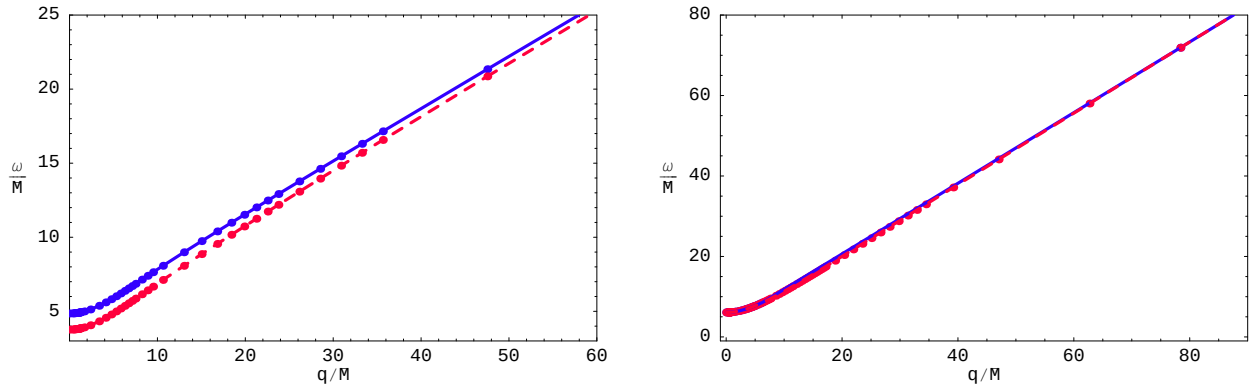

(a) (b)

Figure 2.10: Dispersion relation $\omega(q)$ for Minkowski D7-brane embeddings with (a) $R_0 = 1.20$ ($m = 1.32$) and (b) $R_0 = 2.00$ ($m = 2.00$) in a D3-brane background. The solid blue line corresponds to $\delta\phi$ fluctuations, whereas the red dashed line corresponds to δR fluctuations.

non-relativistic motion (small three-momenta), we expect that the dispersion relation takes the form

$$\omega(q) \simeq M_0 + \frac{q^2}{2M_{kin}}\,, \tag{2.84}$$

where $M_0 = M_0(T)$ is the rest mass calculated above and $M_{kin} = M_{\rm kin}(T)$ is the effective kinetic mass for a moving meson. Although $M_{\rm kin}(T)$ is not the same as $M_0(T)$, for low temperatures the difference between the two quantities is expected to be small. For example, fitting the small-$\tilde{q}$ results for $\tilde{\omega}$ for the lowest δR-mode at $T/\bar{M} = 0.5$ (or $R_0 = 2$) yields

$$\frac{\omega}{\bar{M}} = 6.084 + 0.076\frac{q^2}{\bar{M}^2} + \cdots\,. \tag{2.85}$$

Hence in this case, we find $M_0/\bar{M} \simeq 6.084$ and $M_{\rm kin}/\bar{M} \simeq 6.579$. Recall that at $T = 0$, we would have $M_0 = M_{\rm kin} = M_{\rm gap} = 2\pi\bar{M} \simeq 6.283\bar{M}$ and so both masses have shifted by less than 5%. Note that while the rest mass has decreased, the kinetic mass has increased. The latter is perhaps counter-intuitive as it indicates it is actually easier to set the meson in motion through the plasma than in vacuum. From a gravity perspective, it is perhaps less surprising as the Minkowski branes are bending towards the black hole horizon and so these fluctuations experience a greater redshift than in the pure $AdS_5 \times S^5$ background.

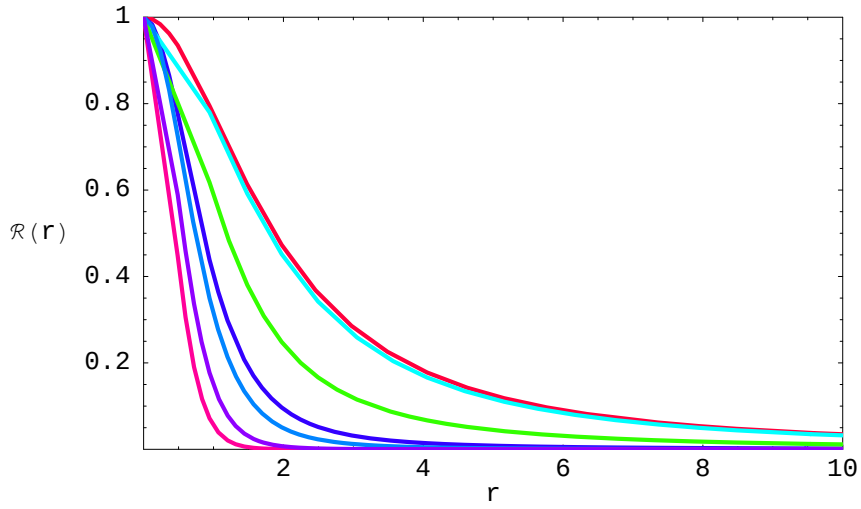

Figure 2.11: The radial profile for δR with $R_0 = 2$ with various spatial momentum. From top to bottom, the profiles correspond to: $k = 0$, 4.96, 18.81, 31.4, 39.2, 62.7, 94.1.

Examining the regime of large three-momenta, we find that ω grows linearly with k. Naively, one might expect that the constant of proportionality should be one, *i.e.,* the speed of light. However, one finds that

$$\frac{\omega}{\bar{M}} = v_m \frac{q}{\bar{M}} + \frac{M_1}{\bar{M}} + O\left(\frac{\bar{M}}{q}\right) , \tag{2.86}$$

with $v_m < 1$, as illustrated in fig. 2.10. There our numerical results show that for $R_0 = 1.2$ ($m = 1.32$), $v_m \simeq 0.353$ and $M_1/\bar{M} \simeq 4.14$ for δR and $v_m \simeq 0.350$ and $M_1/\bar{M} \simeq 4.71$ for $\delta\phi$, while for $R_0 = 2$ ($m = 2$) $v_m \simeq 0.884$ and $M_1/\bar{M} \simeq 2.61$ for either type of fluctuation. Note that in fig. 2.10b the dispersion relations $\omega(k)$ for δR and $\delta\phi$ are nearly coincident for all k because supersymmetry is being restored at low temperatures. Our results show that the strongly coupled plasma has a significant effect on reducing the maximum velocity of the mesons. This effect is easily understood from the perspective of the dual gravity description. The mesonic states have a radial profile which is peaked near R_0, the minimum radius of the Minkowski embedding, as illustrated in fig. 2.11, and so we can roughly think of them as excitations propagating along the bottom of the D7-brane. At large k, the

speed of these signals will be set by the local speed of light

$$c = \sqrt{-\frac{g_{tt}}{g_{zz}}}\bigg|_{r=R_0} = \frac{f(R_0)}{\tilde{f}(R_0)}\,. \tag{2.87}$$

The latter gives $c \simeq 0.349$ for $R_0 = 1.2$ and $c \simeq 0.882$ for $R_0 = 2$, both of which closely match our results for v_m given above. It is interesting that at finite temperature as k increases, the radial profiles of the mesonic states seem to become more peaked towards R_0, as illustrated in fig. 2.11. Recall that at $T = 0$, these profiles are invariant under boosts in the gauge theory directions. Finally we note that we did not discover any simple relation between M_1 in eq. (2.86) and M_0 and M_{kin} in eq. (2.84).

Note that with the approximations made here, our analysis reveals no dragging forces on these low-lying mesons from the thermal bath. We expect that these would only appear through string-loop effects, which in particular would include the Hawking radiation of the background black hole. This would parallel the similar findings for the drag force experienced by large-J mesons composed of heavy quarks [188–194] and by heavy quarks themselves [133–136, 195–197]. These large-J mesons also exhibited a maximum velocity similar to the effect discussed above [188–194].

2.4 The D4/D6 system

We now turn to the D4/D6 system, described by the array

	0	1	2	3	4	5	6	7	8	9
$D4$	×	×	×	×	×					
$D6$	×	×	×	×		×	×	×		

(2.88)

In the decoupling limit, the resulting gauge theory is five-dimensional super-Yang-Mills coupled to fundamental hypermultiplets confined to a four-dimensional defect.[13] In order to obtain a four-dimensional gauge theory at low energies, one may compactify x^4, the D4-brane direction orthogonal to the defect, on a circle. If periodic boundary conditions for the adjoint fermions are imposed, then supersymmetry is preserved and the four-dimensional

[13]Technically, the theory is intrinsically five-dimensional and hence the perturbative theory is non-renormalisable. Note however that the present study is in the strong coupling regime of the gauge theory where the dual gravity description is appropriate – see section 2.1.1.

theory thus obtained is non-confining. In this case the appropriate dual gravitational background at any temperature is (2.1) with x^4 periodically identified. Instead, if antiperiodic boundary conditions for the adjoint fermions are imposed, then supersymmetry is broken and the four-dimensional theory exhibits confinement [59] and spontaneous chiral symmetry breaking [62]. The holographic description at zero-temperature consists then of D6-brane probes in a horizon-free background, whose precise form is not needed here. At a temperature $T_{\rm deconf}$ set by the radius of compactification, the theory undergoes a first order phase transition at which the gluons and the adjoint matter become deconfined. In the dual description the low-temperature background is replaced by (2.1). If $T_{\rm deconf} < T_{\rm fun}$, the D6-branes remain outside the horizon in a Minkowski embedding, and quark-antiquark bound states survive [62]. As T is further increased up to $T_{\rm fun}$ a first order phase transition for the fundamental matter occurs.

Below we study the thermodynamic and dynamical properties of the D6-branes in the black D4 background appearing above the deconfinement phase transition. Along the way we will have to introduce boundary terms to regulate the D6-brane brane action.

2.4.1 D6-brane embeddings

As in section 2.2.3, we begin by transforming to the coordinate system with radial coordinate ρ defined in (2.24), which is better adapted to study the brane embeddings in the background. For $p = 4$, the radial coordinate is then

$$(u_0\rho)^{3/2} = u^{3/2} + \sqrt{u^3 - u_0^3}\,, \tag{2.89}$$

and the black D4-brane metric is

$$ds^2 = \frac{1}{2}\left(\frac{u_0\rho}{L}\right)^{3/2}\left[-\frac{f^2}{\tilde{f}}dt^2 + \tilde{f}dx_4^2\right] + \left(\frac{L}{u_0\rho}\right)^{3/2}\frac{u_0^2\tilde{f}^{1/3}}{2^{1/3}}\left[d\rho^2 + \rho^2 d\Omega_4^2\right]\,, \tag{2.90}$$

where we now have $f(\rho) = 1 - 1/\rho^3$ and $\tilde{f}(\rho) = 1 + 1/\rho^3$. From eq. (2.6), the temperature is given by

$$T = \frac{3}{4\pi}\left(\frac{u_0}{L^3}\right)^{1/2}\,. \tag{2.91}$$

We also have the holographic relations for the dual five-dimensional gauge theory

$$L^3 = \pi g_{\rm s} N_{\rm c} \ell_{\rm s}^3\,, \qquad g_{\rm YM}^2 = 4\pi^2 g_{\rm s}\ell_{\rm s}\,, \tag{2.92}$$

where we remind the reader that the Yang-Mills coupling $g_{\rm YM}$ is now dimensionful.

The D4/D6 intersection is described by the array (2.88). In analogy to the D3/D7 case, we introduce spherical coordinates $\{r, \Omega_2\}$ in the 567-directions, and polar coordinates $\{R, \phi\}$ on the 89-plane. Computing boundary terms is also facilitated by introducing an angular coordinate between the r and R directions so that we have, as before,

$$\rho^2 = r^2 + R^2\,, \quad r = \rho\sin\theta\,, \quad R = \rho\cos\theta\,, \tag{2.93}$$

and

$$\begin{aligned} d\rho^2 + \rho^2 d\Omega_4^2 &= d\rho^2 + \rho^2(d\theta^2 + \sin^2\theta\, d\Omega_2^2 + \cos^2\theta\, d\phi^2) &(2.94)\\ &= dr^2 + r^2 d\Omega_2^2 + dR^2 + R^2 d\phi^2\,. &(2.95)\end{aligned}$$

Following our analysis for the D3/D7 system, we choose coordinates on the brane such that asymptotically the metric naturally splits into a product of the form D4-throat$\times S^2$. We describe the embedding of the D6-brane in terms of $\chi(\rho) = \cos\theta(\rho)$ – note then that $\chi = R/\rho$. Later, we will have to regulate the Euclidean D6-brane by adding local counter-terms written in terms of this 'field.' The induced metric on the D6-brane is then

$$\begin{aligned} ds^2 = \frac{1}{2}\left(\frac{u_0\rho}{L}\right)^{3/2}&\left[-\frac{f^2}{\tilde f}dt^2 + \tilde f dx_3^2\right]\\ &+\left(\frac{L}{u_0\rho}\right)^{3/2}\frac{u_0^2\tilde f^{1/3}}{2^{1/3}}\left[\left(1+\frac{\rho^2\dot\chi^2}{1-\chi^2}\right)d\rho^2 + \rho^2(1-\chi^2)d\Omega_2^2\right]\,, \end{aligned}\tag{2.96}$$

where, as usual, $\dot\chi = d\chi/d\rho$. The D6-brane action takes the form

$$\frac{I_{\rm bulk}}{\mathcal{N}} = \int d\rho\,\rho^2\left(1-\frac{1}{\rho^6}\right)\sqrt{(1-\chi^2)(1-\chi^2+\rho^2\dot\chi^2)}\,, \tag{2.97}$$

where $\mathcal{N}$ is given by (2.26) with $n = 2$:

$$\mathcal{N} = \frac{\pi}{T}N_{\rm f}T_{\rm D6}u_0^3 = \frac{2^2}{3^6}\,N_{\rm f}\,N_{\rm c}\,g_{\rm eff}(T)^4\,T^3\,, \tag{2.98}$$

where $g_{\rm eff}(T)^2 = g_{\rm YM}^2 N_{\rm c} T$. The resulting equation of motion is

$$\begin{aligned} \partial_\rho&\left[\rho^4\left(1-\frac{1}{\rho^6}\right)\frac{\sqrt{1-\chi^2}\dot\chi}{\sqrt{1-\chi^2+\rho^2\dot\chi^2}}\right]\\ &+\rho^2\left(1-\frac{1}{\rho^6}\right)\chi\left[\sqrt{\frac{1-\chi^2+\rho^2\dot\chi^2}{1-\chi^2}}+\sqrt{\frac{1-\chi^2}{1-\chi^2+\rho^2\dot\chi^2}}\right] = 0\,, \end{aligned}\tag{2.99}$$

and χ asymptotically approaches zero as

$$\chi = \frac{m}{\rho} + \frac{c}{\rho^2} + \cdots , \tag{2.100}$$

with m and c related to the quark mass and condensate via eqs. (2.29) and (2.30) with $p = 4, n = 2$:

$$M_{\rm q} = \frac{u_0 m}{2^{5/3}\pi\ell_s^2} = \frac{2^{1/3}}{3^2}\, g_{\rm eff}(T)^2\, T\, m\,, \tag{2.101}$$

$$\langle \mathcal{O}_m \rangle = -2^{5/3}\pi^2\ell_s^2 N_{\rm f} T_{\rm D6} u_0^2 c = -\frac{2^{5/3}}{3^4}\, N_{\rm f}\, N_{\rm c}\, g_{\rm eff}(T)^2 T^3 c\,. \tag{2.102}$$

In this case, we may write $m = \bar{M}^2/T^2$ with

$$\bar{M}^2 = \frac{9}{2^{1/3}} \left(\frac{M_{\rm q}}{g_{\rm eff}(M_{\rm q})}\right)^2 \simeq 7.143 \left(\frac{M_{\rm q}}{g_{\rm eff}(M_{\rm q})}\right)^2 . \tag{2.103}$$

The scale $\bar{M}$ is again related to the mass gap in the meson spectrum of the D4/D6 system at zero temperature. For either background, the latter must be determined numerically. In the case of the supersymmetric background, one finds [101, 102, 154]:

$$m_{\rm gap}^2 = 8\pi^2\,(1.67) \left(\frac{M_{\rm q}}{g_{\rm eff}(M_{\rm q})}\right)^2 \simeq 131.9 \left(\frac{M_{\rm q}}{g_{\rm eff}(M_{\rm q})}\right)^2 \longrightarrow \frac{\bar{M}}{m_{\rm gap}} \simeq 0.233\,. \tag{2.104}$$

One finds essentially the same result for the confining D4 background [62]. The similarity of these results is probably a reflection of the underlying supersymmetric structure of the five-dimensional gauge theory. In the confining theory, the lowest-lying meson is a pseudo-Goldstone boson, whose mass is determined by the Gell-Mann–Oakes–Renner relation, and the latter linear form extrapolates directly to the supersymmetric result at large $M_{\rm q}$ [62].

The equation of motion (2.99) can of course be recast in terms of the R, r coordinates as

$$\partial_r \left[r^2 \left(1 - \frac{1}{\rho^6}\right) \frac{\partial_r R}{\sqrt{1 + (\partial_r R)^2}} \right] = 6\, \frac{r^2}{\rho^8}\, R \sqrt{1 + (\partial_r R)^2}\,, \tag{2.105}$$

which is again suitable to study the Minkowski embeddings.

For arbitrary m we solved for the D6-brane embeddings numerically. Black hole embeddings are most simply described in the χ, ρ coordinates and we used boundary conditions at the horizon: $\chi(\rho = 1) = \chi_0$ and $\dot{\chi}|_{\rho=1} = 0$ for various $0 \leq \chi_0 < 1$. For Minkowski

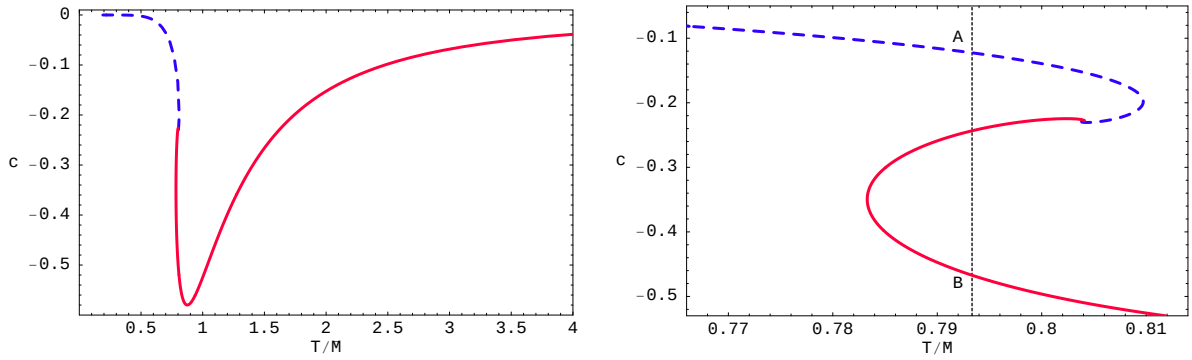

Figure 2.12: Quark condensate c versus temperature $T/\bar{M}$ for a D6-brane in a D4-brane background. The dotted vertical line indicates the precise temperature of the phase transition.

embeddings, we used the R, r coordinates and the boundary conditions at the axis were: $R(r=0) = R_0$ and $\partial_r R|_{r=0} = 0$ for $R_0 > 1$. We computed m and c by fitting the numerical solutions to the asymptotic forms of χ and R given above. In particular, we produced plots of c versus $T/\bar{M}$, as shown in figure 2.12. Again by increasing the resolution, we are able to follow the two families of embeddings spiralling in on the critical solution. However, thermodynamic considerations indicate that a phase transition occurs at the point indicated in the second plot.

2.4.2 D6-brane thermodynamics

As with the D3/D7 system, we wish to compute the contribution of the fundamental matter to the free energy, entropy and energy densities. That is, we will calculate the contributions of the D6-brane to the Euclidean path integral. This requires that we regularise and renormalise the D6-brane action. We will do this by constructing the appropriate counterterms.

Using the asymptotic behaviour (2.100) in (2.97) we find that the D6 action contains a UV divergence, since

$$\frac{I_{\rm bulk}}{\mathcal{N}} \simeq \int_{\rm max}^{\rho} d\rho\, \rho^2 \simeq \frac{\rho_{\rm max}}{3} \tag{2.106}$$

diverges for $\rho_{\rm max} \to \infty$. We expect the counter-terms that must be supplemented to have

the form $\int dt_{\rm E} d^3x \sqrt{\det\gamma}\,(a + b\chi^2 + c\chi^4)$. In the present case, we might expect to pick additional factors of e^{χ} and e^{Φ}. In any event, we would choose the constants to eliminate the divergence. Further for a supersymmetric embedding, we should be able to construct the counter-term action so that the total brane action vanishes.

We take as our ansatz for the counter-terms:

$$I_{\rm bound} = 4\pi L^3 T_{\rm D6} \int dt_{\rm E} d^3x \sqrt{\det\gamma}\, e^{2\sigma + B\Phi} F(\chi)\Big|_{\rho=\rho_{\rm max}}\,, \tag{2.107}$$

where B and $F(\chi)$ are a dimensionless constant and functional of χ, both to be determined. We have also defined $e^{2\sigma} \equiv g_{\theta\theta}$; this factor naturally appears in the measure as it is proportional to the asymptotic volume of the internal S^2. Now the boundary metric γ_{ij} at $\rho = \rho_{\rm max}$ in the effective five-dimensional (brane) geometry is given by

$$ds^2(\gamma) = \frac{1}{2}\left(\frac{u_0\rho_{\rm max}}{L}\right)^{3/2}\left(\frac{f^2(\rho_{\rm max})}{\tilde f(\rho_{\rm max})}\,dt_{\rm E}^2 + \tilde f(\rho_{\rm max}) dx_3^2\right) \tag{2.108}$$

and so $\sqrt{\det\gamma} = \frac{1}{4}\left(\frac{u_0\rho_{\rm max}}{L}\right)^3 f(\rho_{\rm max})\tilde f(\rho_{\rm max})$. In this coordinate system we have

$$e^{2\Phi} = \frac{1}{2}\left(\frac{u_0\rho}{L}\right)^{3/2}\tilde f = e^{6\sigma}\,. \tag{2.109}$$

Now evaluating the counterterm ansatz (2.107) with the supersymmetric background ($u_0 = 0$) with the profile[14] $\chi = m u_0/\varrho$, one finds that the leading divergences cancel if $B = -2/3$ and $F(0) = -1/3$. One also finds that a complete cancellation occurs if we choose

$$F(\chi) = -\frac{1}{3}(1-\chi^2)^{3/2}\,. \tag{2.110}$$

Thus, the complete counter-term action can be chosen as either of the following:

$$I_{\rm bound} = -\frac{4\pi}{3} L^3 T_{\rm D6} \int dt_{\rm E} d^3x \sqrt{\det\gamma}\, e^{2\sigma - 2\Phi/3}(1-\chi^2)^{3/2}\Big|_{\rho=\rho_{\rm max}}\,, \tag{2.111}$$

$$I'_{\rm bound} = -\frac{4\pi}{3} L^3 T_{\rm D6} \int dt_{\rm E} d^3x \sqrt{\det\gamma}\, e^{2\sigma - 2\Phi/3}\left(1 - \frac{3}{2}\chi^2\right)\Big|_{\rho=\rho_{\rm max}}\,. \tag{2.112}$$

In the second expression, we have kept only the terms which contribute to the divergence in the small χ expansion – the next term of $\mathcal{O}(\chi^4)$ vanishes as $\rho_{\rm max} \to \infty$. Computationally, this seems like the easier action with which to work; note however that the first form has

[14] See the discussion below (2.54).

the nice property that, even with finite $\rho_{\rm max}$, it produces a precise cancellation for the supersymmetric configuration, *i.e.,* $I_{\rm D6} = I_{\rm bulk} + I_{\rm bound} = 0$.

Proceeding with $I'_{\rm bound}$ and using (2.100), the boundary term evaluates to

$$I'_{\rm bound} = -\frac{4\pi T_{\rm D6}}{3T}\left(\rho_{\rm max}^3 - \frac{3}{2}m^2\rho_{\rm max} - 3mc\right) , \tag{2.113}$$

where we have divided out the spatial volume V_x – see footnote 5. The total action may then be written as:

$$\frac{I_{\rm D6}}{\mathcal{N}} = G(m) - \frac{1}{3}\left({\rho_{\rm min}}^3 - \frac{3}{2}m^2\rho_{\rm min} - 3mc\right) , \tag{2.114}$$

where the integral is defined as

$$G(m) = \int_{\rho_{\rm min}}^{\infty} d\rho \left[\rho^2\left(1 - \frac{1}{\rho^6}\right)\sqrt{(1-\chi^2)(1-\chi^2+\rho^2\dot{\chi}^2)} - \rho^2 + \frac{m^2}{2}\right] . \tag{2.115}$$

Of course, the free energy follows from this as $F = TI_{\rm D6}$ and then one can compute the entropy $S = -\partial F/\partial T$ and the energy $E = F + TS$. For the computation of the entropy, one must split the free energy into bulk and boundary terms and evaluate the action of the derivative on each of the terms, just as was done for the D3/D7 case. We do not present all the details of the calculation here but simply give the final result:

$$\frac{S}{\mathcal{N}} = -6\,G(m) + 2\left({\rho_{\rm min}}^3 - \frac{3}{2}m^2\rho_{\rm min} - 4mc\right) , \tag{2.116}$$

where the integral G was defined in (2.115). The contribution of the D6-brane to the energy then follows as

$$\frac{E}{\mathcal{N}T} = -5\,G(m) + \frac{5}{3}\left({\rho_{\rm min}}^3 - \frac{3}{2}m^2\rho_{\rm min} - \frac{21}{5}mc\right) . \tag{2.117}$$

Using our numerical results, these thermodynamic quantities are plotted in fig. 2.13. Again the free energy density shows the classic 'swallow tail' form and, to our best numerical accuracy, a first order phase transition takes place at $T_{\rm fun}/\bar{M} = 0.7933$ (or $m = 1.589$), where the free energy curves for the Minkowski and black hole phases cross. The fact that the transition is first order is illustrated by the entropy and energy densities, which make a finite jump at this temperature between the points labelled A and B.

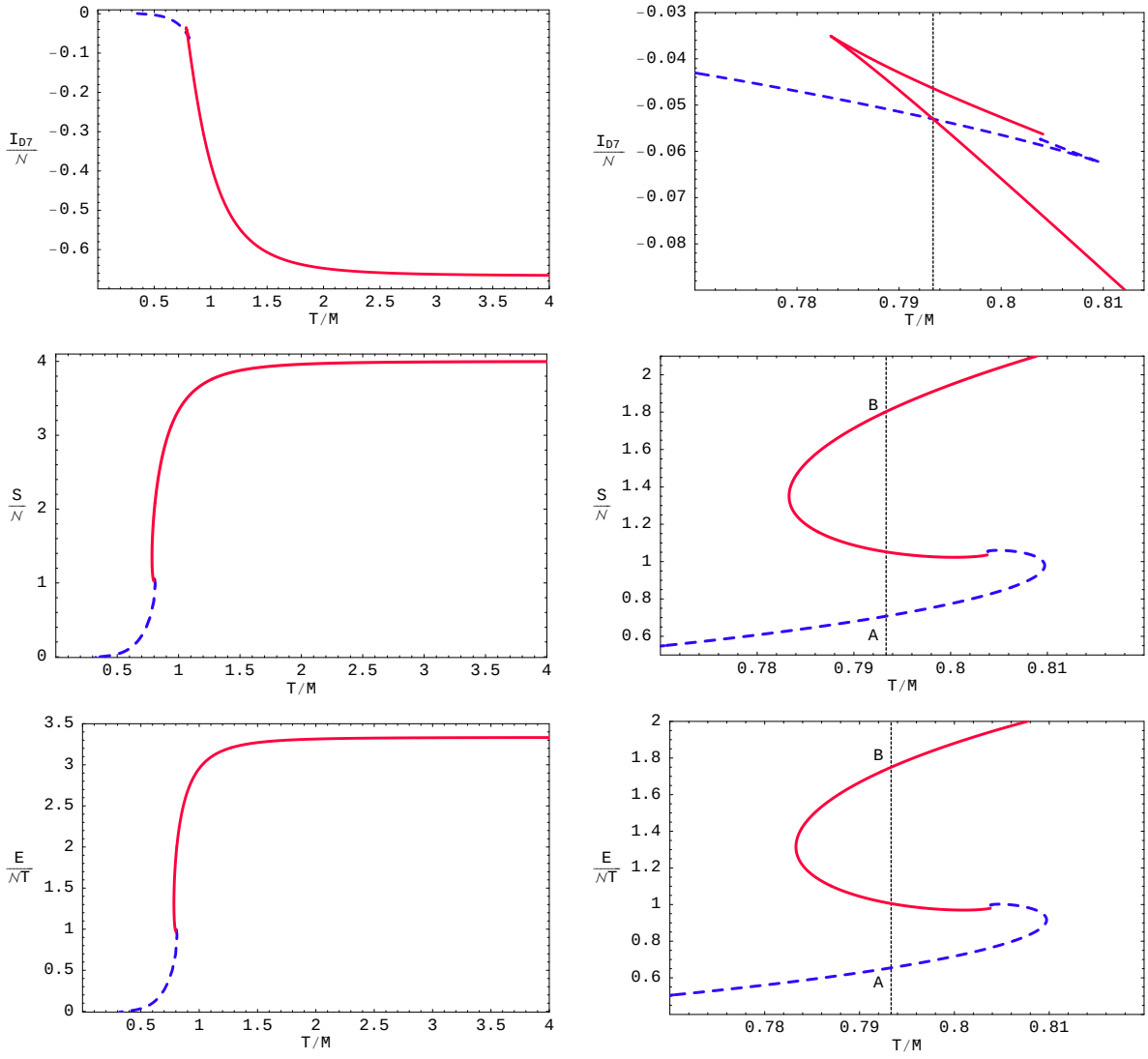

Figure 2.13: Free-energy, entropy and energy densities for a D6-brane in a D4-brane background. The blue dashed (red continuous) curves correspond to the Minkowski (black hole) embeddings. The dotted vertical line indicates the precise temperature of the phase transition.

2.4.3 Meson spectrum for Minkowski embeddings

The meson spectrum corresponding to fluctuations of the D6-brane in the black D4-brane geometry is computed in the same way as for D3/D7. We focus here on Minkowski embeddings for which the spectrum is discrete and stable and consider only scalar mesons here. The excitations of the black hole embeddings will be described by a spectrum of quasinormal modes, as discussed elsewhere [126, 155].

We consider small fluctuations $\delta R, \delta\phi$ about the fiducial embedding, which we now denote by R_v, so that the D6-brane embedding is specified by $R = R_v(r) + \delta R(x^a)$ and $\phi = 0 + \delta\phi(x^a)$, where $R_v(r)$ satisfies (2.105). The pull-back of the bulk metric (2.90) is then

$$P[G]_{ab} = g_{ab} + \left(\frac{L}{u_0\rho}\right)^{3/2} \frac{u_0^2\tilde{f}^{1/3}}{2^{1/3}} \left[\dot{R}_v\left[(\partial_a\delta R)\delta^r_b + (\partial_b\delta R)\delta^r_a\right] + (\partial_a\delta R)\partial_b\delta R + R^2(\partial_a\delta\phi)\partial_b\delta\phi\right], \tag{2.118}$$

where the metric g is given by

$$ds^2(g) = \frac{1}{2}\left(\frac{u_0\rho}{L}\right)^{\frac{3}{2}}\left[-\frac{f^2}{\tilde{f}}dt^2 + \tilde{f}dx_3^2\right] + \left(\frac{L}{u_0\rho}\right)^{\frac{3}{2}}\frac{u_0^2\tilde{f}^{\frac{1}{3}}}{2^{\frac{1}{3}}}\left[(1+\dot{R}_v^2)dr^2 + r^2 d\Omega_2^2\right] \tag{2.119}$$

and, as usual, $\rho^2 = r^2 + R^2$. The DBI action yields the D6-brane Lagrangian density to quadratic order in the fluctuations $\delta R, \delta\phi$:

$$\begin{aligned}\mathcal{L} &= \mathcal{L}_0 - T_{\text{D6}}\frac{u_0^3}{4}r^2\sqrt{h}\sqrt{1+\dot{R}_v^2}\left\{f\tilde{f}\left(\frac{L}{u_0\rho_v}\right)^{3/2}\frac{u_0^2\tilde{f}^{1/3}}{2^{4/3}}\sum_a g_v^{aa}\left[\frac{(\partial_a\delta R)^2}{1+\dot{R}_v^2} + R^2(\partial_a\delta\phi)^2\right]\right. \\ &\quad \left. + \frac{3R_v\dot{R}_v\partial_r(\delta R)^2}{\rho_v^8(1+\dot{R}_v^2)} + \frac{3(\delta R)^2}{\rho_v^8} - \frac{24R_v^2(\delta R)^2}{\rho_v^{10}}\right\},\end{aligned} \tag{2.120}$$

where h is the determinant of the metric on the S^2 of unit radius, $\rho_v^2 = r^2 + R_v^2$, and $\mathcal{L}_0$ is the Lagrangian density for the vacuum embedding:

$$\mathcal{L}_0 = -T_{\text{D6}}\frac{u_0^3}{4}r^2\sqrt{h}\sqrt{1+\dot{R}_v^2}\left(1 - \frac{1}{\rho_v^6}\right). \tag{2.121}$$

Note that terms linear in δR were eliminated from the Lagrangian density $\mathcal{L}$ by integration by parts and by using the equation of motion (2.105) for R_v. Since we are retaining terms only to quadratic order in the fluctuations, the metric g_v in (2.120) is (2.119) with $R = R_v$ and the functions f and $\tilde{f}$ in (2.120) and subsequent expressions are evaluated at ρ_v.

The linearised equations of motion for the fluctuations are then

$$\partial_a \left[f\tilde{f} \left(\frac{L}{u_0 \rho_v} \right)^{3/2} \frac{u_0^2 \tilde{f}^{1/3}}{2^{1/3}} r^2 \sqrt{h} R_v^2 \sqrt{1+\dot{R}_v^2}\, g_v^{ab}\, \partial_b \delta\phi \right] = 0 \tag{2.122}$$

for $\delta\phi$, and

$$\begin{aligned} &\partial_a \left[f\tilde{f} \left(\frac{L}{u_0 \rho_v} \right)^{3/2} \frac{u_0^2 \tilde{f}^{1/3}}{2^{1/3}} \frac{r^2\sqrt{h}}{\sqrt{1+\dot{R}_v^2}}\, g_v^{ab}\, \partial_b \delta R \right] \\ &\qquad = 6\frac{r^2}{\rho_v^8}\sqrt{h}\sqrt{1+\dot{R}_v^2}\left(1-\frac{8R_v^2}{\rho_v^2}\right)\delta R - 6\sqrt{h}\partial_r\left(\frac{r^2}{\sqrt{1+\dot{R}_v^2}}\frac{R_v\dot{R}_v}{\rho_v^8}\right)\delta R \end{aligned}$$

for δR. Proceeding via separation of variables, we take

$$\delta\phi = \mathcal{P}(r)\mathcal{Y}^{\ell_2}(S^2)\, e^{-i\omega t + iqx}, \quad \delta R = \mathcal{R}(r)\mathcal{Y}^{\ell_2}(S^2)\, e^{-i\omega t+iqx} \tag{2.123}$$

where $\mathcal{Y}^{\ell_2}(S^2)$ are spherical harmonics on the S^2 of unit radius satisfying $\nabla^2_{[2]}\mathcal{Y}^{\ell_2} = -\ell_2(\ell_2+1)\mathcal{Y}^{\ell_2}$ where $\nabla^2_{[2]}$ is the Laplacian on the unit two-sphere. In (2.123) we've taken the $x^1 = x$ axis to coincide with the direction of the spatial momentum, *i.e.,* $k = (-\omega, q, 0, 0)$. We obtain the radial differential equation

$$\partial_r\left[\frac{r^2 f\tilde{f}R_v^2}{\sqrt{1+\dot{R}_v^2}}\partial_r\mathcal{P}\right] + fR_v^2\sqrt{1+\dot{R}_v^2}\left[2^{2/3}\frac{r^2}{\rho_v^3}\tilde{f}^{1/3}\left(\frac{\tilde{f}^2}{f^2}\tilde{\omega}^2 - \tilde{q}^2\right) - \ell_2(\ell_2+1)\tilde{f}\right]\mathcal{P} = 0 \tag{2.124}$$

for $\delta\phi$ and

$$\begin{aligned} &\partial_r\left[\frac{r^2 f\tilde{f}}{(1+\dot{R}_v^2)^{\frac{3}{2}}}\partial_r\mathcal{R}\right] + \frac{f}{\sqrt{1+\dot{R}_v^2}}\left[2^{2/3}\frac{r^2}{\rho_v^3}\tilde{f}^{1/3}\left(\frac{\tilde{f}^2}{f^2}\tilde{\omega}^2 - \tilde{q}^2\right) - \ell_2(\ell_2+1)\tilde{f}\right]\mathcal{R} \\ &\qquad = 6\left[\frac{r^2}{\rho_v^8}\sqrt{1+\dot{R}_v^2}\left(1-\frac{8R_v^2}{\rho_v^2}\right) - \partial_r\left(\frac{r^2 R_v\dot{R}_v}{\rho_v^8\sqrt{1+\dot{R}_v^2}}\right)\right]\mathcal{R} \end{aligned}$$

for δR. The dimensionless constant $\tilde{\omega}$ is related to ω via

$$\omega^2 = \tilde{\omega}^2\frac{u_0}{L^3} = \tilde{\omega}^2\left(\frac{4\pi}{3}\right)^2 T^2 = \tilde{\omega}^2\left(\frac{4\pi}{3}\right)^2\frac{\bar{M}^2}{m}\,, \tag{2.125}$$

and analogously for $\tilde{q}$.

We solved (2.125) and (2.124) numerically and determined the eigenvalues $\tilde{\omega}$ using a shooting method, as was done in the D3/D7 case. The masses are given by $M^2 = \omega^2$ in the frame in which the three momentum vanishes: $q = 0$. The spectra $M^2/\bar{M}^2$ versus $T/\bar{M}$ for the angular fluctuations $\delta\phi$ and the radial fluctuations δR are presented in figs. 2.14 and 2.15, respectively (both for $\ell_2 = 0$), and are qualitatively the same as those for the D3/D7 system: the δR and $\delta\phi$ modes become degenerate in the zero-temperature limit, reflecting supersymmetry restoration; in general the meson masses decrease as the temperature increases, especially near the critical solution; and the results for δR fluctuations suggest that a new mode becomes tachyonic at each turn-around of the curves.

2.5 Discussion

We have shown that, in a large class of strongly coupled gauge theories with fundamental fields, this fundamental matter undergoes a first order phase transition at some high temperature $T_{\rm fun} \sim \bar{M}$, where $\bar{M}$ is a scale characteristic of the meson physics. As well as giving the mass gap in the meson spectrum [61], $1/\bar{M}$ is roughly the characteristic size of these bound states [101, 198]. In our models, the gluons and other adjoint fields were already in a deconfined phase at $T_{\rm fun}$, so this new transition is not a confinement/deconfinement transition. Neither is it a chiral symmetry-restoration phase transition, since the chiral condensate $\langle\bar{\psi}\psi\rangle \propto c$ that breaks the axial $U(1)_{\rm A}$ symmetry does not vanish above $T_{\rm fun}$. [15] Rather, the most striking feature of the new phase transition is the change in the meson spectrum and so we refer to it as a 'dissociation' or 'melting' transition.

In the low-temperature phase, below the transition, the mesons are deeply bound and the spectrum is discrete and gapped. To leading order in the large-$N_{\rm c}$ expansion these states are absolutely stable, but at higher orders they may decay into other mesons of lower mass or glueballs. The leading channel is one-to-two meson decay and after examining the interactions in the effective action [61], we find that parametrically the width of a typical

[15] The large-$N_{\rm c}$ theories under consideration enjoy an exact $U(1)_{\rm A}$ symmetry, just like QCD at $N_{\rm c} = \infty$. However, unlike QCD, they do not possess a non-Abelian $SU(N_{\rm f})_{\rm L} \times SU(N_{\rm f})_{\rm R}$ chiral symmetry. Recall also that lattice simulations indicate that, in $N_{\rm c} = 3$ QCD with real-world quark masses, deconfinement and chiral symmetry restoration do not occur with a phase transition but through a smooth cross-over (see, *e.g.,* [199] and references therein).

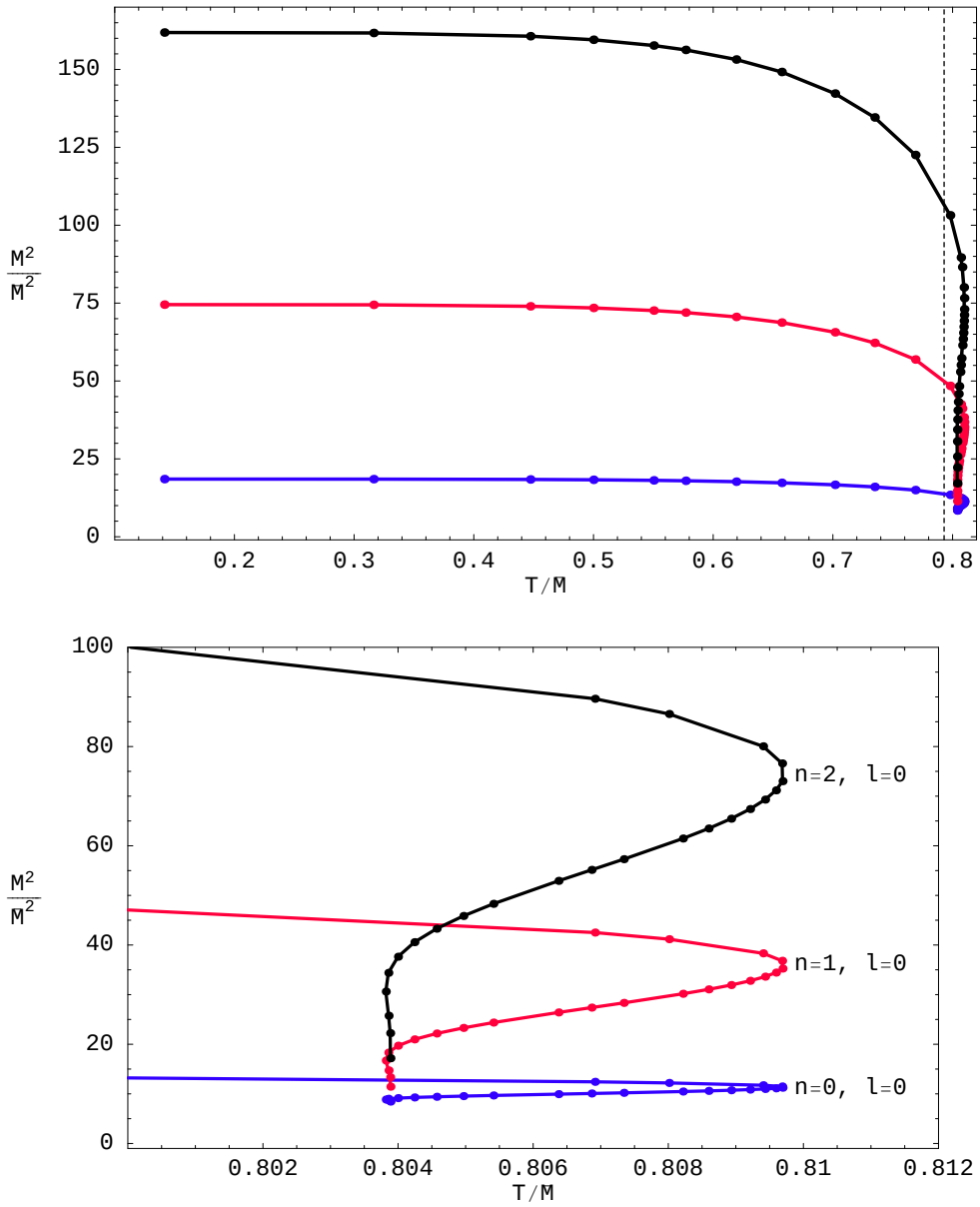

Figure 2.14: Mass spectrum $M^2 = \omega^2|_{q=0}$ for the $\delta\phi$ fluctuations for Minkowski embeddings in the D4/D6 system. The dashed vertical line marks the phase transition.

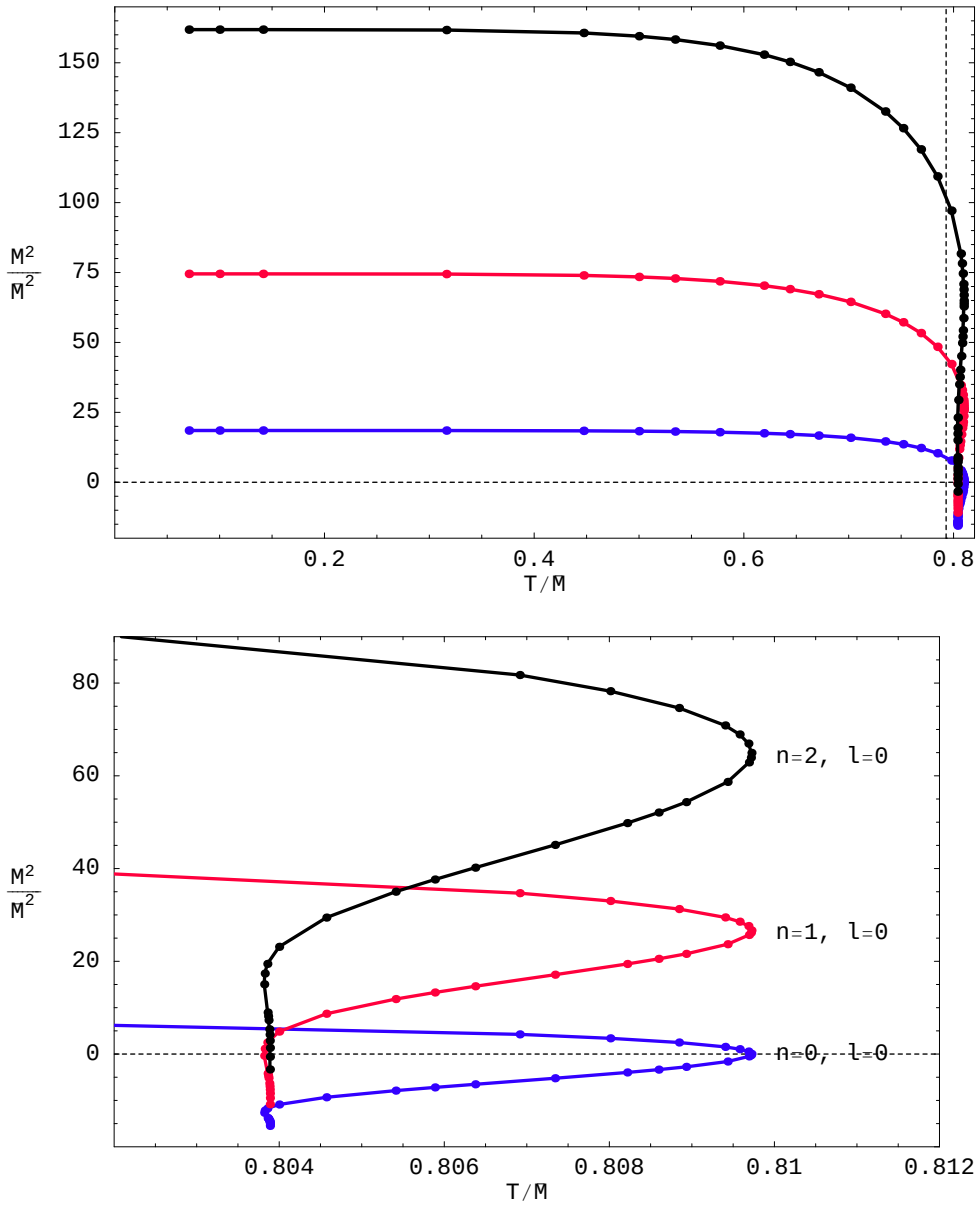

Figure 2.15: Mass spectrum $M^2 = \omega^2|_{q=0}$ for the δR fluctuations for Minkowski embeddings in the D4/D6 system. The dashed vertical line marks the phase transition while the dotted horizontal line marks $M^2 = 0$. Note that some modes become tachyonic.

state is given by $M_{\rm q}/(N_{\rm c}\,\lambda^{3/2}) \simeq M_{\rm gap}/(N_{\rm c}\,\sqrt{\lambda})$. Recall that this is not a confining phase and so we can also introduce free quarks into the system. Of course, such a quark is represented by a fundamental string stretching between the D7-branes and the horizon. At a figurative level, in this phase, we might describe quarks in the adjoint plasma as a 'suspension'. That is, when quarks are added to this phase, they retain their individual identities.

Above the phase transition (*i.e.,* at $T > T_{\rm fun}$), the meson spectrum is continuous and gapless. The excitations of the fundamental fields would be characterised by a discrete spectrum of quasinormal modes on the black hole embeddings [126, 155]. Investigations of the spectral functions in chapter 5 [126] show that some interesting structure remains near the phase transition. Some of these excitations warrant an interpretation in terms of quasiparticle excitations but in any event, there are only a few such states in contrast with the (nominally) infinite spectrum of mesons found in the low temperature phase. An appropriate figurative characterisation of the quarks in this high temperature phase would be as a 'solution'. If one attempts to inject a localised quark charge into the system, it quickly spreads out across the entire plasma and its presence is reduced to diffuse disturbances of the supergravity and worldvolume fields, which are soon damped out [126, 155].

The physics above is potentially interesting in connection with QCD, since lattice simulations indicate that heavy-quark mesons indeed remain bound in a range of temperatures above $T_{\rm deconf}$. For example, for the lightest charmonium states, the melting temperature may be conservatively estimated to be around $1.65T_{\rm deconf} \simeq 249$ to 317 MeV [156–158], depending on the precise value of $T_{\rm deconf}$ [161–163]. Some other studies suggest that the $J/\psi(1S)$ state may persist to $\sim 2.1T_{\rm deconf} \simeq 317$ to 403 MeV [159, 160]. In the D3/D7 model, we see from fig. 2.5 that quark-antiquark bound states melt at $T_{\rm fun} \simeq 0.766\bar{M}$. The scale $\bar{M}$ is related to the mass $M^* = M_{\rm gap}$ of the lightest meson in the theory at zero temperature through eq. (2.48). Therefore we have $T_{\rm fun}(M^*) \simeq 0.122M^*$. For the charmonium states above, taking $M^* \simeq 3000$ MeV gives $T_{\rm fun}(c\bar{c}) \simeq 366$ MeV. Similarly, for the D4/D6 system we have (2.104) which yields $\bar{M} \simeq 0.233M^*$. The transition temperature in this case is then $T_{\rm fun} \simeq 0.793\bar{M} \simeq 0.186M^*$, which gives $T_{\rm fun}(c\bar{c}) \simeq 557$ MeV. Hence it is gratifying that these comparisons lead to a qualitative agreement with the lattice results.

Of course, these comparisons must be taken with some caution, since meson bound states in Dp/Dq systems are deeply bound, *i.e.,* $M^* \ll 2M_q$, whereas the binding energy of charmonium states is a small fraction of the charm mass, *i.e.,* $M_{c\bar{c}} \simeq 2M_c$. It might then

be more appropriate to compare with lattice results for $s\bar{s}$ bound states which are also seen to survive the deconfinement transition. For the ϕ-meson, whose mass is $M_\phi \simeq 1020$ MeV, the formulas above yield $T_{\rm fun}(s\bar{s}) \simeq 124$ MeV (D3/D7) and $T_{\rm fun}(s\bar{s}) \simeq 188$ MeV (D4/D6). Lattice simulations suggest that the melting temperature is around $1.4T_{\rm deconf} \simeq 211$ to 269 MeV [158, 200]. While again we have qualitative agreement, one must observe that at least for the D3/D7 calculation, our result lies below even the lowest estimate for $T_{\rm deconf} \simeq 151$ MeV.

An additional caveat is that here we have identified the melting temperature with $T_{\rm fun}$, above which the discrete meson states disappear. However, the spectral function of some two-point meson correlators in the holographic theory still exhibit some broad peaks in a regime just above $T_{\rm fun}$, which suggests that a few bound states persist just above the phase transition [126]. This is quite analogous to the lattice approach where similar spectral functions are used to examine the existence or otherwise of the bound states. Hence using $T_{\rm fun}$ above should be seen as a (small) underestimate of the melting temperature.

Before leaving this discussion of comparisons with QCD, we reiterate that the present holographic calculations are examining exotic gauge theories and so any agreements above must be regarded with a skeptical eye. However, we would also like to point out one simple physical parallel between all of these systems. The question of charmonium bound states surviving in the quark-gluon plasma was first addressed by comparing the size of the bound states to the screening length in the plasma [201]. While the original calculations have seen many refinements (see, *e.g.,* [202, 203]), the basic physical reasoning remains sound and so we might consider applying the same argument to the holographic gauge theories. Considering first the $\mathcal{N} = 2$ SYM theory arising from the D3/D7 system, the size of the mesons can be inferred from the structure functions in which the relevant length scale which emerges is $\sqrt{\lambda}/M_{\rm q}$ [198]. Holographic studies of Wilson lines in a thermal bath [204, 205] show that the relevant screening length of the SYM plasma is order $1/T$. In fact, the same result emerges from a field theoretic scheme of hard-thermal-loop resummation applied to supersymmetric Yang-Mills theories [206]. In any event, combining these results, the argument that the mesons should dissociate when the screening length is shorter than the size of these bound states yields $T \sim M_{\rm q}/\sqrt{\lambda}$. Of course, the latter matches the results of our detailed calculations in section 2.3. The same reasoning can be applied to the D4/D6 system where the meson size is $O(g_{\rm eff}(M_{\rm q})/M_{\rm q})$ [101] and the screening length is again $O(1/T)$ [103]. Hence this line of reasoning again leads to a dissociation temperature

in agreement with the results of section 2.4. Therefore we see that the same physical reasoning which was used so effectively for the J/ψ in the QCD plasma can also be used to understand the dissociation of the mesons in the present holographic gauge theories.

One point worth emphasising is that there are two distinct processes that are occurring at $T \sim \bar{M}$. If we consider, *e.g.,* the entropy density in fig. 2.5, we see that the phase transition occurs in the midst of a cross-over signalled by a rise in S/T^3. We may write the contribution of the fundamental matter to entropy density as

$$S_{\rm fun} = \frac{1}{8}\lambda\, N_{\rm f}\, N_{\rm c}\, T^3\ H\left(\frac{T^2}{M_{\rm q}^2/\lambda}\right) \tag{2.126}$$

where $H(x)$ is the function plotted in fig. 2.5. H rises from 0 at $x = 0$ to 2 as $x \to \infty$ but the most dramatic part of this rise occurs in the vicinity of $x = 1$. Hence it seems that new degrees of freedom, *i.e.,* the fundamental quarks, are becoming 'thermally activated' at $T \sim \bar{M}$. We might note that the phase transition produces a discontinuous jump in which H only increases by about 0.07, *i.e.,* the jump at the phase transition only accounts for about 3.5% of the total entropy increase. Thus the phase transition seems to play a small role in this cross-over and produces relatively small changes in the thermal properties of the fundamental matter, such as the energy and entropy densities.

As $\bar{M}$ sets the scale of the mass gap in the meson spectrum, it is tempting to associate the cross-over above with the thermal excitation of mesonic degrees of freedom. However, the pre-factor $\lambda\, N_{\rm f}\, N_{\rm c}$ in (2.126) indicates that this reasoning is incorrect. If mesons provided the relevant degrees of freedom,[16] we should have $S_{\rm fun} \propto N_{\rm f}^2$. Instead the factor of $N_{\rm f}N_{\rm c}$ is naturally interpreted as counting the number of degrees of freedom associated with free quarks, with the factor λ demonstrating that the contribution of the quarks is enhanced at strong coupling. A complementary interpretation of (2.126) comes from reorganising the pre-factor as:

$$\lambda\, N_{\rm f}\, N_{\rm c} = (g_{\rm YM}^2\, N_{\rm f})\, N_{\rm c}^2\,. \tag{2.127}$$

[16]In fact we will find a contribution proportional to $N_{\rm f}^2$ for the mesons coming from the fluctuation determinant around the classical D7-brane configuration. One can make an analogy here with the entropy of the adjoint fields of $\mathcal{N} = 4$ SYM on S^3 below the deconfinement transition. In this case, the classical gravity saddle-point yields zero entropy and one must look at the fluctuation determinant to see the entropy contributed by the supergravity modes, *i.e.,* by the gauge-singlet glueballs.

The latter expression makes clear that the result corresponds to the first order correction of the adjoint entropy due to loops of fundamental matter. As we will discuss in chapter 4 [147], we are working in a 'not quite' quenched approximation, in that thermal contributions of the D7-branes represent the leading order contribution in an expansion in $N_{\rm f}/N_{\rm c}$, and so fundamental loops are suppressed but not completely. In chapter 4 [147], we show that the expansion for the classical gravitational back-reaction of D7-brane is controlled by $\lambda N_{\rm f}/N_{\rm c} = g^2_{\rm YM}\, N_{\rm f}$. Hence this expansion corresponds to precisely the expansion in loops of fundamental matter. However, naively the fundamental loops would be suppressed by factors of $T^2/M_{\rm q}^2$ coming from the quark propagators. So from this point of view, the strong coupling enhancement corresponds to the fact that such factors only appear as $\lambda\, T^2/M_{\rm q}^2$ in eq. (2.126).

Hence the strongly coupled theory brings together these two otherwise distinct processes. That is, at strong coupling, the dissociation of the bound states and the thermal activation of the fundamental matter happen at essentially the same temperature. While our discussion above focussed on the D3/D7 system, the D4/D6 results exhibit the same behaviour. Hence this seems to be a universal feature of the holographic gauge theories described by Dp/Dq systems.

The preceding behaviour might be contrasted with that which is expected to occur at weak coupling. In this regime, one expects that the melting of the mesons would also be a cross-over rather than a (first order) phase transition. Moreover, the temperature at which the mesons dissociate would be $T_{\rm fun} \sim E_{\rm bind} \sim g^4_{\rm eff} M_{\rm q}$. On the other hand, the quarks would not be thermally activated until we reach $T_{\rm activ} \sim 2M_{\rm q}$, at which point free quark-antiquark pairs would be readily produced. Of course, the thermal activation would again correspond to a cross-over rather than a phase transition. The key point, which we wish to emphasise, is that these two temperatures are widely separated at weak coupling.

Fig. 2.16 is an 'artistic' representation of the simplest behaviour which would interpolate between strong and weak coupling. One might expect that the melting point and the thermal activation are very close for $g_{\rm eff} \gg 1$. The line of first order phase transitions must end somewhere and so one might expect that it terminates at a critical point around $g_{\rm eff} \sim 1$. Below this point, both processes would only represent cross-overs and their respective temperatures would diverge from one another, approaching the weak coupling behaviour described above.

There are two aspects to enhancement of the thermal densities discussed above. First,

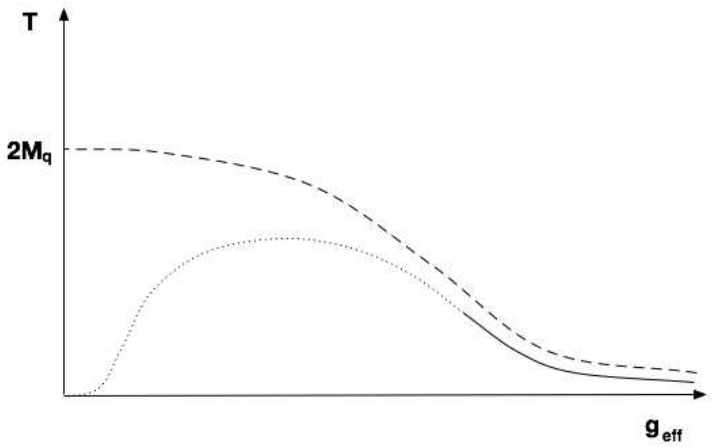

Figure 2.16: A qualitative representation of the simplest possibility interpolating between the weak and the strong coupling regimes. The solid and the dotted lines correspond to $T = T_{\rm fun}$. At strong coupling this corresponds to a first order phase transition (solid line), whereas at weak coupling it corresponds to a cross-over (dotted line). The dashed line corresponds to $T = T_{\rm activ}$. At strong-coupling this takes place immediately after the phase transition, whereas at weak coupling it is widely separated from $T_{\rm fun}$.

at strong coupling the fundamental matter has a stronger effect on the nonabelian plasma than might have been otherwise guessed and second the effect is a positive one. That is, *e.g.,* the energy and entropy densities are raised. Because we are working with $N_{\rm f}/N_{\rm c} \ll 1$, the enhancement we observe is a small correction to the overall properties of the plasma. In fact, it can be added to a list of such correction terms, with others arising as finite-λ [207] and finite-$N_{\rm c}$ effects. Both[17] of these types of corrections are expected to raise the entropy and energy densities of the plasma, as well.

As our calculations were also performed in the limit $N_{\rm c}$, $\lambda \to \infty$ (with $N_{\rm f}$ fixed), it is natural to ask how the detailed results of this chapter depend on this approximation. First of all, the fact that the phase transition is first order implies that it should be stable under small perturbations and so its order and other qualitative details should hold within a finite radius of the $1/N_{\rm c}, 1/\lambda$ expansions. Of course, finite-$N_{\rm c}$ and finite-λ corrections

[17] At finite $N_{\rm c}$, the classical black hole would be surrounded by a gas of Hawking radiation which would increase both the entropy and energy.

may eventually modify the behaviour uncovered here. For example, at large but finite N_c the black hole will Hawking-radiate and each bit of the brane probe will experience a thermal bath at a temperature determined by the local acceleration. This effect becomes more and more important as the lower part of a Minkowski brane approaches the horizon, and may potentially blur the self-similar, scaling behaviour found here. However, at the phase transition, the minimum separation of brane embeddings and the horizon is not parametrically small. For example, $R_0 = 1.1538$ at the transition for D3/D7 system. Hence while the Hawking radiation can be expected to interfere with the self-similar behaviour near the critical embedding, it should not disturb the phase transition for large but finite N_c.

Finite 't Hooft coupling corrections correspond to higher-derivative corrections both to the supergravity action and the D-brane action. These may also blur the details of the structure discussed above. For example, higher-derivative corrections to the D-brane equation of motion are likely to spoil the scaling symmetry of eq. (2.19), and hence the self-similar behaviour. These corrections will again become important near the critical solution, for both Minkowski and black hole embeddings, since the (intrinsic) curvature of the brane becomes large there. However, the phase transition should remain robust for large but finite λ because at this point, the separation of brane embeddings from the critical solution is not parametrically small. We illustrated this for the Minkowski embedding at the phase transition of D3/D7 above but here we can add the same is true for the black hole embedding at this point, which has $\chi_0 = 0.9427$.

Another significant set of corrections come from the gravitational backreaction of the D7-branes (or more generally the probe Dq-branes) on the background spacetime or from fundamental loops in the gauge theory. As indicated above, these are dual descriptions of the same expansion. Our results only represent the first contribution in an infinite series of terms, whose magnitudes are controlled by the ratio N_f/N_c. Given that low energy QCD has $N_f/N_c = 1$, it is of particular interest to study holographic theories in Veneziano's limit of $g_{YM} \to 0$, $N_c \to \infty$ with both λ and N_f/N_c finite [208]. A variety of attempts have been made to construct gravitational backgrounds describing gauge theories in this limit [83, 209–216].

The D2/D6 system provides one interesting background where this limit was studied

at finite temperature [217].[18] In particular, it was found that the energy density scales as $F \sim N_{\rm f}^{1/2} N_{\rm c}^{3/2} T^3$, which obviously differs from (2.33) with $p = 2, d = 2$. This discrepancy is not at all a contradiction and has the same origin as the discrepancy found for the meson spectrum [101, 102, 154]. This is the fact that the calculation in [217] applies in the far infrared of the gauge theory, whereas that presented here applies at high temperatures, *i.e.,* at $T \gg g_{\rm YM}^2$.

We close this section with a few more observations. Ref. [219] argued for the existence of plasma balls in a broad class of confining large-$N_{\rm c}$ theories, which undergo first order deconfinement phase transitions. That is, in these theories, one could form metastable, localised lumps of deconfined gluon plasma. Their dual description should consist of black holes localised along some gauge theory directions. One may imagine an analogous construction for the fundamental matter, based on the first order phase transition discussed here. That is, near $T_{\rm fun}$ one should be able to construct inhomogenous brane configurations in which only a localised region on the branes has fallen through the black hole horizon, *i.e.,* the induced brane metric would contain a localised black hole. The dual gauge theory interpretation would be in terms of a localised bubble inside of which the fundamental matter has melted. Such bubbles may be of interest for understanding how the melting transition actually occurs in a dynamical context.

Finally, we comment on the 'quark condensate' at high temperatures. If one examines fig. 2.4 for example, it is tempting to infer that, since c approaches zero as $T \to \infty$, the quark condensate vanishes in this limit. This vanishing would then be in agreement with the intuition that at high temperatures the thermal fluctuations should destroy any coherent condensate. However, vanishing c is not enough to ensure that $\langle \mathcal{O}_m \rangle$ also vanishes. In fact, if we combine eqs. (2.47) and (2.137), we see that at high temperatures the condensate actually grows as

$$\langle \mathcal{O}_m \rangle \sim N_{\rm c} N_{\rm f} M_{\rm q} T^2 \,. \tag{2.128}$$

At this point, it is important to recall the form of the full operator $\mathcal{O}_m$ given in eq. (2.31). The first two terms are dimension-three operators and so in the high temperature limit we can expect the magnitude of typical fluctuations in these to be $O(T^3)$. Further these operators do not have a definite sign and so presumably their expectation value vanishes when averaging over all fluctuations in the disordered high-temperature system. This, of

[18] The meson spectrum at $T = 0$ including the backreaction of the D6-branes has been studied in [218].

course, is the basis of the intuition that $\langle\bar{\psi}\psi\rangle \to 0$. Now the last term in eq. (2.31) is only a dimension-two operator and so we expect thermal fluctuations to be of $O(T^2)$.[19] The key difference in this case is that the operator only takes positive real values and so averaging over all fluctuations we expect $\langle q^\dagger q\rangle \propto T^2$. Hence our calculations make a precise prediction for this expectation value in the high-temperature phase. Note though that this is a thermal expectation value and not a coherent (zero-momentum) condensate, which we expect that we are observing with $\langle\mathcal{O}_m\rangle \neq 0$ at low temperatures.

Hence it is interesting that the high temperature phase seems to display two distinct regimes of behaviour. At very high temperatures, the physics is dominated by incoherent thermal fluctuations of the fundamental fields, as expected. However, there is also a regime just above the phase transition where the system can support a coherent condensate. This regime would correspond to the region where $|c|/T^3$ is still growing in fig. 2.4. Of course, there is a cross-over between these two regimes and so there is only a rough boundary. It may be natural to define the latter as the point where c is extremized, *i.e.,* $T \simeq 1.2\bar{M}$. Again, this seems to be a universal property of the broad class of holographic theories described by Dp/Dq systems. For example, fig. 2.12 indicates the same behaviour for D6-branes in a D4 background.

The above seems to be one more facet of the rich phenomenology which these holographic theories display at finite temperature. However, this phenomenology presents several puzzles, such as why $T_{\rm fun} \sim \bar{M}$ rather than $M_{\rm q}$ is the scale at which the bound states melt or at which the free quarks are thermally excited. For example, the former seems counterintuitive in view of the fact that, in the regime of strong coupling considered here, this temperature is much lower than the binding energy of the mesons:

$$E_{\rm bind} \sim 2M_{\rm q} - \bar{M} \sim 2M_{\rm q}\,. \tag{2.129}$$

However, this intuition relies on the expectation that the result of melting a meson is a free quark-antiquark pair of mass $2M_{\rm q}$. The gravity description makes it clear that this is not the case at strong coupling. In fact, the constituent quark mass vanishes when the branes fall into the horizon – see section 2.6.4. Rather, in this regime the system is better thought of as a strongly coupled liquid of both adjoint and fundamental fields.

[19] At zero temperature, the supersymmetric theory has a moduli space with many branches where the scalars acquire non-vanishing vacuum expectation values [220, 221]. We are not probing these branches in this study.

In any event, it is gratifying that the holographic description of these gauge theories with fundamental matter provides once more an extremely simple, geometric interpretation of some complicated, strong-coupling physics, such as the existence or otherwise of stable quark-antiquark bound states above the deconfinement temperature. Other well known examples include the geometric characterisations of confinement [59, 103–105] and chiral symmetry breaking [62–64, 93, 106–110, 222].

2.6 Supplementary material for Chapter 2

2.6.1 Embeddings for high and low temperatures for D3/D7

High temperatures (black hole embeddings)

Consider the limit $T/\bar{M} \gg 1$. This corresponds to black hole embeddings with $m = \bar{M}/T \ll 1$. As usual, we use the χ, ρ coordinates. Note that the equatorial D7-brane embedding, $\chi = 0$, is an exact solution of the equation of motion (2.44). To study nearby solutions we expand the bulk portion of the D7-brane action (2.42) to quadratic order in χ

$$\frac{I_{\rm bulk}}{\mathcal{N}} \simeq \int_1^\infty d\rho \left(1 - \frac{1}{\rho^8}\right) \rho^3 \left(1 - \frac{3}{2}\chi^2 + \frac{1}{2}\dot{\chi}^2\right) , \tag{2.130}$$

thus obtaining the linearised equation of motion:

$$\partial_\rho \left[\left(1 - \frac{1}{\rho^8}\right) \rho^5 \dot{\chi}\right] = -3 \left(1 - \frac{1}{\rho^8}\right) \rho^3 \chi \, . \tag{2.131}$$

To solve this equation, it is useful to make the change of variables $x = \rho^2$ so that it becomes:

$$x(x^4 - 1)(4x\chi'' + 2\chi') + 2x(5x^4 + 3)\chi' + 3(x^4 - 1)\chi = 0 \tag{2.132}$$

where $\chi' = d\chi/dx$. The solution of this equation satisfying the boundary condition $\chi'|_{x=1} = 0$ is

$$\tilde{\chi} = \frac{x^{1/2}}{16} F\left(\frac{1}{4}, \frac{1}{2}; \frac{3}{4}; x^4\right) - \frac{1}{4}\left[\frac{\Gamma(3/4)}{\Gamma(1/4)}\right]^2 x^{3/2} F\left(\frac{1}{2}, \frac{3}{4}; \frac{5}{4}; x^4\right) , \tag{2.133}$$

where $F(a, b; c; z)$ is the hypergeometric function satisfying

$$z(1 - z)F'' + [c - (a + b + 1)z]F' - abF = 0. \tag{2.134}$$

The overall normalisation of the solution is arbitrary since, we are solving a linear equation. In the above, we have chosen the normalisation such that

$$\tilde{\chi} \simeq 1/x^{1/2} + \tilde{c}/x^{3/2}\,, \quad x \to \infty \tag{2.135}$$

where

$$\tilde{c} = \frac{\Gamma\left(\frac{-1}{4}\right)\Gamma\left(\frac{3}{4}\right)^2}{\sqrt{2}\pi\Gamma\left(\frac{1}{4}\right)} \simeq -0.456947. \tag{2.136}$$

The tilde on the solution $\tilde{\chi}$ and condensate $\tilde{c}$ indicate that these is the solution for unit mass. The general solution for arbitrary small mass (or equivalently, high temperatures) is simply $\chi = m\tilde{\chi}$ and the condensate is given by

$$c = m\tilde{c}\,. \tag{2.137}$$

Low temperatures (Minkowski embeddings)

Low-temperature solutions correspond to Minkowski embeddings in which the D7 probe is very far from the horizon: $R_0 \gg 1$ or, equivalently, $m = \bar{M}/T \gg 1$. In this case, we expect the brane profile to be nearly flat, *i.e.,* $R(r)$ is approximately constant. This motivates the ansatz $R(r) = R_0 + \delta R(r)$, where R_0 is a large constant. Substituting into eq. (2.49) and expanding to linear order in $\delta R(r)$ gives:

$$\partial_r\left[r^3\left(1 - \frac{1}{(r^2+R_0^2)^4}\right)\partial_r(\delta R)\right] = 8\frac{r^3 R_0}{(r^2+R_0^2)^5}\,. \tag{2.138}$$

Integrating (2.138) and requiring $\partial_r(\delta R)|_{r=0} = 0$ we obtain

$$\begin{aligned}
\delta R(r) \;&\simeq\; -\frac{R_0}{3}\int_0^r dx \frac{1}{x^3}\left(1 - \frac{1}{(x^2+R_0^2)^4}\right)^{-1}\left[\frac{R_0^2+4x^2}{(R_0^2+x^2)^4} - \frac{1}{R_0^6}\right] \\
&=\; -\frac{1}{24R_0^5}\left[2(3R_0^4-1)\arctan\left(\frac{r^2}{1+R_0^2(R_0^2+r^2)}\right)\right. \\
&\quad +(-1-2R_0^2-3R_0^4)\log\left(1+\frac{r^2}{R_0^2-1}\right) \\
&\quad \left.+\,(1-2R_0^2+3R_0^4)\log\left(1+\frac{r^2}{R_0^2+1}\right) + 2R_0^2\log\left(\frac{1+(r^2+R_0^2)^2}{1+R_0^4}\right)\right].
\end{aligned}$$

Note that $\delta R|_{r=0} = 0$ while the limit $r \to \infty$ yields:

$$\begin{aligned}\delta R|_{r\to\infty} \;\simeq\; & \left(\frac{1}{12R_0^5} - \frac{1}{4R_0}\right)\left(\frac{\pi}{2} - \arctan(R_0^2)\right) + \frac{1}{12R_0^3}\log\left(\frac{R_0^4+1}{R_0^4-1}\right) \\ & + \frac{1}{8}\left(\frac{1}{3R_0^5} + \frac{1}{R_0}\right)\log\left(\frac{R_0^2+1}{R_0^2-1}\right) - \frac{1}{6R_0^5}\frac{1}{r^2} + \cdots \end{aligned} \tag{2.139}$$

Recall that for these embeddings $R_0 \gg 1$ so indeed $\delta R \ll R_0$. Note that $R(r \to \infty) \simeq m + c/r^2$ so that in the large R_0, m limit one has $m \simeq R_0 + \delta R|_{r\to\infty}$ and $c \simeq -(6R_0^5)^{-1}$. For very large values of R_0 we can expand (2.139) further to give $m \simeq R_0 + 1/2R_0^7$ as an approximate expression for the quark mass. Inverting this relation yields

$$R_0 \simeq m - \frac{1}{2m^7}\,. \tag{2.140}$$

We will apply this result in our discussion of the constituent quark mass in section 2.6.4.

2.6.2 Computation of the D7-brane entropy

In order to evaluate the expression for the D7-brane entropy density,

$$S = -\frac{\partial F}{\partial T} = -\pi L^2 \frac{\partial F}{\partial u_0}\,, \tag{2.141}$$

we split the free energy into a bulk and a boundary contribution. We also write pertinent expressions in terms of the dimensionful variables

$$\varrho = u_0\,\rho\,, \quad \tilde{c} = u_0^3\,c\,, \quad \tilde{m} = u_0\,m\,, \tag{2.142}$$

to explicitly show the dependences on u_0, or, equivalently, the temperature T.

From eq. (2.54),

$$F_{\text{bound}} = T\,I_{\text{bound}} = -\frac{\pi^2}{8}T_{\text{D7}}\left[(\varrho_{\text{max}}^2 - \tilde{m}^2)^2 - 4\tilde{m}\tilde{c}\right] \tag{2.143}$$

so that the boundary contribution to the entropy is

$$S_{\text{bound}} = -\frac{\pi^3}{2}L^2 T_{\text{D7}}\tilde{m}\frac{\partial \tilde{c}}{\partial u_0}\,, \tag{2.144}$$

as the quark condensate is the only factor in eq. (2.143) which depends on the position of the horizon u_0. Note that both of the divergent regulator contributions in eq. (2.143) have

been eliminated by this differentiation. The bulk contribution to the free energy is given by

$$F_{\rm bulk} = T\, I_{\rm bulk} = \frac{\pi^2}{2} T_{\rm D7} {u_0}^4 \int_{\varrho_{\rm min}/u_0}^{\varrho_{\rm max}/u_0} d\rho\, \rho^3 \left(1 - \frac{1}{\rho^8}\right) \left(1-\chi^2\right) \left(1 - \chi^2 + \rho^2\, \dot{\chi}^2\right)^{1/2} . \quad (2.145)$$

When we differentiate this expression with respect to u_0 following eq. (2.141), the derivative will act in three places: i) the overall factor of ${u_0}^4$; ii) the explicit (and implicit in $\varrho_{\rm min}$) appearance of u_0 in the end-points of the integration; and iii) the field χ which is implicitly a function of the background mass u_0. We consider each of these contributions in turn. First one has:

$$S_i = -2\pi^3 L^2 T_{\rm D7} {u_0}^3 \int_{\varrho_{\rm min}/u_0}^{\varrho_{\rm max}/u_0} d\rho\, \rho^3 \left(1 - \frac{1}{\rho^8}\right) \left(1-\chi^2\right) \left(1 - \chi^2 + \rho^2\, \dot{\chi}^2\right)^{1/2} . \quad (2.146)$$

Note that this contribution by itself is divergent in the limit $\varrho_{\rm max} \to \infty$.

Next consider the contributions from the end-points. At the lower end-point, there are two possibilities depending on whether the brane ends on the horizon or closes off above the horizon. If the brane ends on the horizon, $\varrho_{\rm min} = u_0$ and hence this contribution vanishes since $\partial_{u_0}(\varrho_{\rm min}/u_0) = 0$. (The integrand also vanishes when evaluated at $\rho_{min} = \varrho_{\rm min}/u_0 = 1$.) If the brane closes off above the horizon, $\partial_{u_0}(\varrho_{\rm min}/u_0)$ is nonvanishing but this contribution vanishes because $\chi = 1$ at the end-point. Hence only the upper end-point at $\varrho_{\rm max}$ makes a contribution:

$$\begin{aligned} S_{ii} &= -\frac{1}{2}\pi^3 L^2 T_{\rm D7} {u_0}^4 \left[\rho^3 \left(1 - \frac{1}{\rho^8}\right) \left(1-\chi^2\right) \left(1 - \chi^2 + \rho^2\, \dot{\chi}^2\right)^{1/2}\right]_{\varrho_{\rm max}/u_0} \times \left(-\frac{\varrho_{\rm max}}{{u_0}^2}\right) \\ &= \frac{1}{2u_0}\pi^3 L^2 T_{\rm D7} \left(\varrho_{\rm max}^4 - \tilde{m}^2 \varrho_{\rm max}^2\right) . \end{aligned} \quad (2.147)$$

where we have substituted the asymptotic expansion (2.28) for χ in the second expression.

Finally, we consider the contributions from the dependence of χ on u_0. In this case, $\partial_{u_0}\chi$ inside the integral can be considered as a variation $\delta\chi$. Hence after an integration by parts, this derivative yields the bulk equation of motion for χ inside the integral and a boundary term coming from the integration by parts. Since χ solves the equation of motion, only the boundary term contributes to the entropy with

$$S_{iii} = -\frac{1}{2}\pi^3 L^2 T_{\rm D7} {u_0}^4 \left[\rho^5 \left(1 - \frac{1}{\rho^8}\right) \frac{1-\chi^2}{\left(1 - \chi^2 + \rho^2\, \dot{\chi}^2\right)^{1/2}} \dot{\chi} \partial_{u_0}\chi\right]_{\varrho_{\rm min}/u_0}^{\varrho_{\rm max}/u_0} . \quad (2.148)$$

Arguments similar to those above show that the contribution at the lower endpoint vanishes. If the brane ends on the horizon, the second factor inside the brackets vanishes and also $\dot{\chi}$ vanishes at the horizon. If the brane closes off above the horizon, $\chi = 1$ at the lower end-point and so the numerator in the third factor vanishes and also $\partial_{u_0}\chi = 0$. Hence again, only the upper end-point contributes to the entropy. In order to correctly evaluate this expression, we express the asymptotic expansion (2.45) in terms of $\tilde{m}, \tilde{c}$:

$$\chi = \frac{\tilde{m}/u_0}{\rho} + \frac{\tilde{c}/{u_0}^3}{\rho^3} + \cdots \tag{2.149}$$

Then in eq. (2.148), we have

$$\begin{aligned} \dot{\chi} = \partial_\rho \chi &= -\frac{\tilde{m}/u_0}{\rho^2} - 3\frac{\tilde{c}/{u_0}^3}{\rho^4} + \cdots \\ \partial_{u_0}\chi &= -\frac{\tilde{m}/{u_0}^2}{\rho} - 3\frac{\tilde{c}/{u_0}^4}{\rho^3} + \frac{\partial_{u_0}\tilde{c}/{u_0}^3}{\rho^3} + \cdots \end{aligned} \tag{2.150}$$

Note that it would be incorrect to evaluate $\partial_{u_0}\chi \simeq \partial_{u_0}(\tilde{m}/\rho) = 0$ because in the integral we have assumed that $\partial_{u_0}\rho = 0$ and so $\partial_{u_0}\varrho \neq 0$. Inserting these expansions in (2.148) yields

$$S_{iii} = -\frac{1}{2u_0}\pi^3 L^2 T_{\mathrm{D7}} \left[\tilde{m}^2 \varrho_{\max}^2 + 6\tilde{m}\tilde{c} - \tilde{m}^4 - u_0(\partial_{u_0}\tilde{c})\tilde{m}\right] . \tag{2.151}$$

Finally, gathering all the entropy contributions yields:

$$\begin{aligned} S &= S_i + S_{ii} + S_{iii} + S_{\mathrm{bound}} \\ &= -\frac{1}{2u_0}\pi^3 L^2 T_{\mathrm{D7}} \left[4{u_0}^4 \int_{\rho_{\min}/u_0}^{\rho_{\max}/u_0} d\rho\, \rho^3 \left(1 - \frac{1}{\rho^8}\right)\left(1-\chi^2\right)\left(1 - \chi^2 + \varrho^2\,\dot{\chi}^2\right)^{1/2} \right. \\ &\qquad \left. -\rho_{\max}^4 + 2\tilde{m}^2\rho_{\max}^2 + 6\tilde{m}\tilde{c} - \tilde{m}^4 \right] . \end{aligned} \tag{2.152}$$

Note that the boundary terms have provided precisely the correct $\rho_{\max}$ terms to regulate the integral. Hence using (2.26), (2.55) and (2.57), we can express the final result for the entropy as

$$\frac{S}{\mathcal{N}} = -4G(m) + ({\rho_{\min}}^2 - m^2)^2 - 6mc\,. \tag{2.153}$$

2.6.3 Positivity of the entropy

Here we present an analytic proof that the plot of the Dq-brane probe Euclidean action $I_{\rm E}$ versus m must exhibit mathematical kinks and not just rapid turn overs.[20] Recall that this is necessary for the entropy $S = -\partial F/\partial T$ to be positive. We focus here on the case of black hole embeddings of the D7-brane in the D3-brane background for concreteness, but the analogous arguments applies to Minkowski embeddings and to other Dp/Dq systems.

The argument proceeds by thinking of the plot $I_{\rm E}(m)$ as a parametric plot $(m(\chi_0), I_{\rm E}(\chi_0))$, where χ_0, which plays the role of the parameter along the curve, is the value of χ at the 'horizon' $\rho = 1$. This is in fact the way we construct the plot: We choose χ_0 as a boundary condition at the horizon and we integrate the differential equation 'outwards', thus obtaining a solution $\psi(\rho;\chi_0)$, from whose asymptotic behaviour we read off $m(\chi_0)$ and $c(\chi_0)$. Substituting the solution into the D7-brane action we then obtain $I_{\rm E}(\chi_0)$.

Now the key observation is that if the tangent vector to the curve never vanishes, then there can be no kinks. In order to have a kink there must be a point at which both $m' \equiv \partial m/\partial\chi_0$ and $I' \equiv \partial I_{\rm E}/\partial\chi_0$ vanish simultaneously. We know that there are certainly an infinite number of points at which $m' = 0$, because close to criticality the function $m(\chi_0)$ is an oscillatory function with both maxima and minima. We will now see that at each of these points we also have $I'_{\rm E} = 0$.

The renormalised D7-brane action is $I_{\rm E} = I_{\rm bulk} + I_{\rm bound}$, with

$$I_{\rm bulk} = \int_{\rho_{\rm min}}^{\rho_{\rm max}} d\rho\, \mathcal{L}(\chi,\dot\chi) = \int_{\rho_{\rm min}}^{\rho_{\rm max}} d\rho \left(1 - \frac{1}{\rho^8}\right) \rho^3 \,(1-\chi^2)\sqrt{1-\chi^2+\rho^2\dot\chi^2}\,, \qquad (2.154)$$

and

$$I_{\rm bound} = -\frac{1}{4}\left(\rho_{\rm max}^4 - 2m^2\rho_{\rm max}^2 - 4mc + m^4\right)\,, \qquad (2.155)$$

where we have set $\mathcal{N} = 1$ for simplicity. Using the equation of motion, we see that the derivative of $I_{\rm E}$ is

$$I'_{\rm E} = \frac{\partial I_{\rm E}}{\partial\chi_0} = \left[\frac{\partial\mathcal{L}}{\partial\dot\chi}\frac{\partial\chi}{\partial\chi_0}\right]_{\rho_{\rm min}}^{\rho_{\rm max}} = \left[\left(1-\frac{1}{\rho^8}\right)\rho^3\,(1-\chi^2)\frac{\rho^2\dot\chi}{\sqrt{1-\chi^2+\rho^2\dot\chi^2}}\frac{\partial\chi}{\partial\chi_0}\right]_{\rho_{\rm min}}^{\rho_{\rm max}}. \qquad (2.156)$$

[20] For the sake of this discussion it is irrelevant whether we plot $I_{\rm E}$ versus m or versus $1/m$, as in the main text.

The contribution at $\rho = \rho_{\min}$ clearly vanishes because $\rho_{\min} = 1$ and $\dot{\chi}(1) = 0$. Asymptotically we have

$$\chi = \frac{m}{\rho} + \frac{c}{\rho^3} + \mathcal{O}(\rho^{-4}) \,, \tag{2.157}$$

and therefore

$$\frac{\partial \chi}{\partial \chi_0} = \frac{m'}{\rho} + \frac{c'}{\rho^3} + \mathcal{O}(\rho^{-4}) \,. \tag{2.158}$$

Substituting this into (2.156) we find

$$I_{\rm E}' = \left[-mm'\rho^2 + m^3 m' - 3cm' - mc' + \mathcal{O}(\rho^{-1}) \right]_{\rho=\rho_{\max}} \,. \tag{2.159}$$

The derivative of the boundary action is just

$$I_{\rm bound}' = mm'\rho_{\max}^2 + mc' + cm' - m^3 m' \,, \tag{2.160}$$

so adding everything together we arrive at a simple result in the limit in which the regulator is removed:

$$I_{\rm E}{}' \equiv \frac{\partial I_{\rm E}}{\partial \chi_0} = -2cm' \,. \tag{2.161}$$

This formula is useful for a number of reasons. First, it shows that $I_{\rm E}'$ vanishes if and only if m' vanishes, as we wanted to see. Second, applying the chain rule we find

$$\frac{\partial I_{\rm E}}{\partial m} = -2c \,. \tag{2.162}$$

Physically we expect that $c < 0$ always, because the brane is attracted to the horizon, and this is confirmed by our numerical results. It then follows that $I_{\rm E}$ is an increasing function of m, or equivalently a decreasing function of $1/m$, and hence that the entropy is positive. Third, it provides an alternative expression for $I_{\rm E}$, namely

$$I_{\rm E}(\chi_0) = -\frac{1}{2} - 2\int_0^{\chi_0} dx\, c(x) m'(x) \,, \tag{2.163}$$

where we have imposed the boundary condition $I_{\rm E}(\chi_0 = 0) = -1/2$, which follows from a straightforward calculation of the action of the equatorial embedding. This expression can be used to evaluating $I_{\rm E}$ numerically. Moreover, close to criticality one knows the analytic form of $m(\chi_0)$ and $c(\chi_0)$, which should allow one to compute $I_{\rm E}(\chi_0)$ analytically.

2.6.4 Constituent quark mass in the D3/D7 system

In this section we compute the constituent quark mass $M_{\rm c}$ for temperatures below and near the critical temperature for the D3/D7 brane system. A similar analysis has already been provided in [133].

Our holographic dictionary relates the quark mass $M_{\rm q}$ to the asymptotic constant m with eq. (2.46). However this is the bare mass parameter appearing in the microscopic Lagrangian of the gauge theory. We must expect the physical or constituent mass of a free quark in the deconfined plasma to receive thermal corrections. Since a free quark corresponds to a string in the D3-brane geometry hanging from a probe D7-brane (Minkowski embedding) down to the horizon, the constituent quark mass corresponds to the energy of this configuration.

In the notation of the metric (2.36), (2.40), the string worldsheet is extended in the t, R directions, localized at $r = 0$, with induced metric:

$$ds^2 = -\frac{1}{2}\left(\frac{u_0 R}{L}\right)^2 \frac{f^2}{\tilde{f}} dt^2 + \frac{L^2}{R^2} dR^2. \tag{2.164}$$

The Nambu-Goto string action then becomes

$$I_{\rm string} = -\frac{u_0}{2\pi\ell_{\rm s}^2}\int dt dR\, f/\sqrt{2\tilde{f}}\,, \tag{2.165}$$

where, since $r = 0$, $f = 1 - 1/R^4$ and $\tilde{f} = 1 + 1/R^4$. Identifying the constituent quark mass with minus the action per unit time of this static configuration, we have

$$M_{\rm c} = \frac{u_0}{2\pi\ell_{\rm s}^2\sqrt{2}}\int_1^{R_0} dR \left(1 - \frac{1}{R^4}\right)\left(1 + \frac{1}{R^4}\right)^{-1/2} = \frac{u_0}{2\pi\ell_{\rm s}^2\sqrt{2}}\left[R_0\sqrt{1 + \frac{1}{R_0^4}} - \sqrt{2}\right], \tag{2.166}$$

where we recall that $R_0 = R(r = 0)$ is the minimal radius reached by the probe brane. Given the definition (2.46) for the bare quark mass, we find that

$$\frac{M_{\rm c}}{M_{\rm q}} = \frac{1}{m}\left[R_0\sqrt{1 + \frac{1}{R_0^4}} - \sqrt{2}\right]. \tag{2.167}$$

Plots of $M_{\rm c}/M_{\rm q}$ versus $T/\bar{M}$ are given in figure 2.17. In the vicinity of the critical solution, there are again multiple embeddings for a fixed value of $T/\bar{M}$ and so the plots of $M_{\rm c}$ show

an oscillatory behaviour in this regime. From eq. (2.167), it is clear that as we approach the critical solution, *i.e.,* $R_0 \to 1$, the constituent quark mass goes to zero. Note however that the phase transition occurs at $T/\bar{M} \simeq 0.7658$, which corresponds to $R_0 \simeq 1.15$ – which is marked with the vertical dotted line in fig. 2.17. Hence the exotic behaviour in the vicinity of the critical solution will again not be manifest in the physical system.

As the temperature goes to zero, $M_{\rm c}/M_{\rm q} \to 1$. This is expected, since for small temperatures we have $m \gg 1$ and we can use the approximate relation (2.140) in (2.167) to find

$$\frac{M_{\rm c}}{M_{\rm q}} \simeq 1 - \frac{\sqrt{2}}{m} + \frac{1}{2m^4} - \frac{5}{8m^8} + \cdots . \tag{2.168}$$

Since $m = 2M_{\rm q}/\sqrt{\lambda}T$, this can be finally converted into

$$\frac{M_{\rm c}}{M_{\rm q}} \simeq 1 - \frac{\sqrt{\lambda}T}{\sqrt{2}M_{\rm q}} + \frac{1}{2}\left(\frac{\sqrt{\lambda}T}{2M_{\rm q}}\right)^4 - \frac{5}{8}\left(\frac{\sqrt{\lambda}T}{2M_{\rm q}}\right)^8 + \cdots . \tag{2.169}$$

The same expansion appears in [133] but here we have provided an analytic derivation for the coefficient of the fourth term, which was obtained in [133] by a numerical fit. Note that the two expansions precisely coincide, however, one must replace $\lambda \to 2\lambda$ above because [133] uses a different normalisation for the 't Hooft coupling. This difference arises from the implicit normalisation of the $U(N_{\rm c})$ generators: $\mathrm{Tr}(T_a\, T_b) = d\,\delta_{ab}$. The standard field theory convention used in [133] is $d = 1/2$ while our choice is $d = 1$, as is prevalent in the D-brane literature. For temperatures above the phase transition, the branes fall into the horizon and so naively the constituent quark mass vanishes. Rather it is probably inappropriate to speak in terms of free quarks in this strongly coupled phase.

2.6.5 Holographic Renormalisation of the D4-brane

The gauge/gravity duality was originally extended to non-AdS backgrounds in [58]. However, until recently the discussion of the boundary counter-terms needed for holographic renormalisation [180] was largely limited to asymptotically AdS backgrounds. It was shown that these techniques can also be applied in backgrounds describing cascading gauge theory [223–227]. In principle, we believe it should be possible to extend these techniques to general gauge/gravity dualities, in some sense by definition to complete the holographic framework. Here we discuss the construction of surface terms which will regulate the Euclidean action of a black Dp-brane throat geometry. Again, while formally this may be

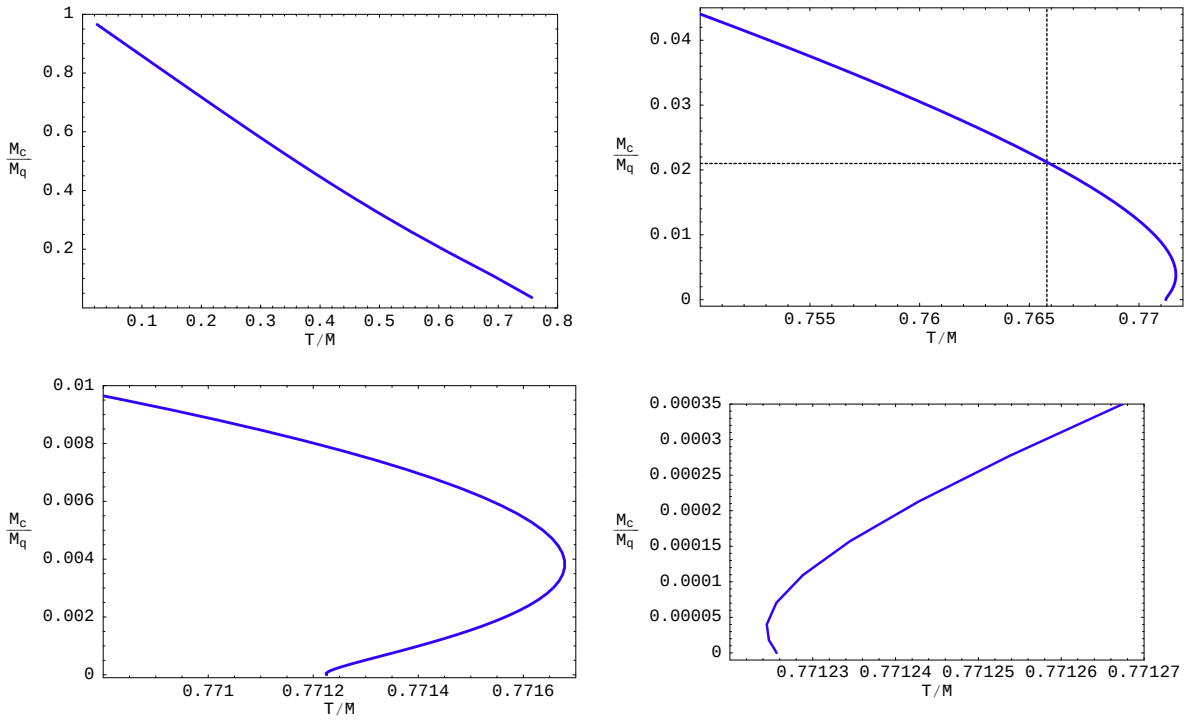

Figure 2.17: Constituent quark mass M_c/M_q as a function of temperature $T/\bar{M}$. The vertical dotted line indicates the temperature of the phase transition while the horizontal line indicates that the constituent quark mass is roughly $M_c/M_q \simeq 0.0212$ at the phase transition. Some plots zooming in on the spiral behaviour for temperatures slightly above the transition temperature are also shown.

problematic as generally the supergravity description is breaking down in the asymptotic region, some such approach should be possible if we believe a gauge/gravity duality exists. We begin a with discussion on the D4-brane background since this is an interesting place given that it lifts to an (asymptotically) $AdS_7 \times S^4$ background for which the counter-terms are known. Hence in principle, all we have to do is dimensionally reduce the latter to express them in terms of the D4-brane description. Given our results for the D4-brane, we make some brief comments on the general Dp-brane backgrounds.

Let us begin by introducing the Euclidean background for a black D4-brane:

$$\begin{aligned} ds^2 &= \left(\frac{r}{L}\right)^{3/2}\left(f(r)\,d\tau^2+d\vec{x}^{\,2}\right)+\left(\frac{L}{r}\right)^{3/2}\left(\frac{dr^2}{f(r)}+r^2d\Omega_4^2\right) \\ C^{(4)}_{\tau 1234} &= -i\left(\frac{r}{L}\right)^3\,, \qquad e^{2\Phi}=\left(\frac{r}{L}\right)^{3/2}\,, \end{aligned} \tag{2.170}$$

where

$$f(r)=1-\frac{{u_0}^4}{r^4} \tag{2.171}$$

and the metric above is in string frame. Recall that the temperature (2.91) and the holographic relations (2.92) for the dual five-dimensional gauge theory are given in section 2.4.

The string-frame geometry lifts to eleven dimensions as usual:

$$ds^2_{11}=e^{-2\Phi/3}(ds^2_{10})+e^{4\Phi/3}dz^2\,, \tag{2.172}$$

which for (2.170) yields

$$\begin{aligned} ds^2 &= \frac{r}{L}\left(f(r)\,d\tau^2+d\vec{x}^{\,2}+dz^2\right)+\left(\frac{L}{r}\right)^2\frac{dr^2}{f(r)}+L^2d\Omega_4^2 \\ &= \left(\frac{u}{\tilde{L}}\right)^2\left(f(u)\,d\tau^2+d\vec{x}^{\,2}+dz^2\right)+\left(\frac{\tilde{L}}{u}\right)^2\frac{du^2}{f(u)}+L^2d\Omega_4^2\,, \end{aligned} \tag{2.173}$$

with $r/L=(u/\tilde{L})^2$, $f(u)=1-(\tilde{\omega}/u)^6$, $\tilde{L}=2L$ and $\tilde{\omega}^2=4Lu_0$. For later discussion, it will be convenient to express the throat geometry as

$$ds^2_{11}=e^{-2\Phi/3}\left(ds^2_{(p+2)-throat}+e^{2\sigma}L^2d\Omega^2_{8-p}\right)+e^{4\Phi/3}dz^2\,. \tag{2.174}$$

Here the geometry described by $ds^2_{(p+2)-throat}$ replaces the AdS space, while the $(p+2)$-dimensional field $e^{2\sigma}$ describes the running of the internal S^{8-p}, and L is the scale which we will use to replace the AdS scale.

Now in the standard holographic story for AdS/CFT one refers to the gravity action in the same dimension as the AdS space. A similar reduction can be done for the Dp-brane throats, *i.e.,* integrate out the internal S^{8-p}, however it seems more natural to think of them as ten-dimensional geometries. Therefore we will consider the bulk action and the Gibbons-Hawking surface term in terms of the full ten (or eleven) dimensions. Note that

in the usual $\mathrm{AdS}_n \times S^m$ examples, these contributions to the action are identical in n and $n+m$ dimensions. In particular, note that the sphere factor is constant and so it does not contribute to the extrinsic curvature in the Gibbons-Hawking term. So the relevant bosonic terms in the Euclidean actions are:

$$I_{\text{bulk}} = -\frac{1}{16\pi G_{11}} \int d^{11}x\sqrt{G}\left(R(G) - \frac{1}{2\cdot 4!}(F^{(4)})^2\right) \tag{2.175}$$

$$= -\frac{1}{16\pi G_{10}} \int d^{10}x\sqrt{g}\left[e^{-2\Phi}\left(R(g) + 4(\nabla\Phi)^2\right) - \frac{1}{2\cdot 4!}(F^{(4)})^2\right], \tag{2.176}$$

where we have only kept the terms needed to evaluate the action for the above solution. Also we have $16\pi G_{11} = (2\pi)^8\ell_P^9$ and $16\pi G_{10} = (2\pi)^7\ell_{\text{s}}^8 g_{\text{s}}^2 = (2\pi)^7\ell_P^9/R_{11}$. One subtlety is that these two bulk actions are only equal up to an integration by parts. As surface terms play an important role in the following, we must keep track of this term. So in reducing the M-theory action to the IIA action, one picks up an additional surface term:

$$-\frac{1}{8\pi G_{10}} \oint d^9x\sqrt{h}\,\frac{14}{3}e^{-2\Phi}\, n\cdot\nabla\Phi\,, \tag{2.177}$$

where h_{ab} denotes the boundary metric in string frame and n is a unit radial vector. Note that the norm of the latter is fixed by the ten-dimensional string-frame metric. Now we also need the Gibbons-Hawking surface term, which in eleven dimensions is:

$$I_{\text{GH}} = -\frac{1}{8\pi G_{11}} \oint d^{10}x\sqrt{H}\,K_{11}(G) \tag{2.178}$$

$$= -\frac{2\pi R_{11}}{8\pi G_{11}} \oint d^9x\sqrt{h}\,e^{-2\Phi}\left(K_{10}(g) - \frac{8}{3}\,n\cdot\nabla\Phi\right). \tag{2.179}$$

Combining the two ten-dimensional surface terms yields

$$I'_{\text{GH}} = -\frac{1}{8\pi G_{10}} \oint d^9x\sqrt{h}\,e^{-2\Phi}\left(K_{10}(g) + 2\,n\cdot\nabla\Phi\right). \tag{2.180}$$

Note that for the D4 throat geometry, the internal S^4 varies with the radial position, and so the full ten-dimensional geometry contributes to $K_{10}(g)$. Hence part of the role of the additional term proportional to the radial gradient of Φ is to cancel the sphere contribution, as the four-sphere does not contribute in the M-theory calculation. One can check that the 'unexpected' dilaton term in eq. (2.180) arises from transforming the standard gravity action from Einstein to string frame.

Now the construction of the remaining boundary counter-terms requires a Kaluza-Klein reduction from ten dimensions [228]. For the case of the D4-brane, we can in principle simply dimensionally reduce the counter-terms for AdS_7, which include a constant or volume term, as well as terms proportional to $\mathcal{R}$ (the intrinsic curvature) and $\mathcal{R}^2$. However, we only want to consider the D4-brane in Poincaré coordinates, *i.e.,* we consider the dual field theory in a flat background geometry. Hence the intrinsic curvature contributions will vanish and we need only consider the volume term. Note that the prefactor for the AdS_7 counter-terms involves $(8\pi G_7)^{-1}$ and so we can think that this arose from dimensionally reducing over the internal S^4. Hence we write the counter-term as:

$$\begin{aligned} I_{ct} &= \frac{1}{8\pi G_{11}} \int_{S^4} d^4x\sqrt{\gamma} \oint_{\partial(AdS_7)} d^6x\sqrt{H}\,\frac{5}{\tilde{L}} \\ &= \frac{1}{8\pi G_{11}}\Omega_4\, L^4 \oint_{\partial M} d^5x\sqrt{h}\,2\pi R_{11}\,\frac{5}{2L}\,\left(e^{2\sigma-2\Phi/3}\right)^{4/2}\left(e^{4\Phi/3}\right)^{1/2}\left(e^{-2\Phi/3}\right)^{5/2} \\ &= \frac{5}{2}\,\frac{\Omega_4\, L^3}{8\pi G_{10}} \oint_{\partial M} d^5x\sqrt{h}\,e^{4\sigma}\,e^{-7\Phi/3}\,. \end{aligned} \tag{2.181}$$

So now given the background (2.170), one calculates the Euclidean action I_E as the sum of the three terms above in eqs. (2.176), (2.180) and (2.181). As usual we divide out by the spatial volume (see footnote 5), in which case all of the thermodynamic quantities are actually densities. In this way we arrive at

$$I_E = -\frac{\Omega_4 L^4}{16\pi G_{10}}\frac{\beta {u_0}^3}{2L^4} = -\frac{2^{10}\pi^7}{3^7 G_{10}}\frac{L^9}{\beta^5} = -\frac{2^5\pi^2}{3^7}\,\lambda\, N_{\rm c}^2\, T^5\,, \tag{2.182}$$

which yields the free energy density given in eq. (2.10). One can also check that this result matches that for a planar AdS_7 black hole [169].

Now one can probably extend the counter-term above to general Dp-brane throats. The prefactor for the $(n-1)$-dimensional counter-terms in $AdS_n \times S^m$ examples involves $(8\pi G_n \tilde{L})^{-1}$. Hence we have implicitly dimensionally reduced over the internal S^m and it seems natural that, for the Dp-branes, the prefactor involve $\Omega_{8-p}L^{7-p}/(8\pi G_{10})\,e^{(8-p)\sigma} = (8\pi G_{p+2}L)^{-1}\,e^{(8-p)\sigma}$. Then it seems the general rule should be that the counter-term takes the form

$$I_{ct} = \frac{A}{8\pi G_{p+2}\,L}\oint_{\partial M} d^{p+1}x\sqrt{h}\,e^{(8-p)\sigma}\,e^{B\Phi}\,, \tag{2.183}$$

where we have written the boundary metric in the string frame, as read off from the ten-dimensional or $(p+2)$-dimensional string-frame metric, *i.e.,* $ds^2_{(p+2)-throat}$ in eq. (2.174).

Then A and B are dimensionless constants which are chosen experimentally to cancel the relevant divergence coming from the bulk and Gibbons-Hawking contributions to the action.

Chapter 3

Holographic phase transitions at finite baryon density

In the previous chapter we studied the thermodynamics of a large class of strongly coupled, large-N_c gauge theories with N_f flavours of fundamental matter using the gravity dual of N_f Dq-brane probes in the near horizon geometry induced by N_c black Dp-branes. It was shown that a universal, first order phase transition occurs at some critical temperature T_{fun}. At low temperatures, the Dq-branes sit outside the black hole in what was dubbed a 'Minkowski' embedding (see figure 2.1), and stable meson bound states exist. In this phase the meson spectrum exhibits a mass gap and is discrete. Above some critical temperature T_{fun} the branes fall through the horizon in what were dubbed 'black hole' embeddings. In this phase the meson spectrum is gapless and continuous. This large-N_c, strong coupling phase transition is therefore associated with the melting of the mesons. In theories that undergo a confinement/deconfinement phase transition at some temperature $T_{deconf} < T_{fun}$, mesonic states thus remain bound in the deconfined phase for the range of temperatures $T_{deconf} < T < T_{fun}$.

As discussed in section 2.5, this physics is in qualitative agreement with that of QCD, in which $s\bar{s}$ and $c\bar{c}$ states, for example, seem to survive the deconfinement phase transition at $T_{deconf} \simeq 175$ MeV [156–160]. It is thus interesting to ask how this physics is modified at finite baryon density. In the presence of N_f flavours of equal mass, the gauge theory possesses a global $U(N_f) \simeq SU(N_f) \times U(1)_q$ symmetry. The $U(1)_q$ charge counts the net number of quarks, *i.e.,* the number of baryons times N_c – see appendix A for details. In

the gravity description, this global symmetry corresponds to the $U(N_{\rm f})$ gauge symmetry on the worldvolume of the $N_{\rm f}$ D-brane probes. The conserved currents associated to the $U(N_{\rm f})$ symmetry of the gauge theory are dual to the gauge fields on the D-branes. Thus, the introduction of a chemical potential $\mu_{\rm b}$ or a non-zero density $n_{\rm b}$ for the baryon number in the gauge theory corresponds to turning on the diagonal $U(1) \subset U(N_{\rm f})$ gauge field on the D-branes.[1,2]

In this chapter we study the gauge theory at constant baryon number density $n_{\rm b}$ [151]. We find that, for any finite value of the baryon number density, the Minkowski embeddings, *i.e.,* embeddings where the probe branes close off above the horizon, are physically inconsistent. Hence at finite $n_{\rm b}$, we focus our study on black hole embeddings. Despite this difference with the $n_{\rm b} = 0$ case, the first order phase transition found there continues to exist here for sufficiently small baryon number density. In this case, however, the transition is between two black hole embeddings. For a sufficiently large baryon number density, there is no phase transition as a function of the temperature. The phase transition ceases to exist at a critical value $n_{\rm b}^*$. These results are summarised in fig. 3.1. This phase diagram also shows a shaded region where the black hole embeddings are found to be thermodynamically unstable. While the boundary of this region shown in the diagram is qualitative, we have found that the unstable region has a limited extent to the left of the line of first order phase transitions. Hence the system must find a new stable phase, at least, in this small region – see section 3.2.

We focus on four-dimensional $\mathcal{N} = 4$ super-Yang-Mills theory coupled to fundamental matter, whose dual description consists of $N_{\rm f}$ D7-branes in the background of $N_{\rm c}$ black D3-branes, but our results hold in other dimensions. Investigations of other holographic systems with a chemical potential have appeared previously in [220, 233–235]. An overview of the chapter is as follows: In section 3.1, we solve for the embedding of the D7-branes in the black D3-brane geometry. Our discussion includes a brief review of the black hole background, the equations of motion determining the embedding, and a careful analysis of the required boundary conditions. In this section, we also discuss the effect of finite

[1]This should not be confused with the chemical potential for R-charge (as considered in, *e.g.,* [229–232]) which is dual to internal angular momentum on the S^5 in the gravity description.

[2]The theories studied here are supersymmetric and hence contain scalars. For these scalars, the chemical potential effectively acts as a negative mass squared. While this leads to an instability for free massless scalars, we expect that the interactions in the present study will stabilise this.

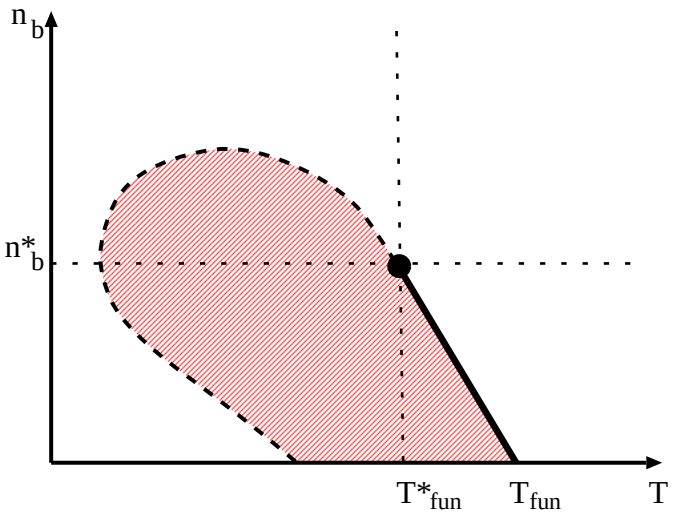

Figure 3.1: Phase diagram: Baryon number n_b versus temperature T. The line of first order phase transitions ends with a critical point at $(T^*_{\rm fun}, n^*_{\rm b})$. The phase which we study is intrinsically unstable in the shaded (red) region. This plot shows only a small portion of the full phase diagram near the critical point. The origin of the axes above corresponds to $(n_{\rm b}, T) = (0, 0.986\, T_{\rm fun})$.

$n_{\rm b}$ on the critical solution and self-similar scaling found at $n_{\rm b} = 0$ in chapter 2 [111, 112]. Finally, we present the results of numerically solving for the embeddings at various values of the baryon number density. Section 3.2 examines the thermal properties of the D7-branes, including their stability or lack thereof. Section 3.3 concludes this chapter with a discussion of results.

3.1 Holographic framework

3.1.1 Black D3-branes

In this section we review relevant aspects of the throat geometries and thermodynamics of black D3-branes, reviewing some formulae from sections 2.1 and 2.3.1 for $p = 3$ which will be needed in this chapter.

As first proposed in [52], $\mathcal{N} = 4$ super-Yang-Mills (SYM) with gauge group $SU(N_{\rm c})$

is holographically dual to type IIB string theory on $AdS_5 \times S^5$ with N_c units of RR five-form flux. The dictionary relating the two sides of the duality equates $g_s = g^2_{YM}/2\pi$ and $L^4/\ell_s^4 = 2g^2_{YM}N_c \equiv 2\lambda$, where L is the AdS curvature scale – for a review, see [53]. In the limit of large N_c and large λ, the string side of the duality reduces to (weakly coupled) classical gravity. At a finite temperature, a black hole appears in the supergravity background [59]. The black hole metric was given in (2.36) and with $\varrho = u_0\rho$ can be written as

$$ds^2 = \frac{1}{2}\left(\frac{\varrho}{L}\right)^2\left[-\frac{f^2}{\tilde{f}}dt^2 + \tilde{f}dx_3^2\right] + \frac{L^2}{\varrho^2}\left[d\varrho^2 + \varrho^2 d\Omega_5^2\right] , \tag{3.1}$$

where

$$f(\varrho) = 1 - \frac{u_0^4}{\varrho^4}, \quad \tilde{f}(\varrho) = 1 + \frac{u_0^4}{\varrho^4} . \tag{3.2}$$

The gauge theory temperature is equivalent to the Hawking temperature of the black hole horizon: $T = u_0/\pi L^2$ – see section 2.1.

As discussed in section 2.1.2, this holographic framework allows the thermal behaviour of the strongly coupled gauge theory to be further studied with standard semiclassical gravity techniques [164]. In particular, the entropy density can be calculated as the geometric Hawking-Bekenstein entropy of the horizon [59, 172][3]

$$S = \frac{\mathcal{A}}{4G\,V_x} = \frac{\pi^6}{4G}\frac{L^8}{\beta^3} = \frac{\pi^2}{2}N_c^2\,T^3 , \tag{3.3}$$

where we have used $16\pi G = (2\pi)^7\ell_s^8\,g_s^2$. The parametric dependence $S \propto N_c^2$ reflects the fact that the gauge theory is deconfined. Remarkably, this strong coupling result differs from that calculated at weak coupling by merely a factor of 3/4 [172].

3.1.2 D7-brane embeddings

As discussed previously, all fields in the $\mathcal{N} = 4$ SYM theory transform in the adjoint representation of the $SU(N_c)$ gauge group and fields transforming in the fundamental representation can be included by introducing an additional set of D-branes on the string theory side of the duality [60, 153]. As in section 2.3.1, we consider the decoupling limit of the intersection of N_c D3-branes and N_f D7-branes described by the array (2.34). The

[3] We divide out by the (formally infinite) three-dimensional volume V_x of the Minkowski space in which the gauge theory is formulated to yield the (finite) entropy density (3.3).

resulting dual gauge theory is $\mathcal{N}=4$ super-Yang-Mills coupled to $N_{\rm f}$ $\mathcal{N}=2$ fundamental hypermultiplets [60, 153] at temperature T in $3+1$ dimensions.

Assuming $N_{\rm f} \ll N_{\rm c}$, the decoupling limit leads to $N_{\rm f}$ probe D7-branes in the background (3.1), with the intersection parametrised by the coordinates $\{t, x^i\}$. As in section 2.3.1, we introduce spherical coordinates $\{r, \Omega_3\}$ in 4567-directions and polar coordinates $\{R, \phi\}$ in the 89-directions and use θ to denote the angle between these two spaces. Taking $\chi = \cos\theta$ to describe the embedding of the D7-branes, translational symmetry in the 0123-space and rotational symmetry in the 4567-directions motivate us to take $\chi = \chi(\varrho)$. The induced metric on the D7-branes is then:

$$ds^2 = \frac{1}{2}\left(\frac{\varrho}{L}\right)^2\left[-\frac{f^2}{\tilde{f}}dt^2 + \tilde{f}dx_3^2\right] + \frac{L^2}{\varrho^2}\left[\frac{1-\chi^2+\varrho^2(\partial_\varrho\chi)^2}{1-\chi^2}\right]d\varrho^2 + L^2(1-\chi^2)d\Omega_3^2\,. \quad (3.4)$$

We also introduce a $U(1)$ gauge field on the worldvolume of the D7-branes. As discussed in detail in appendix A, in order to study the gauge theory at finite chemical potential or baryon number density, it suffices to turn on the time component of the gauge field, A_t. Again, symmetry considerations lead us to take the ansatz $A_t = A_t(\varrho)$. The action of the D7-branes then becomes:

$$I_{\rm D7} = -N_{\rm f}T_{\rm D7}\int d^8\sigma\frac{\varrho^3}{4}f\tilde{f}(1-\chi^2)\sqrt{1-\chi^2+\varrho^2(\partial_\varrho\chi)^2 - 2(2\pi\ell_{\rm s}^2)^2\frac{\tilde{f}}{f^2}(1-\chi^2)F_{\varrho t}^2}\,, \quad (3.5)$$

where $F_{\varrho t} = \partial_\varrho A_t$ is a radial electric field.

The equation of motion for A_t (Gauss' law) gives

$$\partial_\varrho\left[\frac{\varrho^3}{2}\frac{\tilde{f}^2}{f}\frac{(1-\chi^2)^2\partial_\varrho A_t}{\sqrt{1-\chi^2+\varrho^2(\partial_\varrho\chi)^2 - 2(2\pi\ell_{\rm s}^2)^2\frac{\tilde{f}}{f^2}(1-\chi^2)(\partial_\varrho A_t)^2}}\right] = 0\,. \quad (3.6)$$

In the limit that $\varrho\to\infty$, this equation reduces to $\partial_\varrho(\varrho^3\partial_\varrho A_t)\simeq 0$ and so the asymptotic solution approaches

$$A_t \simeq \mu - \frac{a}{\varrho^2} + \cdots\,. \quad (3.7)$$

The constants μ and a are (proportional to) the chemical potential for and the vacuum expectation value of the baryon number density, respectively (see appendix A). The equation of motion (3.6) clearly indicates that there is a constant of motion, which we write

as

$$d \equiv N_{\rm f} T_{D7} (2\pi\ell_{\rm s}^2)^2 \frac{\varrho^3}{2} \frac{\tilde{f}^2}{f} \frac{(1-\chi^2)^2 \partial_\varrho A_t}{\sqrt{1-\chi^2+\varrho^2(\partial_\varrho\chi)^2 - 2(2\pi\ell_{\rm s}^2)^2 \frac{\tilde{f}}{f^2}(1-\chi^2)(\partial_\varrho A_t)^2}} \,. \tag{3.8}$$

With this normalisation, this constant is precisely the electric displacement, $d = \delta I_{\rm D7}/\delta F_{\varrho t}$. Taking the large-$\varrho$ limit of eq. (3.8) with the asymptotic form (3.7), we find:

$$d = N_{\rm f} T_{\rm D7} (2\pi\ell_{\rm s}^2)^2 \, a. \tag{3.9}$$

Now one could proceed to derive the equation of motion for the D7-brane profile $\chi(\varrho)$ from the action (3.5) and then use eq. (3.8) to eliminate A_t in favor of the constant d. Instead, we first construct the Legendre transform of eq. (3.5) with respect to d to eliminate A_t directly at the level of the action. The result is:

$$\begin{aligned} \tilde{I}_{\rm D7} &= I_{\rm D7} - \int d^8\,\sigma F_{\varrho t} \frac{\delta I}{\delta F_{\varrho t}} \\ &= -N_{\rm f} T_{\rm D7} \int d^8\sigma \, \frac{\varrho^3}{4} f\tilde{f}(1-\chi^2)\sqrt{1-\chi^2+\varrho^2(\partial_\varrho\chi)^2}\sqrt{1+\frac{8\,d^2}{(2\pi\ell_{\rm s}^2 N_{\rm f} T_{\rm D7})^2 \varrho^6 \tilde{f}^3 (1-\chi^2)^3}} \,. \end{aligned} \tag{3.10}$$

The gauge field equations resulting from this Legendre transform are simply $\partial_\varrho d = \delta\tilde{I}_{\rm D7}/\delta A_t$ and $\partial_\varrho A_t = -\delta\tilde{I}_{\rm D7}/\delta d$. The first of these reproduces the fact that d is a fixed constant and we will return to the second one below.

Before deriving the equation of motion for the D7-brane profile $\chi(\varrho)$, it is convenient to introduce dimensionless quantities:

$$\rho = \frac{\varrho}{u_0} \,, \qquad \tilde{d} = \frac{d}{2\pi\ell_{\rm s}^2 u_0^3 N_{\rm f} T_{\rm D7}} \,. \tag{3.11}$$

The χ equation from eq. (3.10) can then be written as

$$\begin{aligned} &\partial_\rho \left[\frac{\rho^5 f\tilde{f}(1-\chi^2)\dot{\chi}}{\sqrt{1-\chi^2+\rho^2\dot{\chi}^2}} \sqrt{1+\frac{8\tilde{d}^2}{\rho^6\tilde{f}^3(1-\chi^2)^3}} \right] \\ &= -\frac{\rho^3 f\tilde{f}\chi}{\sqrt{1-\chi^2+\rho^2\dot{\chi}^2}} \sqrt{1+\frac{8\tilde{d}^2}{\rho^6\tilde{f}^3(1-\chi^2)^3}} \left[3(1-\chi^2) + 2\rho^2\dot{\chi}^2 - 24\tilde{d}^2 \frac{1-\chi^2+\rho^2\dot{\chi}^2}{\rho^6\tilde{f}^3(1-\chi^2)^3+8\tilde{d}^2} \right] , \end{aligned} \tag{3.12}$$

where the dot denotes derivatives with respect to ρ, *i.e.,* $\dot{\chi} = \partial_\rho\chi$. With $\rho \to \infty$, this equation becomes, at leading order, $\partial_\rho(\rho^5\dot{\chi}) \simeq -3\rho^3\,\chi$. Hence asymptotically the profile behaves as

$$\chi = \frac{m}{\rho} + \frac{c}{\rho^3} + \cdots \,, \tag{3.13}$$

which is the same asymptotic behaviour found for $n_{\rm b} = 0$ – see section 2.3. As before, the dimensionless constants m and c are proportional to the quark mass and condensate, with the precise relations given in appendix A, eqs. (A.7) and (A.11), respectively [111, 112].

Returning to the gauge field, we begin by introducing a convenient dimensionless potential and chemical potential:

$$\tilde{A}_t = \frac{2\pi\ell_{\rm s}^2}{u_0} A_t \,, \quad \tilde{\mu} = \frac{2\pi\ell_{\rm s}^2}{u_0} \mu \,. \tag{3.14}$$

Then as described above, (3.10) yields the following equation

$$\partial_\rho \tilde{A}_t = 2\tilde{d} \frac{f\sqrt{1-\chi^2+\rho^2\dot{\chi}^2}}{\sqrt{\tilde{f}(1-\chi^2)[\rho^6\tilde{f}^3(1-\chi^2)^3+8\tilde{d}^2]}} \,. \tag{3.15}$$

Integrating yields the potential difference between two radii,

$$\tilde{A}_t(\rho) - \tilde{A}_t(\rho_{\rm min}) = 2\tilde{d}\int_{\rho_{\rm min}}^{\rho} d\rho \frac{f\sqrt{1-\chi^2+\rho^2\dot{\chi}^2}}{\sqrt{\tilde{f}(1-\chi^2)[\rho^6\tilde{f}^3(1-\chi^2)^3+8\tilde{d}^2]}} \,. \tag{3.16}$$

We will see below that all embeddings of interest extend down to the horizon at $\rho = 1$, so $\rho_{\rm min} = 1$ provides a convenient reference point. Further we set $\tilde{A}_t(\rho = 1) = 0$ by the following argument: The event horizon of the background (3.1) can be characterised as a Killing horizon, which implies that it contains the bifurcation surface where the Killing vector ∂_t vanishes [236]. If the potential $\tilde{A}$ as a one-form is to be well defined, then $\tilde{A}_t$ must vanish there. Hence we can use (3.16) to calculate the chemical potential, *i.e.,* $\tilde{A}_t(\infty)$, as

$$\tilde{\mu} = 2\tilde{d}\int_1^{\infty} d\rho \, \frac{f\sqrt{1-\chi^2+\rho^2\dot{\chi}^2}}{\sqrt{\tilde{f}(1-\chi^2)[\rho^6\tilde{f}^3(1-\chi^2)^3+8\tilde{d}^2]}} \,. \tag{3.17}$$

3.1.3 Near-horizon embeddings

In chapter 2 an important role was played by the analysis of the probe brane embeddings in the near-horizon region of the geometry (3.1) [111, 112]. In this section we will see how this analysis is affected by the presence of the electric field on the D7-branes. In fact, we generalise the analysis to consider probe Dq-branes in a black Dp-brane background, along the lines of section 2.2 [111]. These calculations will lead to two main conclusions: The

first is that smooth Minkowski embeddings are unphysical for any non-zero baryon density. The second is that we expect the first order phase transition found in chapter 2 [111, 112] to persist for small values of the baryon density, but to disappear for sufficiently large densities.

In order to focus on the near-horizon region, we set

$$\varrho = u_0 + \frac{L}{u_0} z \,, \quad \theta = \frac{y}{L} \,, \tag{3.18}$$

and expand the metric (2.36) to lowest order in z, y. This yields Rindler space together with some spectator directions which we omit since they play no role in the following:

$$ds^2 = -(2\pi T)^2 z^2 dt^2 + dz^2 + dy^2 + y^2 d\Omega_n^2 + \cdots \,. \tag{3.19}$$

Recall that $T = u_0/\pi L^2$. The integer n is equal to the dimension of the internal sphere wrapped by the probe Dq-branes. For the D3/D7 system $n = 3$, but as stated above our analysis in this section will apply to more general Dp/Dq systems, for which n may not be 3; for example, $n = 2$ for the D4/D6 system studied in section 2.4. The horizon is of course at $z = 0$. The coordinates z and y are the near-horizon analogues of the global coordinates R and r in (2.40), respectively.

In order to describe the embedding of the Dq-branes, we choose the static gauge for all their coordinates except the radial coordinate on the brane, which we denote as σ. The Dq-brane embedding may then be described parametrically as: $z = z(\sigma)$, $y = y(\sigma)$. We modify the analysis of section 2.2 by adding a radial electric field $E \equiv \ell_s^2 \dot{A}_t / T$, where the dot denotes differentiation with respect to σ. For simplicity, in this section we will ignore the overall normalisation of the Dq-branes' action and take $I_{\rm D7} \propto \int d\sigma \mathcal{L}$, where

$$\mathcal{L} = -y^n \sqrt{z^2(\dot{z}^2 + \dot{y}^2) - E^2} \,. \tag{3.20}$$

This action is homogeneous of degree $2 + n$ under the rescaling

$$z \to \alpha z \,, \quad y \to \alpha y \,, \quad E \to \alpha^2 E \,, \tag{3.21}$$

which means that the equations of motion will be invariant under such a transformation. Recall that as first described in [173–175], this scaling symmetry was a key ingredient for self-similarity of the brane embeddings in chapter 2 [111, 112]. However, in the present case with $E \neq 0$, the symmetry does not act within the family of embedding solutions with

a fixed electric field (or rather fixed d – see eq. (3.23) below). Hence we can not expect to find exactly the same self-similar behaviour for branes supporting a fixed chemical potential or baryon density. However, we argue below that the embeddings should behave in approximately the same way at least where the gauge field is a small perturbation on the Dq-brane.

As in the previous subsection, it is convenient to work with the electric displacement

$$d = \frac{\partial \mathcal{L}}{\partial E} = \frac{y^n E}{\sqrt{z^2(\dot{z}^2 + \dot{y}^2) - E^2}}\,, \tag{3.22}$$

which is constant by virtue of Gauss' law. This is the near-horizon analogue of the quantity with the same name introduced in the previous subsection.[4] Note that under the scaling (3.21) d transforms as

$$d \to \alpha^n d\ . \tag{3.23}$$

Inverting the relation (3.22) above, one finds

$$E^2 = \frac{d^2 z^2(\dot{z}^2 + \dot{y}^2)}{d^2 + y^{2n}}\,. \tag{3.24}$$

It is also useful to note the relation

$$\sqrt{z^2(\dot{z}^2 + \dot{y}^2) - E^2} = y^n z \left[\frac{\dot{z}^2 + \dot{y}^2}{d^2 + y^{2n}}\right]^{1/2}\ . \tag{3.25}$$

To eliminate E in favour of d and obtain a functional for $y(\sigma)$ and $z(\sigma)$, we perform a Legendre transformation by defining

$$\tilde{\mathcal{L}} = \mathcal{L} - Ed = -z\sqrt{\dot{z}^2 + \dot{y}^2}\sqrt{d^2 + y^{2n}}\,, \tag{3.26}$$

in analogy with (3.10). It is easily verified that the equations of motion obtained from $\tilde{\mathcal{L}}$ are the same as those obtained by first varying $\mathcal{L}$ and then using eq. (3.24) to eliminate E.

We can conclude from eq. (3.24) that Minkowski embeddings which close off smoothly at the y-axis, such as those considered in chapter 2, are unphysical if $d \neq 0$ [111, 112]. These embeddings are most appropriately described in the gauge $y = \sigma$, and they are characterised by the condition that the brane reaches $y = 0$ at some finite $z = z_0 > 0$. For the brane geometry to be smooth there, we must impose the boundary condition

[4] Note, however, that they differ in their normalisation.

$\dot{z}(0) = 0$. Eq. (3.24) then yields $E^2 = z_0^2$ at $y = 0$. Now even though E remains finite, the tensor field $E dy \wedge dt$ is ill-defined at the origin and so one should conclude that these configurations are singular. This singularity is made clearer by considering the electric displacement d which also remains constant at the origin. However, one should note that as defined in eq. (3.22) d is actually a tensor density and so the norm of the associated tensor field is $\left|\frac{d}{\sqrt{-g}}\frac{\partial}{\partial y}\frac{\partial}{\partial t}\right|^2 \sim d^2/y^{2n}$, which clearly diverges at the origin. The physical reason why Minkowski embeddings are inconsistent is, of course, that the radial electric field lines have nowhere to end if the brane closes off above the horizon. This makes it clear that, although we have obtained this result in the near-horizon approximation, the same conclusion follows from an analysis in the full geometry (2.36).

For D-branes, an electric field on the worldvolume can also be associated with fundamental strings 'dissolved' in the D7-brane [237] – see also the discussion around eq. (A.13). Hence the above statement that the electric field lines have nowhere to end can also be viewed as the fact that the strings have nowhere to end if the brane closes off. However, rather than simply viewing the Minkowski embeddings as unphysical, this point of view lends itself to the interpretation that these embeddings by themselves are incomplete. That is, one could imagine constructing a physical configuration by attaching a bundle of fundamental strings to the brane at $y = 0$ and letting these stretch down to the horizon. The strings resolve the singularity in the electric field since they act as point charges which are the source of this field. However, in such a configuration, the strings and the brane must satisfy a force balance equation at the point where they are connected. It is clear that if the brane closes off smoothly with $\dot{z}(0) = 0$, then they can not exert any vertical force in the z direction to balance the tension of the strings and so this can not be an equilibrium configuration. One might then consider 'cuspy' configurations which close off with a finite $\dot{z}(0)$ but still at some $z = z_0 > 0$. In this case, the branes exert a vertical force and so one must examine the configuration in more detail to determine if the two forces can precisely balance. This analysis requires a more careful treatment of the normalisation of the brane action and the fields than we have presented here. Hence we defer the detailed calculations to the next subsection where we will examine the D7-branes in more detail. However, let us state the conclusion here: no Minkowski embeddings can achieve an equilibrium for any (finite) value of $\dot{z}(0)$. Therefore we discard Minkowski embeddings for the rest of our analysis.

Hence we now turn to consider black hole embeddings which intersect the horizon. Since these reach the horizon $z = 0$ at some $y = y_0$ they are conveniently described in the gauge $z = \sigma$. The appropriate boundary condition in this case is then $\dot{y}(0) = 0$, and the equation that follows from $\tilde{\mathcal{L}}$ is

$$(y^{2n} + d^2)\left[zy\ddot{y} + (1 + \dot{y}^2)y\dot{y}\right] - y^{2n}(1 + \dot{y}^2)nz = 0\,. \tag{3.27}$$

In view of this equation it is clear that we should expect two qualitatively different behaviours for solutions with $y_0^n \gg d$ and $y_0^n \ll d$. In the first case, it is easy to see that $y^n \gg d$ all along the solution, and so we effectively recover the equations of motion for $d = 0$ from chapter 2, namely eq. (2.19) [111, 112], and therefore oscillatory behaviour around a critical solution for large y:

$$y \simeq \sqrt{n}\, z + \xi\,, \quad \xi = \frac{T^{-1}}{(Tz)^{\frac{n}{2}}}\left[a\,\sin(\alpha \log Tz) + b\,\cos(\alpha \log Tz)\right]\,, \tag{3.28}$$

where a, b are determined by y_0. As shown in section 2.2 [111, 112], this oscillatory behaviour eventually leads to the property that the quark condensate is multi-valued as a function of the quark mass, and hence to a first order phase transition (see figure 3.4 and the discussion in the next subsection). We thus expect a similar transition if $y_0^n \gg d$.

Incidentally, note that, unlike in the case $d = 0$, here the 'critical solution' $y = \sqrt{n}\, z$ is not an exact solution of eq. (2.19) but only an approximate solution for large y. In particular, there is no exact solution of the form $y \propto z$ that just touches the horizon except the $y = 0$ solution. Note also that for black hole embeddings eq. (3.24) gives $E \sim z$ as $z \to 0$, leading to a well defined tensor field at the horizon $z = 0$.

We now turn to the case $y_0^n \ll d$, for which the equation of motion (3.27) reduces to

$$z\ddot{y} + (1 + \dot{y}^2)\dot{y} \simeq 0\,, \tag{3.29}$$

whose exact solution is

$$\dot{y} = \frac{z_1}{\sqrt{z^2 - z_1^2}}\,, \tag{3.30}$$

$$y = y_0 + z_1\,\log\left(z + \sqrt{z^2 - z_1^2}\right)c\,, \tag{3.31}$$

where y_0 and z_1 are integration constants. Recall that the boundary conditions should be $y(z = 0) = y_0$ and $\dot{y}(z = 0) = 0$. It is impossible to satisfy these conditions with the

logarithm in eq. (3.31). It is also clearly seen in eq. (3.30) that the general solution is problematic (at $z = z_1$) unless $z_1 = 0$. Hence the only physical solution in this regime is precisely the constant solution: $y = y_0$.

Further, we note that the embedding starts very near the horizon with $y = y_0$ where $y_0^n \ll d$ and so we ask how it makes a transition to some more interesting profile of the full equation (3.27) far from the horizon. The point is that the term $ny^{2n}z$ will eventually grow large and require y to deviate from a constant. Quantitatively, one finds that the transition occurs for $z \sim y_0\,(d/y_0^n)$ where the leading solution has the form

$$y = y_0 + \frac{n}{4}\left(\frac{y_0^n}{d}\right)^2 \frac{z^2}{y_0} + \cdots . \tag{3.32}$$

Hence we see the $O(z^2)$ correction to the constant embedding is enormously suppressed in this regime $y_0^n \ll d$. Note that at $z \sim y_0\,(d/y_0^n)$, the second term is comparable to the first and so the Taylor series is breaking down. However, at this point, we still have $y^n \ll d$ and $\dot{y} \ll 1$. In summary, the solution in this regime is a long spike that emanates from the horizon almost vertically, resembling a bundle of strings.

The analysis above thus leads to the following physical picture. If d is small enough, then there is a set of embeddings in the near-horizon region for which $y_0^n \gg d$, whose physics is similar to that of the $d = 0$ case, explored in chapter 2. In particular, we expect a first order phase transition to occur as a function of the temperature. As d increases, the region where the condition $y_0^n \gg d$ holds gets pushed outside the regime in which the near-horizon analysis is applicable, suggesting that the phase transition as a function of temperature should cease to exist for sufficiently large d. This is precisely what the phase diagram in figure 3.1 confirms. In contrast, the condition $y_0^n \ll d$ can always be met in the near-horizon region, indicating that solutions for which the part of the brane near the horizon behaves as a narrow cylinder of almost constant size, resembling a bundle of strings, exist for all values of d. This is also confirmed by our numerical analysis in the full geometry (as illustrated in figure 3.2), since such type of embeddings can always be realised, for any fixed d, by increasing the quark mass (or equivalently by decreasing the temperature). In the next subsection we analyse some properties of these embeddings more closely.

3.1.4 Strings from branes

The near-horizon analysis above revealed the existence of solutions for which the brane resembles a long narrow cylinder that emanates from the horizon. One's intuition is that this spike represents a bundle of strings stretching between the asymptotic brane and the black hole. Examples in which fundamental strings attached to a D-brane are described as an electrically charged spike solution of the DBI action are well known in flat space [238, 239], in AdS space [240–244] and in other brane backgrounds [245]. Here we would like to formalise this intuition by investigating the core region of our D7-brane embeddings in more detail. This analysis allows us to investigate the boundary conditions for the Minkowski-like embeddings in detail.

We begin by rewriting the Legendre-transformed action (3.10) as

$$\tilde{I}_{\rm D7} = -\frac{T_{\rm D7}}{\sqrt{2}}\int d^8\sigma \frac{f}{\tilde{f}^{1/2}}\sqrt{1+\frac{\varrho^2(\partial_\varrho\chi)^2}{1-\chi^2}}\left[\frac{d^2}{(2\pi\ell_{\rm s}^2 T_{\rm D7})^2}+\frac{N_{\rm f}^2}{8}\varrho^6\tilde{f}^3(1-\chi^2)^3\right]^{1/2}. \qquad (3.33)$$

Now recall that $\chi=\cos\theta$ and consider the last factor in the integrand. If the embedding is very near the axis, *i.e.,* $\chi\simeq 1$, then the second contribution in this factor can be neglected and eq. (3.33) becomes

$$\begin{aligned}\tilde{I}_{\rm D7} &\simeq -n_{\rm q}V_x\frac{1}{2\pi\ell_{\rm s}^2}\int dt\, d\varrho\, \frac{f}{(2\tilde{f})^{1/2}}\sqrt{1+\varrho^2(\partial_\varrho\theta)^2}\\ &= -n_{\rm q}V_x\frac{1}{2\pi\ell_{\rm s}^2}\int dt\, d\varrho\, \sqrt{-g_{tt}\left(g_{\varrho\varrho}+g_{\theta\theta}(\partial_\varrho\theta)^2\right)}\,, \end{aligned} \qquad (3.34)$$

where we have used the relation (A.14) between d and the density of strings $n_{\rm q}$. We recognise the result above as the Nambu-Goto action for a bundle of fundamental strings stretching in the ϱ direction but free to bend away from $\theta=0$ on the S^5. It is interesting to note that the term that was dropped provides precisely the measure factor associated with the x^i and S^3 directions in the limit where the d term vanishes (or is small). In this sense then, the D7-brane forgets about its extent in those directions.

Let us consider the boundary conditions for the configurations which reach the axis $\theta=0$ at some finite ϱ, *i.e.,* for Minkowski-like embeddings. These embeddings would in general have a cusp if $\partial_\varrho\theta$ remains finite at $\theta=0$ (a smooth embedding would correspond to $\partial_\varrho\theta\to\infty$). As discussed in the previous subsection, to produce a potentially physical configuration, we would attach a bundle of fundamental strings to the tip of the brane

(with precisely the density $n_{\rm q}$). However, to produce a consistent static configuration, there must be a balance between the forces exerted by these external strings and the brane along the ϱ-direction. The effective tension of the branes can be evaluated in many ways, but here we consider the calculation:

$$T_{\varrho\varrho} = \frac{2}{\sqrt{-g}}\frac{\delta \tilde{I}_{\rm D7}}{\delta g^{\varrho\varrho}} \simeq n_{\rm q} V_x \, \frac{1}{2\pi\ell_{\rm s}^2}\frac{g_{\varrho\varrho}}{\sqrt{1+g^{\varrho\varrho}g_{\theta\theta}(\partial_\varrho\theta)^2}}\,. \tag{3.35}$$

Now if we wish to calculate the effective tension for a bundle of strings smeared out of the x^i-directions with density $n_{\rm q}$, the same calculation would apply since eq. (3.34) is precisely the fundamental string action. However, these strings would lie vertically along the axis and so we would evaluate eq. (3.35) with $\partial_\varrho\theta = 0$. Hence for a cusp with any non-zero $\partial_\varrho\theta$, the effective tension (3.35) is less than that of the vertical strings. Hence none of these Minkowski-like embeddings can achieve an equilibrium with the attached strings for any finite value of $\partial_\varrho\theta$.[5] We might consider these configurations as the initial data in a dynamical context. Then, given the results above, we see that the strings will pull the brane down the axis to the horizon – a similar discussion appears in a different context in [246]. In any event, we will not consider any of these Minkowski-like embeddings in the remainder of our analysis.

Now let us consider the black hole embeddings that arise from eq. (3.34). In fact, the equations resulting from this action were studied as (a special case of) the string configurations describing Wilson loops in the AdS/CFT correspondence [204, 247, 248]. In general these solutions are loops which begin and end at large ϱ. Hence these are inappropriate in the present context.[6] In this context, at finite temperature, there is another class of string configurations, namely strings that fall straight into the horizon, which display the screening of the quark-antiquark potential. Using this experience, we conclude that the *only* solutions for eq. (3.34) which reach the horizon will be the constant configurations $\theta = \theta_0$. Hence, as we saw in the near horizon analysis, the black hole embeddings near the $\theta = 0$ axis are long narrow cylinders of constant (angular) cross-section.

One should ask how far out these constant profiles are valid as approximate solutions of the full equations derived from eq. (3.33). The approximation that allowed us to derive

[5]The same conclusion applies for the general Dq/Dp-brane configurations discussed in subsection 3.1.3.

[6]If we use only a portion of these solutions, *i.e.,* the configuration is cut-off before reaching the loop's minimum ϱ, the profile describes the cuspy configurations discussed above.

eq. (3.34) required $\tilde{d}^{1/3} \gg \rho \sin\theta$, assuming $\rho \gg 1$. Hence the constant solutions $\theta = \theta_0$ should remain approximate solutions out to $\rho_{\text{transition}} \sim \tilde{d}^{1/3}/\theta_0$ for small $\theta_0 \ll 1$. Beyond this radius we expect the profile should expand out and approach an asymptotically flat brane. However, we can push this transition out to an arbitrarily large radius by taking $\theta_0 \to 0$. This again suggests that with $d \neq 0$, there are D7-brane embeddings which reach the horizon no matter how far the (asymptotic) brane is from the black hole. We will verify this result with numerical investigations of the full solutions for the action (3.33) in the next subsection.

Our analysis of the static D7-brane profiles near $\chi \sim 1$ have confirmed the idea that the embeddings develop a narrow spike that behaves like a bundle of strings stretching between the asymptotic brane and the black hole. It is interesting to extend this idea further by investigating the dynamical properties of these spikes. As a step in this direction, let us consider our framework with the more general ansatz: $\chi(\varrho, t)$ and $A_t(\varrho)$.[7] After a straightforward calculation the Legendre-transformed action becomes

$$\tilde{I}_{\text{D7}} = -T_{\text{D7}} \int d^8\sigma \frac{f}{(2\tilde{f})^{1/2}} \sqrt{1 + \varrho^2(\partial_\varrho\theta)^2 - \frac{2L^4}{\varrho^2}\frac{\tilde{f}}{f^2}(\partial_t\theta)^2} \left[\frac{d^2}{(2\pi\ell_{\text{s}}^2 T_{\text{D7}})^2} + \frac{N_{\text{f}}^2}{8}\varrho^6\tilde{f}^3\sin^6\theta\right]^{1/2} . \tag{3.36}$$

As above, we restrict our attention to the embeddings when they are very close to the axis $\theta \simeq 0$. In this regime, the second contribution in the last factor can be neglected and eq. (3.36) becomes

$$\tilde{I}_{\text{D7}} \simeq -n_{\text{q}} V_x \frac{1}{2\pi\ell_{\text{s}}^2} \int dt\, d\varrho\, \frac{f}{(2\tilde{f})^{1/2}} \sqrt{1 + \varrho^2(\partial_\varrho\theta)^2 - \frac{2L^4}{\varrho^2}\frac{\tilde{f}}{f^2}(\partial_t\theta)^2} . \tag{3.37}$$

Once again we recognise this result as the Nambu-Goto action for a bundle of fundamental strings stretching in the ϱ-direction with dynamical fluctuations in the θ-direction. Hence we are beginning to see that not just the static properties of the spikes, such as the tension, but also their dynamical spectrum of perturbations matches that of a collection of strings; similar results have been seen for the dynamics of the BIon spikes on branes in asymptotically flat spacetime [249]. In this sense we see that, although no fundamental strings are initially manifest, the D7-brane spectrum still captures the presence of these strings. This is a satisfying result since these strings stretching between the horizon and

[7] The symmetries of the problem ensure that this ansatz leads to a consistent solution.

the asymptotic D7-branes are dual to the quarks in the field theory, for which we are turning on the chemical potential μ. It would be interesting to investigate these issues in more detail.

3.1.5 Numerical embeddings

We now return to the detailed analysis of the D7-brane embeddings in the black D3-brane background. In general, it is not feasible to analytically solve eq. (3.12), which determines the profile $\chi(\rho)$, so we resorted to numerics. We numerically integrated eq. (3.12), specifying boundary conditions on the horizon $\rho_{\min} = 1$: $\chi(1) = \chi_0$ for various $0 \leq \chi_0 < 1$ and $\partial_\rho \chi|_{\rho=1} = 0$. In order to compute the constants m, c corresponding to each choice of boundary condition at the horizon, we fitted the solutions to the asymptotic form (3.13). Several representative D7-brane profiles are depicted in figure 3.2. In particular, we see explicitly here the formation of long narrow spikes reaching down to the horizon as χ_0 approaches 1.

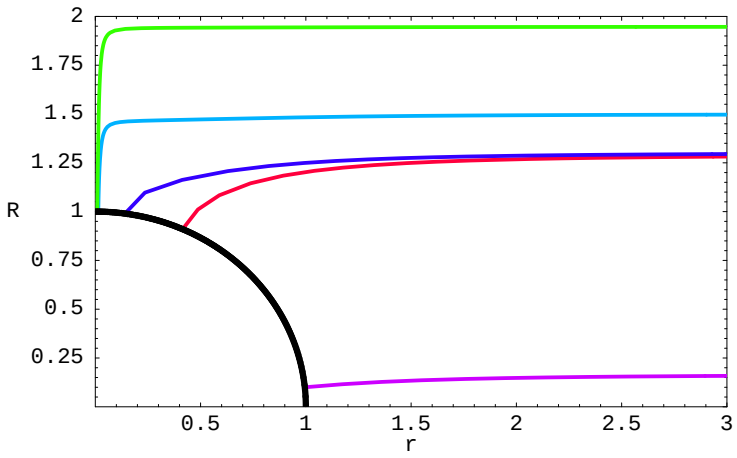

Figure 3.2: Profiles of various D7-brane embeddings in the D3-brane background for $\tilde{d} = 10^{-4}/4$. The black circle represents the horizon.

We can make the appearance of these spikes quantitative here by examining how varying the boundary condition χ_0 changes the quark mass m – recall that the latter is proportional to the distance which the branes reach along the vertical axis of figure 3.2. Figure 3.3 shows

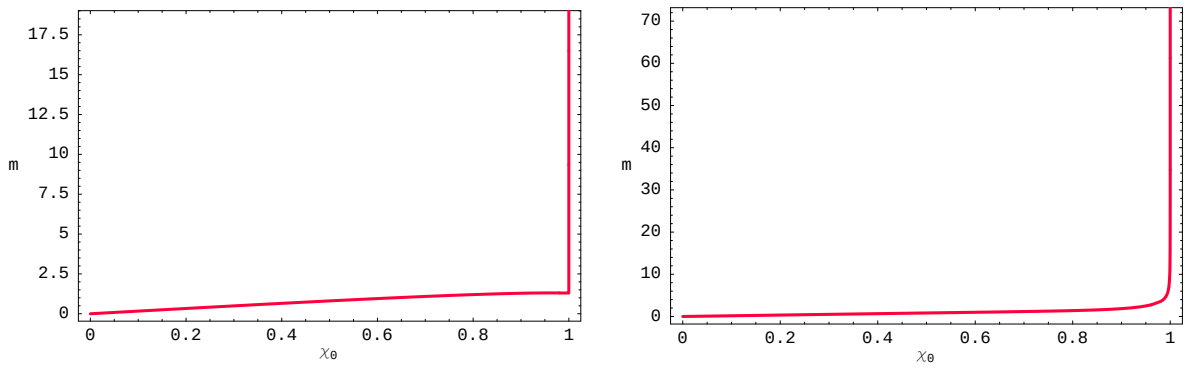

(a) (b)

Figure 3.3: Quark mass m versus boundary condition χ_0 on the horizon for (a) $\tilde{d} = 10^{-4}/4$ and (b) $\tilde{d} = 1/4$.

plots of m versus χ_0 for $\tilde{d} = 10^{-4}/4$ and $1/4$. Note that in both cases, as $\chi_0 \to 1$, the quark mass is diverging. Hence with $\tilde{d} \neq 0$, there are D7-brane embeddings which reach the horizon no matter how large the (asymptotic) separation between the brane and the black hole becomes. Since $m \propto M_{\rm q}/T$ as shown in eq. (A.7), $m \to \infty$ corresponds to $T \to 0$ for a fixed quark mass $M_{\rm q}$. Hence the previous result is equivalent to saying that the D7-branes intersect the horizon for all values of T when $d \neq 0$. Contrast this with the $\tilde{d} = 0$ case of section 2.3, where embeddings of the D7-branes which intersect the horizon (*i.e.,* black hole embeddings) only existed above some minimum temperature [111, 112]. At low temperatures the D7-branes were described by embeddings which smoothly closed off above the horizon (*i.e.,* Minkowski embeddings). For nonzero baryon density, there are black hole embeddings corresponding to all temperatures in the gauge theory. For small temperatures, or large quark mass, most of the brane is very far away from the horizon with only a very thin long spike extending down to touch the horizon. Far from the black hole, this embedding would look very much like a Minkowski embedding in the low temperature phase of $\tilde{d} = 0$. It differs only by the narrow spike going down to touch the horizon.

Figures 3.4, 3.5 and 3.6 illustrate the dependence of the quark condensate c on the temperature T. Several such plots of c versus T with varying degrees of resolution are given in figure 3.4 for small values of the baryon density: $\tilde{d} = 0$, $10^{-6}/4$ and $10^{-4}/4$. In the first two plots, the differences between the curves is virtually indiscernable. In particular

then, they all begin to show the spiralling behaviour that was characteristic of the self-similar scaling discovered for $\tilde{d} = 0$ in chapter 2 [111, 112]. Of course, section 3.1.3 argued that these spirals should persist to a certain level at small $\tilde{d}$. Note that in the highest resolution plot (the last one in fig. 3.4), one sees that for $\tilde{d} = 10^{-4}/4$ the small scale spirals have been eliminated. In any event, the plots in figure 3.4 explicitly demonstrate that, for small baryon density $\tilde{d}$, the black hole embeddings are mimicking the behaviour of both the black hole and Minkowski branches of the theory at $\tilde{d} = 0$. Hence certain features of the physics will be continuous between the theories with vanishing and non-vanishing baryon number density. In particular, the spiralling or rather the multi-valuedness of c indicates there will be a first order phase transition and so the 'melting' transition found in chapter 2 [111, 112] persists to small values of the baryon density.

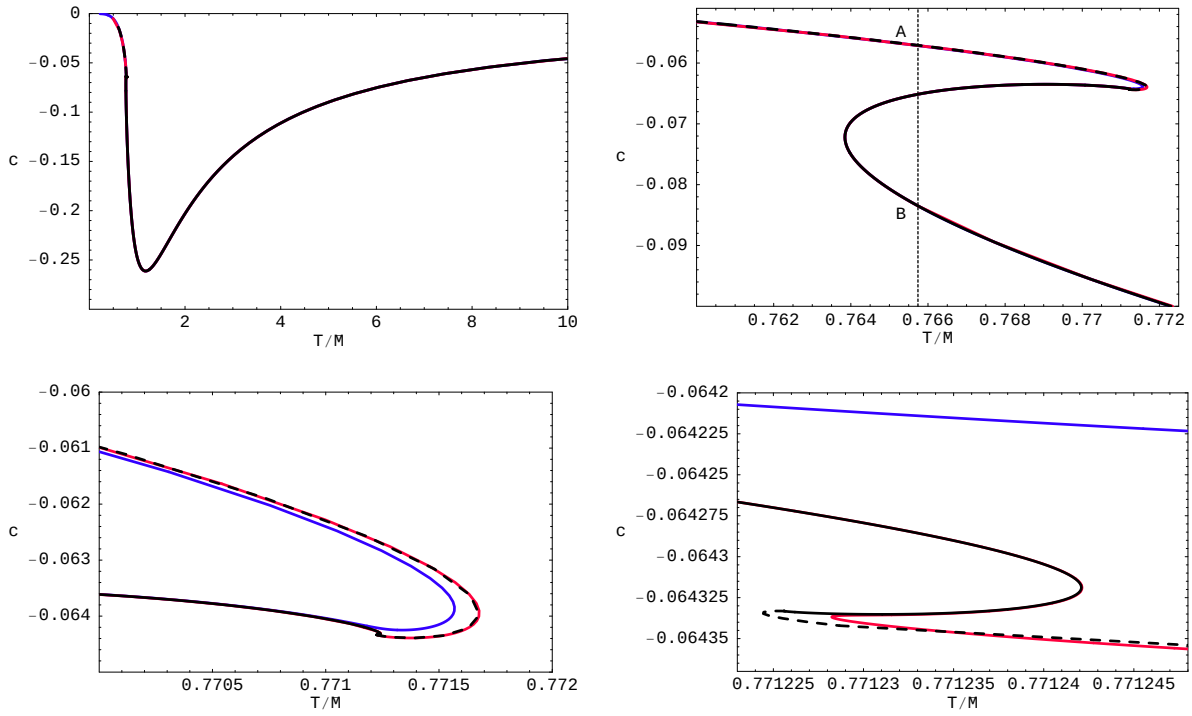

Figure 3.4: Quark condensate c versus temperature $T/\bar{M}$ for $\tilde{d} = 0$, $10^{-6}/4$ and $10^{-4}/4$ on the black, red and blue curves, respectively. At low resolution, these curves are all nearly identical and display a similar spiralling behaviour.

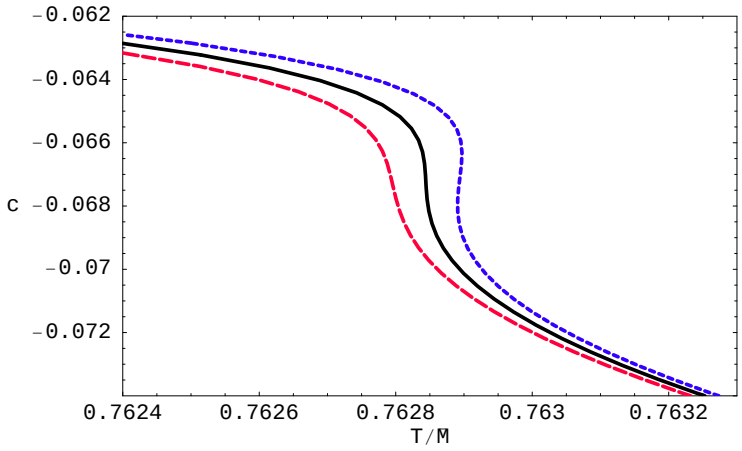

Figure 3.5: Quark condensate c versus temperature $T/\bar{M}$ near the critical point. The solid black curve corresponds to the critical baryon density $\tilde{d}^* = 0.00315$. The dashed curves above (blue) and below (red) correspond to $\tilde{d} = 0.0031$ and 0.0032, respectively.

As $\tilde{d}$ is increased, the self-similar, spiralling behaviour becomes less and less pronounced and eventually c becomes a single-valued function of $T/\bar{M}$. To the best numerical accuracy that we could achieve, the critical value at which the phase transition disappears is $\tilde{d}^* = 0.00315$. Figure 3.5 shows c in the vicinity of the transition around this critical value. For $\tilde{d} = 0.0031$, the curve shows a slight S-shape and so a small first order phase transition would still occur. For the critical value $\tilde{d}^* = 0.00315$, the curve is monotonic but with a singular slope near the centre. In this case, the phase transition would be reduced to second order. Finally for $\tilde{d} = 0.0032$, the curve is monotonic with a finite slope everywhere and so the phase transition has disappeared.

For completeness, we also show the behaviour of the quark condensate at much larger values of the baryon density in figure 3.6. Figure 3.6a corresponds to $\tilde{d} = 1/4$ where some interesting structure still persists around $T/\bar{M} \sim 1$, which was where c shows a minimum in figure 3.4 at smaller densities. Figure 3.6b corresponds to $\tilde{d} = 10$, where c has become a monotonically increasing (towards zero) function of T.

We integrated (3.17) numerically to solve for the chemical potential. Plots of $\tilde{\mu}$ versus temperature all show an apparent divergence as $T/\bar{M} \to 0$, as illustrated in figure 3.7a. However, this behaviour is misleading as we now explain. As discussed in the previous

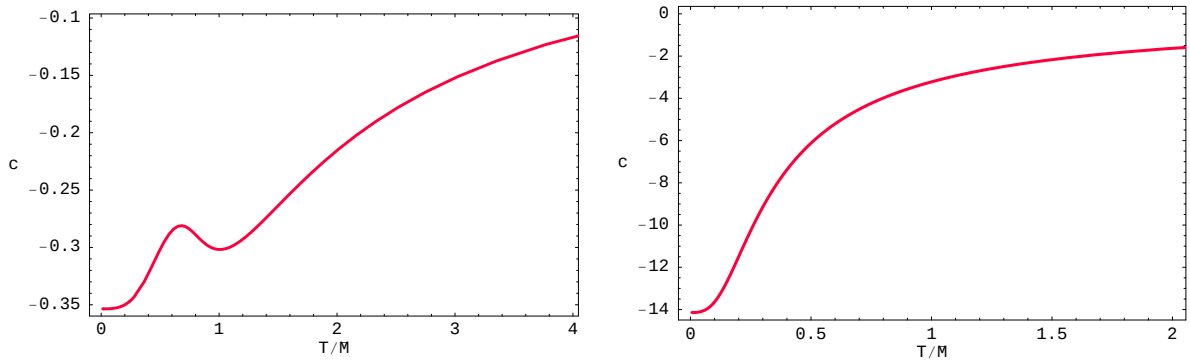

(a) (b)

Figure 3.6: Quark condensate c versus temperature $T/\bar{M}$ for (a) $\tilde{d} = 1/4$ and (b) $\tilde{d} = 10$.

subsections, a common feature of the D7-brane embeddings at small temperatures is the long narrow spike close to the $\theta = 0$ axis. This spike dominates eq. (3.17) for small $T/\bar{M}$ and so the latter formula can be simplified to

$$\mu \simeq \frac{1}{\sqrt{2}2\pi\ell_s^2}\int_{u_0}^{u_0 m} d\varrho\, f/\tilde{f}^{1/2} \simeq M_{\rm q}\,, \tag{3.38}$$

where we have restored the dimensions of the chemical potential and the radial coordinate. Hence in this limit, the chemical potential is essentially given by the quark mass, as one might have expected. Hence the divergence in figure 3.7a arises simply because $\tilde{\mu} \propto \mu/T$, as shown in eq. (A.20). This spurious behaviour is eliminated by plotting $\mu/M_{\rm q} = \sqrt{2}\tilde{\mu}/m$, as shown in figure 3.7b. The latter plot exhibits the small temperature limit $\mu/M_{\rm q} \to 1$ for T approaching zero, as is implied by eq. (3.38). Note that if one calculates μ in the vicinity of the phase transition, it shows a multi-valuedness similar to that shown for the quark condensate above.

3.2 D7-brane thermodynamics: Free energy, entropy and stability

We now wish to study the thermal properties of the fundamental hypermultiplets at finite baryon number. As in chapter 2, our holographic framework translates this question into

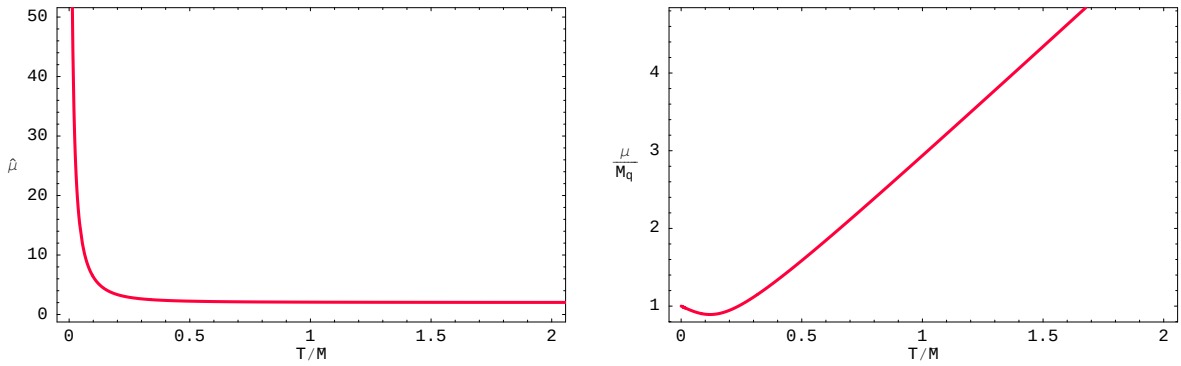

(a) (b)

Figure 3.7: Chemical potential for $\tilde{d} = 10$ versus temperature displayed as: (a) $\tilde{\mu}$ and (b) $\mu/M_{\rm q}$.

one of investigating the thermal contributions of the D7-branes on the gravity side. As usual, we use the standard technique [164] of Wick rotating the time direction. The Euclidean time circle of the black D3-brane background then becomes the thermal circle in a finite temperature path integral, and the leading contribution to the free energy is determined by evaluating the Euclidean action. As we are interested in the contributions of the fundamental matter, we only study the action of the D7-branes. As in section 2.3.2, evaluating the bulk brane action leads to a formally divergent result and the AdS/CFT correspondence provides a prescription to remove these divergences: One introduces a finite-radius UV cut-off and a set of boundary counterterms to renormalise the action [178]. This approach for the branes is completely analogous to the same calculations which are performed for the gravity background [165–169]. This holographic renormalisation of the D7-brane action was discussed in more detail in section 2.3.2 [111, 112], which we follow closely here.

We begin by writing the Euclidean action for the D7-branes in terms of dimensionless

quantities, introduced in section 3.1.2, as[8]

$$I_{\rm bulk} = \int d^8\sigma\, \mathcal{L}_{\rm E} = \mathcal{N}\int d\rho\, \rho^3 f\tilde{f}(1-\chi^2)\sqrt{1-\chi^2+\rho^2\dot{\chi}^2 - \frac{2\tilde{f}}{f^2}(1-\chi^2)\dot{\tilde{A}}_t^2}\,, \tag{3.39}$$

where $\mathcal{N}$ is the normalisation constant introduced in eq. (2.43) [111, 112]:[9]

$$\mathcal{N} = \frac{2\pi^2 N_{\rm f} T_{\rm D7} u_0^4}{4T} = \frac{\lambda N_{\rm c} N_{\rm f} T^3}{32}\,.$$

The normalisation factor illustrates the fact that the leading contributions of the fundamental matter are proportional to $N_{\rm c}\, N_{\rm f}$, in accord with the large-$N_{\rm c}$ counting rules of the gauge theory. Note then that these contributions are subleading to those of the adjoint fields which scale as $N_{\rm c}^2$ – see, for example, the entropy density in eq. (3.3).

As commented above, this bulk action (3.39) contains large-ρ, UV divergences. Fortunately, however, these are the same as in the absence of the gauge field, and therefore no new counterterms are required beyond those derived in section 2.3.2 [111, 112], which take the form

$$\frac{I_{\rm bound}}{\mathcal{N}} = -\frac{1}{4}\left(\rho_{\rm max}^4 - 2m^2\rho_{\rm max}^2 + m^4 - 4mc\right)\,, \tag{3.40}$$

where $\rho_{\rm max}$ is the UV cut-off. The regularised D7-brane action is then $I_{\rm E} = I_{\rm bulk} + I_{\rm bound}$. It can most simply be written as:

$$\frac{I_{\rm E}}{\mathcal{N}} = G(m) - \frac{1}{4}\left[({\rho_{\rm min}}^2 - m^2)^2 - 4mc\right]\,, \tag{3.41}$$

where $G(m)$ is the integral:

$$G(m) = \int_{\rho_{\rm min}}^{\rho_{\rm max}} d\rho \left(\rho^3 f\tilde{f}(1-\chi^2)\sqrt{1-\chi^2+\rho^2\dot{\chi}^2 - \frac{2\tilde{f}}{f^2}(1-\chi^2)\dot{\tilde{A}}_t^2} - \rho^3 + m^2\rho\right)\,. \tag{3.42}$$

The limit $\rho_{\rm max}\to\infty$ may now be taken, since this integral converges.

[8] For simplicity, we have left A_t untouched here rather than introducing a Wick rotated potential $A_{t_{\rm E}} = -i\, A_t$. As is well-known, such a Euclidean potential would have to be treated as an imaginary field in the present context because the chemical potential and particle density must remain real constants – see, *e.g.,* [229, 230].

[9] Note that this constant does not include the three-volume V_x along the gauge theory directions. Rather in this section we will divide out these factors everywhere and so all extensive quantities are actually densities per unit volume; for example, (3.39) is the Euclidean action density.

As usual, we wish to identify the action with a thermodynamic free energy. However, in the present case, there are various possibilities depending on the ensemble under consideration, *i.e.,* the Gibbs free energy for the grand canonical ensemble with fixed μ and the Helmholtz free energy for the canonical ensemble with fixed $n_{\rm b}$. Experience with similar calculations for charged black holes, *e.g.,* [229, 230], suggests that the Gibbs free energy is given by the Euclidean action while the Helmholtz free energy is associated with the Legendre transform of $I_{\rm E}$.

In the following, we confirm these expectations. Using the equations of motion, the variation of the action reduces to a boundary term:

$$\delta I_{\rm E} = \left[\frac{\partial \mathcal{L}_{\rm E}}{\partial \dot{\chi}} \delta\chi + \frac{\partial \mathcal{L}_{\rm E}}{\partial \dot{\tilde{A}}_t} \delta\tilde{A}_t \right]_{\rho_{\rm min}}^{\rho_{\rm max}} . \tag{3.43}$$

Combining this with the variation of the boundary action $I_{\rm bound}$ (3.40) yields

$$\delta I_{\rm E} = -2\mathcal{N} c\, \delta m - \frac{n_{\rm q}}{T} \delta\mu \tag{3.44}$$

where $n_{\rm q}$ was defined in (A.14). Recalling that $m = \bar{M}/T$ we see that the natural thermodynamic variables of the Euclidean action are the temperature T and the chemical potential μ. Hence we must identify $I_{\rm E} = \beta W$, where $W(T,\mu)$ is the thermodynamic potential in the grand canonical ensemble, namely the Gibbs free energy.

Since we wish to work at fixed charge density, *i.e.,* in the canonical ensemble, we perform a Legendre transformation by defining

$$\tilde{I}_{\rm E} = I_{\rm E} + \frac{n_{\rm q}\,\mu}{T} , \tag{3.45}$$

which of course is a function of the temperature and the charge density:

$$\delta\tilde{I}_{\rm E} = -2\mathcal{N}\, c\, \delta m + \frac{\mu}{T}\, \delta n_{\rm q} . \tag{3.46}$$

We thus identify $\tilde{I}_{\rm E} = \beta F$ where $F(T, n_{\rm q})$ is the Helmholtz free energy.

The bulk part of $\tilde{I}_{\rm E}$ is of course the Euclidean analogue of (3.10):

$$\frac{\tilde{I}_{\rm bulk}}{\mathcal{N}} = \int d\rho\, \rho^3\, f\tilde{f}(1-\chi^2)\sqrt{1-\chi^2+\rho^2\dot{\chi}^2} \left[1 + \frac{8\tilde{d}^2}{\rho^6 \tilde{f}^3 (1-\chi^2)^3} \right]^{1/2} . \tag{3.47}$$

Since the divergences of this bulk action are the same as those of the $\tilde{d} = 0$ case, the analogous expression to eq. (3.41) is now

$$\frac{\tilde{I}_{\rm E}}{\mathcal{N}} = \widetilde{G}(m) - \frac{1}{4}\left[(m^2-1)^2 - 4mc\right] , \tag{3.48}$$

where $\widetilde{G}(m)$ is the integral:

$$\widetilde{G}(m) = \int_1^\infty d\rho \left[\rho^3 f \tilde{f}(1-\chi^2)\sqrt{1-\chi^2+\rho^2\dot{\chi}^2}\sqrt{1+\frac{8\tilde{d}^2}{\rho^6\tilde{f}^3(1-\chi^2)^3}} - \rho^3 + m^2\rho\right] . \tag{3.49}$$

In both of these expressions, we have replaced $\rho_{\rm min} = 1$ since all of the embeddings which we consider terminate at the horizon.

We evaluated the free energy numerically for various $\tilde{d}$ and representative results are given in figures 3.8 and 3.9. The behaviour of the action versus temperature in figure 3.8 for $\tilde{d} = 10^{-4}/4$ is nearly identical to that for $\tilde{d} = 0$ – see fig. 2.5. The results for $\tilde{d} = 10^{-4}/4$ are typical for small values of $\tilde{d}$ with the classic 'swallow tail' shape. Of course, the crossing point of the two branches coming in from small and large T marks the temperature of the phase transition. By varying $\tilde{d}$, one can then map out the phase diagram shown above in figure 3.1. A more detailed diagram is shown here in figure 3.10. We see here that the first order phase transition occurs along a segment starting at $T_{\rm fun}/\bar{M} = .7658$ at $\tilde{d} = 0$ and ending at the critical point at $T^*_{\rm fun}/\bar{M} = .7629$ and $\tilde{d}^* = 0.00315$.

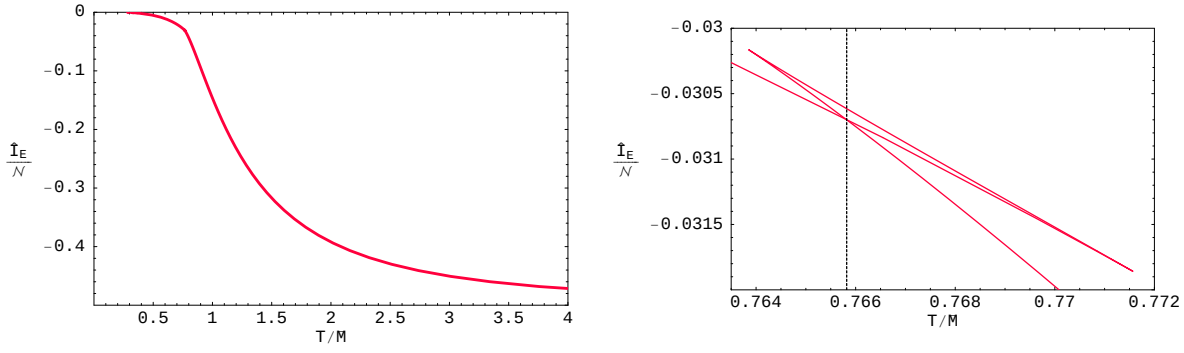

Figure 3.8: Legendre transform of the action, $\tilde{I}_{\rm D7}$, versus temperature for $\tilde{d} = 10^{-4}/4$. The phase transition temperature is denoted by the dotted vertical line in the second plot.

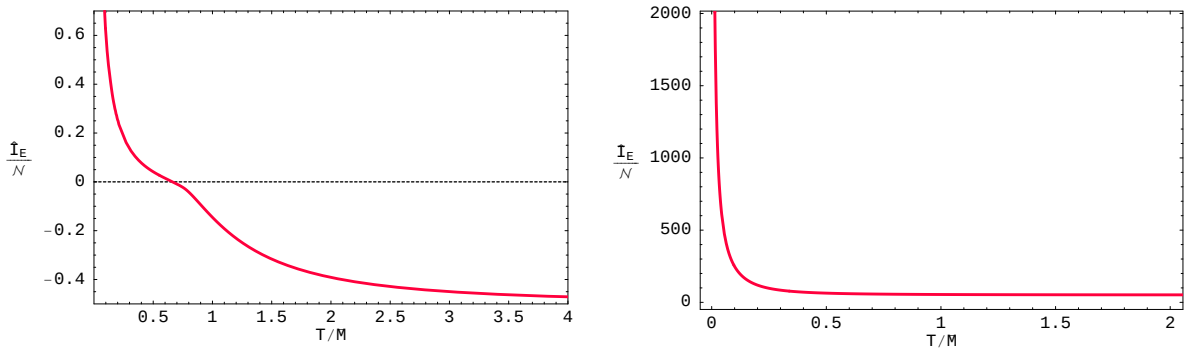

Figure 3.9: Legendre transform of the action, $\tilde{I}_{\rm D7}$, versus temperature for (a) $\tilde{d} = 10^{-1}/4$ and (b) $\tilde{d} = 10$. There is no phase transition for these values of $\tilde{d}$.

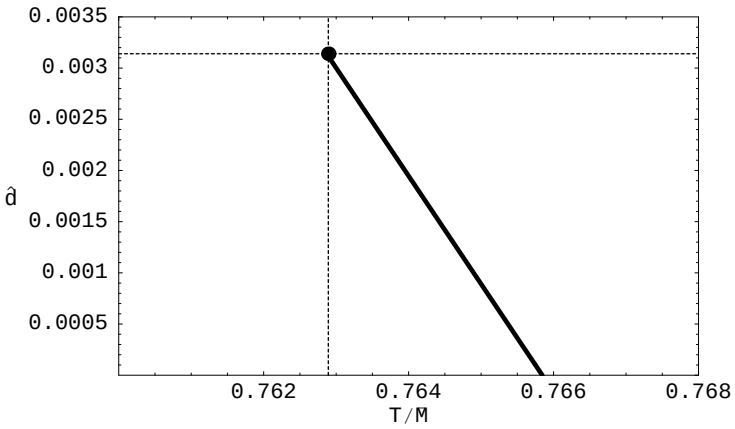

Figure 3.10: Phase diagram: Baryon density $\tilde{d}$ versus temperature $T/\bar{M}$.

For completeness, we show some representative plots for large values of $\tilde{d}$ in figure 3.9, where there is no crossing and no phase transition. Note that these plots show an apparent divergence as $T \to 0$ but this is a spurious effect in analogy to the discussion of the plots for the chemical potential. This artifact is actually present in all of the free energy plots but the width becomes very narrow at small $\tilde{d}$.

We now turn to the entropy density. This can be obtained by differentiating the Helmholtz free energy density $F(T,d) = T\tilde{I}_{\rm E}$ with respect to T as

$$S = -\frac{\partial F}{\partial T} = -\pi L^2 \frac{\partial F}{\partial u_0}\,, \tag{3.50}$$

where we used the relation $u_0 = \pi L^2 T$. Following the calculations described in section 2.6.2 [112], one must carefully consider all of the implicit u_0 dependence in (3.48). The only new contribution comes here from the appearance of $\tilde{d}$ in (3.49) since from (3.11), we can see that

$$\frac{\partial \tilde{d}}{\partial u_0} = -\frac{3}{u_0}\tilde{d}\,. \tag{3.51}$$

Gathering all the contributions, the entropy can be expressed as

$$\frac{S}{\mathcal{N}} = -4\widetilde{G}(m) + 24\tilde{d}^2 H(m) + (m^2-1)^2 - 6mc\,, \tag{3.52}$$

where we have defined the integral

$$H(m) = \int_1^\infty d\rho\, \frac{f\sqrt{1-\chi^2+\rho^2\dot{\chi}^2}}{\rho^3\tilde{f}^2(1-\chi^2)^2}\left[1+\frac{8\tilde{d}^2}{\rho^6\tilde{f}^3(1-\chi^2)^3}\right]^{-1/2}\,. \tag{3.53}$$

Comparing this expression to eq. (3.17), we see that $H = \tilde{\mu}/2\tilde{d}$. Hence we may write the final result as

$$\frac{S}{\mathcal{N}} = -4\widetilde{G}(m) + 12\,\tilde{d}\tilde{\mu} + (m^2-1)^2 - 6mc\,. \tag{3.54}$$

We evaluated the entropy numerically for various $\tilde{d}$ and some typical results are given in figs. 3.11 and 3.12. The behaviour of the entropy versus temperature in figure 3.11 for $\tilde{d} = 10^{-4}/4$ is nearly identical to that for $\tilde{d} = 0$ – see figure 2.5. In particular, near the phase transition point, the curve is multi-valued because there are several embeddings with the same values of $\tilde{d}$ and $T/\bar{M}$. Figure 3.12 shows the behaviour of the entropy for larger values of $\tilde{d}$ beyond the critical point.

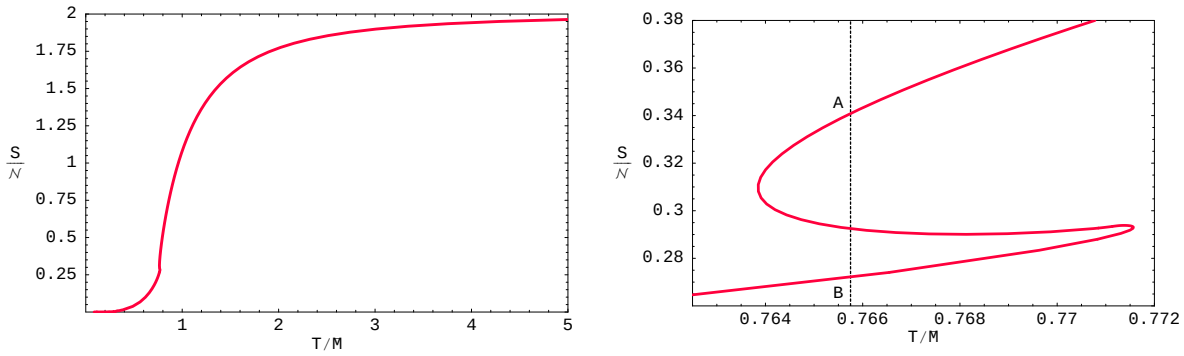

Figure 3.11: The entropy $S/\mathcal{N}$ versus temperature $T/\bar{M}$ for $\tilde{d} = 10^{-4}/4$. The position of the phase transition is marked by the dotted vertical line in the second figure.

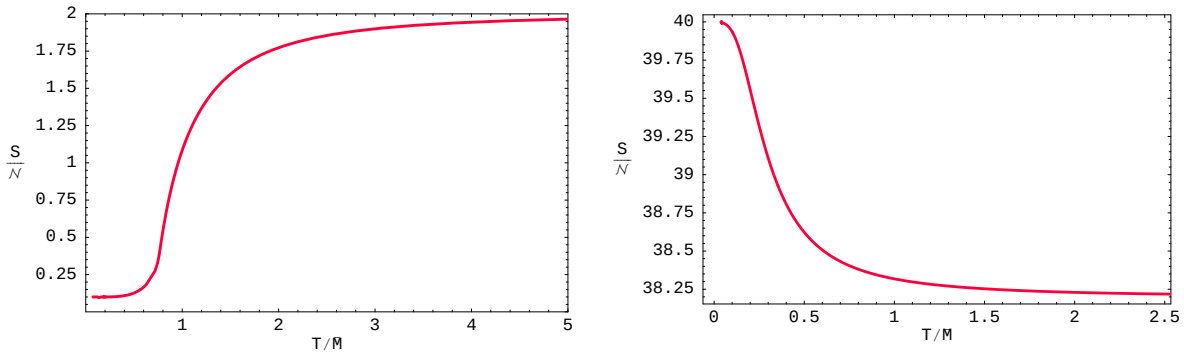

(a) (b)

Figure 3.12: The entropy $S/\mathcal{N}$ versus temperature $T/\bar{M}$ for (a) $\tilde{d} = 10^{-1}/4$ and (b) $\tilde{d} = 10$.

The thermodynamic identity $E = F + T\,S = T(\tilde{I}_{\rm E} + S)$ allows us to determine the contribution of the D7-brane to the energy density:

$$\frac{E}{\mathcal{N}T} = -3\widetilde{G}(m) + 12\,\tilde{d}\tilde{\mu} + \frac{3}{4}\left[(m^2-1)^2 - \frac{20}{3}mc\right] . \tag{3.55}$$

While we did calculate E for many values of $\tilde{d}$, we do not present any plots here as qualitatively their behaviour is similar to that in the plots of the entropy.

Finally, we turn to the thermodynamic stability of the system. There are various ways to write the requirements for the intrinsic stability of our fixed-charge ensemble. We investigated stability here with the conditions:

$$\frac{\partial S}{\partial T} > 0 \ , \qquad \frac{\partial \mu}{\partial n} > 0 \ . \tag{3.56}$$

The first one requires that the system be stable against fluctuations in energy and seems to be satisfied everywhere. The second constraint for electrical stability is more interesting, as we found that it was not satisfied for all $\tilde{d}$ and T. Our investigations of the region of instability remain preliminary, but figure 3.1 roughly illustrates the extent of the unstable zone as the shaded (red) region. In particular, the line of the phase transition seems to be part of the boundary of the unstable region between $T^*_{\rm fun}$ and $T_{\rm fun}$. This would indicate that the black hole embeddings do not correctly describe the true ground state in this small region and in particular, just below the phase transition. We hope to return to this matter in the future. We comment more on the implications of the instability in the discussion section below.

3.3 Discussion

In chapter 2 [111, 112] we identified a universal, first order thermal phase transition in holographic Dp/Dq systems. This was characterised by a jump of the Dq-branes between a Minkowski embedding and a black hole embedding in the background of the black Dp-branes. In the gauge theory this transition is associated with the melting of the mesons.

In the present chapter we have shown that Minkowski embeddings become inconsistent at any finite baryon (or equivalently, quark) number density. The physical reason is that a non-zero density which is dual to a worldvolume electric field translates into a finite number of strings being dissolved into the Dq-branes. Hence the brane is not allowed to

close off smoothly as the strings cannot simply terminate. We considered the possibility of Minkowski-like embeddings where the branes close off above the horizon and external fundamental strings are attached at this point and extend down to the horizon. However, examining the forces between the cusp in the brane embedding and the external strings, one finds that no equilibrium configuration is possible. Rather the strings would pull the tip of the brane down to meet the horizon. We note here though that this is not the only possibility for a Minkowski-like embedding. One must simply attach a source for the strings and one obvious alternative for such a source is the baryon vertex [240–244]. In a Dp-brane background, the baryon vertex consists of a D(8–p)-brane wrapping the internal S^{8-p}. Hence it may be that there is a family of Minkowski-like embeddings, where a gas of baryons absorbs the strings dissolved on the probe branes. It would be interesting to investigate this possibility further.

On the other hand, we did find that with any non-zero baryon density $n_{\rm b}$, black hole embeddings where the Dq-branes intersect the horizon exist for all values of the temperature. In contrast, such embeddings do not exist below a certain temperature for $n_{\rm b} = 0$ and the system must be described by a Minkowski embedding beyond this point. In any event, we focussed here on studying the behaviour of the black hole embeddings at finite $n_{\rm b}$ in the specific example of the D3/D7 system. Our results indicate that the physics is essentially continuous around $n_{\rm b} = 0$. The reason is that black hole embeddings with very small $n_{\rm b}$ mimic the behaviour of both $n_{\rm b} = 0$ Minkowski embeddings and $n_{\rm b} = 0$ black hole embeddings. Moreover, the near-horizon analysis strongly suggested that the universal phase transition found in chapter 2 [111, 112] should persist for sufficiently small baryon densities, but that it should cease to exist above some critical value $n_{\rm b} = n_{\rm b}^*$. This was confirmed by our detailed numerical analysis for the D3/D7 system. We emphasise though that the transition at small baryon density occurs between two black hole embeddings.

At zero baryon number density, the spectrum on Minkowski embeddings consists of a gapped, discrete set of stable mesons (in the large-$N_{\rm c}$, strong coupling limit), together with stable, massive, free constituent quarks – see chapter 2 [111, 112]. Instead, mesons on black hole embeddings have melted and and the spectrum is continuous and gapless. In fact, little evidence of the previously stable states remains in this continuous spectrum – see chapter 5 [126]. In addition, constituent quarks are massless. In the presence of a non-zero baryon density, all embeddings are of black hole type and hence no strictly stable mesons exist. Note, however, that the decay width is very small if the quark mass is very

large, or if the meson is very heavy. Indeed, the decay width of a meson is proportional to the support of its wave function on the near-axis region where the spike attaches to the branes. This region becomes small as the quark mass increases. Alternatively, the peak of the meson wave function occurs further and further away from the axis as the meson mass increases – which, for fixed quark mass, can be achieved by, for example, increasing the meson radial quantum number. We plan to study these issues in more detail elsewhere.

Similarly, it may seem that the free constituent quarks represent a puzzle in this framework. Recall that the dual gauge theory is deconfined and so free quarks should play a role, in particular since we introduce a chemical potential. The analysis at $n_{\rm b} = 0$ suggests that at least at low temperatures a constituent quark is dual to a string extending from the horizon to the brane (at large radius). However, at finite $n_{\rm b}$, our embeddings are all of the black hole type and so if we attach such a string to the brane, it will quickly slip away behind the horizon. Hence the puzzle is: How do the D7-branes capture the physics of a gas of constituent quarks at low temperatures when there are no stable excitations corresponding to macroscopic strings?

Of course, the resolution of this puzzle is provided by the analysis in subsection 3.1.4. The near-horizon analysis of the Dp/Dq system suggested that, for any value of the baryon density, there should exist Dq-brane embeddings which closely resemble Minkowski embeddings everywhere except for a long thin spike stretching all the way down to the black Dp-branes horizon. This was confirmed for the D3/D7 case by our numerical results, which demonstrate that such embeddings correspond to large quark masses (or low temperatures). Further, we showed that not only do these spikes match the tension of a bundle of fundamental strings, but also their dynamics. Hence these spikes provide a brane realisation of the desired gas of constituent quarks. Since the fields describing the D7-branes are dual to meson operators (*i.e.,* operators with $n_{\rm q} = 0$) in the gauge theory, we may say that, in a very precise sense, quarks are being built out of mesons here, in the limit of large quark masses.

In considering the discussion above, one must remember that part of our phase diagram 3.1 corresponds to unstable embeddings. In particular, the line of the phase transition seems to be part of the boundary of the unstable region. This would indicate that the black hole embeddings do not correctly describe the true ground state of the phase immediately below the phase transition. Hence while one should not doubt the existence of a phase transition, the precise location of the transition can be called into question. Recall however,

that for small $\tilde{d} \neq 0$ the behaviour of the black hole embeddings matched everywhere the known behaviour of the system with $\tilde{d} = 0$ very closely, as illustrated in fig. 3.4. Hence we expect that the true line of phase transitions must be very close to that indicated in fig. 3.10 for small $\tilde{d}$ but it may deviate to the right at larger values of $\tilde{d}$. We also reiterate that we are still refining our results on the boundary of the unstable region and that fig. 3.1 only gives a qualitative representation beyond $T^*_{\rm fun}$. It may also be that the region below the phase transition line very close to $T_{\rm fun}$ is stable.

The instability arises in the region where

$$\left(\frac{\partial \mu}{\partial n_{\rm b}}\right)_T = \left(\frac{\partial^2 F}{\partial n_{\rm b}^2}\right)_T < 0\,. \tag{3.57}$$

It would be interesting to identify what the stable ground state is in this region. One indication comes from the nature of the instability itself. In the region where (3.57) holds the free energy F is a concave function of the baryon density, which means that the system can lower its free energy by separating into two phases with densities $n_{\rm b}^1 < n_{\rm b} < n_{\rm b}^2$ such that

$$\gamma n_{\rm b}^1 + (1-\gamma) n_{\rm b}^2 = n_{\rm b}\,, \quad \gamma F(n_{\rm b}^1) + (1-\gamma) F(n_{\rm b}^2) < F(n_{\rm b})\,. \tag{3.58}$$

One way in which this would be realised in the gravity description would be that it becomes thermodynamically favourable for the $N_{\rm f}$ D-brane probes to distribute the $U(1)_q$ charge unequally among constituent branes, presumably through some mechanism involving the non-Abelian nature of their dynamics. This would imply that the flavour symmetry is spontaneously broken in the infrared. Alternatively, such a separation in different-$n_{\rm b}$ phases may be realised by going to a spatially inhomogeneous phase where $n_{\rm b}$ varies from point to point. The Minkowski-like embeddings carrying a gas of baryons may play a role in this regime.

In this chapter we concentrated on the phase structure of gauge theories at constant temperature and charge density, namely on their description in the canonical ensemble. It will be interesting to consider the phase structure of these theories in the grand canonical ensemble, *i.e.,* as a function of the temperature and the chemical potential. This should be particularly interesting in terms of a potential comparison with the phase structure of QCD. However, it is important to keep in mind that much of the interesting physics in QCD at finite density – see, *e.g.,* [250, 251] – is associated with the fact that baryon number in QCD is only carried by fermionic fields (quarks). This leads to the existence

of a Fermi surface at finite chemical potential. In gauge theories dual to Dp/Dq systems such as those considered here, baryon number is also carried by scalar fields, and so the physics at finite chemical potential is likely to be very different. In particular, a chemical potential for charged scalars acts effectively as a negative mass squared. In the case of free massless scalars this leads to an instability. The theories considered here, however, contain interaction, quartic terms in the fundamental scalars, and so the chemical potential will presumably lead to condensation of the scalars if these are sufficiently light.

As the paper [151] on which this chapter is based was being prepared, we became aware of [252] which overlaps considerably with this work. We thank Sang-Jin Sin for informing us of their project before publication. Unfortunately, we find no evidence of two phase transitions as reported in [252]. We believe their result is spurious, arising from including unphysical Minkowski embeddings in their analysis.

Chapter 4

Holographic viscosity of fundamental matter

A universal bound was recently proposed [125, 140] for the ratio of the shear viscosity to the entropy density of any physical system as $\eta/S \geq 1/4\pi$. In particular, this bound is conjectured to hold for all relativistic quantum field theories at finite temperature that exhibit hydrodynamic behaviour at long wavelengths. Perhaps surprisingly, experimental results from the Relativistic Heavy Ion Collider (RHIC) suggest that, for QCD just above the deconfinement phase transition, the value of η/S is close to saturating this bound [149, 150]. This would indicate that the quark-gluon plasma formed at RHIC is almost a perfect liquid.

Unfortunately, there are currently no theoretical tools with which to calculate transport coefficients in QCD in this strong coupling regime, *e.g.,* the viscosity. However, as we've seen in earlier chapters, the gauge/gravity correspondence makes the strong coupling regime of a large class of gauge theories accessible. In fact, the proposal [125,140] for a universal bound on η/S originated with calculations in this holographic context. Explicit calculations [119,121,128,137,141,142,144,145,253] and general arguments [125,138–140,146] have demonstrated that the bound is exactly saturated by a large class of holographic theories in the limit cited above – for a review, see [118]. In order to approach real-world QCD, it is clearly important to consider $1/\lambda$ and $1/N_c$ corrections. For four-dimensional $\mathcal{N} = 4$ super-Yang-Mills (SYM), the leading correction of the first type was shown to raise the value of η/S above the bound [127, 148]. That is, at finite coupling the bound still

holds but is no longer saturated.

A feature common to all of the gauge theories considered in these hydrodynamic studies is that the matter degrees of freedom transform in the adjoint representation of the gauge group.[1] In this chapter, we study the effect of adding matter fields transforming in the fundamental representation. In particular, we focus on four-dimensional $SU(N_c)$ SYM coupled to N_f fundamental hypermultiplets with $N_f \ll N_c$. Large-N_c counting rules imply that, in the deconfined phase, the contribution of the gluons and adjoint matter to physical quantities is of order N_c^2. Further, the first correction in the absence of fundamental matter is of order 1, *i.e.,* it is suppressed by $1/N_c^2$. Instead, the relative contribution of fundamental matter is only suppressed by N_f/N_c, and therefore it constitutes the leading correction in the large-N_c limit. This is particularly important in theories for which the bound is exactly saturated at $N_c = \infty$, since in these cases whether or not the bound is violated at large but finite N_c is completely determined by the leading $1/N_c$ correction.

As seen in earlier chapters, the dual gravity description of a four-dimensional gauge theory containing fundamental matter is given by N_f D7-brane probes [60, 153] in the background geometry of N_c D3-branes. At finite temperature the geometry contains a black hole [59]. Determining modifications of the shear viscosity requires that we go beyond the usual probe approximation and begin to account for the backreaction of the D7-branes. However, to leading order in N_f/N_c, the calculation of the η/S ratio can be effectively reduced to one in five-dimensional Einstein gravity coupled to a scalar field. General results [125,138–140] then guarantee that $\eta/S = 1/4\pi$. Since the D7-brane contribution to the entropy density is known to be of order $S_{\text{fun}} \sim \lambda N_c N_f T^3$ – see section 2.3.2 [111, 112]– this implies that the contribution of the fundamental matter to the shear viscosity at strong 't Hooft coupling is enhanced with respect to that dictated solely by large-N_c counting rules.

In section 4.3 we will argue that an analogous enhancement takes place for other transport coefficients. We will also explain how our results extend straightforwardly to other holographic gauge theories described by Dp/Dq systems, studied in chapter 2 [62,111,112], or Dp/Dq/D$\bar{\text{q}}$ systems [63, 64, 107–110, 222, 234, 254–256], as well as to systems with a non-zero baryon number chemical potential, such as those studied in chapter 3.

[1] An exception is ref. [212], where fundamental matter was considered. However, the construction involves D5-branes and so the temperature is not a free parameter.

4.1 Holographic Framework

The shear viscosity of the gauge theory in a two-plane labelled by x^i, x^j may be extracted from the retarded correlator of two stress energy tensors via Kubo's formula (see, for example, [118] and references therein)

$$\eta = \lim_{\omega\to 0} \frac{1}{2\omega} \int dt\, d^3x\, e^{i\omega t} \left\langle [T_{ij}(x), T_{ij}(0)] \right\rangle \,, \tag{4.1}$$

where no summation over i, j is implied. The stress energy tensor is dual on the string side to a metric perturbation H_{ij} polarised along the same two-plane. The two-point function above may be calculated by taking two functional derivatives of the on-shell string effective action with respect to this perturbation [123, 124]. In the large-$N_{\rm c}$, large-λ limit, this effective action reduces to the type IIB supergravity action coupled to the worldvolume action of the D7-branes, $I = I_{\rm IIB} + I_{\rm D7}$. Schematically, we have:

$$I = \frac{1}{16\pi G} \int d^{10}x \sqrt{-g} R - N_{\rm f} T_{\rm D7} \int d^8x \sqrt{-g_{\rm ind}} + \cdots \,, \tag{4.2}$$

where $g_{\rm ind}$ is the induced metric on the D7-branes. In terms of the string length and coupling:

$$16\pi G = (2\pi)^7 \ell_s^8 g_s^2 \,, \quad T_{\rm D7} = 2\pi/(2\pi\ell_s)^8 g_s \,. \tag{4.3}$$

The ratio between the normalisations of the two terms above is

$$\varepsilon = 16\pi G N_{\rm f} T_{\rm D7} = \frac{\lambda}{2\pi} \frac{N_{\rm f}}{N_{\rm c}} \,, \tag{4.4}$$

where $\lambda = g_{\rm YM}^2 N_{\rm c} = 2\pi g_s N_{\rm c}$ is the 't Hooft coupling. This ratio controls the relative magnitude of the D7-branes' contribution to physical quantities, *e.g.,* the entropy density– see section 2.3.2 [111, 112]. We will assume that $\varepsilon \ll 1$ and hence that the D7-branes can be treated as a small perturbation; for fixed λ this is achieved by taking $N_{\rm f} \ll N_{\rm c}$. We will begin by examining contributions of order ε in the next section. In the last section, we will comment on effects of order ε^2 and higher.

As seen in section 2.3, in the absence of D7-branes the supergravity background dual to four-dimensional $\mathcal{N} = 4$ SYM at temperature T is

$$ds^2 = ds_5^2 + L^2 d\Omega_5^2 \,, \tag{4.5}$$

$$ds_5^2 = \frac{(\pi L T \rho)^2}{2} \left[-\frac{f^2}{\tilde{f}} dt^2 + \tilde{f} dx_i^2 \right] + \frac{L^2}{\rho^2} d\rho^2 \,, \tag{4.6}$$

where $f(\rho) = 1 - 1/\rho^4\,, \quad \tilde{f}(\rho) = 1 + 1/\rho^4$, and $L = (4\pi g_s N_{\rm c})^{1/4}\ell_s$ is the asymptotic AdS radius. There are also $N_{\rm c}$ units of Ramond-Ramond flux through the five-sphere while the remaining supergravity fields vanish. The metric (4.5,4.6) possesses an event horizon at $\rho = 1$. The entropy density of the gauge theory is then the geometric entropy of the horizon [172]:

$$S = \frac{\pi^3}{4G_5} L^3 T^3 = \frac{\pi^2}{2} N_{\rm c}^2\, T^3\,, \tag{4.7}$$

where $G_5 = G/\pi^3 L^5$ is the five-dimensional Newton's constant obtained by dimensional reduction on the five-sphere.

As in previous chapters, we introduce D7-branes oriented such that five worldvolume directions match those of the five-dimensional black hole (4.6), $y \equiv \{t, x^i, \rho\}$, and the remainder wrap an S^3 (with a possibly varying radius) inside the S^5 of (4.5) – see array (2.34). We adapt coordinates in this internal space such that

$$d\Omega_5^2 = d\theta^2 + \sin^2\theta d\Omega_3^2 + \cos^2\theta d\phi^2 \tag{4.8}$$

and, as before, describe the D7-branes embedding by χ, with $\chi = \cos\theta$. To order ε^0, this is determined by extremising the D7-brane action in the background (4.5,4.6) – see section 2.3.1.

4.2 Viscous Branes

As alluded to above, the calculation of the shear viscosity proceeds as follows. First, one solves the (linearised) equation of motion for a metric perturbation H around the appropriate background. Next, one evaluates the appropriate action for the perturbed background to quadratic order in H. A second derivative of the on-shell action then yields the desired two-point function [123, 124] with which the Kubo formula (4.1) is evaluated.

In the absence of D7-branes the appropriate action is $I_{\rm IIB}$ and the background is given by (4.5). In the presence of the D7-branes the relevant action is supplemented by $I_{\rm D7}$. To first order in the ε-expansion, this affects the calculation of the viscosity in three ways. First, the branes will produce $\mathcal{O}(\varepsilon)$ corrections to the metric (4.5), as well as to the dilaton and the RR axion, since they act as new sources in the field equations arising from the combined action. These background corrections then lead to modifications of the field equation satisfied by H. Second, the branes will also modify the H field equation directly

through extra source terms originating from the variation of $I_{\rm D7}$ with respect to H. Third, the second-derivative of the on-shell action, which yields the correlator in Kubo's formula, may acquire contributions from $I_{\rm D7}$.

Further effects would enter a full calculation of η at higher orders in ε. For example, the background corrections modify the brane embedding, but this only begins to contribute to the on-shell action at $\mathcal{O}(\varepsilon^2)$. In fact, we will now show that only the first two types of possible modifications contribute at $\mathcal{O}(\varepsilon)$. Moreover, the only relevant background correction is the zero-mode (on the five-sphere) of the five-dimensional black hole metric (4.6).

We begin by considering the third set of possible contributions listed above. Expanding the brane action around the $\mathcal{O}(\varepsilon^0)$ background, one finds that, because H enters the action non-derivatively, the H^2 terms do not have a form which will contribute in the Kubo formula [123, 124]. However, turning on H also induces a correction $\delta\chi = \mathcal{O}(H^2)$ in the embedding of the branes. This leads to a surface term in the variation of the D7-brane action,

$$\delta I_{\rm D7} \sim \left.\frac{\partial \mathcal{L}_{\rm D7}}{\partial(\partial_\rho \chi)}\delta\chi\right|_{\rho_{\rm max}}, \tag{4.9}$$

of the right form to contribute to the two-point correlator. However, arguments similar to those in section 2.6.3 imply that any variation of the action is proportional to δm [111,112]:

$$\delta I_{\rm D7} = -2c\delta m\,. \tag{4.10}$$

Hence this contribution must vanish as the variation of the action with respect to H must be taken while keeping the quark mass fixed.

Consider now corrections to the background (4.5). While there are $\mathcal{O}(\varepsilon)$ corrections to the dilaton and RR axion, these only produce $\mathcal{O}(\varepsilon^2)$ contributions to the H field equation because they enter the supergravity action quadratically (in the Einstein frame). We are thus left to consider the contributions of corrections to the spacetime metric. To order ε, the background metric is

$$g = g_0 + \varepsilon g_1^{(0)} + \varepsilon \sum_{\ell\neq 0} g_1^{(\ell)}\,, \tag{4.11}$$

where the corrections $g_1^{(\ell)}$ are organised by their properties under the $SO(6)$ rotations on S^5, with $\ell = 0$ denoting invariant contributions.[2] Since the D7-branes only fill an S^3 in

[2]As the metric is a tensor, invariant means $g_1^{(0)}$ has vanishing Lie derivatives under the $SO(6)$ Killing

the internal space, they also source the $g_1^{(\ell)}$ corrections with $\ell \neq 0$. For the following, an important point is that the functions $g_1^{(0)}$ and $g_1^{(\ell)}$ respect the symmetries of the background geometry (4.5) and the brane embedding, *i.e.,* translations in $\{t, x^i\}$ and $SO(3)$ rotations in x^i, as well as $SO(4)$ rotations in the internal S^3 (wrapped by the D7-brane). The perturbation H has a similar decomposition:

$$H = H_0 + \varepsilon H_1^{(0)} + \varepsilon \sum_{\ell \neq 0} H_1^{(\ell)} \,. \tag{4.12}$$

Implicitly, H_0 is an $SO(6)$ singlet and in the absence of D7-branes it is consistent to restrict the perturbation in this sector [119, 137]. However, in the presence of the D7-branes, nontrivial $H_1^{(\ell)}$ are sourced when H_0 is turned on.[3] Indeed, after integration over the S^5, the supergravity action produces couplings of the schematic form $\varepsilon^2 \int d^5y\, H_0 H_1^{(\ell)} g_1^{(\ell)}$. Similarly, the D7-branes action produces couplings like $\varepsilon^2 \int d^5y\, H_0 H_1^{(\ell)}$, for modes that are constant on the S^3 wrapped by the D7-branes. However, as indicated, both types of terms are of order ε^2 and so we may neglect their contribution here since we only wish to determine the correlator (4.1) up to order ε.

We therefore conclude that, to order ε, we need only consider the zero-modes $g_1^{(0)}(y)$ and $H_1^{(0)}(y)$, and may drop all modes with non-trivial dependence on the S^5 directions. Hence in working to order ε, evaluation of the viscosity actually reduces to a five-dimensional calculation. We can make the latter concrete by dimensionally reducing the action (4.2) to five dimensions ignoring all the Kaluza-Klein modes on the five-sphere, as well as the other supergravity fields. By the previous arguments, the resulting action still captures all of the relevant fields for the calculation of the viscosity to this order. The five-dimensional action can be written as

$$I_{_5} = \frac{1}{16\pi G_{_5}} \int d^5y \sqrt{-g} \left[R + \frac{12}{L^2} - \frac{2\,\varepsilon}{\pi L^2}(1-\chi^2)\sqrt{1-\chi^2+L^2 g^{\rho\rho}(\partial_\rho \chi)^2} \right] , \tag{4.13}$$

where g denotes the five-dimensional metric. The first two terms originate from the reduction of $I_{\rm IIB}$, whereas the last one comes from the reduction of $I_{\rm D7}$ – see eq. (2.42). Note

symmetries of the background (4.5). Hence as well as perturbations of the AdS black hole (4.5), $g_1^{(0)}$ includes perturbations in the size of the five sphere. However, this scalar is removed from the $\mathcal{O}(\varepsilon)$ calculation by going to the Einstein frame in the reduced action (4.13). This fixes the five dimensional Newton's constant as $G_5 = G/\pi^3 L^5$.

[3] With D7-branes, H_0 also sources other supergravity fields at $\mathcal{O}(\varepsilon H_0^2)$. However, these perturbations do not contribute to the shear viscosity at $\mathcal{O}(\varepsilon)$.

that, in the action (4.13), we have only allowed scalar field configurations depending on the radial coordinate, since this suffices for our purposes. This system is just five-dimensional Einstein gravity coupled to a cosmological constant and a(n unusual) scalar field χ. In an ε-expansion, the black hole solutions generated by this auxiliary theory will match the asymptotically AdS part of the original ten-dimensional solution to order ε, *i.e.,* the brane profile $\chi(\rho)$ and the background metric (4.6) plus the order-ε correction $g_1^{(0)}(\rho)$.

The viscosity may now be obtained by calculating the perturbation H_{ij} around the five-dimensional solution and taking the second functional derivative of the action (4.13) evaluated on-shell. However, the black hole solutions of our auxiliary five-dimensional system satisfy the symmetries required in [125, 140], namely translational and rotational invariance in the x^i directions, and hence the result is guaranteed to satisfy $\eta/S = 1/4\pi$. We thus conclude that this universal bound is still saturated in the full ten-dimensional string theory when working to first order in ε. An immediate consequence is that the contributions of the fundamental matter to the viscosity and the entropy density are related (within our approximations) as $\eta_{\rm fun} = S_{\rm fun}/4\pi$. With the known results for $S_{\rm fun}$ from section 2.3.2 [111, 112], we have

$$\eta_{\rm fun} = \frac{\pi}{8} N_{\rm c}^2 T^3 \left[1 + \frac{\lambda}{8\pi^2}\frac{N_{\rm f}}{N_{\rm c}}\, h\left(\frac{\lambda T}{M_{\rm q}}\right) + \cdots\right] , \tag{4.14}$$

where the function $h(x)$ satisfies $h(0) = 0$, $h(\infty) = 1$, and makes a cross-over between both values around $x \sim 1$. Note that this cross-over includes a small discontinuity arising from a first-order phase transition of the fundamental matter – see chapter 2 [111, 112]. We therefore conclude that both $S_{\rm fun}$ and $\eta_{\rm fun}$ are enhanced at strong 't Hooft coupling with respect to the $\mathcal{O}(N_{\rm c}N_{\rm f})$-value dictated solely by large-$N_{\rm c}$ counting rules.

The calculation of $S_{\rm fun}$ in chapter 2 [111,112] was performed by identifying the Euclidean action of the D7-branes with $F_{\rm fun}/T$, where $F_{\rm fun}$ is the free energy contribution of the fundamental matter. The entropy is then determined as $S_{\rm fun} = -\partial F_{\rm fun}/\partial T$. This entropy should, of course, coincide with the change in the horizon area induced by the presence of the D7-branes. The latter can be checked explicitly for the case of massless quarks, for which $\chi = 0$ and, from section 2.3.2, $S_{\rm fun} = \lambda N_{\rm f} N_{\rm c} T^3/16$. From (4.13) we see that the net effect of these 'equatorial' branes is to shift the effective cosmological constant. The corresponding black hole solution is still given by (4.6) with the replacement $L^2 \to L^2/(1 - \varepsilon/6\pi)$. The same replacement in (4.7) shifts the entropy to order ε by $\delta S = \lambda N_{\rm f} N_{\rm c} T^3/16$, in precise agreement with the result from section 2.3.2.

4.3 Discussion

We have seen that the calculation of the contribution of fundamental matter to the shear viscosity may be effectively reduced to a calculation in five dimensions. An analogous simplification takes place for other transport coefficients that can be extracted from correlators involving local operators with vanishing R-charge, since these are dual to modes that carry no angular momentum on the S^5. Examples involving components of the stress-energy tensor include the speed of sound v_s and the bulk viscosity ξ. Other transport coefficients that involve R-charged operators, such as the R-charge diffusion constant [119], or extended strings, such as the jet quenching parameter $\hat{q}$ [133–135], may require a ten-dimensional calculation. Generically, however, we expect the relative contribution of the fundamental matter to be of order $\varepsilon \sim \lambda N_{\rm f}/N_{\rm c}$, since this controls the backreaction of the branes.

Above, our discussion focussed on the D3/D7 system, but the arguments are easily extended to a more general Dp/Dq system intersecting over d common directions. These constructions are dual to a finite-temperature SYM theory in $p+1$ dimensions coupled to fundamental matter confined to a $(d+1)$-dimensional defect. One new feature in these generalised configurations is that the defect breaks translational invariance along the $p-d$ orthogonal directions. In order to calculate the shear viscosity[4] along the translationally invariant directions parallel to the defect, the simplest approach is to compactify these extra directions.[5] The arguments in the previous section go through essentially unchanged except for the fact that the index ℓ now labels momentum modes both along the S^{8-p} transverse to the Dp-branes and along the $p-d$ directions orthogonal to the defect. In this case the problem of calculating the leading contribution of the fundamental matter to the viscosity/entropy ratio can be reduced to a calculation in $(d+2)$-dimensional Einstein gravity coupled to a set of scalar fields. In addition to the scalar χ above, this set now includes the dilaton and the metric components governing the size of the internal S^{8-p} of the background geometry and the size of the $(p-d)$-dimensional space orthogonal to the

[4]The framework for the calculation of correlators is less well developed for such backgrounds, which are not asymptotically AdS. Cascading gauge theories are an interesting case where these techniques are being developed [129, 223–227].

[5]Compactifying is also required to make the $(d+2)$-dimensional Newton's constant finite. Since Newton's constant cancels in the ratio η/S, there is no obstruction to taking the infinite volume limit at the end.

defect.[6] This lower dimensional theory again captures all of the relevant fields to calculate the viscosity to leading order in $N_{\rm f}/N_{\rm c}$. Further, the form of the $(d+2)$-dimensional gravity theory and the background guarantees that $\eta/S = 1/4\pi$. The leading result for the entropy density was determined in chapter 2 [111, 112] and hence we have

$$\eta_{\rm fun} \sim N_{\rm c} N_{\rm f}\, T^d\, g_{\rm eff}(T)^{\frac{2(d-1)}{5-p}}\ , \tag{4.15}$$

where $g^2_{\rm eff}(T) = \lambda T^{p-3}$ is the dimensionless effective 't Hooft coupling for a $(p+1)$-dimensional theory at temperature T [58]. Here the gauge/gravity duality is only valid in the strongly coupled regime [58] and hence we again see an enhancement beyond the large-$N_{\rm c}$ counting. The same line of argument can also be implemented for the Dp/Dq/D$\bar{\rm q}$ systems which have also been studied recently [63, 64, 107–110, 222, 234, 254–256].

The $U(N_{\rm f}) \simeq SU(N_{\rm f}) \times U(1)_{\rm B}$ gauge symmetry on the Dq-branes is a global, flavour symmetry of the dual gauge theory. The results above also hold when a baryon number chemical potential for the $U(1)_{\rm B}$ charge is introduced. As we saw in chapter 3, this is dual to turning on the time component of the gauge potential on the Dq-branes, $A_t(\rho)$ [151, 234].[7] The arguments of the previous section again go through essentially unchanged, except for the fact that an additional vector A_μ is added to the reduced $(d+2)$-dimensional Einstein gravity theory. Thus the saturation of the bound is not affected by the introduction of a chemical potential.

Above we have worked to the lowest order in the parameter $\varepsilon \sim \lambda N_{\rm f}/N_{\rm c}$ that controls the backreaction of the D7-branes on the D3-brane geometry. We have argued that to this order one may ignore all effects of this backreaction except for those on the non-compact part of the metric. We regard the agreement between the entropy density as calculated in section 2.3 [111, 112] and as obtained in the previous section from the change in the horizon area as a quantitative consistency check of this approach. In calculating beyond order ε, the internal modes, *e.g.*, $g_1^{(\ell)}(y)$, and other supergravity fields, will all play a role. Further, at

[6] One might similarly worry about the RR field sourced by the Dq-branes. This will be of order ε and so naturally contributes to the stress tensor at order ε^2. However, there may also be order-ε cross-terms if this RR field already appears as part of the background generated by the Dp-brane. For supersymmetric cases [101, 102, 257], this only happens for the D3/D3, D2/D4 and D1/D5 systems. In all of these, the defect is (1+1)-dimensional and so the shear viscosity is not defined.

[7] This baryon number chemical potential should not be confused with the R-charge chemical potential considered in *e.g.* [142, 144–146, 253], which is dual in the string description to angular momentum on the sphere.

$\mathcal{O}(\varepsilon^2)$ quantum effects will have to be considered.[8] Closed string loop corrections naturally appear in an expansion in $g_s^2 \sim \lambda^2/N_c^2$. Thus if as above N_f is fixed, the loop corrections may be of the same magnitude as the higher order D7-brane contributions, *i.e.,* $g_s^2 \sim \varepsilon^2$ if $N_f = \mathcal{O}(1)$.

The holographic field theories with fundamental matter are naturally organised according to three expansions in $1/\lambda$, $1/N_c$, and N_f/N_c. To suppress string loop corrections with respect to the backreaction of the D7-branes (or more generally the Dq-branes), one must keep N_f/N_c fixed while taking $N_c \to \infty$. The resulting classical solution would resum the effects of the fundamental matter in the N_f/N_c expansion, keeping the leading order contributions in $1/\lambda$ and $1/N_c$. A fully backreacted solution is singular for the D3/D7 system [214, 215], since the dual gauge theory possesses a Landau pole at some finite high-energy scale Λ_{UV}. This of course should not affect the hydrodynamic behaviour as long as the other scales in the problem, the temperature and the quark mass, are much lower than Λ_{UV} (just like the transport properties of an electromagnetic plasma are not affected by the Landau pole in QED). Similarly, in the case of a general Dp-brane background (with $p \neq 3$), one finds strong coupling or curvature divergences in the far UV, which are irrelevant for the long-wavelength hydrodynamics. In these cases, the *classical* backreacted solution would effectively resum the effects of the fundamental matter to leading order in the $1/\lambda$, $1/N_c$ expansions. It may be possible to prove that the viscosity bound is still saturated by these solutions by extending the arguments of [138, 139, 146]. The finite-temperature backgrounds of [212, 217] represent a step towards this goal.

[8] We expect Hawking radiation contributes at order N_f^2/N_c^2. In the presence of N_f D7-branes, there are (at least) $\mathcal{O}(N_f^2)$ species or degrees of freedom into which the black hole can Hawking radiate. However, this is still suppressed by $1/\lambda^2$ relative to ε^2 at strong 't Hooft coupling.

Chapter 5

Holographic spectral functions and diffusion constants for fundamental matter

From the previous chapter it is clear that the dynamics of strongly coupled plasmas may be studied using gravity models. The study of these dynamics continues in this chapter through calculations of spectral functions and diffusion constants for fundamental matter in the $\mathcal{N} = 2$ four-dimensional theory dual to the D3/D7 brane system.

As shown in chapter 2, fundamental matter in the D3/D7 system undergoes a first order phase transition characterised by a discontinuous jump of the D7-branes from Minkowski embeddings, which close off above the black hole, to black hole embeddings, which intersect the black hole (fig. 2.1). In the dual field theory this phase transition is exemplified by discontinuities in various physical quantities, *e.g.,* the quark condensate. The most striking feature of the phase transition is found in the meson spectrum. In the low-temperature or Minkowski phase, the mesons are stable (to leading order in the large-N_c and large 't Hooft coupling limit) and the spectrum is discrete with a finite mass gap. In the high-temperature or black hole phase, mesons are destabilised and the spectrum of excitations is continuous and gapless. Hence the first order phase transition may be characterised by the dissociation or 'melting' of mesons.

The phases of the theory may be studied via spectral functions for mesons. In the low temperature phase of the theory, $T < T_{\rm fun}$, where mesons are stable, the spectral

function consists of a series of delta-function-like peaks,[1,2] *i.e.,* resonances centred on mass eigenvalues – see fig. 5.1a. These masses were calculated in section 2.3.3 and the spectra appear in figures 2.7, 2.8, and 2.9 for pseudoscalar, scalar, and vector mesons, respectively. In the high temperature phase, $T > T_{\rm fun}$, the spectral function is essentially featureless,[3] – see fig. 5.1b. More interesting behaviour is observed when the system evolves from the high-temperature phase into the low-temperature phase through the metastable 'supercooled' phase. In this case, the serene landscape of fig. 5.1b is distorted by peaks corresponding to quasiparticle excitations, and these excitations are eventually transformed into the stable resonances shown in fig. 5.1a.

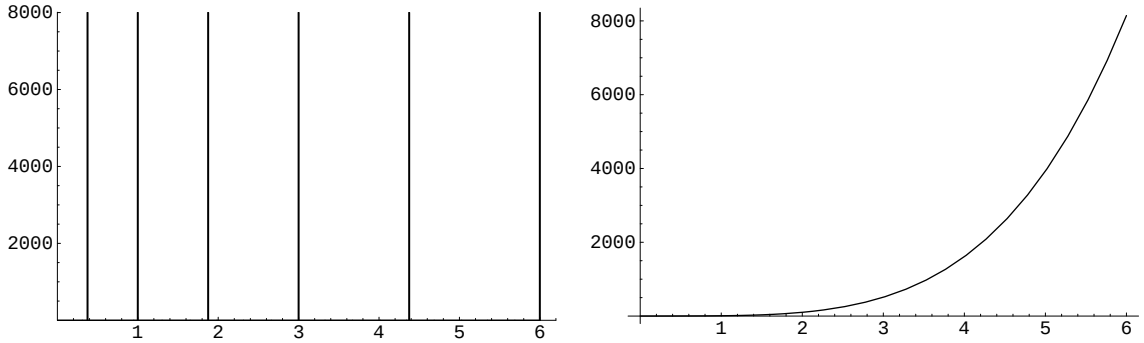

Figure 5.1: Sketch of typical spectral functions in the (a) low-temperature (Minkowski) and (b) high-temperature (black hole) phases.

These features of the spectral functions are controlled by the analytic structure of the corresponding retarded correlators in the complex frequency plane. In the high-temperature phase, the poles of the retarded correlators (with the exception of the poles corresponding to hydrodynamic excitations) are located at a finite distance from the real axis, thus making the spectral function featureless. As the temperature is lowered relative to the quark mass, the poles move closer to the real axis and the spectral functions exhibit

[1]The decay width of these particles and the continuum contribution of multi-particle states are both suppressed by factors of $1/N_{\rm c}$.

[2]A derivation of the scalar meson spectral function at $T = 0$ appears in section 5.6.1.

[3]The temperature-dependent part of the spectral functions exhibits damped oscillations with the period proportional to a Matsubara frequency, see section 5.1.3 for details.

distinct peaks. Holographically, the poles of the retarded correlators correspond to quasinormal modes of the gravitational background [123, 258]. The numerical investigation of the full quasinormal spectrum of the D3/D7 system faces certain technical difficulties. In this chapter we focus on computing the spectral functions for which the numerical methods are reliable.

In addition to characterising quasiparticle excitations of a thermal system, spectral functions also carry information about the medium's transport properties. Adapting techniques from [119, 125, 259], we compute the quark diffusion constant as a function of the parameter M_q/T in the high-temperature phase, and attempt to give a qualitative description of its dependence on the coupling for the full range of temperatures.

The thermal dissociation of mesons and the transport properties of the quark-gluon plasma can be studied in lattice QCD with the help of indirect methods, *e.g.,* the maximal entropy method [156, 157, 260–266]. These studies suggest, in particular, that mesons survive as relatively well-defined resonances at temperatures well above T_c $(2-3T_c)$. While the uncertainties of these lattice methods remain large, the holographic approach used in this chapter serves as a source of quantitative and often analytically exact results for qualitatively similar finite-temperature models.

An overview of this chapter is as follows: In section 5.1 we review properties of thermal spectral functions in field theory and outline methods of computing spectral functions from the dual gravity theory. These methods are illustrated by a simple example of computing the spectral function and diffusion constant for R currents in $\mathcal{N} = 4$ SYM. For vanishing spatial momentum, the correlator, quasinormal spectrum, and the spectral function can be computed analytically. In section 5.2 we revisit the D3/D7-brane framework, previously introduced in section 2.3, reviewing the D7-brane embeddings and pertinent aspects of the thermodynamics [111, 112]. In section 5.3, we turn to the calculation of the spectral function for various mesonic operators in the high temperature phase of the $\mathcal{N} = 2$ gauge theory. We consider a vector operator in section 5.3.1. In the special case of vanishing quark mass, we determine the spectral function analytically. In general, for arbitrary quark mass, the vector spectral function is computed numerically. In section 5.3.2, we turn to spectral functions for scalar and pseudoscalar operators, which are again bilinear in the fundamental fields. Section 5.4 presents three independent computations of the diffusion constant for 'light' quarks, using the membrane paradigm method [125], the Green-Kubo formula, and by calculating the lowest quasinormal frequency for the vector field on the

D7-branes. Section 5.5 contains some observations and a discussion of our results. Some details of our analysis are relegated to section 5.6: Section 5.6.1 contains a derivation of the scalar spectral function at $T = 0$; section 5.6.2 provides a derivation of the high frequency asymptotics for the spectral functions; section 5.6.3 provides a partial analysis of the quasinormal modes for the pseudoscalar and scalar excitations; and, finally, section 5.6.4 extends the computation of the quark diffusion constant, described in section 5.4.1, to the holographic framework described by a Dq-brane probe in a near-extremal Dp-brane throat.

5.1 Prelude: spectral functions and holography

In general, finite-temperature correlation functions of conserved charge densities carry information about a medium's transport properties and quasiparticle excitations. This information is given, roughly, by the poles and the corresponding residues of the correlators, or, equivalently, by their spectral functions. Recently, the study of these objects has been used to great effect in a holographic framework to study the thermal properties of various strongly coupled field theories [118]. In a holographic setting, the spectral functions are often easier to compute than the full correlators on the gravity side. According to the holographic dictionary, the poles are determined by the quasinormal spectrum of a dual bulk field fluctuation, whereas the spectral function is given by the imaginary part of the retarded correlator which is independent of the radial coordinate [123,184]. In this section, we combine the necessary tools for computing the spectral functions from dual gravity and analysing their properties, and then illustrate this technique using the simple example of strongly coupled $\mathcal{N} = 4$ supersymmetric $SU(N_c)$ Yang-Mills (SYM) theory at large N_c. In this case, the R-current spectral function has been analysed elsewhere [184, 267, 268] but we present a new analytic result (for vanishing spatial momentum).

5.1.1 Field theory picture

A thermal spectral function of an operator $\mathcal{O}$ is defined as[4]

$$\mathfrak{R}(\omega, \mathbf{q}) = \int d^4x \; e^{-i\omega t + i\mathbf{q}\mathbf{x}} \langle [\mathcal{O}(t, \mathbf{x}), \mathcal{O}(0)] \rangle \,, \tag{5.1}$$

where the correlator is computed in thermal equilibrium at a temperature T. The spectral function is proportional to the imaginary part of the retarded correlator,

$$\mathfrak{R}(\omega, \mathbf{q}) = -2 \, \mathrm{Im} \, G^R(\omega, \mathbf{q}) \,, \tag{5.2}$$

where

$$G^R(\omega, \mathbf{q}) = -i \int d^4x \, e^{-i\omega t + i\mathbf{q}\mathbf{x}} \, \theta(x^0) \langle [\mathcal{O}(t, \mathbf{x}), \mathcal{O}(0)] \rangle \,. \tag{5.3}$$

If $\mathcal{O}$ is an operator of a density of a conserved charge in a rotation invariant theory, the retarded thermal two-point function is determined by two independent scalar functions. In Fourier space, the correlator can be decomposed into the transverse and longitudinal parts [184]

$$G^R_{\mu\nu}(\omega, q) = P^T_{\mu\nu} \, \Pi^T(\omega, q) + P^L_{\mu\nu} \, \Pi^L(\omega, q) \,, \tag{5.4}$$

where the index structure is absorbed into two mutually orthogonal projectors $P^T_{\mu\nu}$ and $P^L_{\mu\nu}$. Without loss of generality we can take the spatial momentum oriented along the x direction, so that $k_\mu = (-\omega, q, 0, 0)$, with $k^2 = -\omega^2 + q^2$. Then one has [184]

$$G^R_{yy}(k) = G^R_{zz}(k) = \Pi^T(\omega, q) \;. \tag{5.5}$$

Other components of the current-current correlator are

$$G^R_{tt}(k) = -\frac{q^2}{q^2 - \omega^2} \, \Pi^L(\omega, q) \;, \tag{5.6}$$

$$G^R_{tx}(k) = -\frac{\omega q}{q^2 - \omega^2} \, \Pi^L(\omega, q) \;, \tag{5.7}$$

$$G^R_{xx}(k) = -\frac{\omega^2}{q^2 - \omega^2} \, \Pi^L(\omega, q) \;. \tag{5.8}$$

[4]Our metric convention, here, as with everywhere else in the thesis, is $(-, +, +, +)$. We assume translation invariance to be an unbroken symmetry of the theory.

In the long-time, long-wavelength limit (*i.e.,* for $\omega/T \ll 1$, $q/T \ll 1$) the functions $\Pi^T(\omega, q)$ and $\Pi^L(\omega, q)$ have a universal behaviour dictated by hydrodynamics: $\Pi^T(\omega, q)$ is nonsingular as a function of the frequency, while $\Pi^L(\omega, q)$ has a simple pole at

$$\omega = -iDq^2\,, \tag{5.9}$$

where D is the charge diffusion constant.

The rotation invariance implies that in the limit of vanishing spatial momentum at fixed $\omega > 0$ the two scalar functions coincide: $\Pi^T(\omega, 0) = \Pi^L(\omega, 0) = \Pi(\omega)$. Correspondingly, at $q = 0$ one can define

$$\mathfrak{R}(\omega) \equiv \mathfrak{R}_{xx}(\omega, 0) = \mathfrak{R}_{yy}(\omega, 0) = \mathfrak{R}_{zz}(\omega, 0)\,. \tag{5.10}$$

The Green-Kubo formula relates the diffusion constant to the zero-frequency limit of the spectral function $\mathfrak{R}(\omega)$:

$$D\,\Xi = \lim_{\omega\to 0} \frac{1}{2\omega}\mathfrak{R}(\omega)\,. \tag{5.11}$$

Here Ξ is the charge susceptibility. The susceptibility is determined by the thermodynamics of the system in a grand canonical ensemble,

$$\Xi = \left.\frac{\partial n(\mu)}{\partial \mu}\right|_{\mu=0}\,, \tag{5.12}$$

where $n(\mu)$ is the charge density, μ is the corresponding chemical potential.

In addition to hydrodynamic poles, the retarded correlators may have other singularities located in the lower half-plane of complex frequency. Assuming one of these singularities is a simple pole,

$$G^R \sim \frac{1}{\omega - \Omega(q,\alpha) + i\Gamma(q,\alpha)}\,,$$

where α represents a set of parameters relevant for a particular theory, for the spectral function one has

$$\mathfrak{R}(\omega) \sim \frac{\Gamma}{(\omega-\Omega)^2 + \Gamma^2}\,.$$

Thus in the vicinity of $\omega = \Omega$, the spectral function has a peak characterised by a width $\sim \Gamma$ and a height ('lifetime') $\sim 1/\Gamma$. The peak has a quasiparticle interpretation if $\Gamma \ll \Omega$.

The spectral function $\mathfrak{R}(\omega)$ also has a characteristic form in the high frequency limit. This behaviour is determined by the leading short-distance singularity

$$\lim_{(t^2-\mathbf{x}^2)\to 0}\langle \mathcal{O}(t,\mathbf{x})\,\mathcal{O}(0)\rangle = \frac{\mathcal{A}}{|t^2-\mathbf{x}^2|^{\Delta}} + \cdots\,, \tag{5.13}$$

where Δ denotes the dimension of the operator $\mathcal{O}$ and $\mathcal{A}$ is a dimensionless constant. A Fourier transform then leads to the following contribution to the spectral function

$$\mathfrak{R}(\omega) \sim \mathcal{A}\,\omega^{2\Delta-4}\,. \tag{5.14}$$

5.1.2 Gravity picture

In the dual gravity picture, the conserved current J_μ couples to a boundary value of the gauge field fluctuation A_μ propagating in a specific gravitational background. One can form two gauge-invariant combinations of the fluctuation whose equations of motion (supplemented with appropriate boundary conditions) contain (in the limit where the gravity description is valid) full information about the functions $\Pi^T(\omega,q)$ and $\Pi^L(\omega,q)$ introduced in section 5.1.1. These gauge invariant combinations are the transverse and longitudinal (with respect to a chosen direction of the spatial momentum) components E_T, E_L of the electric field in curved space [184]. Quasinormal spectra of the fluctuations E_T and E_L determine the position of the poles of $\Pi^T(\omega,q)$ and $\Pi^L(\omega,q)$ in the complex ω plane.

5.1.3 A simple example: spectral function of R currents in $\mathcal{N}=4$ SYM

Correlators of R-currents in strongly coupled $\mathcal{N}=4$ $SU(N_c)$ supersymetric Yang-Mills (SYM) theory at large N_c were previously studied by means of the AdS/CFT correspondence both at zero [269, 270] and finite temperature [119, 183, 184, 267, 268].

In thermal $\mathcal{N}=4$ SYM, the retarded two-point correlators of the $SU(4)_R$ R-symmetry currents J^a_μ are determined by two independent scalar functions[5], $\Pi^T(\omega,q)$ and $\Pi^L(\omega,q)$.

The holographic dual of thermal $\mathcal{N}=4$ SYM in flat space is well known. The supergravity background describing the decoupling limit of N_c black D3-branes was given in

[5]In an equilibrium state without chemical potentials for the R-charges, the correlation function of R currents j^a_μ has the form $C^{ab}_{\mu\nu} = \delta^{ab}C_{\mu\nu}(x)$. In all expressions, the factor δ^{ab} is omitted.

section 2.1 as (see, *e.g.,* [53])

$$ds^2 = \frac{u^2}{L^2}\left(-f(u)dt^2 + dx_3^2\right) + \frac{L^2}{u^2}\left(\frac{du^2}{f(u)} + u^2 d\Omega_5^2\right), \qquad C_{0123} = -\frac{u^4}{L^4}, \tag{5.15}$$

where $f(u) = 1 - u_0^4/u^4$ and the dilaton is constant. The horizon lies at $u = u_0$ and the radius of curvature L is defined in terms of the string coupling constant $g_{\rm s}$ and the string length scale $\ell_{\rm s}$ as $L^4 = 4\pi\, g_{\rm s} N_{\rm c}\, \ell_{\rm s}^4$. According to the duality, originally proposed by Maldacena [52], type IIB string theory on this background is dual to four-dimensional $\mathcal{N} = 4$ super-Yang-Mills $SU(N_{\rm c})$ gauge theory. The holographic dictionary between the theories relates the Yang-Mills and string coupling constants $g_{\rm YM}^2 = 2\pi g_{\rm s}$. The temperature of the gauge theory is equivalent to the Hawking temperature of the black hole horizon, related to u_0 via eq. (2.6), *i.e.,* $T = u_0/\pi L^2$.

In the supergravity approximation (corresponding to the limit $N_{\rm c} \to \infty$, $\lambda = g_{\rm YM}^2 N_{\rm c} \to \infty$ in the field theory), full information about functions $\Pi^T(\omega, q)$ and $\Pi^L(\omega, q)$ can be obtained by solving the linearised Maxwell equations for the bulk electric field components E_T, E_L [184]

$$E_T'' + \frac{f'}{f}E_T' + \frac{\mathfrak{w}^2 - \mathfrak{q}^2 f}{(1-\bar{x})f^2}E_T = 0\,, \tag{5.16}$$

$$E_L'' + \frac{\mathfrak{w}^2 f'}{f(\mathfrak{w}^2 - \mathfrak{q}^2 f)}E_L' + \frac{\mathfrak{w}^2 - \mathfrak{q}^2 f}{(1-\bar{x})f^2}E_L = 0\,, \tag{5.17}$$

where $'$ indicates a derivative with respect to $\bar{x} \equiv 1 - u_0^2/u^2$. We have also introduced the dimensionless quantities

$$\mathfrak{w} = \frac{\omega}{2\pi T}, \qquad \mathfrak{q} = \frac{q}{2\pi T}. \tag{5.18}$$

An analysis of eqs. (5.16) and (5.17), including the perturbative solution for small $\mathfrak{w}$, $\mathfrak{q}$, can be found in [184]. Here we focus on the particular case of vanishing spatial momentum which admits an analytic solution for arbitrary frequency.

For $\mathfrak{q} = 0$, the components $E_T = E_L \equiv E$ obey the same equation

$$E'' + \frac{f'}{f}\,E' + \frac{\mathfrak{w}^2}{(1-\bar{x})f^2}\,E = 0\,. \tag{5.19}$$

Writing

$$E(\bar{x}) = \bar{x}^{-i\mathfrak{w}/2}\,(2-\bar{x})^{-\mathfrak{w}/2}\,F(\bar{x})\,, \tag{5.20}$$

where $F(\bar{x})$ is by construction regular at the horizon $\bar{x}=0$, we obtain the equation

$$F''+\frac{2i\mathfrak{w}+2(\bar{x}-1)-(1+i)\mathfrak{w}\bar{x}}{(\bar{x}-2)\bar{x}}\,F'+\frac{\mathfrak{w}((1+i)(1-\bar{x})-i\mathfrak{w}((1+2i)-\bar{x}))}{2\bar{x}(2-3\bar{x}-\bar{x}^2)}\,F=0\,. \quad (5.21)$$

Two linearly independent solutions of eq. (5.21) are written in terms of the Gauss hypergeometric function

$$F_1(\bar{x})=(1-\bar{x})^{\frac{(1+i)\mathfrak{w}}{2}}{}_2F_1\left(1-\frac{(1+i)\mathfrak{w}}{2}\,,-\frac{(1+i)\mathfrak{w}}{2}\,;1-i\mathfrak{w};\frac{\bar{x}}{2(\bar{x}-1)}\right)\,, \quad (5.22)$$

$$F_2(\bar{x})=\bar{x}^{i\mathfrak{w}}\,(1-\bar{x})^{\frac{(1-i)\mathfrak{w}}{2}}{}_2F_1\left(1-\frac{(1-i)\mathfrak{w}}{2}\,,-\frac{(1-i)\mathfrak{w}}{2}\,;1+i\mathfrak{w};\frac{\bar{x}}{2(\bar{x}-1)}\right)\,. \quad (5.23)$$

To compute the retarded correlators, we need a solution obeying the incoming wave boundary condition at $\bar{x}=0$ [123]. The correct solution is thus given by eq. (5.22).

The retarded correlation functions can be computed from the boundary supergravity action using the Lorentzian AdS/CFT prescription [123]. For vanishing spatial momentum, the result reads [184, 268]

$$\Pi(\omega)=\frac{N_c^2T^2}{8}\lim_{\bar{x}\to 1}\frac{E'(\bar{x})}{E(\bar{x})}\,. \quad (5.24)$$

Substituting the solution (5.22) into eq. (5.24) we obtain

$$\Pi(\omega)=\frac{N_c^2T^2}{8}\left\{i\,\mathfrak{w}+\mathfrak{w}^2\left[\psi\left(\frac{(1-i)\mathfrak{w}}{2}\right)+\psi\left(-\frac{(1+i)\mathfrak{w}}{2}\right)\right]\right\}\,, \quad (5.25)$$

where $\psi(z)$ is the logarithmic derivative of the gamma-function. The spectral function is given by

$$\mathfrak{R}(\omega)=-\frac{N_c^2T^2}{4}\,\mathrm{Im}\left\{i\,\mathfrak{w}+\mathfrak{w}^2\left[\psi\left(\frac{(1-i)\mathfrak{w}}{2}\right)+\psi\left(-\frac{(1+i)\mathfrak{w}}{2}\right)\right]\right\}\,. \quad (5.26)$$

Using the property of the digamma function $\psi(z)-\psi(-z)=-\pi\cot\pi z-1/z$, the spectral function (5.26) can be written in a more compact form

$$\mathfrak{R}(\omega)=\frac{N_c^2T^2}{4}\,\frac{\pi\mathfrak{w}^2\sinh\pi\mathfrak{w}}{\cosh\pi\mathfrak{w}-\cos\pi\mathfrak{w}}\,. \quad (5.27)$$

These analytic results for the retarded Green's function (5.25) and the spectral function (5.26), (5.27) are new and allow their various features to be easily examined. The asymptotics of the spectral function for large and small frequency can be computed:

$$\mathfrak{R}(\omega) = \frac{\pi N_c^2T^2\mathfrak{w}^2}{4}\left(1+2e^{-\pi\mathfrak{w}}\cos\pi\mathfrak{w}+\cdots\right)\,,\qquad \mathfrak{w}\to\infty\,, \quad (5.28)$$

$$\mathfrak{R}(\omega) = \frac{N_c^2T^2\mathfrak{w}}{4}\left(1+\frac{\pi^2\mathfrak{w}^2}{6}+\cdots\right)\,,\qquad \mathfrak{w}\to 0\,. \quad (5.29)$$

As expected, the high frequency asymptotic coincides with the zero-temperature result for the spectral function [123]

$$\mathfrak{R}^{T=0}(\omega) = \frac{N_c^2\omega^2}{16\pi}\,. \tag{5.30}$$

The retarded correlator (5.25) is a meromorphic function of $\mathfrak{w}$ with poles located at[6]

$$\mathfrak{w} = \pm n - i\,n\,, \qquad n = 1, 2, \ldots\,. \tag{5.31}$$

The position of the poles coincides with the quasinormal spectrum of the fluctuations $E(\bar{x})$ determined by the Dirichlet condition $E(1) = 0$. For each pole, the imaginary part has the same magnitude as the real one, and thus none of the singularities can be given a 'quasiparticle' interpretation. Indeed, as shown in fig. 5.2a, the spectral function is quite featureless, although not monotonic: its finite-temperature part, $\mathfrak{R}(\omega) - \mathfrak{R}^{T=0}(\omega)$, exhibits damped oscillations reflecting the diminishing influence of the sequence of poles receding farther and farther away from the real axis in the complex frequency plane (fig. 5.2b). The oscillatory behaviour of the finite-temperature part of the spectral function is evident from eq. (5.28).

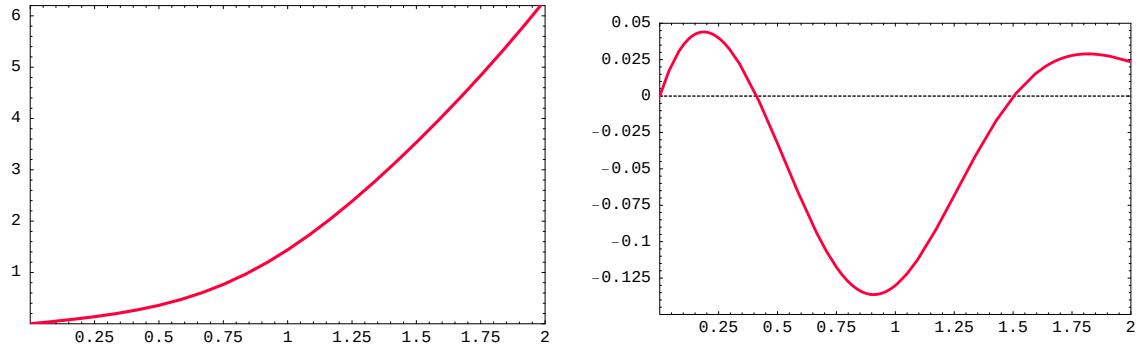

(a) (b)

Figure 5.2: The $\mathcal{N} = 4$ SYM R-current spectral function at zero spatial momentum $\mathfrak{R}(\omega)$ (a) and its finite temperature part $\mathfrak{R}(\omega) - N_c^2\omega^2/16\pi$ (b) in units of $N_c^2T^2/2$ as a function of $\mathfrak{w} = \omega/2\pi T$.

Using the Green-Kubo formula (5.11) and the low frequency limit (5.29) of the spectral function at zero spatial momentum one finds the product of the R-charge diffusion constant

[6]The exact location of the poles was previously found in [183] using the continued fraction method.

and the charge susceptibility

$$D\Xi = \frac{N_c^2 T}{16\pi}\,. \tag{5.32}$$

The susceptibility is determined from thermodynamics according to eq. (5.12). The dependence of the charge density on the chemical potential was found in [142]. For small μ, one has

$$n(\mu) = \frac{N_c^2 T^2}{8}\,\mu + \cdots\,, \tag{5.33}$$

and thus from eq. (5.12), $\Xi = N_c^2 T^2/8$. We conclude that the R charge diffusion constant is given by $D = 1/2\pi T$, in agreement with the result of an earlier calculation [119], where the value of D was determined from the hydrodynamic pole of the longitudinal part of the correlator at small but nonvanishing spatial momentum.

5.2 Adding flavour: D7-brane embedding and thermodynamics

We saw in section 2.3 that fields transforming in the fundamental representation of the gauge group can be introduced to the near horizon geometry of N_c black D3-branes via the introduction of N_f D7-branes [60, 153]. As before, we consider the decoupling limit of the D3- and D7-branes, described by the array (2.34). Of course, the dual field theory is now an $\mathcal{N} = 2$ gauge theory consisting of the original SYM theory coupled to N_f fundamental hypermultiplets. Taking the decoupling limit with $N_f \ll N_c$, the D7-branes may be treated as probes in the black D3-brane geometry (5.15).

As in section 2.3.1, we work with radial coordinate ρ and describe the D7-branes' profile by $\chi(\rho) = \cos\theta(\rho)$. The induced metric on the D7-branes was given in eq. (2.41) and equation of motion for χ appears in eq. (2.44). The field asymptotically approaches zero as described by eq. (2.45), *i.e.*, $\chi = m/\rho + c/\rho^3$. The operator dual to χ is the supersymmetric extension of the quark mass term, defined in (A.2). Holography then relates the dimensionless constants m and c to the quark mass and condensate via (A.7) and (A.11). Eq. (A.7) implies the relationship $m = \bar{M}/T$ between the dimensionless quantity m, the temperature T and the mass scale $\bar{M}$ defined in eq. (2.48).

In the limits of large and small m it is possible to find approximate analytic solutions for the embeddings – see section 2.6.1 [112]. However, for arbitrary m we numerically

integrated (2.44) – see section 2.3.1 [111, 112]. In the present case, we are studying the high temperature phase and so we are interested in the black hole embeddings, which are found by imposing the following boundary conditions at the event horizon $\rho_{\rm min} = 1$: $\chi = \chi_0$ and $d\chi/d\rho = 0$ for $0 \leq \chi_0 < 1$. In order to compute the constants m, c corresponding to each value of χ_0, we fitted the numerical solutions to the asymptotic form (2.45).

5.2.1 Thermodynamics of the brane

As studied in detail in chapter 2, at finite temperature there are two classes of embeddings for the D7-branes and a first-order phase transition going between these classes. For temperatures below the phase transition $T < T_{\rm fun}$, the D7-branes close off above the black hole horizon (Minkowski embeddings), while above the transition ($T > T_{\rm fun}$), the D7-branes extend through the horizon (black hole embeddings). The thermodynamics of the D3/D7 brane system were studied in detail in section 2.3.2 and we review a few salient facts here.

Plots of the free energy versus temperature appeared in fig. 2.5. A zoom in view of the area near the phase transition is given in fig. 5.3 and this shows the 'swallow tail' which is typical of first order phase transitions. Starting from low temperatures, we follow the blue dotted line depicting Minkowski embeddings to the point where this line intersects the solid red line for black hole embeddings. The phase transition occurs at this point, and the physical embedding jumps from a Minkowski embedding, a finite distance from the black hole horizon, to the black hole embedding with $\chi_0 \simeq 0.94$. At this temperature, the quark condensate, entropy, and energy density each exhibit a finite discontinuity, indicating that the phase transition is first order.

It is interesting to ask whether the D7-brane embeddings beyond the phase transition, *e.g.,* between A_1 and A_2 on the black hole branch, still represent metastable configurations. If so, the corresponding states of the gauge theory might be accessed by a process analogous to 'supercooling' the system. Examining the specific heat $c_{\rm V} = \partial E/\partial T$ reveals that $c_{\rm V}$ becomes negative as the curves (*e.g.,* of the condensate, entropy or energy density as a function of T) spiral around the critical solution, indicating that the system should be unstable for these embeddings (see the discussion in section 2.3.2). In particular, the specific heat first becomes negative at A_2 on the black hole branch and A_3 on the Minkowski branch. Examining the scalar fluctuation spectrum of the D7-brane Minkowski embeddings (corresponding to the meson spectrum in the low temperature phase of the dual

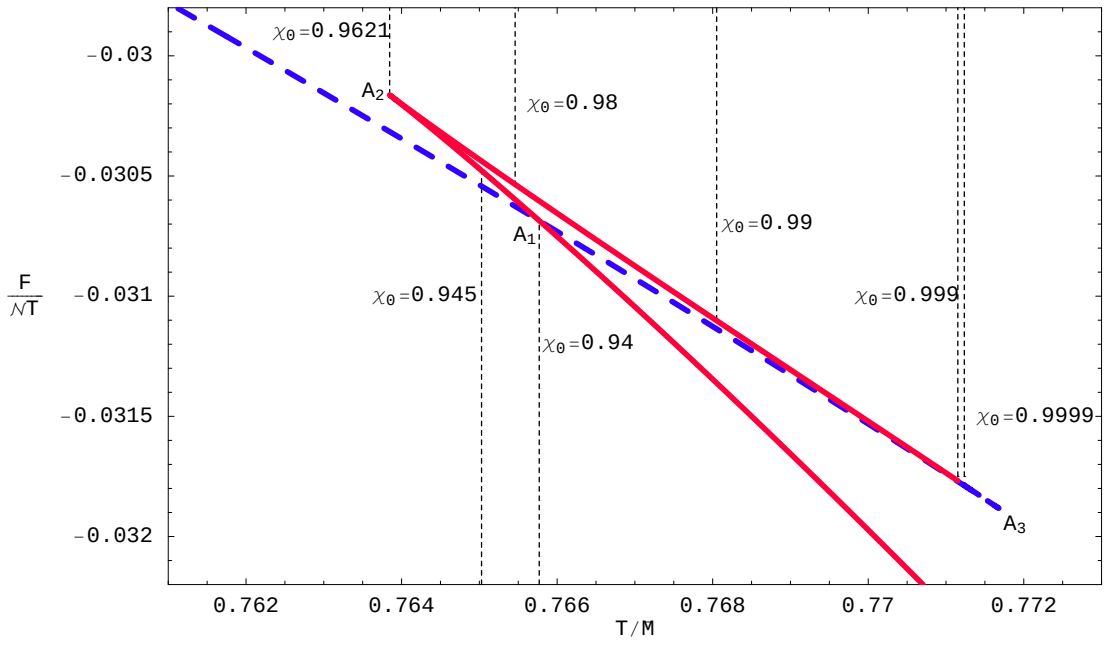

Figure 5.3: The free energy $F/\mathcal{N}T$ versus temperature $T/\bar{M}$ for a D7-brane in the black D3-brane geometry where $\mathcal{N} = \lambda N_{\rm f} N_{\rm c} T^3/32$ – see eq. (2.43). The blue dashed (red continuous) curves correspond to the Minkowski (black hole) embeddings. The values of χ_0 for certain black hole D7-brane embeddings are noted for future reference. The phase transition is indicated by the vertical dashed line labelled $\chi_0 = 0.94$.

gauge theory) –see section 2.3.3 – reveals that a dynamical instability appears precisely at A_3: At the first kink in the free energy, the lowest-lying scalar mode on the D7-branes becomes tachyonic. In fact, at the second kink, the second lowest-lying scalar mode becomes tachyonic and new tachyonic modes seem to appear at each such kink [112].

Hence the behaviour on the Minkowski branch is clear: Continuing along the Minkowski branch past the phase transition, the system exhibits a dynamical instability, which matches the thermodynamic prediction, at the point A_3 in fig. 5.3, which is the first kink in the free energy on the Minkowski branch and corresponds to the first turn-around in the spiral. Hence while these configurations remain metastable between A_1 and A_3, all of the embeddings beyond A_3 are simply unstable. In fact, more and more instabilities appear as the

embeddings approach the critical solution, as described above.

On the black hole branch we expect similar phenomena. At point A_2 in fig. 5.3, the specific heat becomes negative, indicating a thermodynamic instability. Though the full calculation of the quasinormal spectrum remains to be performed – preliminary results appear in [155] – we will see in section 5.3.2 that the scalar spectral function provides evidence that new tachyonic modes again appear at each turn in the spiral along the black hole branch. Section 5.6.3 presents a complementary analysis which also supports the appearance of tachyons in the quasinormal spectrum of the scalar fluctuations. Hence we expect that only the configurations between A_1 and A_2 on the black hole branch represent metastable states of the gauge theory.

5.3 Spectral functions for excitations of fundamental fields

In this section, we compute spectral functions for excitations of fundamental fields in the high temperature phase of the theory, $T > T_{\rm fun}$, by studying vector and scalar fluctuations of the D7-brane probes. The spectrum of these fluctuations in the Minkowski phase of the theory was found in section 2.3.3. The details of the holographic dictionary relating the fluctuations of the probe branes to the hypermultiplet operators of the gauge theory are described in appendix A. For each of the vector, pseudoscalar, and scalar mesons we begin by considering modes constant on the internal S^3 and then extend the analysis to include modes with nonzero angular momentum on this space. The latter modes are dual to higher dimension operators which are charged under the global $SO(4)$ symmetry, as outlined in appendix A.4.

5.3.1 Vector

In the gravity dual, the vector is one of several possible excitations of the worldvolume gauge field on the D7-branes [101]. The holographic dictionary outlined in appendix A reveals that the vector is dual to the current $J^\mu_{\rm q}$ which is the conserved current corresponding to the diagonal $U(1)_{\rm q}$ of the global flavour symmetry.

We begin by considering modes constant on the internal S^3. In this case, vector modes

are characterised by having only $A_{t,x,y,z}$ nonzero with $A_\rho = A_{S^3} = 0$ [101]. The full action (2.79) for the gauge fields on a D7-brane contains the Dirac-Born-Infeld (DBI) action plus a Wess-Zumino term, as discussed in section 2.3.3. However, for gauge fields with $A_\rho = A_{S^3} = 0$ only the DBI portion of the action is relevant. Further, since we only study linearised fluctuations about the background, the gauge field action is only needed to quadratic order and it is simply

$$I = -\frac{(2\pi\ell_{\rm s}^2)^2}{4} T_{\rm D7} N_{\rm f} \int d^8\sigma \sqrt{-g}\, g^{cd} g^{ef} F_{fc} F_{de}\,, \tag{5.34}$$

where the Latin indices run over the D7 worldvolume directions and g_{ab} is the induced metric on the D7-brane given in (2.36).

Assuming that the gauge field is independent of the coordinates on the S^3, we can easily reduce (5.34) to an effective action in five-dimensions. The induced metric in these directions is

$$ds^2(\tilde{g}) = \frac{1}{2}\left(\frac{u_0\rho}{L}\right)^2 \left[-\frac{f^2}{\tilde{f}} dt^2 + \tilde{f} dx_3^2\right] + \frac{L^2}{\rho^2}\left(\frac{1-\chi^2+\rho^2\dot{\chi}^2}{1-\chi^2}\right) d\rho^2\,, \tag{5.35}$$

and so the determinant of the full induced metric (2.36) can be written as

$$\sqrt{-g} = \frac{\sqrt{-\tilde{g}}}{\tilde{g}_{eff}^2(\rho)}\sqrt{h}\,, \qquad \frac{1}{\tilde{g}_{eff}^2(\rho)} \equiv L^3(1-\chi^2)^{\frac{3}{2}}\,. \tag{5.36}$$

Here h is the determinant of the metric on the S^3 of unit radius and $\tilde{g}_{eff}$ is a radially-dependent 'effective coupling'. Integrating over the three-sphere, the action (5.34) reduces to

$$I = -\frac{(2\pi\ell_{\rm s}^2)^2}{4}\Omega_3 T_{\rm D7} N_{\rm f} \int dt d^3x d\rho \sqrt{-\tilde{g}}\, \frac{F^{\alpha\beta}F_{\alpha\beta}}{\tilde{g}_{eff}^2(\rho)}\,, \tag{5.37}$$

where $\alpha, \beta = t, x, y, z, \rho$. Of course, Maxwell's equations follow as

$$\partial_\alpha\left(\frac{\sqrt{-\tilde{g}}}{\tilde{g}_{eff}^2} F^{\alpha\beta}\right) = 0. \tag{5.38}$$

Using the equation of motion (5.38), the action (5.37) can be written as

$$I = -\frac{(2\pi\ell_{\rm s}^2)^2}{2} T_{\rm D7}\Omega_3 N_{\rm f} \int dx^4 d\rho\, \partial_\alpha\left[\frac{\sqrt{-\tilde{g}}}{\tilde{g}_{eff}^2} A_\beta F^{\alpha\beta}\right]\,. \tag{5.39}$$

Retaining only the terms at the ρ-boundaries and using the metric (5.35), this becomes

$$I = -\frac{(2\pi\ell_{\rm s}^2)^2}{2} T_{\rm D7}\Omega_3 \frac{{u_0}^2}{2} N_{\rm f} \int d^4x \left[\frac{f\rho^3(1-\chi^2)^2}{\sqrt{1-\chi^2+\rho^2\dot{\chi}^2}} \left(A_i \partial_\rho A_i - \frac{\tilde{f}^2}{f^2} A_t \partial_\rho A_t \right) \right]_{\rho\to 1}^{\rho\to\infty} ,$$

where i is summed over x, y, z. Following [184], we take the Fourier transform of the gauge field and with $k_\mu = (-\omega, q, 0, 0)$,

$$A_\mu = \int \frac{d\omega\, dq}{(2\pi)^2} e^{-i\omega t + iqx} A_\mu(k,\rho) \,, \tag{5.40}$$

(with $A_\rho = 0$, as discussed earlier), and the boundary action can be written as

$$I = -\frac{N_{\rm f}N_{\rm c}T^2}{2^4} \int \frac{d\omega dq}{(2\pi)^2} \left[\frac{f\rho^3(1-\chi^2)^2}{\sqrt{1-\chi^2+\rho^2\dot{\chi}^2}} \left(A_i(\rho,-k)\partial_\rho A_i(\rho,k) - \frac{\tilde{f}^2}{f^2} A_t(\rho,-k)\partial_\rho A_t(\rho,k) \right) \right]_{\rho\to 1}^{\rho\to\infty} .$$

We construct gauge-invariant components of the electric field: $E_x \equiv qA_t + \omega A_x$ and $E_{y,z} \equiv \omega A_{y,z}$. Note that in the language of section 5.1, E_x corresponds to the longitudinal electric field E_L while $E_{y,z}$ correspond to the transverse electric field E_T. With these gauge-invariant fields, the action can be rewritten as (using eq. (5.47) below)

$$\begin{aligned} I \;=\; & -\frac{N_{\rm f}N_{\rm c}T^2}{2^4} \int \frac{d\omega dq}{(2\pi)^2} \left[\frac{f\rho^3(1-\chi^2)^2}{\sqrt{1-\chi^2+\rho^2\dot{\chi}^2}} \left(\frac{E_x(\rho,-k)\partial_\rho E_x(\rho,k)}{\omega^2 - q^2 f^2/\tilde{f}^2} \right.\right. \\ & \left.\left. -\frac{1}{\omega^2}\left(E_y(\rho,-k)\partial_\rho E_y(\rho,k) + E_z(\rho,-k)\partial_\rho E_z(\rho,k)\right) \right) \right]_{\rho\to 1}^{\rho\to\infty} . \end{aligned} \tag{5.41}$$

Focussing on the longitudinal electric field, we write

$$E_x(k,\rho) = E_0(k) \frac{E_k(\rho)}{E_k(\rho_{\rm max})} \,, \tag{5.42}$$

where it is understood that eventually the limit $\rho_{\rm max} \to \infty$ will be taken. We can then define the flux factor for E_x as [123]:

$$\mathcal{F} = -\frac{N_{\rm f}N_{\rm c}T^2}{2^4} \left[\frac{f\rho^3(1-\chi^2)^2}{\sqrt{1-\chi^2+\rho^2\dot{\chi}^2}} \frac{E_{-k}(\rho)\partial_\rho E_k(\rho)}{(\omega^2 - q^2 f^2/\tilde{f}^2) E_{-k}(\rho_{\rm max}) E_k(\rho_{\rm max})} \right] . \tag{5.43}$$

The usual AdS/CFT prescription tells us to evaluate it at the boundary $\rho \to \infty$ to find the retarded Green's function for E_x [123]:

$$G = -2\mathcal{F} = \frac{N_{\rm f}N_{\rm c}T^2}{2^3} \left[\frac{f\rho^3(1-\chi^2)^2}{\sqrt{1-\chi^2+\rho^2\dot{\chi}^2}} \frac{E_{-k}(\rho)\partial_\rho E_k(\rho)}{(\omega^2 - q^2 f^2/\tilde{f}^2) E_{-k}(\rho_{\rm max}) E_k(\rho_{\rm max})} \right]_{\rho\to\infty} . \tag{5.44}$$

The retarded Green's function for A_x is the above expression times ω^2, which for $q = 0$ gives

$$G_{xx} = \frac{N_{\rm f}N_cT^2}{8}\left[\rho^3\frac{\partial_\rho E_k(\rho)}{E_k(\rho)}\right]_{\rho\to\infty}\,, \tag{5.45}$$

upon using the asymptotic expansion (2.45) for χ. Of course, this is the analogue of the expression in eq. (5.24) for the example discussed in section 5.1.3. The spectral function for $q = 0$ is then

$$\mathfrak{R}_{xx}(\omega,0) = -2{\rm Im}G_{xx}(\omega,0) = -\frac{N_{\rm f}N_cT^2}{4}{\rm Im}\left[\rho^3\frac{\partial_\rho E_k(\rho)}{E_k(\rho)}\right]_{\rho\to\infty}\,. \tag{5.46}$$

In order to evaluate the spectral function, we must solve the equations of motion (5.38). For $A_\rho = A_{S^3} = 0$ and A_μ an s-wave on the S^3, the equations for A_t and A_x are

$$\tilde{g}^{tt}\omega\dot{A}_t - \tilde{g}^{xx}q\dot{A}_x = 0\,, \tag{5.47}$$

$$\partial_\rho\left(\frac{\sqrt{-\tilde{g}}}{\tilde{g}^2_{eff}}\tilde{g}^{tt}\tilde{g}^{\rho\rho}\dot{A}_t\right) - \frac{\sqrt{-\tilde{g}}}{\tilde{g}^2_{eff}}\tilde{g}^{tt}\tilde{g}^{xx}\left(\omega q A_x + q^2 A_t\right) = 0\,, \tag{5.48}$$

$$\partial_\rho\left(\frac{\sqrt{-\tilde{g}}}{\tilde{g}^2_{eff}}\tilde{g}^{\rho\rho}\tilde{g}^{xx}\dot{A}_x\right) - \frac{\sqrt{-\tilde{g}}}{\tilde{g}^2_{eff}}\tilde{g}^{tt}\tilde{g}^{xx}\left(\omega q A_t + \omega^2 A_x\right) = 0\,. \tag{5.49}$$

Given the longitudinal field $E_x = qA_t + \omega A_x$, the system of equations (5.47)-(5.49) yields

$$\ddot{E}_x + \left[\frac{4\omega^2\tilde{f}\dot{f}}{f(\omega^2\tilde{f}^2 - q^2f^2)} + \partial_\rho\ln\left(\frac{\sqrt{-\tilde{g}}}{\tilde{g}^2_{eff}}\tilde{g}^{tt}\tilde{g}^{\rho\rho}\right)\right]\dot{E}_x + \frac{\tilde{g}^{xx}}{\tilde{g}^{\rho\rho}}\left(\frac{\tilde{f}^2}{f^2}\omega^2 - q^2\right)E_x = 0. \tag{5.50}$$

Substituting for the induced metric in (5.50), the equation of motion for E_x is:

$$\begin{aligned}\ddot{E}_x + \left[\frac{4\mathfrak{w}^2\tilde{f}\dot{f}}{f(\mathfrak{w}^2\tilde{f}^2 - \mathfrak{q}^2f^2)} + \frac{f}{\tilde{f}^2}\frac{\sqrt{1-\chi^2+\rho^2\dot{\chi}^2}}{\rho^3(1-\chi^2)^2}\partial_\rho\left(\frac{\tilde{f}^2\rho^3(1-\chi^2)^2}{f\sqrt{1-\chi^2+\rho^2\dot{\chi}^2}}\right)\right]\dot{E}_x \\ +8\frac{1-\chi^2+\rho^2\dot{\chi}^2}{\rho^4\tilde{f}(1-\chi^2)}\left(\frac{\tilde{f}^2}{f^2}\mathfrak{w}^2 - \mathfrak{q}^2\right)E_x = 0\,,\end{aligned} \tag{5.51}$$

where the dimensionless frequency $\mathfrak{w}$ and momentum $\mathfrak{q}$ were defined in eq. (5.18).

Returning to the transverse electric field $E_T = E_{y,z}$, the equation of motion is

$$\partial_\rho\left[\frac{\sqrt{-\tilde{g}}}{\tilde{g}^2_{eff}}g^{\rho\rho}g^{yy}\partial_\rho E_T\right] - \frac{\sqrt{-\tilde{g}}}{\tilde{g}^2_{eff}}g^{yy}\left(\omega^2 g^{tt} + q^2 g^{xx}\right)E_T = 0\,. \tag{5.52}$$

For vanishing spatial momentum $q = 0$, this equation and that for E_x (eq. (5.51)) coincide. Thus, as discussed in section 5.1, for $q = 0$, the spectral functions are identical *i.e.,* $\mathfrak{R}_{xx}(\omega, 0) = \mathfrak{R}_{yy}(\omega, 0) = \mathfrak{R}_{zz}(\omega, 0)$ and we denote these by $\mathfrak{R}(\omega)$ henceforth.

We proceed to compute the spectral function $\mathfrak{R}(\omega)$ by solving the equation of motion (5.51) with $\mathfrak{q} = 0$. First we note that the case of massless quarks corresponds to the equatorial embedding of the D7-branes for which $\chi(\rho) = 0$. Hence g^2_{eff} in eq. (5.37) is constant and the induced metric (5.35) matches precisely that of the AdS_5 black hole. Hence except for an overall normalisation, the calculation of $\mathfrak{R}(\omega)$ is identical to that in the example discussed in section 5.1.3 and so in this case, it is possible to solve (5.51) exactly. We leave this exercise for the following subsection as it is a special case of the general analysis of charged vector operators, for which the case $M_{\rm q} = 0$ is also exactly soluble.

For massive quarks ($m \neq 0$), the embedding equation (2.44) must be solved numerically and hence it was necessary to numerically integrate (5.51) to solve for E_x. Near the horizon ($\rho \to 1$), eq. (5.51) implies that $E_x \sim (\rho - 1)^{\pm i\mathfrak{w}}$. Choosing the negative sign enforces incoming wave boundary conditions at the horizon. Thus, for each choice of quark mass, we solved (5.51) numerically, taking $E_x(\rho) = (\rho - 1)^{-i\mathfrak{w}} F(\rho)$ and where $F(\rho)$ is regular at the horizon with $F(1) = 1$ and $\partial_\rho F(1) = i\mathfrak{w}/2$ for real $\mathfrak{w}$.

The spectral function was evaluated using the numerical solutions for E_x and eq. (5.46). In the high frequency limit, the spectral function asymptotes to $N_{\rm f}N_{\rm c}\omega^2/4\pi$ – see section 5.6.2. Figure 5.4 provides plots of the finite-temperature part of the spectral function,[7] $\mathfrak{R}(\omega) - N_{\rm f}N_{\rm c}\omega^2/4\pi$, for various D7-brane embeddings, specified by $\chi_0 = \chi(\rho = 1)$ (or equivalently by m). The upper plot shows the finite temperature part of the spectral function for temperatures above the phase transition: $\chi_0 = 0$ ($m = 0$), $\chi_0 = 0.1$ ($m = 0.1667$), $\chi_0 = 0.5$ ($m = 0.8080$), $\chi_0 = 0.8$ ($m = 1.2026$), $\chi_0 = 0.94$ ($m = 1.3059$) – the last of these corresponds to $T/M_{\rm q}$ for the phase transition. Note that the $\chi = 0$ and $\chi_0 = 0.1$ lines are virtually coincident. The lower plot shows the finite temperature part of the spectral function for values of χ_0 corresponding to black hole embeddings after the phase transition, *i.e.,* along the lines A_1 to A_2 and A_2 to A_3 on the black hole branch in fig. 5.3. Note that as χ_0 approaches 1, the finite temperature part of the spectral function displays

[7] In using the wording 'finite temperature part of the spectral function,' we are adopting the language used previously for $\mathcal{N} = 4$ SYM in section 5.1.3 and ref. [184]. In the present case, this refers to the spectral function minus its high frequency asymptotics.

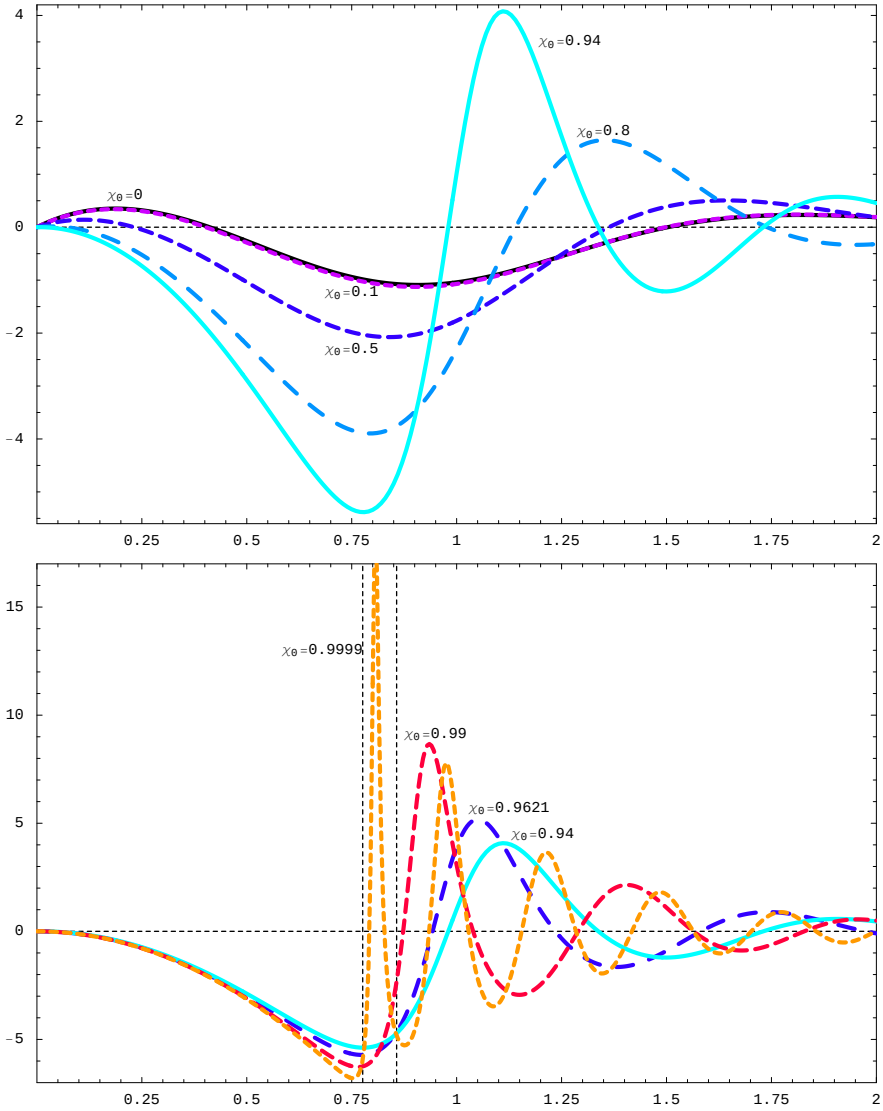

Figure 5.4: The finite temperature part of the vector spectral function, *i.e.*, $\mathfrak{R} - N_{\rm f}N_{\rm c}\omega^2/4\pi$, in units of $N_{\rm f}N_{\rm c}T^2/4$, versus $\mathfrak{w} = \omega/2\pi T$ for various values of χ_0 corresponding to different values of $m = \bar{M}/T$. The upper plot shows values of χ_0 corresponding to temperatures above the phase transition while the lower plot is for values of χ_0 past the transition. The vertical dotted lines represent the mass of the lowest and first excited vector mesons in the low temperature (Minkowski) phase for a near-critical Minkowski embedding.

high peaks. Further, as $\chi_0 \to 1$, the peaks in the spectral function grow sharper, become more closely spaced, and move towards lower frequencies. For example, the peaks in the $\chi_0 = 0.9999$ line are much more closely spaced than those in the $\chi_0 = 0.99$ line.

It is interesting to compare the positions of these peaks to the masses of the lowest vector mesons in the Minkowski phase, computed in section 2.3.3. The vertical dotted line at $\mathfrak{w} \simeq 0.776$ represents the mass of the lowest vector meson for a Minkowski embedding very close to the critical embedding. It seems that the position of the first peak of the spectral function is converging to a very similar value as $\chi_0 \to 1$ – certainly for $\chi_0 = 0.9999$, the first peak is very close to $\mathfrak{w} \simeq 0.776$. The second vertical dotted line at $\mathfrak{w} \simeq 0.857$ represents the mass of the first excited vector meson ($n = 1, \ell = 0$) as the Minkowski embedding approaches the critical solution. In this case, it is likely that the second peak in the spectral function is approaching this value, but certainly it is not converging on this position as rapidly as the first peak. Note that in the Minkowski phase, $\mathfrak{w} \simeq 0.98$ corresponds to the mass of the lowest vector meson just at the phase transition. This is significantly above both masses quoted above near the critical solution – recall from section 2.3.3 that in general the meson masses decreased as the critical embedding was approached [112]. Further then, this mass does not seem to be correlated with the positions of the spectral peaks for the black hole embedding at the phase transition, beyond being in the same general range.

The high peaks in the spectral function for $\chi_0 \to 1$ may be interpreted in terms of quasiparticle states because their width Γ is much less than their frequency Ω: $\Gamma \ll \Omega$. Section 5.6.3 presents a complementary discussion which reaches the same conclusion. Only the pseudoscalar modes are explicitly discussed in section 5.6.3, however, the results for the vector are almost identical. In particular, the effective potential shown in section 5.6.3 develops a finite barrier at intermediate values of the radius as $\chi_0 \to 1$. This suggests the existence of metastable states in the corresponding Schroedinger problem which, as discussed in section 5.6.3, should correspond to quasinormal frequencies with $\Gamma \ll \Omega$ in this regime.

Charged vectors

The $\mathcal{N} = 2$ gauge theory under study here has an internal $SO(4) = SU(2) \times SU(2)$ global symmetry, which is dual to rotations on the D7-branes' internal S^3. The vector modes

which are considered above are all singlets under this symmetry. However, these operators only correspond to the lowest dimension operators in an infinite family of vector operators transforming in the $(\ell/2, \ell/2)$ representation of the internal symmetry [61]. As outlined in appendix A.4, these operators are built up by combining the adjoint hypermultiplet fields (scalars) with the fundamental fields appearing in the singlet operators.

Evaluating the spectral function for these vectors with $\ell \neq 0$ follows closely the analysis in the previous subsection and so only salient steps are presented here. Of course, the first step is to consider an expansion of the world-volume vector in terms of spherical harmonics on the S^3,

$$A_\mu = \sum_\ell \mathcal{Y}^\ell(S^3)\, A^\ell_\mu(\rho, x^\mu)\,, \tag{5.53}$$

where the spherical harmonics on the unit three-sphere satisfy (2.76).[8] Examining the eight-dimensional Maxwell equations arising from eq. (5.34), one finds that with $\ell \neq 0$ (and $T \neq 0$) A^ℓ_ρ cannot be set to zero in general. Hence the general analysis becomes somewhat more elaborate. However, if we focus on spatially independent fluctuations, *i.e.,* the $q \to 0$ limit taken above, then both $A^\ell_{\rho,t}$ decouple and the calculations are greatly simplified. In this case then, the analogue of eq. (5.41) becomes

$$I_\ell = -\frac{N_{\rm f} N_{\rm c} T^2}{2^6\pi^2} \int \frac{d\omega}{\omega^2} \left[\frac{f\rho^3(1-\chi^2)^2}{\sqrt{1-\chi^2+\rho^2\dot\chi^2}} E^\ell_i(\rho,-k)\partial_\rho E^\ell_i(\rho,k) \right]^{\rho\to\infty}_{\rho\to 1}\,, \tag{5.54}$$

where i is summed over x, y, z and $E^\ell_i \equiv \omega A^\ell_i$. Recall that with vanishing spatial momenta, there is no distinction between longitudinal and transverse electric fields (in the language of section 5.1).

Examining the asymptotic behaviour of any of the electric field components, we write

$$E^\ell_i(\omega,\rho) = E^\ell_0(\omega) \frac{(\pi T)^\ell}{2^{\ell/2}} \rho^\ell_{\rm max} \frac{E_{\ell,\omega}(\rho)}{E_{\ell,\omega}(\rho_{\rm max})}\,, \tag{5.55}$$

where it is understood that eventually the limit $\rho_{\rm max} \to \infty$ will be taken. Note the factor of $\rho^\ell_{\rm max}$ required to obtain the correct asymptotic behaviour – see appendix A.4. As above,

[8] Of course, the spherical harmonics for a given ℓ are also labeled by two further $SU(2)$ quantum numbers, but we drop these as they are irrelevant in the following. Implicitly, our normalisation is such that $\mathcal{Y}^{\ell=0}_{m=0,n=0}(S^3) = 1$ and so $\int d^3\Omega\sqrt{h}\, \mathcal{Y}^{*\ell'}_{m'n'} \mathcal{Y}^\ell_{mn} = 2\pi^2\, \delta_{\ell\ell'}\, \delta_{mm'}\, \delta_{nn'}$.

taking variations of $E_0^\ell(k)$ then yields the flux factor $\mathcal{F}_\ell$ for E_i^ℓ. This then leads to the following expression for the spectral function for A_i:

$$\mathfrak{R}_{ii}^\ell(\omega) \equiv -2\mathrm{Im}G_{ii}^\ell(\omega) = -\frac{\pi^{2\ell}}{2^{\ell+2}} N_{\rm f} N_{\rm c} T^{2\ell+2} \mathrm{Im}\left[\rho^{2\ell+3} \frac{\partial_\rho E_{\ell,\omega}(\rho)}{E_{\ell,\omega}(\rho)}\right]_{\rho\to\infty} . \tag{5.56}$$

with no sum on i. Instead, for any value of $i = x, y, z$, the spectral functions are identical, *i.e.*, $\mathfrak{R}_{xx}^\ell(\omega) = \mathfrak{R}_{yy}^\ell(\omega) = \mathfrak{R}_{zz}^\ell(\omega)$, because we are limiting our analysis here to the case of vanishing spatial momentum. Hence in the following we denote these spectral functions by $\mathfrak{R}_\ell(\omega)$.

In order to evaluate the spectral functions, we must solve the Maxwell equations arising from the eight-dimensional action (5.34). Expressed in terms of the electric field components, the relevant equation of motion is

$$\ddot{E}_{\ell,\omega} + \left[\frac{4\dot{f}}{\tilde{f}\, f} + \frac{f}{\tilde{f}^2}\frac{\sqrt{1-\chi^2+\rho^2\dot{\chi}^2}}{\rho^3(1-\chi^2)^2}\partial_\rho\left(\frac{\tilde{f}^2\rho^3(1-\chi^2)^2}{f\sqrt{1-\chi^2+\rho^2\dot{\chi}^2}}\right)\right]\dot{E}_{\ell,\omega} + \frac{1-\chi^2+\rho^2\dot{\chi}^2}{\rho^2(1-\chi^2)^2}\left[\frac{8(1-\chi^2)\tilde{f}}{\rho^2 f^2}\mathfrak{w}^2 - \ell(\ell+2)\right]E_{\ell,\omega} = 0\,. \tag{5.57}$$

We now proceed to compute the spectral function $\mathfrak{R}_\ell(\omega)$, first for massless quarks ($m = 0$) and then for quarks with a finite mass.

Recall that the case of massless quarks corresponds to the equatorial embedding of the D7-branes for which $\chi(\rho) = 0$. In the previous section, we noted that for the $\ell = 0$ vector, the calculation of $\mathfrak{R}(\omega)$ then becomes the same as that in our example of section 5.1.3. In particular, an analytic solution can be found for $q = 0$ because it is possible to solve (5.51) exactly when $\chi = 0$. Here we show that in fact the general equation (5.57) for any ℓ has an analytic solution in this case of massless quarks.

Setting $\chi = 0$ and making the change of variables $\bar{x} = 1 - 2/\rho^2\tilde{f} = 1 - 2\rho^2/(1+\rho^4)$, the equation for the fluctuation $E_{\ell,\omega}(\bar{x})$ is

$$E''_{\ell,\omega} + \frac{f'}{f}E'_{\ell,\omega} + \left[\frac{\mathfrak{w}^2}{(1-\bar{x})f^2} - \frac{\ell(\ell+2)}{4(1-\bar{x})^2 f}\right]E_{\ell,\omega} = 0\,, \tag{5.58}$$

where the prime denotes a derivative with respect to $\bar{x}$. As in eq. (5.20), the solution is given by[9]

$$E_{\ell,\omega}(\bar{x}) = \bar{x}^{-i\mathfrak{w}/2}\,(2-\bar{x})^{-\mathfrak{w}/2}\,F(\bar{x})\,, \tag{5.59}$$

[9]Note that near the horizon $\bar{x} \simeq 2(\rho-1)^2$ and so the small $\bar{x}$ behaviour here is consistent with the boundary condition at the horizon discussed for the numerical solution.

where the regular function $F(\bar{x})$ is a straightforward generalisation of the result (5.22):

$$F(\bar{x}) = (1-\bar{x})^{\frac{(1+i)\mathfrak{w}}{2}}\, {}_2F_1\left(1+\frac{\ell}{2}-\frac{(1+i)\mathfrak{w}}{2}\,, -\frac{\ell}{2}-\frac{(1+i)\mathfrak{w}}{2}\,; 1-i\mathfrak{w}; \frac{\bar{x}}{2(\bar{x}-1)}\right) . \quad (5.60)$$

The spectral function is then given by

$$\mathfrak{R}_\ell(\omega) = -\lim_{\epsilon\to 0}\frac{\pi^{2\ell}}{2^\ell} N_{\rm f} N_{\rm c} T^{2\ell+2}\, \mathrm{Im} f(\bar{x}) \left(\frac{1+\sqrt{f}}{1-\bar{x}}\right)^\ell \frac{E(\bar{x},-\mathfrak{w})}{E(1-\epsilon,-\mathfrak{w})}\frac{E'(\bar{x},\mathfrak{w})}{E(1-\epsilon,\mathfrak{w})} . \quad (5.61)$$

The right hand side of eq. (5.61) is independent of the radial coordinate [123] and thus can be computed at any value of $\bar{x}$, *e.g.,* at $\bar{x}=0$. We obtain

$$\mathfrak{R}_\ell(\omega) = \frac{2^\ell \pi^{2\ell-1}}{(\ell!)^2}\, N_{\rm f} N_{\rm c} T^{2\ell+2} \sinh \pi\mathfrak{w} \left|\Gamma\left(1+\frac{\ell}{2}-\frac{\mathfrak{w}}{2}-\frac{i\mathfrak{w}}{2}\right)\Gamma\left(1+\frac{\ell}{2}+\frac{\mathfrak{w}}{2}-\frac{i\mathfrak{w}}{2}\right)\right|^2 , \quad (5.62)$$

which shows that the poles of the retarded correlator corresponding to $\mathfrak{R}_\ell(\omega)$ are located at

$$\mathfrak{w} = \pm\left(n+1+\frac{\ell}{2}\right)(1\mp i)\,, \qquad n=0,1,\ldots . \quad (5.63)$$

Note that there is an interesting degeneracy in the positions of these quasinormal modes in that their position only depends on $n+\ell/2$. This is reminiscent of the unexpected degeneracy found in [61], where the meson masses only depended on the combination $n+\ell$ (at $T=0$). For $\ell=0$, eq. (5.62) reduces (up to the normalisation) to the result (5.27). For odd and even $\ell>0$, respectively, eq. (5.62) can be written in the form

$$\begin{aligned}
\mathfrak{R}_{\ell=2n-1}(\omega) &= \frac{\pi^{2\ell}}{2^\ell} N_{\rm f} N_{\rm c} T^{2\ell+2}\, \frac{2^{4n}\Gamma^4(n+1/2)}{2\pi[(2n-1)!]^2}\, \frac{\sinh\pi\mathfrak{w}}{\cosh\pi\mathfrak{w}+\cos\pi\mathfrak{w}} \prod_{k=1}^{n}\left(1+\frac{4\mathfrak{w}^4}{(2k-1)^4}\right), \\
\mathfrak{R}_{\ell=2n}(\omega) &= \frac{\pi^{2\ell}}{2^\ell} N_{\rm f} N_{\rm c} T^{2\ell+2}\, \frac{2^{4n}(n!)^4}{[(2n)!]^2}\, \frac{\pi\mathfrak{w}^2\sinh\pi\mathfrak{w}}{\cosh\pi\mathfrak{w}-\cos\pi\mathfrak{w}} \prod_{k=1}^{n}\left(1+\frac{\mathfrak{w}^4}{4k^4}\right),
\end{aligned}$$

where $n=1,2,\ldots$. The asymptotics of the spectral function for large and small frequency are

$$\begin{aligned}
\mathfrak{R}_\ell(\omega) &= \frac{\pi^{2\ell+1}}{(\ell!)^2} N_{\rm f} N_{\rm c} T^{2\ell+2}\, \mathfrak{w}^{2\ell+2}\left(1+(-1)^\ell 2e^{-\pi\mathfrak{w}}\cos\pi\mathfrak{w}\right)\left(1+O(1/\mathfrak{w}^4)\right), \quad (5.64) \\
&\qquad\qquad \mathfrak{w}\to\infty\,, \\
\mathfrak{R}_\ell(\omega) &= \frac{2^\ell\pi^{2\ell}}{(\ell!)^2} N_{\rm f} N_{\rm c} T^{2\ell+2}\Gamma^4(1+\frac{\ell}{2})\,\mathfrak{w}\,, \qquad \mathfrak{w}\to 0\,. \quad (5.65)
\end{aligned}$$

In particular, we have the $\ell = 1$ spectral function:

$$\mathfrak{R}_1(\omega) = \frac{\pi^3}{4} N_{\rm f} N_{\rm c} T^4 \frac{(1+4\mathfrak{w}^4)\sinh \pi\mathfrak{w}}{\cosh \pi\mathfrak{w} + \cos \pi\mathfrak{w}} \,. \tag{5.66}$$

The large frequency asymptotics of $\mathfrak{R}_1(\omega)$ is

$$\mathfrak{R}_1(\omega) \to \bar{\mathfrak{R}}_1(\omega) = \frac{\pi^2}{2} N_{\rm f} N_{\rm c} T^4 \left[2\pi\mathfrak{w}^4 \left(1 - 2e^{-\pi\mathfrak{w}} \cos \pi\mathfrak{w}\right) + \frac{\pi}{2} \right] , \tag{5.67}$$

where we have dropped $\mathcal{O}(e^{-\pi\mathfrak{w}})$ terms. Thus for sufficiently large values of $\mathfrak{w}$ the finite temperature part of the spectral function, $\mathfrak{R}_1(\omega) - \pi^3 N_{\rm f} N_{\rm c} T^4 \mathfrak{w}^4$, exhibits damped oscillations around $\pi^3 N_{\rm f} N_{\rm c} T^4/4$ – see fig. 5.5. Note that for $\ell \geq 2$ the finite temperature part of the spectral function asymptotes to $\mathfrak{w}^{2\ell+2}$ for large $\mathfrak{w}$ and thus the oscillatory behaviour again becomes a subdominant effect.

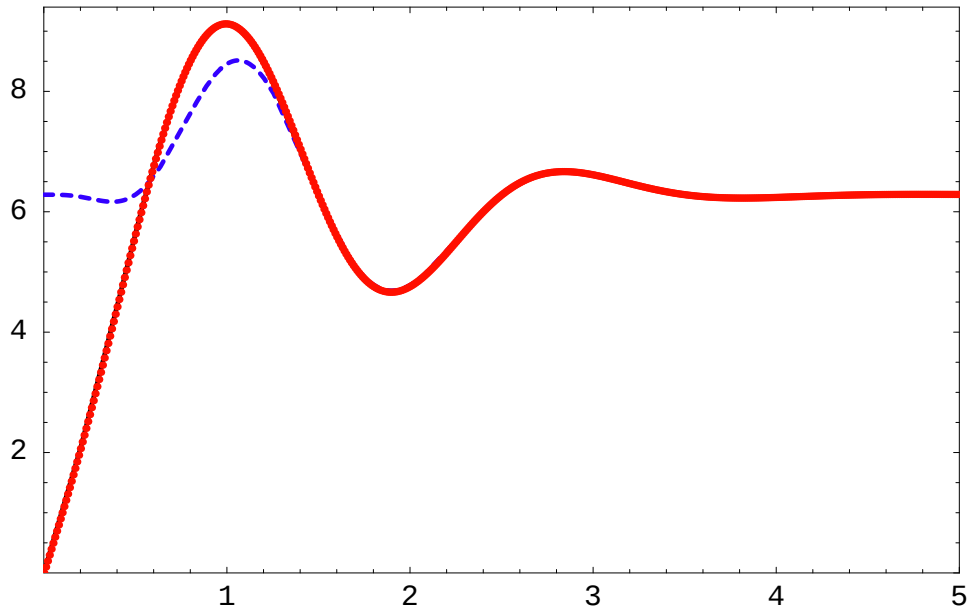

Figure 5.5: The finite temperature parts of the $M_{\rm q} = 0$ ($\chi_0 = 0$), $q = 0$, $\ell = 1$ vector spectral function ($\mathfrak{R}_1 - N_{\rm f} N_{\rm c} \omega^4/16\pi$) and of its high frequency asymptotics (5.67) ($\bar{\mathfrak{R}}_1 - N_{\rm f} N_{\rm c} \omega^4/16\pi$) (dashed blue line), in units of $\pi^2 N_{\rm f} N_{\rm c} T^4/8$, versus $\mathfrak{w} = \omega/2\pi T$. Note the figure also demonstrates the precise agreement between the numerical results (red dots) and the exact result (solid black line, which is essentially invisible above).

As in the previous section, for massive quarks ($\chi_0 \neq 0$), both the embedding equation (2.44) and the vector equation of motion (5.57) must be solved numerically. Solving for $E_{\ell,\omega}$ requires special attention to the boundary conditions near the horizon ($\rho \to 1$). As for the $\ell = 0$ case, the appropriate incoming wave conditions are imposed by taking $E_{\ell,\omega}(\rho) = (\rho-1)^{-i\mathfrak{w}} F(\rho)$ with $F(1) = 1$ and $\partial_\rho F(1) = i\mathfrak{w}/2$.

The vector spectral function for $\ell = 1$ is shown for various values of χ_0 in fig. 5.6. For all values of χ_0, the $\ell = 1$ spectral functions approach $N_{\rm f}N_{\rm c}\omega^4/16\pi$ at large ω – see section 5.6.2. While this common behaviour is not clear in fig. 5.6, it can be seen by going to larger $\mathfrak{w}$. Note that the spectral functions in the upper plot, which correspond to values of the $T/M_{\rm q}$ above the phase transition, seem to be essentially featureless. In contrast, the lower plot shows that as the critical embedding is approached (with $\chi_0 \to 1$) some peaks are appearing in the spectral function. The masses of the lowest two $\ell = 1$ vector mesons in the low temperature phase for a near-critical Minkowski embedding have been included in this plot as well. While these lines lie close to the first peak for the $\chi_0 = 0.9999$ spectral function, the peaks do not seem to be converging to these positions nearly as rapidly as was seen for $\ell = 0$.

The peaks in the spectral function for $\chi_0 \to 1$ may again be interpreted in terms of quasiparticle states when their width Γ and is much less than their frequency Ω: $\Gamma \ll \Omega$. Hence, as discussed for $\ell = 0$, it appears that the quasinormal frequencies are approaching the real axis in this regime. However, we stress that this approach is occurring much more slowly for the $\ell > 0$ modes. In particular, the spectral function remains essentially structureless for $\chi_0 = 0.94$, which corresponds to the phase transition between the black hole and Minkowski embeddings. Therefore the mesonic states corresponding to the higher-ℓ vector operators dissociate immediately at the phase transition.

Note the complementary discussion in section 5.6.3 would lead to similar conclusions. In particular, a barrier in the effective potential develops as in the $\ell = 0$ analysis but only for values of χ_0 much closer to one when $\ell > 0$. Hence metastable states in the corresponding Schroedinger problem would only appear in this regime for χ_0 very close to one.

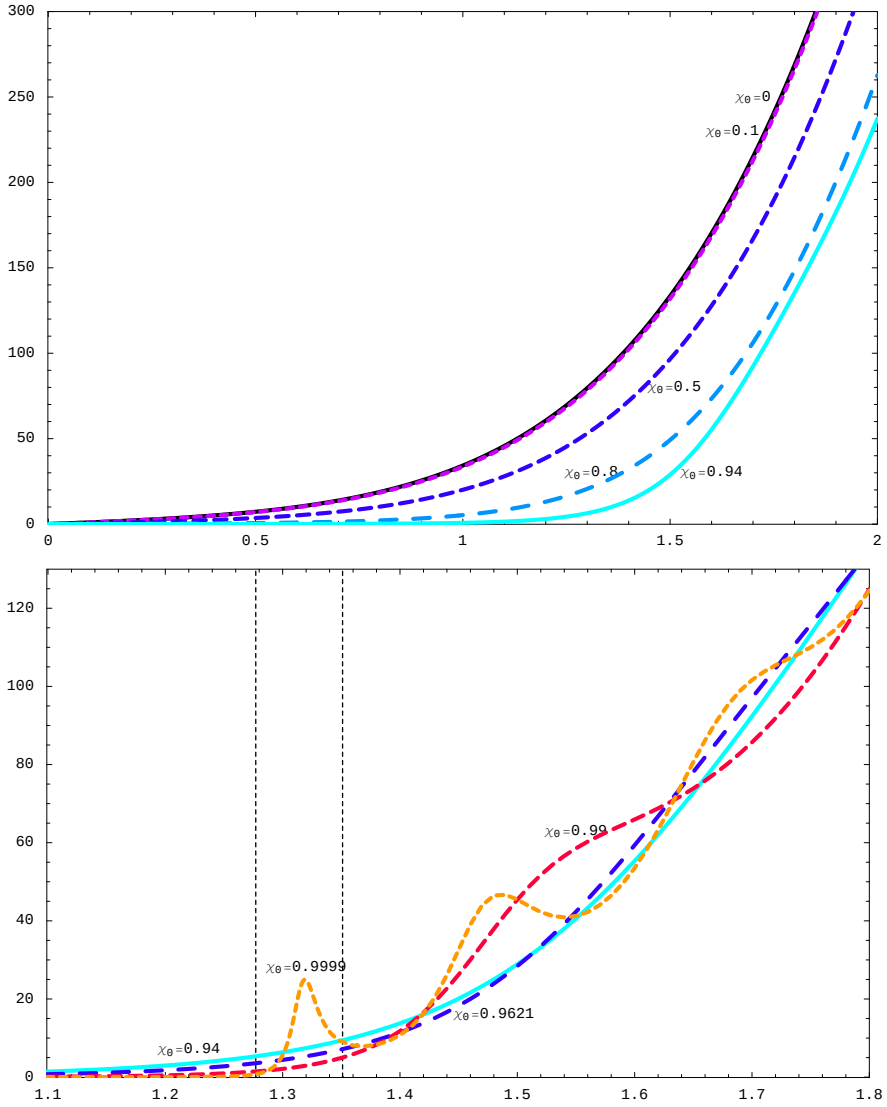

Figure 5.6: The vector spectral function for $\ell = 1$ in units of $\pi^2 N_{\rm f} N_{\rm c} T^4/8$ versus $\mathfrak{w}$. The upper plot shows values of χ_0 corresponding to temperatures above the phase transition while the lower plot is for values of χ_0 past the phase transition. In the lower plot we focus on values of $\mathfrak{w}$ for which the spectral function shows structure. The vertical dotted lines represent the mass of the lowest and first excited vector mesons for $\ell = 1$ in the low temperature (Minkowski) phase for a near-critical embedding.

5.3.2 Scalars

We now turn to scalar and pseudoscalar excitations of the fundamental fields. In the dual gravity picture, these correspond to scalar fluctuations of the D7-brane probes in the black D3 geometry (2.36) about the fiducial embedding given by $\theta_v(\rho)$:

$$\theta(\sigma^a) = \theta_v(\rho) + \delta\theta(\sigma^a)\,, \qquad \phi = 0 + \delta\phi(\sigma^a)\,, \tag{5.68}$$

where σ^a denotes the D7-branes' worldvolume coordinates. Appendix A describes the holographic dictionary relating the scalar $\delta\theta$ and the pseudoscalar $\delta\phi$ to the corresponding gauge theory operators.

The pull-back of the bulk metric (2.36) to the D7 worldvolume is:

$$ds^2 = ds^2(g) - \frac{2L^2\dot\chi}{\sqrt{1-\chi^2}}\partial_a(\delta\theta)dx^a d\rho + L^2\left[\partial_a(\delta\theta)\partial_b(\delta\theta) + \chi^2\partial_a(\delta\phi)\partial_b(\delta\phi)\right]dx^a dx^b$$

where

$$ds^2(g) = \frac{1}{2}\left(\frac{u_0\rho}{L}\right)^2\left[-\frac{f^2}{\tilde f}dt^2 + \tilde f dx_3^2\right] + \frac{L^2}{\rho^2}\left[\left(1+\frac{\rho^2\dot\chi^2}{1-\chi^2}\right)d\rho^2 + \rho^2\sin^2(\theta_v+\delta\theta)d\Omega_3^2\right]. \tag{5.69}$$

As before, we've put $\chi(\rho) = \cos\theta_v(\rho)$. Using the DBI action and retaining terms only to quadratic order in the fluctuations, the Lagrangian density is

$$\begin{aligned}\mathcal{L} \;=\; & \mathcal{L}_0 + -\frac{N_{\rm f}T_{\rm D7}{u_0}^4}{4}\sqrt{h}\,\partial_\rho\left[-\frac{\rho^5 f\tilde f(1-\chi^2)^{3/2}\dot\chi}{\sqrt{1-\chi^2+\rho^2\dot\chi^2}}\delta\theta - \frac{3}{2}\frac{\rho^5 f\tilde f(1-\chi^2)\chi\dot\chi}{\sqrt{1-\chi^2+\rho^2\dot\chi^2}}(\delta\theta)^2\right] \\ & -\frac{N_{\rm f}T_{\rm D7}{u_0}^4}{4}\sqrt{h}\,\rho^3 f\tilde f\sqrt{1-\chi^2+\rho^2\dot\chi^2}\left[-\frac{3}{2}\frac{1-\chi^2}{1-\chi^2+\rho^2\dot\chi^2}(\delta\theta)^2\right. \\ & \left.+\frac{L^2}{2}(1-\chi^2)g_v^{ab}\left(\frac{(1-\chi^2)\partial_a(\delta\theta)\partial_b(\delta\theta)}{1-\chi^2+\rho^2\dot\chi^2} + \chi^2\partial_a(\delta\phi)\partial_b(\delta\phi)\right)\right],\end{aligned} \tag{5.70}$$

where g_v^{ab} is the metric (5.69) with $\delta\theta = 0$ and $\mathcal{L}_0$ is the Lagrangian density for the fiducial embedding χ (given in (2.42)). We eliminated terms linear in $\delta\theta$ by integrating by parts and using the equation of motion (2.44) for χ.

The equations of motion for the fluctuations follow from (5.70) as

$$\partial_a\left[\sqrt{h}\,\rho^3 f\tilde f(1-\chi^2)\chi^2\sqrt{1-\chi^2+\rho^2\dot\chi^2}\,g_v^{ab}\,\partial_b(\delta\phi)\right] = 0 \tag{5.71}$$

for $\delta\phi$ and

$$L^2\partial_a\left[\frac{\sqrt{h}\,\rho^3 f\tilde{f}(1-\chi^2)^2}{\sqrt{1-\chi^2+\rho^2\dot{\chi}^2}}\,g_v^{ab}\,\partial_b(\delta\theta)\right]+3\frac{\sqrt{h}\,\rho^3 f\tilde{f}(1-\chi^2)}{\sqrt{1-\chi^2+\rho^2\dot{\chi}^2}}\delta\theta=0 \tag{5.72}$$

for $\delta\theta$.

Pseudoscalar $\delta\phi$

The relevant portion of the action (5.70) for the pseudoscalar $\delta\phi$ is

$$I_{\delta\phi}=-\frac{T_{\rm D7}N_{\rm f}{u_0}^4L^2}{8}\int d^8\sigma\,\partial_a\left[\sqrt{h}\,\rho^3 f\tilde{f}(1-\chi^2)\chi^2\sqrt{1-\chi^2+\rho^2\dot{\chi}^2}\,g_v^{ab}\,\delta\phi\,\partial_b\delta\phi\right], \tag{5.73}$$

where we've integrated by parts and used the equation of motion (5.71). To evaluate the spectral function we only need the complex part of (5.73) and hence in the following we retain only the term involving the ρ derivative. Exanding the fluctuation in terms of spherical harmonics on the S^3 of unit radius,

$$\delta\phi=\sum_\ell \mathcal{Y}^\ell(S^3)\delta\phi_\ell(\rho,x^\mu)\,, \tag{5.74}$$

the term needed to evaluate the spectral function for the ℓth mode is

$$I_{\delta\phi_\ell}=-\frac{T_{\rm D7}N_{\rm f}{u_0}^4\Omega_3}{8}\int d^4x\,\left[\frac{\rho^5 f\tilde{f}(1-\chi^2)^2\chi^2}{\sqrt{1-\chi^2+\rho^2\dot{\chi}^2}}\,\delta\phi_\ell\,\partial_\rho\delta\phi_\ell\right]_{\rho\to\infty}. \tag{5.75}$$

We take the Fourier transform of $\delta\phi_\ell$ with $k=(-\omega,q,0,0)$,

$$\delta\phi_\ell(\rho,x^\mu)=\int\frac{d\omega dq}{(2\pi)^2}e^{-i\omega t+iqx}\delta\phi_\ell(\rho,k)\,, \tag{5.76}$$

and write

$$\delta\phi_\ell(\rho,k)=\delta\phi_\ell^0(k)\frac{(\pi T)^\ell}{2^{\ell/2}}\rho_{\rm max}^\ell\frac{\mathcal{P}_{\ell,k}(\rho)}{\mathcal{P}_{\ell,k}(\rho_{\rm max})}\,, \tag{5.77}$$

where the limit $\rho_{\rm max}\to\infty$ will eventually be taken. Note the factor of $\rho_{\rm max}^\ell$ required to obtain the correct asymptotic behaviour $\delta\phi_\ell(\rho_{\rm max},k)=\delta\phi_\ell^0(k)\rho_{\rm max}^\ell$ – see appendix A. We can then define the flux factor for the ℓth mode as

$$\mathcal{F}_{\phi_\ell}=-\frac{\pi^{2\ell}}{2^{\ell+6}}\lambda N_{\rm f}N_{\rm c}T^{2\ell+4}\left[\frac{\rho^5 f\tilde{f}(1-\chi^2)^2\chi^2}{\sqrt{1-\chi^2+\rho^2\dot{\chi}^2}}\,\frac{\rho_{\rm max}^{2\ell}\,\mathcal{P}_{\ell,-k}(\rho)\,\partial_\rho\mathcal{P}_{\ell,k}(\rho)}{\mathcal{P}_{\ell,-k}(\rho_{\rm max})\,\mathcal{P}_{\ell,k}(\rho_{\rm max})}\right]_{\rho\to\infty}. \tag{5.78}$$

The retarded Green's function is then $G = -2\mathcal{F}$ [123] from which we obtain the spectral function $\mathfrak{A} = -2\mathrm{Im}\ G$ for $q = 0$ as

$$\mathfrak{A}_{\phi_\ell}(\omega, 0) = -\frac{\pi^{2\ell}}{2^{\ell+4}} \lambda N_{\mathrm{f}} N_{\mathrm{c}} T^{2\ell+4} m^2 \lim_{\rho\to\infty} \mathrm{Im}\left[\rho^{3+2\ell} \frac{\partial_\rho \mathcal{P}_{\ell,k}(\rho)}{\mathcal{P}_{\ell,k}(\rho)}\right], \tag{5.79}$$

where we simplified using eq. (2.45).

For the $\ell = 0$ mode, the holographic dictionary in appendix A describes how the variation $\delta\phi^0(k)$ introduced an insertion of the operator $M_{\mathrm{q}}\,\mathcal{O}_\phi$. Hence to get the spectral function for the dimension-three operator $\mathcal{O}_\phi$, we should normalise the spectral function by an extra factor $1/M_{\mathrm{q}}^2$. We expect that this should also hold for $\ell > 0$, in which case the operator $\mathcal{O}_{\phi_\ell}$ has dimension $\ell + 3$. Recalling that $m^2 = 4M_{\mathrm{q}}^2/\lambda T^2$, we arrive at:

$$\tilde{\mathfrak{A}}_{\phi_\ell}(\omega) = \frac{1}{M_{\mathrm{q}}^2}\mathfrak{A}_{\phi_\ell}(\omega, 0) = -\frac{\pi^{2\ell}}{2^{\ell+2}} N_{\mathrm{f}} N_{\mathrm{c}} T^{2\ell+2} \lim_{\rho\to\infty} \mathrm{Im}\left[\rho^{3+2\ell} \frac{\partial_\rho \mathcal{P}_k(\rho)}{\mathcal{P}_k(\rho)}\right]. \tag{5.80}$$

Using (5.76) and (5.77), the equation of motion (5.71) becomes

$$\begin{aligned}
&\partial_\rho\left[\frac{\rho^5 f\tilde{f}(1-\chi^2)^2\chi^2}{\sqrt{1-\chi^2+\rho^2\dot{\chi}^2}}\partial_\rho\mathcal{P}_{\ell,k}\right] \\
&= -\rho^3 f\tilde{f}\chi^2\sqrt{1-\chi^2+\rho^2\dot{\chi}^2}\left[\frac{8(1-\chi^2)}{\rho^2\tilde{f}}\left(\frac{\tilde{f}^2}{f^2}\mathfrak{w}^2 - \mathfrak{q}^2\right) - \ell(\ell+2)\right]\mathcal{P}_{\ell,k}\,.
\end{aligned} \tag{5.81}$$

Near the horizon ($\rho \to 1$) we impose incoming wave boundary conditions so that taking

$$\mathcal{P}_{\ell,k}(\rho) \simeq (\rho-1)^{-i\mathfrak{w}}\left[1 + \frac{i\mathfrak{w}}{2}(\rho-1) + \mathcal{O}(\rho-1)^2\right] \quad \text{for } \rho \to 1\,, \tag{5.82}$$

we were able to solve (5.81) numerically to evaluate the spectral function (5.80). The high frequency asymptotics of the spectral function are described in section 5.6.2.

Figure 5.7 provides plots of the finite temperature part of the spectral function, $\tilde{\mathfrak{A}}_\phi - N_{\mathrm{f}}N_{\mathrm{c}}\omega^2/4\pi$, for the pseudoscalar $\delta\phi$, $\ell = 0$, for various values of χ_0. Qualitatively the results are the same as for the vector spectal function shown in figure 5.4.[10] The quasiparticle peaks in spectral function quickly dissipate above the phase transition, *i.e.,* for $\chi_0 < 0.94$. High sharp peaks develop as $\chi_0 \to 1$. As before, the position of these peaks may be compared with the masses of the lowest pseudoscalar mesons on the Minkowski branch.

[10] The $\ell = 1$ spectral function for the pseudoscalar closely resembles that for the vector, shown in fig. 5.6.

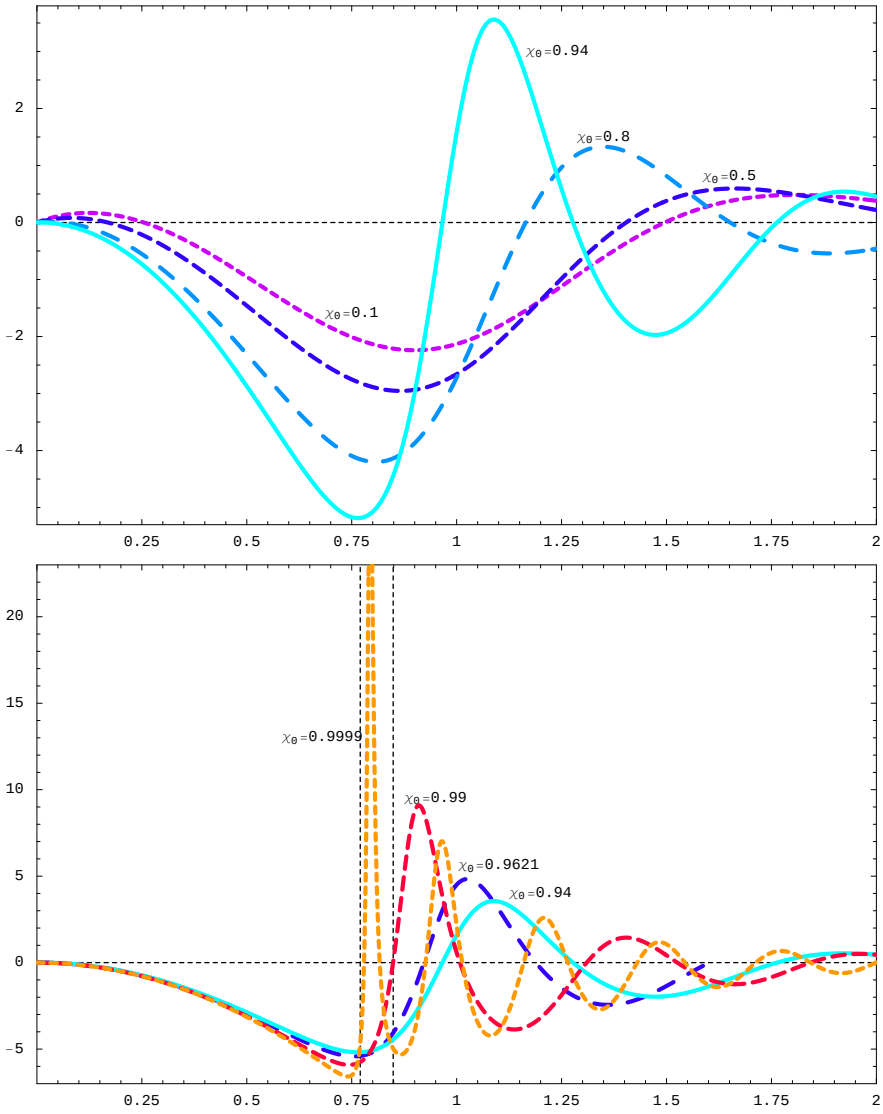

Figure 5.7: The finite temperature part of the $\delta\phi$, $\ell = 0$, spectral function, $\tilde{\mathfrak{R}}_\phi - N_{\rm f}N_{\rm c}\omega^2/4\pi$, in units of $N_{\rm f}N_{\rm c}T^2/4$ versus $\mathfrak{w} = \omega/2\pi T$ for various values of χ_0.The upper plot shows the spectral function for values of χ_0 corresponding to temperatures above the phase transition while the lower plot is for values of χ_0 past the transition. The vertical dotted lines represent the masses of the lowest two pseudoscalar mesons for a near-critical Minkowski embedding.

The vertical dotted lines mark the masses ($\mathfrak{w} \simeq 0.770$ and 0.849) of the lowest two $\delta\phi$ mesons (with $\ell = 0$) for a near-critical Minkowski embedding. Note that the first peak in the $\chi_0 = 0.9999$ line is nearly centred on the first value of $\mathfrak{w}$. The second peak of this spectral function also seems to be converging towards the mass of the next meson.

As before, the sharp peaks which develop in the spectral function as χ_0 approaches 1 may be interpreted in terms of quasiparticle states. Section 5.6.3 presents a complementary discussion of the quasinormal spectrum which reaches the same conclusion.

Scalar $\delta\theta$

The derivation of the spectral function for the scalar $\delta\theta$ is entirely analogous to that for the pseudoscalar. The portion of the action for the $\delta\theta$ fluctuations is, from (5.70),

$$I_{\delta\theta} = -\frac{N_{\rm f}T_{\rm D7}{u_0}^4}{4}\int d^8\sigma\,\left\{\sqrt{h}\partial_\rho\left[-\frac{\rho^5 f\tilde{f}(1-\chi^2)^{3/2}\dot{\chi}}{\sqrt{1-\chi^2+\rho^2\dot{\chi}^2}}\delta\theta - \frac{3}{2}\frac{\rho^5 f\tilde{f}(1-\chi^2)\dot{\chi}\chi}{\sqrt{1-\chi^2+\rho^2\dot{\chi}^2}}(\delta\theta)^2\right]\right.$$
$$\left. + \frac{L^2}{2}\partial_a\left[\frac{\sqrt{h}\rho^3 f\tilde{f}(1-\chi^2)^2}{\sqrt{1-\chi^2+\rho^2\dot{\chi}^2}}g_v^{ab}\delta\theta\partial_b\delta\theta\right]\right\},$$

where we've integrated by parts and used the equation of motion (5.72). As discussed above, to evaluate the spectral function we only need the imaginary part of the Green's function and hence of this action. Thus, only the ρ derivative term from the second line is needed. We expand the scalar in terms of spherical harmonics on the S^3 (as in (5.74)), take the Fourier transform (as in (5.76)), and express the ℓth mode as

$$\delta\theta_\ell(\rho,k) = \delta\theta_\ell^0(k)\,\frac{(\pi T)^\ell}{2^{\ell/2}}\rho_{\rm max}^{\ell-1}\frac{\mathcal{R}_{\ell,k}(\rho)}{\mathcal{R}_{\ell,k}(\rho_{\rm max})}, \tag{5.83}$$

where we will eventually take the limit $\rho_{\rm max}\to\infty$. Note that the factor of $\rho_{\rm max}^{\ell-1}$ is inserted to obtain the correct asymptotic behaviour – see appendix A.

Following the same procedure as with the pseudoscalars, we identify

$$\mathcal{F}_{\theta_\ell} = -\frac{\pi^{2\ell}}{2^{\ell+6}}\lambda N_{\rm f}N_{\rm c}T^{2\ell+4}\left[\frac{\rho^5 f\tilde{f}(1-\chi^2)^3}{(1-\chi^2+\rho^2\dot{\chi}^2)^{3/2}}\frac{\rho_{\rm max}^{2\ell-2}\mathcal{R}_{\ell,-k}(\rho)\partial_\rho\mathcal{R}_{\ell,k}(\rho)}{\mathcal{R}_{\ell,-k}(\rho_{\rm max})\mathcal{R}_{\ell,k}(\rho_{\rm max})}\right]_{\rho\to\infty}. \tag{5.84}$$

The spectral function then follows as

$$\mathfrak{R}_{\theta_\ell}(\omega,0) = -\frac{\pi^{2\ell}}{2^{\ell+4}}\lambda N_{\rm f}N_{\rm c}T^{2\ell+4}\lim_{\rho\to\infty}\,{\rm Im}\,\left[\rho^{3+2\ell}\frac{\partial_\rho\mathcal{R}_{\ell,k}(\rho)}{\mathcal{R}_{\ell,k}(\rho)}\right], \tag{5.85}$$

where we've used (2.45) to simplify.

Now recall $\chi = \cos\theta$ and asymptotically $\chi \simeq m/\rho$ where m is determined by gauge theory quantities in eq. (A.7). Note that asymptotically we can relate a variation in θ with a variation in χ: $\delta\chi = -\delta\theta$. Hence, a variation of the coefficient of the operator $\mathcal{O}_m$ in the gauge theory action (*i.e.,* figuratively we might say $\delta M_{\rm q}(k)$) corresponds to $(\sqrt{\lambda}\,T/2)\delta\theta_0(k)$ in eq. (5.83). In the correlator (5.85) two factors of $\delta\theta_0$ have been stripped off, so in order to normalise the correlator so that only the variations of the gauge theory coefficient are removed, we should multiply by a factor of $4/\lambda T^2$:

$$\tilde{\mathfrak{K}}_{\theta_\ell}(\omega) = \frac{4}{\lambda T^2}\,\mathfrak{K}_{\theta_\ell}(\omega,0) = -\frac{\pi^{2\ell}}{2^{\ell+2}} N_{\rm f} N_{\rm c} T^{2\ell+2} \lim_{\rho\to\infty} \mathrm{Im}\left[\rho^{3+2\ell}\frac{\partial_\rho \mathcal{R}_k(\rho)}{\mathcal{R}_k(\rho)}\right]. \tag{5.86}$$

With the Fourier transform of $\delta\theta$ and using the notation (5.83), the equation of motion (5.72) for $\delta\theta$ becomes

$$\begin{aligned}&\partial_\rho\left[\frac{\rho^5 f\tilde{f}(1-\chi^2)^3}{(1-\chi^2+\rho^2\dot{\chi}^2)^{3/2}}\partial_\rho\mathcal{R}_{\ell,k}\right]\\ &= -\frac{\rho^3 f\tilde{f}(1-\chi^2)}{\sqrt{1-\chi^2+\rho^2\dot{\chi}^2}}\left[\frac{8(1-\chi^2)}{\rho^2\tilde{f}}\left(\frac{\tilde{f}^2}{f^2}\mathfrak{w}^2-\mathfrak{q}^2\right)-(\ell+3)(\ell-1)\right]\mathcal{R}_{\ell,k}\,.\end{aligned} \tag{5.87}$$

As with the vector and pseudoscalar, we set $\mathfrak{q}=0$ and impose incoming wave boundary conditions at the horizon, requiring that the field behave as

$$\mathcal{R}_{\ell,k}(\rho) \simeq (\rho-1)^{-i\mathfrak{w}}\left[1+\frac{i\mathfrak{w}}{2}(\rho-1)+\mathcal{O}(\rho-1)^2\right] \tag{5.88}$$

near $\rho=1$.

We solved (5.87) numerically and evaluated the spectral function using (5.86). The high frequency asymptotics of the spectral function appear in section 5.6.2. Plots of the finite temperature part of the s-wave spectral function, $\tilde{\mathfrak{K}}_\theta - N_{\rm f}N_{\rm c}\omega^2/4\pi$, are provided in fig. 5.8 for D7-brane embeddings corresponding to temperatures above the phase transition. The spectral function shows no high peaks and little structure at temperatures above the phase transition.

Figure 5.9 provides plots of the spectral function for values of $0.94 < \chi_0 < 1$, corresponding to black hole embeddings past the phase transition, *i.e.,* continuing along the black hole branch in fig. 5.3 past point A_1. For $0.94 < \chi_0 < 0.96$, prior to the first kink in

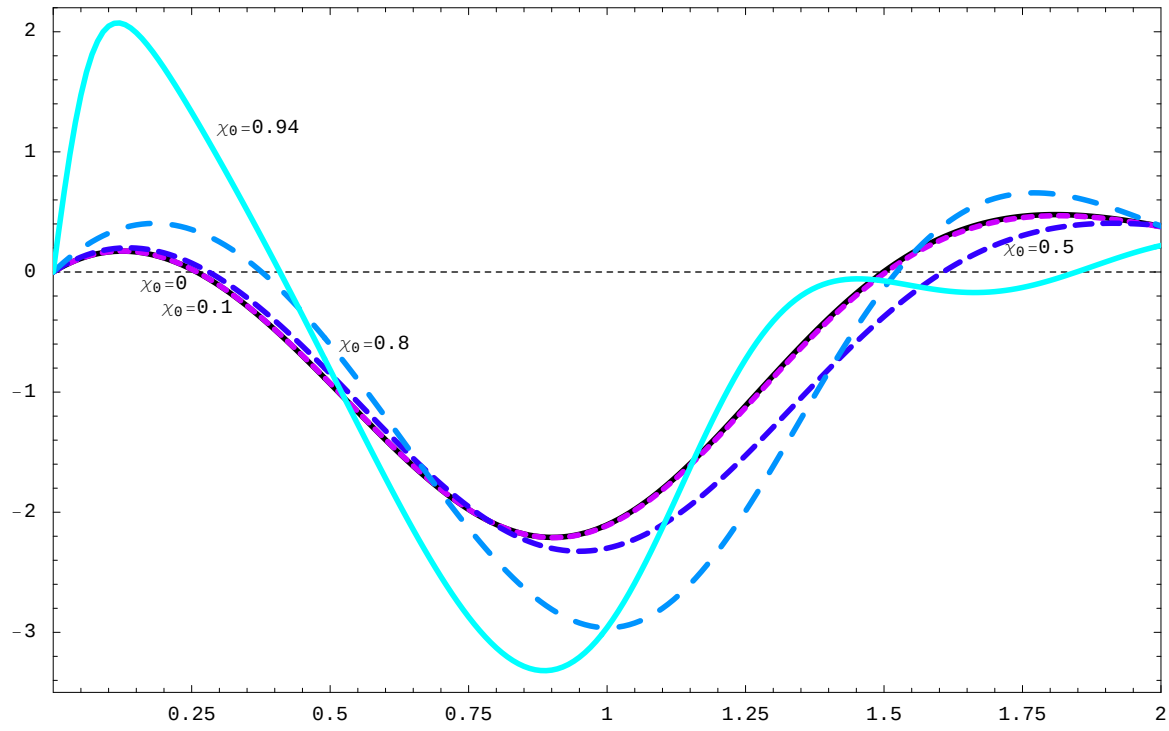

Figure 5.8: The finite temperature part of the s-wave ($\ell = 0$) scalar ($\delta\theta$) spectral function, $\tilde{\mathfrak{K}}_\theta - N_{\rm f}N_{\rm c}\omega^2/4\pi$, in units of $N_{\rm f}N_{\rm c}T^2/4$ for $\chi_0 \leq 0.94$, corresponding to temperatures above the phase transition.

the free energy (between A_1 and A_2 in fig. 5.3), no striking peaks appear in the spectral function. However, for $\chi_0 = 0.9621$, point A_2 in fig. 5.3, a very high peak appears in the spectral function, centred on $\omega = 0$. Taking a value of χ_0 slightly larger (smaller), say $\chi_0 = 0.964$ ($\chi_0 = 0.96$), fig. 5.9 shows that the peak is diminishing and is centred on a small but nonzero value of ω. A bit further away from the first kink, *e.g.,* $\chi_0 = 0.97\,, 0.98$ no peak is evident. Following the D7-brane embeddings to the second kink, which occurs for $\chi_0 = 0.99973885$, the same behaviour is evident: Near this value of χ_0 a small peak starts to appear in the spectral function and at $\chi_0 = 0.99973885$ a high peak, centred on $\omega = 0$ appears. As we will discuss in section 5.5, this behaviour is a result of quasinormal eigenfrequencies crossing the real axis from the lower to upper half of the complex ω-plane. As a result, these black hole embeddings become unstable beyond $\chi_0 = 0.9621$, in precise agreement with the thermodynamic discussion of section 5.2.1.

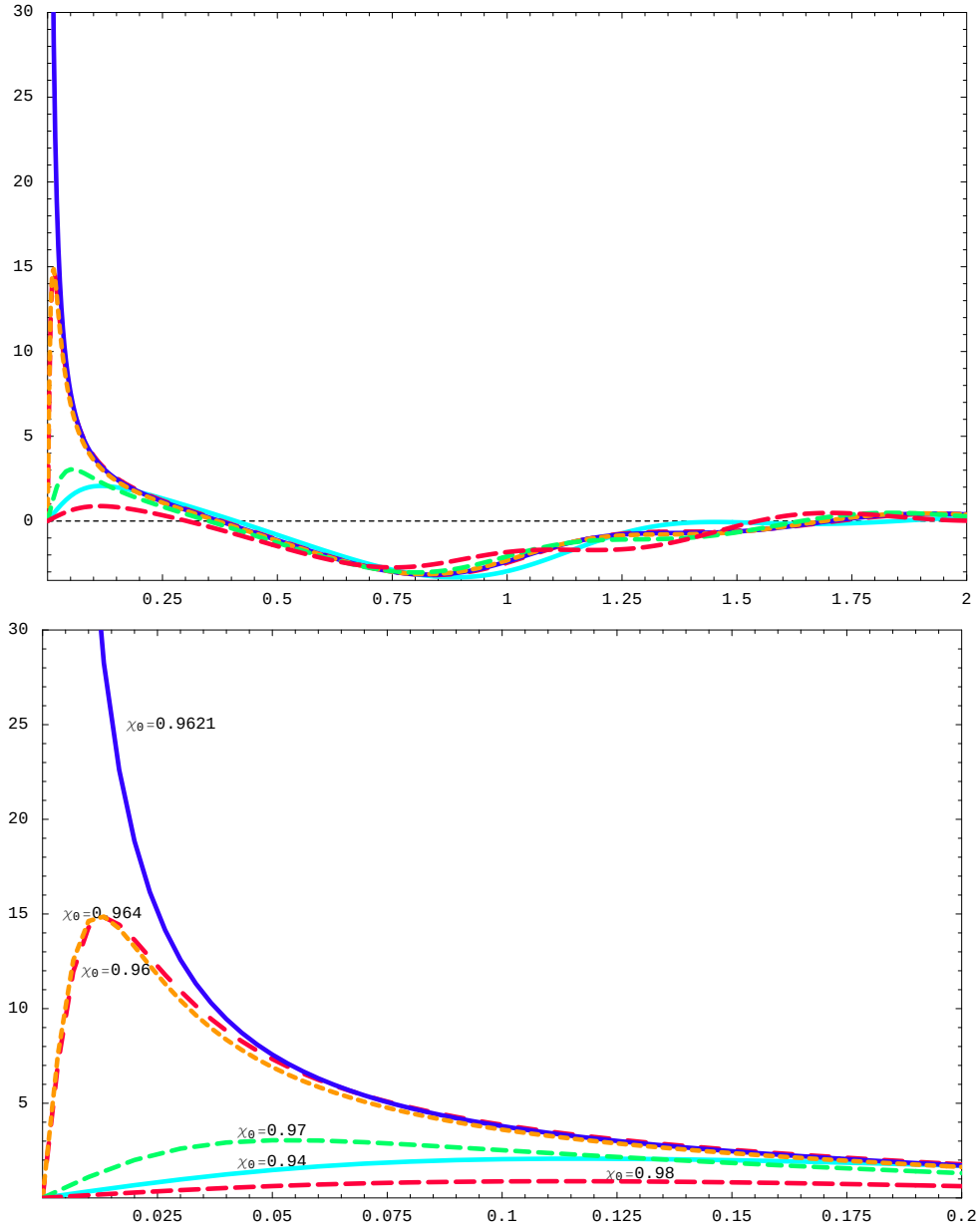

Figure 5.9: The finite temperature part of the scalar ($\delta\theta$) spectral function for $\ell = 0$ in units of $N_{\rm f}N_{\rm c}T^2/4$ for values of χ_0 past the phase transition. The lower plot focusses on the region near $\mathfrak{w} = 0$ where a peak appears in the spectral for $\chi_0 = 0.9621$, corresponding to the first kink in the plot of the free energy versus temperature.

Fig. 5.10 provides a plot of the scalar spectral function for the $\ell = 1$ mode. The spectral function does not show any structure for any values of χ_0, or, equivalently, m. In particular, we see no evidence for $\ell = 1$ of quasinormal eigenfrequencies crossing the real axis from the lower to upper half of the complex ω-plane. This is expected from section 2.3.3 where, in the low temperature (Minkowski) phase, we saw no evidence of tachyonic modes appearing for $\ell > 0$ [112].

We close this section with one final observation. While the pseudoscalar equation of motion (5.81) is singular in the massless limit, the spectral function should have a well defined limit. Further, if we compare the $\chi \to 0$ limits in the pseudoscalar and scalar channels in figures 5.7 and 5.8, it seems that they converge on the same spectral function. The fact that the spectral functions coincide in this limit should be a reflection of the restoration of an additional $U(1)$ global symmetry, corresponding to rotations in the 89-plane in the array (2.34), in the limit of vanishing quark mass. In the massless limit, this symmetry relates the two scalar operators.

5.4 Diffusion constant for 'light' quarks

The worldvolume gauge field A_μ is dual to a conserved current J^μ_q in the dual gauge theory – see appendix A. One then expects to see the diffusion of the conserved charge, *i.e.,* quark charge, according to Fick's law, $\vec{J}_q = -D\vec{\nabla}J^t_q$, with a certain diffusion constant. This expectation can be confirmed in a holographic context [119, 125] and in fact, the computation of the diffusion constant can be performed in a number of different ways. In the present D3/D7 brane system, we have explicitly computed the diffusion constant in three different ways: (a) using the membrane paradigm [125]; (b) the Green-Kubo formula; and (c) the lowest quasinormal frequency in the diffusion channel. In this section, we describe these different computations and our results confirm the internal consistency of the holographic framework, in that we show these different methods all give the same result.

5.4.1 Membrane paradigm method

The computation of the diffusion constant via the membrane paradigm was discussed in [125] where explicit formulae for various transport coefficients in terms of metric compo-

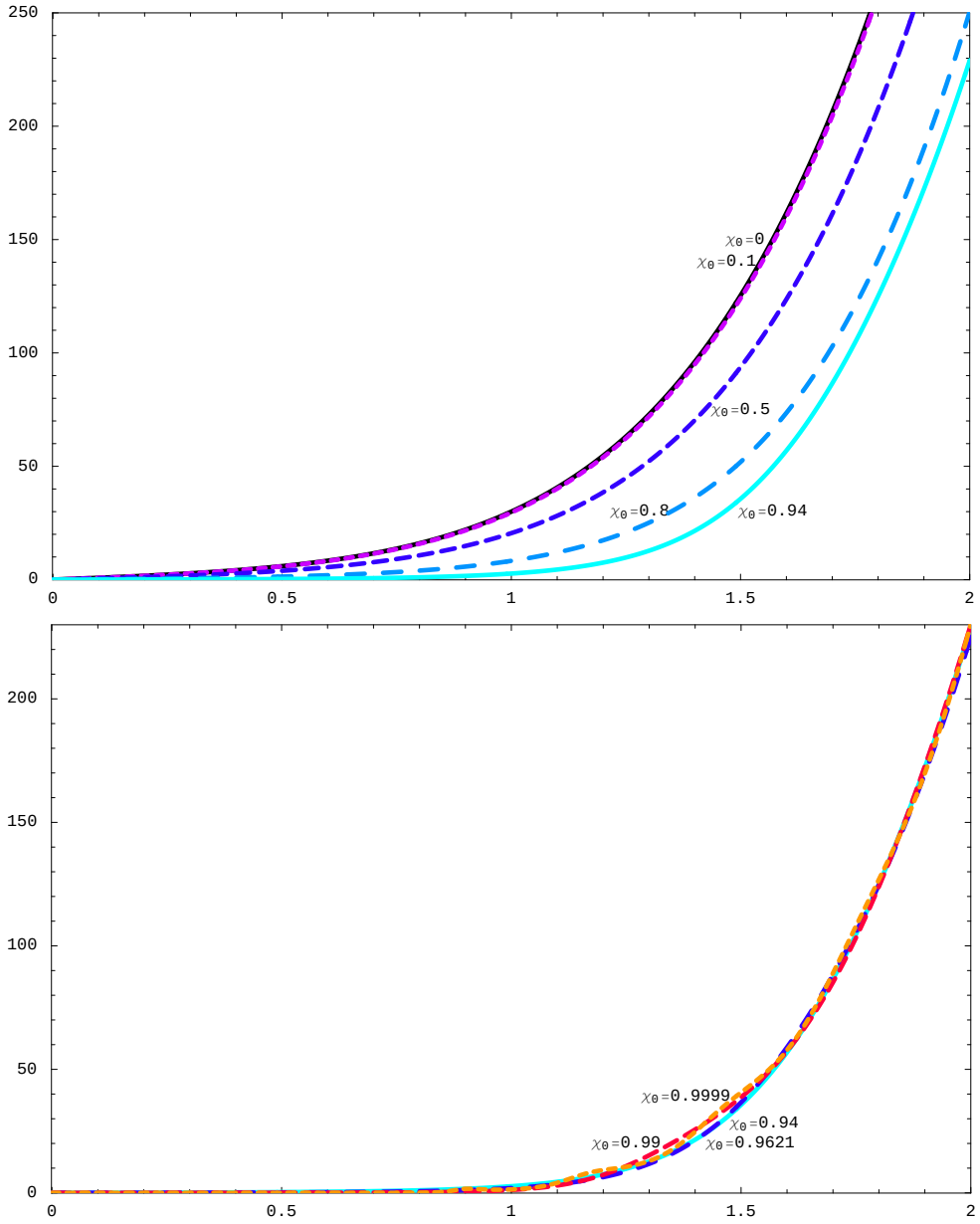

Figure 5.10: The scalar spectral function for $\ell = 1$ in units of $\pi^2 N_{\rm f} N_{\rm c} T^4/8$ versus $\mathfrak{w}$. The upper plot is for values of χ_0 corresponding to temperatures above the phase transition while the lower plot is for χ_0 past the phase transition. Note in the lower plot that the lines for $\chi_0 = 0.9621, 0.99, 0.9999$ roughly coincide with that for $\chi_0 = 0.94$ and that there is no structure suggesting the existence of quasiparticle states.

nents for a wide class of metrics were derived. There, the authors considered perturbations of a black brane background and a formula for the diffusion constant (eq. (2.27) in [125], also quoted here in eq. (5.135)) resulted from a derivation of Fick's law. An analogous computation can be performed for the D7-branes' vector field for black hole embeddings and it gives[11]

$$\begin{aligned} D &= \frac{\sqrt{-g}}{\sqrt{h}}\frac{1}{g_{xx}\sqrt{-g_{tt}g_{\rho\rho}}}\bigg|_{\rho=1}\int d\rho\,(-g_{tt})\,g_{\rho\rho}\frac{\sqrt{h}}{\sqrt{-g}} \\ &= \frac{2(1-\chi_0)^{3/2}}{\pi T}\int_1^\infty d\rho\frac{f\sqrt{1-\chi^2+\rho^2\dot{\chi}^2}}{\tilde{f}^2\rho^3(1-\chi^2)^2}\,, \end{aligned} \tag{5.89}$$

where, in the first expression, the metric g is the induced metric on the D7-branes (2.41) and h is the determinant of the metric on the S^3 of unit radius.

Using the numerical solutions for the embedding χ, we numerically integrated (5.89) to find DT. The results are plotted in figs. 5.11 and 5.12. Fig. 5.11 clearly shows that at high temperatures, DT approaches $1/2\pi$. This coincides with the result for the diffusion constant of R-charges in $\mathcal{N}=4$ SYM [119]. At a pragmatic level, this coincidence arises because both results are constructed from correlators of a Maxwell field in an AdS_5 black hole background. As the quark mass is increased, the induced geometry on the D7-branes deviates from that of the background geometry. Hence one finds a departure of DT away from $1/2\pi$ as the ratio $T/\bar{M}$ decreases. Close to the phase transition, there is a rapid decrease and $DT = 0.036 \simeq 0.226/2\pi$ at the phase transition. If we continue following the black hole branch beyond the phase transition, DT continues to fall and it also becomes a multi-valued function of temperature, as shown in fig. 5.12. The latter simply reflects the fact that multiple embeddings can be found for a single temperature in the vicinity of the critical solution.

5.4.2 Green-Kubo formula

As discussed in section 5.1.1, the diffusion constant may also be computed using the Green-Kubo formula (5.11) which relates the product of the diffusion constant D and

[11]Note that the same method can be applied to compute the diffusion constant for the gauge theory corresponding to the supergravity configuration of a Dq-brane probe in the near-horizon black Dp-brane geometry – see section 5.6.4.

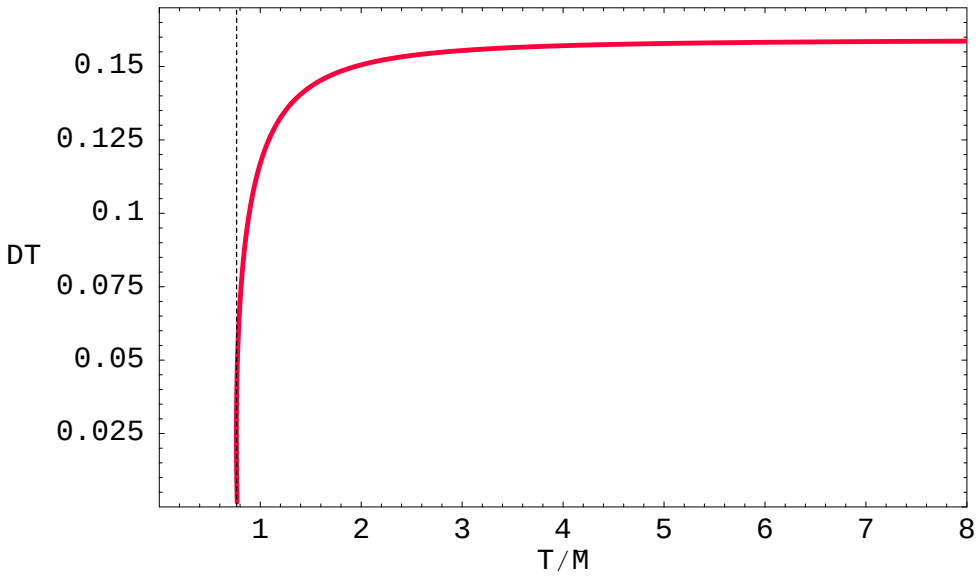

Figure 5.11: The diffusion constant D times the temperature T versus temperature $T/\bar{M}$ for D7-brane probes in the black D3-brane geometry. The dotted vertical line marks the temperature of the phase transition.

the susceptibility Ξ to the slope of the vector spectral function ($\ell = 0$) for $\omega \to 0$: $D\Xi = \lim_{\omega\to 0} \mathfrak{K}(\omega)/2\omega$. The susceptibility is $\Xi = \partial n_q/\partial\mu|_{\mu=0}$ where n_q is the charge density and μ is the chemical potential, both for fundamental matter (quarks or their supersymmetric generalisation). In order to compute the susceptibility, one must consider the D3/D7 brane system at finite baryon number and chemical potential, as in chapter 3 [151]. The susceptibility can be computed directly from eq. (3.17) which applies for any black hole embeddings. From appendix A, μ and n_q are related to dimensionless counterparts $\tilde{\mu}$ and $\tilde{d}$ via eqs. (A.20) and (A.21), respectively. Combining these definitions, we have

$$\frac{\partial\tilde{d}}{\partial\tilde{\mu}} = \frac{4}{N_{\rm f}N_{\rm c}T^2}\frac{\partial n_{\rm q}}{\partial\mu}\,, \tag{5.90}$$

which, interestingly, is independent of the 't Hooft coupling λ.

Note from eq. (3.17) that $\tilde{\mu} = 0$ is equivalent to $\tilde{d} = 0$ which means that we can calculate $\partial\tilde{\mu}/\partial\tilde{d}|_{\tilde{d}=0}$ from this equation and take the inverse for the desired derivative.

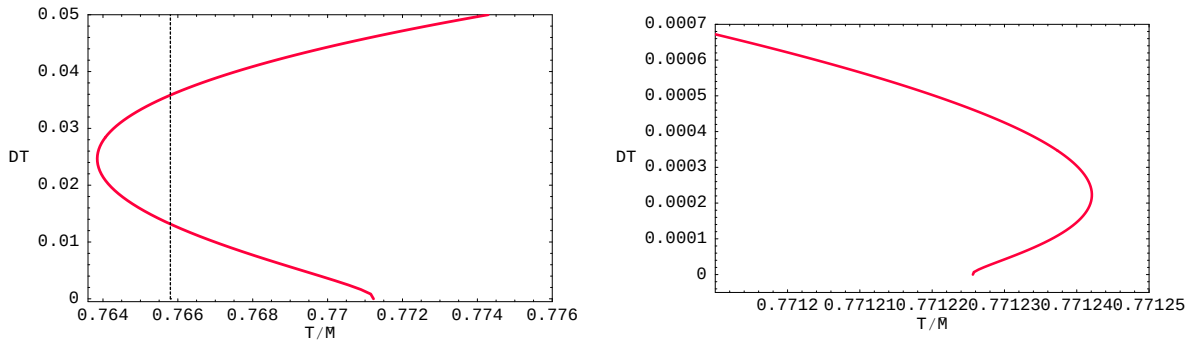

Figure 5.12: Plots of the diffusion constant D times the temperature T versus temperature $T/\bar{M}$ for D7-brane probes in the black D3-brane geometry, zooming in on the spiral behaviour for temperatures near the phase transition.

Hence a straightforward calculation yields

$$\frac{\partial\tilde{\mu}}{\partial\tilde{d}} = 2\int_1^\infty d\rho\, \frac{\rho^6 f \tilde{f}^4 (1-\chi^2)^4 \sqrt{1-\chi^2+\rho^2\dot{\chi}^2}}{\Big(\tilde{f}(1-\chi^2)[\rho^6\tilde{f}^3(1-\chi^2)^3+8\tilde{d}^2]\Big)^{3/2}}\,, \tag{5.91}$$

and evaluating at $\tilde{d}=0$ gives

$$\left.\frac{\partial\tilde{\mu}}{\partial\tilde{d}}\right|_{\tilde{d}=0} = 2\int_1^\infty d\rho\, \frac{f\sqrt{1-\chi^2+\rho^2\dot{\chi}^2}}{\tilde{f}^2\rho^3(1-\chi^2)^2}\,. \tag{5.92}$$

Combining eqs. (5.90) and (5.92), our final result is

$$\Xi \equiv \left.\frac{\partial n_{\rm q}}{\partial\mu}\right|_{\mu=0} = \frac{N_{\rm f}N_{\rm c}}{4}\,T^2\,\left\{\left.\frac{\partial\tilde{\mu}}{\partial\tilde{d}}\right|_{\tilde{d}=0}\right\}^{-1}\,. \tag{5.93}$$

Note that in limit of massless quarks (*i.e.*, $\chi=0$), these expressions have a simple form

$$\left.\frac{\partial\tilde{\mu}}{\partial\tilde{d}}\right|_{\tilde{d}=0} = \frac{1}{2}\,, \qquad \Xi = \frac{N_{\rm f}N_{\rm c}}{2}\,T^2\,. \tag{5.94}$$

Numerically evaluating the low frequency limit of the spectral function $\mathfrak{A}$ and the susceptibility (using (5.93) and (5.92)), we computed the diffusion constant using (5.11), and the results confirm those displayed in figure 5.11.

Further, if we combine (5.93) and (5.89), we are led to write

$$D\,\Xi = \frac{(1-\chi_0^2)^{3/2}}{4\pi}\,N_{\rm f}N_{\rm c}\,T\,, \tag{5.95}$$

which, in view of (5.11), provides a simple analytic expression for the low frequency ($\omega \to 0$) limit of the vector spectral function:

$$\mathfrak{R}(\omega) = \frac{(1-\chi_0^2)^{3/2}}{2\pi} N_{\rm f}N_{\rm c}T\omega + \cdots\,. \tag{5.96}$$

5.4.3 Lowest quasinormal frequency (in the diffusion channel)

The final computation of the diffusion constant comes from examining the hydrodynamic dispersion relation, corresponding to the lowest quasinormal frequency. At small three-momentum q, the diffusion constant can be extracted from: $\omega = -iDq^2 + \mathcal{O}(q^4)$ [125]. In principle, the calculation of the quasinormal mode spectrum from eq. (5.51) proceeds as follows: For $\rho \to \infty$, eq. (5.51) implies that $E_x \simeq A + B\rho^{-2}$ for some constants A, B. Normalizable modes will be those with $A = 0$. Hence one method to determine the quasinormal frequencies is to use a two-dimensional shooting method, *i.e.,* solving (5.51) numerically with incoming wave boundary conditions at the horizon and then tuning the (complex) frequency to find a solution behaving as ρ^{-2} asymptotically. For small q we solved (5.51) for various m to determine the lowest quasinormal frequency and our results for the diffusion constant are identical to those plotted in fig. 5.11.

5.5 Discussion

In this chapter, we used holography to investigate various aspects of the high temperature phase of an $\mathcal{N} = 2$ super-Yang-Mills theory with fundamental matter. The holographic description consists of probe D7-branes in the near-horizon background of D3-branes (in the limit of large-$N_{\rm c}$ and large-λ with fixed $N_{\rm f}$). In the high temperature phase, the D7-branes extend through the event horizon of the AdS_5 black hole, which describes the theory at finite temperature. In chapter 2 [111, 112], this phase was denoted as the black hole branch since the metric induced on the worldvolume of the D7-branes is itself a black hole. Even though the latter geometry no longer obeys Einstein's equations, the analysis of the hydrodynamic physics found previously for bulk fields, *e.g.,* [118], is readily

transferred to the worldvolume fields on the D7-branes. Hence we were able to examine the spectral function for various mesonic operators in section 5.3, following [259, 267], and we calculated the diffusion constant for the quark charge in section 5.4, adapting techniques from [119, 125].

As discussed in section 2.3.1, the induced geometry on the D7-branes is determined by solving for the embedding profile from eq. (2.44). Given the complexity of eq. (2.44), these geometries are only known in general from numerical integration. However, there is one particularly simple case, namely that of zero quark mass. In this case, the embedding is trivial, *i.e.,* $\chi = 0$ everywhere, and the induced geometry (2.41) is precisely that of (the direct product of) an AdS_5 black hole (with a constant S^3). Hence our analysis in sections 5.3.1 and 5.4 reduces to studying a Maxwell field in an AdS_5 black hole geometry and the results precisely match those found previously for bulk gauge fields. For example, the quark diffusion constant (with $M_q = 0$) matches precisely with the R-charge diffusion constant calculated in [119, 125].

As the quark mass is increased (or T/M_q decreases), the induced black hole geometry on the D7-brane begins to deviate from that of the background. In particular, the main differences arise near the event horizon where χ is largest. For example, eq. (2.41) shows that the size of the S^3 and hence the induced horizon area shrinks as χ_0 grows. Hence the physical properties of the fundamental fields were seen to depart (dramatically, in some cases) from the standard results with the growth of the quark mass. Recall that some of the most interesting behaviour appeared as $\chi_0 \to 1$, *i.e.,* approaching the critical solution for which the effective horizon area vanishes. Hence this behaviour can be seen as a precursor of the phase transition to the low temperature phase or the Minkowski branch, in which the D7-brane smoothly closes off above the event horizon.

In the low temperature phase, the spectrum of mesons is characterised by a discrete set of stable states (see section 2.3.3) [61, 112] and the spectral function is a series of delta-function-like peaks, as illustrated in fig.5.1a. A derivation of the spectral function for the scalar meson at $T = 0$ appears in section 5.6.1. These mesonic states correspond to open string excitations which are essentially living at the minimum radius of the D7-branes. Since in the high temperature phase the D7-branes extend through the event horizon, these states are destabilised. In this phase, the spectrum can be characterised by a discrete set of quasinormal modes in the effective black hole metric induced on the D7-branes [155]. The spectral functions calculated in section 5.3 reveal interesting information

about this quasinormal spectrum. We focussed on three particular operators, which are bilinears of the fundamental fields – the details appear in appendix A – corresponding vector, pseudoscalar and scalar channels.

The behaviours of the vector and pseudoscalar spectral functions are very similar, as can be seen in figures 5.4 and 5.7. The following physical picture emerges from these plots: At very high temperatures, the spectral function closely resembles that for a vector in $\mathcal{N} = 4$ SYM. (Of course, as discussed above, the bulk and worldvolume vector results are identical for $T/M_{\rm q} \to \infty$.) In this regime, the spectral function shows essentially no structure and the eigenfrequencies of quasinormal modes must all be deep in the (lower) complex plane. As the temperature decreases (with fixed quark mass), both the real and imaginary parts of a given quasinormal frequency decrease but the formation of peaks in the spectral function suggests that the imaginary part decreases more rapidly. At temperatures just above the phase transition, there are vector and pseudoscalar quasiparticles. Continuing along the black hole branch to even lower temperatures beyond the phase transition (*i.e.,* following the black hole line through A_1 in fig. 5.3), peaks grow very sharp and even more prominent indicating that the quasinormal modes have $\mathrm{Re}(\omega) \gg \mathrm{Im}(\omega)$ in this regime.

Section 5.6.3 presents a complementary discussion which reaches the same conclusion. Plots of the effective potential for the pseudoscalar (and vector) excitations in section 5.6.3 show a finite potential barrier developing at intermediate values of the radius as $\chi_0 \to 1$. This suggests the existence of metastable states in the corresponding Schroedinger problem which, as discussed in section 5.6.3, would correspond to a quasinormal frequency with $\Gamma \ll \Omega$ *i.e.,* the eigenfrequency approaches the real axis in this regime. Of course, while this intuitive picture developed from the effective potential matches the behaviour of the spectral functions discussed above, it only gives a very schematic picture of the quasinormal spectrum. Hence it would be interesting to develop a more detailed picture with a full calculation of the quasinormal modes [155].

If we examine the positions of the peaks in the spectral functions more closely as the black hole embedding approaches the critical solution, it appears that the real parts of the quasinormal frequencies roughly match with the spectrum of the lowest (vector and pseudoscalar) mesons on a near-critical Minkowski embedding. Hence one notable feature of the spectral functions is that as $\chi_0 \to 1$, the peaks are becoming sharper but also more closely spaced and moving towards lower frequencies. For example, in figure 5.7, the peaks in the $\chi_0 = 0.9999$ line are much more closely spaced than those in the

$\chi_0 = 0.99$ line. This behaviour is similar to what is seen for the $\delta\phi$ spectrum for near-critical Minkowski embeddings: For these near-critical embeddings, the tower of masses appears to be collapsing to the mass of the lowest meson – see figs. 2.7, 2.8, and 2.9. As the phase transition occurs well away from the critical solution (*i.e.,* $\chi_0 = 0.94$ versus 1), the positions of the spectral peaks are not closely matched with the corresponding meson spectrum for the Minkowski embedding at the phase transition. Of course, both spectra are still characterised by the same general mass scale, as given in eq. (2.48).

We also examined the spectral functions for $\ell > 0$ in vector and pseudoscalar channels. These modes of the worldvolume fields correspond to higher dimension operators in the field theory, which are charged under the internal symmetry group $SO(4) = SU(2)\times SU(2)$ – see the discussion in appendix A. For these modes, the results are qualitatively similar to those for $\ell = 0$ as one approaches the critical embedding. However, the rate at which the quasinormal frequencies approach the real axis is much slower – that is, the spectral functions only develop pronounced peaks very close to $\chi_0 = 1$. In fact, these peaks are already washed out at the phase transition, *i.e.,* $\chi_0 = 0.94$. Hence the corresponding mesons with $\ell > 0$ do not survive as quasiparticles through the phase transition. An analogous observation applies to the excited mesons with $\ell = 0$ and $n \geq 1$. Examining the spectral functions in figs. 5.4 and 5.7, one finds that only the first peak remains pronounced at $\chi_0 = 0.94$. Hence it seems that only the ground state mesons (with $n = 0 = \ell$) can be said to survive the phase transition as quasiparticles. However, even these resonances have disappeared in the quark-gluon plasma by $\chi_0 \simeq 0.8$ or $T \simeq 1.1T_{\rm fun}$, where $T_{\rm fun}$ is the temperature of the phase transition.

As shown in figures 5.8 and 5.9, the behaviour of the scalar spectral function is qualitatively different from that found in the vector and pseudoscalar channels, shown in figs. 5.4 and 5.7. As before, at high temperatures, the spectral function shows no distinguished structure, indicating that the quasinormal eigenfrequencies are all deep in the (lower) complex plane. As the temperature decreases, a small peak develops near the origin although it is still not very prominent at the phase transition. However, continuing to the D7-brane embeddings on the black hole branch for temperatures below the phase transition, this single peak grows and becomes extremely sharp and centred at $\omega = 0$, precisely at the first kink in the free energy, *i.e.,* $\chi_0 = 0.9621$. Beyond this point, the peak decays and moves away from $\omega = 0$. Our interpretation of this behaviour is that the lowest (pair) of the quasinormal frequencies approaches the origin and actually crosses the real axis at

the point A_2 in fig. 5.3. Continuing beyond this point, this eigenfrequency moves into the upper half plane, where it actually corresponds to an unstable mode.

This interpretation of the behaviour of the scalar spectral function is confirmed by the qualitative analysis of the corresponding quasinormal modes in section 5.6.3. Examining the effective potential for the scalar excitations shows that a negative potential well develops and grows as $\chi_0 \to 1$. As discussed in the section 5.6.3, when this well is large enough, it can support long-lived 'bound' states for which (the real part of) the effective energy is negative. These modes are distinguished since $\Gamma^2 > \Omega^2$ and further $\Gamma < 0$, so that these bound states correspond to instabilities of the D7-brane. The spike (or pole) at $\omega = 0$ in the scalar spectral function discussed above results from the formation of the first bound state where the eigenfrequency crosses the real axis. Of course, it would be interesting to develop a detailed picture with a full calculation of the quasinormal modes [155].

Recall that the thermodynamic discussion of sections 2.3.2 and 5.2.1 predicted that the system should become unstable at the point A_2 in fig. 5.3 because the specific heat of the black hole branch becomes negative there. Hence our analysis above is in precise agreement with this result and it shows that the instability corresponds to a pair of unstable 'quasinormal' modes appearing on the D7-branes.

In fact, we found the scalar spectral function also displays a spike at $\omega = 0$ at the second kink in the free energy, *i.e.,* $\chi_0 = 0.99973885$. Hence it appears that the second lowest quasinormal modes become unstable at this point. It is natural to conjecture then that each time the free energy turns, two new 'tachyonic' modes appears in the scalar spectrum. In fact, the spectrum of scalar mesons on the Minkowski branch was found to display precisely this behaviour (see section 2.3.3) [112].

The spectral functions of mesonic operators which we calculated exhibited interesting features which can be interpreted in terms of the spectrum of quasinormal modes. It would, of course, be interesting to confirm these behaviours by a direct investigation of the quasinormal modes [155]. In the present chapter, the spectral functions were only calculated for zero spatial momentum for computational simplicity. Another natural extension of this work is to consider the behaviour at nonvanishing spatial momentum. In particular, the spectral functions for general time-like and light-like four-momentum can be used to calculate photon and dilepton production rates, respectively [268]. An analysis of these results for the present $\mathcal{N} = 2$ gauge theory will appear shortly [271].

The other main result of this chapter was the calculation of the diffusion constant for

the quark charge. We used a number of techniques developed for bulk black holes in the calculation of the R-charge diffusion constant: the membrane paradigm method [125], the Green-Kubo formula [119] (which relied on the studies of this system at finite quark density from chapter 3, [151]), and the lowest quasinormal frequency [125]. It is gratifying that, as demanded by the internal consistency of the holographic framework, all three of these independent calculations yield the same results, shown in figure 5.11.

At very high temperatures (*i.e.,* $T/\bar{M} \gg 1$), the diffusion constant approaches $2\pi D\,T = 1$, which, as discussed above, matches the R-charge diffusion constant for the $\mathcal{N} = 4$ super-Yang-Mills theory [125]. As $T/\bar{M}$ decreases, the product $D\,T$ decreases. Intuitively, we might understand this result as the rate of diffusion decreasing at a fixed temperature when the quark mass is increased. In fact, the decrease is remarkably small at first, *e.g.,* $2\pi D\,T = 0.9$ at $T/\bar{M} \simeq 1.5$. However, figure 5.11 then shows a dramatic decline as we approach the phase transition at $T/\bar{M} = 0.7658$. At the phase transition, $2\pi D\,T \simeq 0.226$, but if we continue following the black hole branch it appears that $D\,T$ continues to decrease and would vanish at the critical embedding. The membrane paradigm approach to calculating D, as described in section 5.4.1, provides a straightforward understanding of this vanishing from the bulk perspective. Examining the expression in eq. (5.89), we see that in the critical limit, the integral remains finite but the prefactor vanishes because $\sqrt{-g} \to 0$. Hence the dominant effect which causes D to decrease is the reduction of the effective horizon area of the brane geometry (2.41) as we approach the critical embedding. That is, $(1 - \chi_0^2) \to 0$ in advancing toward the critical embedding. Further, this area vanishes precisely at the critical embedding, confirming that D should vanish there.

We have considered the $\mathcal{N} = 2$ gauge theory to have $N_{\rm f}$ flavours of quarks. Hence it is worth noting that the results for the quark diffusion constant in the present holographic framework are independent of both $N_{\rm f}$ and $N_{\rm c}$. Of course, the same independence of $N_{\rm c}$ was seen with the R-charge [125]. This must certainly arise because we are working in the limit of large $N_{\rm c}$ and large λ.

There has also been a great deal of interest in the diffusion of 'heavy quarks' in holographic theories recently [133–136] – see also [192, 195, 272] and the references therein. In the present context, this simply refers to the quark diffusion constant in the low temperature phase where the D7-branes are some finite distance away from the black hole horizon. In the low temperature or Minkowski embedding phase, a quark is represented by a fundamental string stretching between the D7-brane and the horizon. As such, a heavy

quark is holographically represented by a macroscopic object (on a similar footing with the probe D7-branes) and classically this object will remain at rest (*i.e.,* it does not 'diffuse'). It is only when semiclassical effects are taken into account that the heavy quarks diffuse through the appearance of Hawking radiation from the effective black hole metric induced on the string worldsheet [135]. This process should be contrasted with the diffusion process in the high temperature phase which we have been considering here. As stressed above, in this phase the induced metric on the D7-brane is a black hole metric and so if quark number is injected into the system, the holographic description of diffusion is simply the classical process of the corresponding worldvolume excitations falling towards the event horizon. Given these two disparate descriptions, it is not surprising that the diffusion constant takes a qualitatively and quantitatively different form in the two phases. In the low temperature phase, the diffusion constant is governed by the heavy quark result [133,135][12]

$$2\pi\, D\, T = \sqrt{8/\lambda}\,. \tag{5.97}$$

On the other hand, after the phase transition to the high temperature phase, we found above that $2\pi\, D\, T = O(1)$. Note that the holographic analysis applies for strong 't Hooft coupling (*i.e.,* $\lambda \gg 1$) and so these results show the expected suppression of quark diffusion in the low temperature phase.

We comment on a possible puzzle with the above description of the diffusion of heavy quarks as due to semiclassical Hawking radiation. As such, the diffusion constant would be expected to vanish in the limit $\hbar \to 0$ for the bulk theory. Now the standard AdS/CFT dictionary would associate Planck's constant $\hbar$ in the bulk supergravity with $1/N_{\rm c}$ in the dual gauge theory [53]. However, above, we see the result (5.97) is seen to be independent of $N_{\rm c}$ and D certainly does not vanish in the limit $N_{\rm c} \to \infty$. The resolution of this puzzle is that we have misidentified the correct 'semiclassical' nature of the diffusion process here. Above we observed that the heavy quarks diffuse because of the appearance of Hawking radiation in the effective field theory on the string worldsheet dual to such a heavy quark. That is, the 'fields' on the worldsheet are the transverse coordinates describing the embedding of the string and so fluctuations in these fields (arising from Hawking radiation)

[12]Note we present this result with the same normalisation for the 't Hooft coupling used throughout this chapter and thesis. Ref. [133] uses a convention such that $\tilde{\lambda} = 2\lambda$. This difference arises from the implicit normalisation of the $U(N_{\rm c})$ generators: $\mathrm{Tr}(T_a\, T_b) = d\,\delta_{ab}$. The standard field theory convention used in [133] is $d = 1/2$ while our choice is $d = 1$, which is prevalent in the D-brane literature.

corresponds to fluctuations in the position of the quark (*i.e.,* diffusion of the quark). As usual, $\hbar$ for the worldsheet theory is identified with the inverse string tension, $\alpha' = \ell_s^2$. More correctly, the dimensionless $\hbar$ in the nonlinear sigma model on the worldsheet is identified with the ratio of α' and the background curvature scale, *i.e.,* $\hbar_{ws} \simeq \ell_s^2/L^2 \simeq 1/\sqrt{\lambda}$. Now we see this physical picture matches precisely with the calculated result (5.97) and the limit $\lambda \to \infty$ is the semiclassical limit on the string worldsheet.

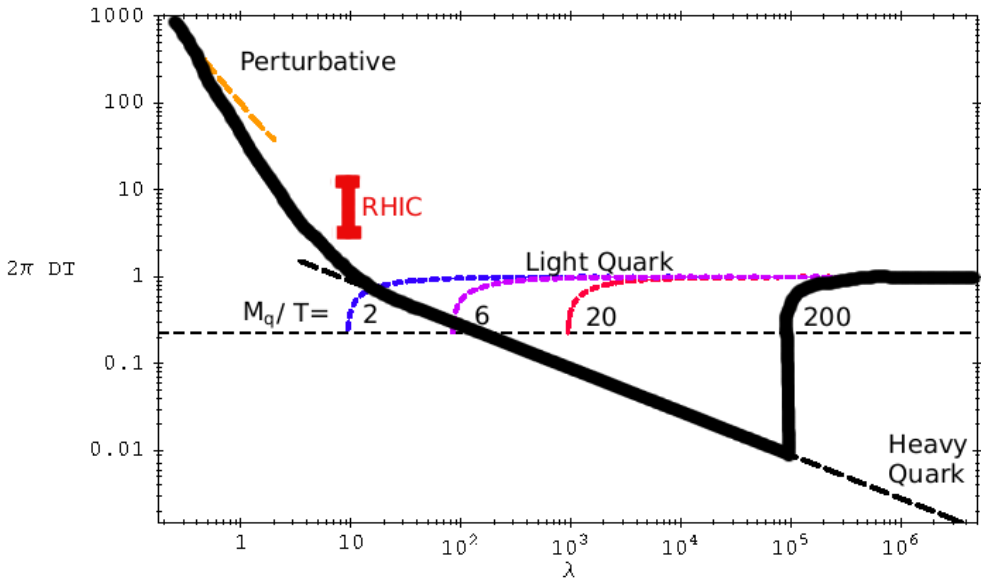

Figure 5.13: Sketch of $2\pi\, D\, T$ versus λ for a canonical $\mathcal{N} = 2$ gauge theory with $M_q/T = 200$. The perturbative regime [273] is to the far left and it crosses over to the 'heavy' quark behaviour (5.97). Above the transition to the black hole phase ($\lambda \simeq 9.4 \times 10^4$), the curve reflects the light quark behaviour of fig. 5.12. The light quark curves are also shown for $M_q/T = 2$, 6, and 20. The horizontal dotted line marks the value of $2\pi\, D\, T$ for the 'light' quarks at the phase transition.

The results for the diffusion constant in both the high and low temperature phases are combined in figure 5.13, where the diffusion constant is shown as a function of λ (for fixed M_q/T). The thick black curve shows a canonical result for the $\mathcal{N} = 2$ gauge theory, which we are displaying for $M_q/T = 200$. The diffusion constant starts at very large values on the left in nearly perturbative results. The dashed 'perturbative' line is the extrapolation of

the perturbative calculation of [273] for $\mathcal{N} = 4$ super-Yang-Mills at large N_c. As the curve shows, we expect $D\,T$ to make a transition to the $\lambda^{-1/2}$ behaviour of heavy quarks in the low temperature phase. For infinite quark mass, this behaviour would extend out to infinite 't Hooft coupling. However, for a finite mass, increasing λ eventually takes the system to the high temperature phase. It would be interesting to understand the corrections to the heavy quark result (5.97), as we approach the phase transition. For $M_q/T = 200$, the latter occurs at $\lambda \simeq 9.4 \times 10^4$ [111, 112]. At this first order phase transition, $2\pi\, D\, T$ jumps discontinuously up to the 'light quark' curve where $2\pi\, D\, T = 0.226$ and it quickly reaches the asymptotic value of 1 as λ continues to increase.

Much of the recent interest in holographic calculations of the diffusion constant was generated by the possibility to compare these strong coupling results with experimental results for the QCD quark-gluon plasma measured at RHIC [274]. It is interesting then to place the RHIC results in the context of the phenomenology of the $\mathcal{N} = 2$ gauge theory studied here. In fig. 5.13, the bar labeled RHIC corresponds to $\alpha_{strong} = 0.5$ (or $\lambda = 3\pi$) and the range $2\pi\, D\, T = 3 \sim 12$, for which the simultaneous fit of the nuclear modification factor and elliptic flow amplitude for heavy (charm) quarks is acceptable – see [274] for details. This value of the 't Hooft coupling is well away from the light quark behaviour of our canonical theory but also lies in an intermediate regime between the heavy quark and perturbative regimes. Hence a direct comparison of either approach for the $\mathcal{N} = 2$ theory to the experimental data for QCD is difficult [273, 275]. We emphasise that in this intermediate region our canonical curve is simply an 'artistic' impression of the cross-over between these two regimes.

For the canonical theory, we chose $M_q/T = 200$ so that the phase transition between the low and high temperature regimes took place for a value of λ that we could confidently characterise as strong coupling. We can extend the discussion of RHIC results by noting that the charm quark has a mass of roughly 1500 MeV while the temperatures achieved in the RHIC collisions are in the regime 250 MeV. Hence in these experiments, we are considering $M_q/T \simeq 6$. As illustrated in figure 5.13, the effect of reducing this ratio is to slide the light quark curve to the left. That is, the phase transition occurs at smaller and smaller values of λ, *e.g.,* , $\lambda_c \simeq 85$ for $M_q/T \simeq 6$. However, it seems that this critical value is still well away from the value of the coupling relevant for RHIC. Further it seems that the same will still be true for charm quarks even at the higher temperatures that might be achieved in the future at the LHC. Thus it is unlikely that a dramatic jump in

the diffusion constant, such as that seen for our canonical theory, can ever be expected to appear in these experiments. It is noteworthy that in any event, the experimentally favoured values of the heavy quark diffusion constant are in fact above those calculated in the high temperature phase. Hence it would seem that a QCD phase transition would be characterised by a sudden decrease rather than a sudden increase in the diffusion constant.

While our results for the diffusion constant do not seem relevant for 'heavy quarks', they might be considered as that for 'light quarks' in QCD. Note that our holographic model gave $2\pi\, D\, T \leq 1$ where the effect of a finite quark mass was to give a slight (less than order one) reduction below the asymptotic value of 1. Section 5.6.4 extends the computation of the diffusion constant described in section 5.4.1 to more general holographic theories. In particular, figure 5.17 shows the results for the D4/D6-brane system, which is the basis for the construction of one holographic model which mimics QCD at large $N_{\rm c}$ [62]. The results are similar to those above with $2\pi\, D\, T \leq 3/2$ with finite mass effects giving a small reduction from the asymptotic value. Another interesting holographic model of a QCD-like theory comes from introducing D8 and anti-D8 probe branes in a D4-brane background [63, 64]. The resulting diffusion constant is simply $2\pi\, D\, T = 1$. In this model, the current quark mass vanishes and so no finite mass effects appear. We might also recall the results for the R-charge diffusion constants $2\pi\, D\, T = 1$ and $3/4$, for the near-extremal D3- and D4-brane backgrounds [125]. Hence in all these cases then, we find that the calculations yield $2\pi\, D\, T = O(1)$. This might suggest that in QCD the diffusion constant associated with the light quarks falls dramatically at strong coupling, as compared to the perturbative results [276], but that they should saturate around this level. One might note then that these diffusion constants would be smaller than for heavy quarks at presently accessible energies but not much smaller. However, we must recall that these calculations are all performed at large λ and large $N_{\rm c}$ (with $N_{\rm f}/N_{\rm c} \ll 1$) and so it would be interesting to understand the corrections to these results at finite λ and finite $N_{\rm c}$.

In the present study, we focussed on calculating the diffusion constant for the overall quark charge. Of course, with $N_{\rm f}$ flavours of quark with identical masses, the $\mathcal{N} = 2$ gauge theory has a global $U(N_{\rm f})$ flavour symmetry and in the dual gravity description, the worldvolume theory of the D7-brane contains a nonabelian $U(N_{\rm f})$ gauge field. Our calculations have only considered the diagonal $U(1)$ component of this gauge field. However, as noted in appendix A, one can easily examine the nonabelian $SU(N_{\rm f})$ flavour currents with the corresponding components of the worldvolume gauge field – see, *e.g.,* eq. (A.6). In princi-

ple, we would describe the diffusion of the full set of flavour currents with a diffusion matrix D_{ab}, rather than a single constant. However, our calculations of the diffusion constant in section 5.4 only relied on knowing the quadratic action for the dual gauge field and hence the nonabelian character of the gauge fields would play no role. Hence the diffusion matrix is, in fact, diagonal: $D_{ab} = D\,\delta_{ab}$ where D is precisely the constant determined for the $U(1)$ charge. On general grounds, this is of course the expected result for the $\mathcal{N} = 2$ gauge theory in the absence of any chemical potentials. With a nonvanishing chemical potential, the diffusion matrix will not take this simple form [277]. Similar comments to those above also apply for extending our calculations of the spectral function to operators that are no longer $SU(N_{\rm f})$ singlets.

5.6 Supplementary material for chapter 5

5.6.1 Spectral function for scalar meson at $T = 0$

In the low temperature phase of the D3/D7 brane theory, we expect the scalar spectral function to be a series of delta-function resonances centred on mass eigenvalues. In this appendix we compute the scalar spectral function for the theory at zero temperature. The spectrum of mesons in this theory was studied in detail in ref. [61].

The background geometry corresponding to the field theory at $T = 0$ is that of (5.15) with $u_0 = 0$ so that $f(u) = 1$, *i.e.,* the background no longer contains a black hole. We embed $N_{\rm f}$ D7-branes in this geometry as described by the array (2.34), at a distance $m_0 = 2\pi\ell_{\rm s}^2 M_{\rm q}$ from the D3-branes. The resulting theory is supersymmetric with eight supercharges preserved. Using spherical polar coordinates in the 4567-space with radial coordinate $\bar\varrho = m_0\varrho$, the induced metric on the D7-branes is

$$ds^2 = \frac{m_0^2}{L^2}(1+\varrho^2)\left(-dt^2 + dx_3^2\right) + \frac{L^2}{1+\varrho^2}\left(d\varrho^2 + \varrho^2 d\Omega_3^2\right)\,. \tag{5.98}$$

Following the same procedure as described in section 5.3.2, we consider small scalar fluctuations δR of the D7-branes about this fiducial embedding, *i.e.,* taking polar coordinates ϕ and $\bar R = m_0 R$ in the 89-directions, we consider $\phi = 0$ and $\bar R = m_0(1+\delta R)$. Expanding the DBI action to quadratic order in δR, we find

$$I = -\frac{L^2}{2} T_{\rm D7} \int d^8\sigma \frac{\sqrt{-g}}{1+\varrho^2}\, g^{ab}\,\partial_a\delta R\,\partial_b\delta R\,. \tag{5.99}$$

The corresponding equation of motion is

$$\partial_a \left[\frac{\sqrt{-g}}{1+\varrho^2} g^{ab}\, \partial_b \delta R \right] = 0\,, \tag{5.100}$$

where g is the metric (5.98).

We take the fluctuations to be s-waves on the internal S^3. Then, integrating over the S^3 and integrating by parts, the action (5.99) becomes:

$$I = -\pi^2 m_0^4 T_{\rm D7} \int d^4x \left[\varrho^3 \delta R\, \partial_\varrho \delta R \right]_{\varrho\to\infty}\,. \tag{5.101}$$

Expanding the fluctuation in terms of Fourier modes, we take

$$\delta R(k,\varrho) = \delta R_0(k) \frac{\mathcal{R}_k(\varrho)}{\mathcal{R}_k(\varrho_{\rm max})}$$

as the solution of eq. (5.100) regular at $\varrho = 0$ and normalised to $\delta R_0(k)$ at $\varrho = \varrho_{\rm max}$. The correlation function is given by[13]

$$G = 2\pi^2 m_0^4 T_{\rm D7} N_{\rm f} \left[\varrho^3 \frac{\mathcal{R}_{-k}(\varrho)\, \partial_\varrho \mathcal{R}_k(\varrho)}{\mathcal{R}_{-k}(\varrho_{\rm max}) \mathcal{R}_k(\varrho_{\rm max})} \right]_{\varrho\to\infty} = 2\pi^2 m_0^4 T_{\rm D7} N_{\rm f} \left[\varrho^3 \frac{\partial_\varrho \mathcal{R}_k(\varrho)}{\mathcal{R}_k(\varrho)} \right]_{\varrho\to\infty}\,. \tag{5.102}$$

Changing the radial coordinate from ϱ to $\bar z = \varrho^2/(1+\varrho^2)$, the equation of motion (5.100) for a fluctuation with vanishing spatial momentum can be written as

$$\partial_{\bar z}^2 \mathcal{R}_k(\bar z) + \frac{2}{\bar z} \partial_{\bar z} \mathcal{R}_k(\bar z) + \frac{\bar\omega^2}{4\bar z(1-\bar z)} \mathcal{R}_k(\bar z) = 0\,, \tag{5.103}$$

where $\bar\omega^2 = \omega^2 L^4/m_0^2$. The solution regular at $\bar z = 0$ is given by a hypergeometric function

$$\mathcal{R}_k(\bar z) = {}_2F_1\left(\frac{1}{2} + \frac{1}{2}\sqrt{1+\bar\omega^2},\, \frac{1}{2} - \frac{1}{2}\sqrt{1+\bar\omega^2};\, 2;\, \bar z \right)\,. \tag{5.104}$$

The correlator (5.102) becomes[14]

$$G = \frac{2\,\pi^2\, m_0^4\, T_{\rm D7}\, N_{\rm f}}{M_{\rm q}^2}\, \bar\omega^2 \left[\psi\left(\frac{1}{2} + \frac{1}{2}\sqrt{1+\bar\omega^2} \right) - \frac{\pi}{2} \tan \frac{\pi\sqrt{1+\bar\omega^2}}{2} \right]\,, \tag{5.105}$$

[13]Note that in the low-temperature phase the spectrum is discrete and the correlator as a function of frequency is expected to have poles on the real axis. The difference between various types of correlators (retarded, advanced, Feynman etc) then comes from the usual choice of an integration contour in the complex frequency plane.

[14]In order to obtain the appropriate normalisation we must multiply G by $1/M_{\rm q}^2$ (see section 5.3.2).

where we dropped contact terms. The correlator (5.105) has poles at $\omega_k^2 = 4k(k+1)m_0^2/L^4$, $k = 1, 2, ...$, corresponding to the meson mass spectrum found in [61]. Using the expansion

$$\frac{\pi}{4a}\tan\frac{\pi a}{2} = \sum_{k=0}^{\infty}\frac{1}{(2k+1)^2 - a^2}$$

and Sokhotsky's formula

$$\lim_{\epsilon\to 0}\frac{1}{x \pm i\epsilon} = \mp i\pi\delta(x) + \mathcal{P}\left(\frac{1}{x}\right) ,$$

we find

$$\mathfrak{R} = -2\,\mathrm{Im}\; G = \frac{N_{\rm f}N_{\rm c}}{\pi}\sum_{k=1}^{\infty}\omega_k^2\sqrt{1+\bar{\omega}_k^2}\,\delta\left(\bar{\omega}^2 - \bar{\omega}_k^2\right) . \tag{5.106}$$

This expression confirms our expectations for the spectral function in the low temperature phase of the theory, illustrated in fig. 5.1a: the spectral function is a sum of delta-function peaks centred on meson mass eigenvalues. Note that with

$$\delta\left(\bar{\omega}^2 - \bar{\omega}_k^2\right) = \frac{\delta\left(\bar{\omega} - \bar{\omega}_k\right) + \delta\left(\bar{\omega} + \bar{\omega}_k\right)}{2\bar{\omega}_k} , \tag{5.107}$$

and assuming $\omega \geq 0$, the spectral function can also be expressed as

$$\mathfrak{R} = \frac{N_{\rm f}N_{\rm c}}{2\pi}\sum_{k=1}^{\infty}\omega_k^2\sqrt{1+\frac{1}{\bar{\omega}_k^2}}\,\delta\left(\bar{\omega} - \bar{\omega}_k\right) . \tag{5.108}$$

For large frequencies ω_k, corresponding to large k, eq. (5.108) can be written as

$$\mathfrak{R} \sim \frac{N_{\rm f}N_{\rm c}\omega^2}{4\pi}\sum_{k}\;\Delta\bar{\omega}_k\,\delta\left(\bar{\omega} - \bar{\omega}_k\right) , \tag{5.109}$$

where $\Delta\bar{\omega}_k = \bar{\omega}_{k+1} - \bar{\omega}_k \simeq 2$ is the spacing between delta functions for large k. Note that the prefactor $N_{\rm f}N_{\rm c}\omega^2/4\pi$ is in agreement with the high frequency asymptotics – see eq. (5.116).

5.6.2 Spectral function high frequency asymptotics

In this section we find expressions for the vector, pseudoscalar and scalar spectral functions in the high frequency limit, *i.e.,* ω much larger than all scales: $\omega \gg T, M_{\rm q}$. Note that in a sense this limit is equivalent to taking the limit of zero temperature and quark mass.

The spectral functions, $\tilde{\mathfrak{K}}_{\theta_\ell}(\omega)$, $\tilde{\mathfrak{K}}_{\phi_\ell}(\omega)$, $\mathfrak{K}_\ell(\omega)$, are collectively denoted by $\mathfrak{K}^\ell_s(\omega)$ here and are defined as

$$\mathfrak{K}^\ell_s = -\frac{\pi^{2\ell}}{2^{\ell+2}} N_{\rm f} N_{\rm c} T^{2\ell+2} \mathrm{Im}\left[\rho^{3+2\ell}\frac{\partial_\rho \Phi_\ell}{\Phi_\ell}\right]_{\rho\to\infty}, \tag{5.110}$$

where $\Phi_\ell = \rho\mathcal{R}_{\ell,k}, \mathcal{P}_{\ell,k}, E_{\ell,k}$ for the scalar, pseudoscalar, and vector fluctuations, respectively. The desired limit is achieved by considering both $\rho \to \infty$ and $\mathfrak{w}^2 - \mathfrak{q}^2 \to +\infty$. In this limit, the embedding function is $\chi \sim m/\rho$, and the three equations of motion, (5.57) for $E_{\ell,k}$, (5.81) for $\mathcal{P}_{\ell,k}$, and (5.87) for $\mathcal{R}_{\ell,k}$, reduce to

$$\partial^2_\rho \Phi_\ell + \frac{3}{\rho}\partial_\rho \Phi_\ell - \left[\frac{\ell(\ell+2)}{\rho^2} - \frac{8(\mathfrak{w}^2-\mathfrak{q}^2)}{\rho^4}\right]\Phi_\ell = 0. \tag{5.111}$$

Changing variables first from ρ to the 'standard' radial coordinate u using (2.35) (which becomes $u = \rho u_0/\sqrt{2}$ asymptotically) and then to $z = L^2/u$, we obtain

$$\Phi''_\ell(z) - \frac{1}{z}\Phi'_\ell(z) - \left(\frac{\ell(\ell+2)}{z^2} + k^2\right)\Phi_\ell = 0\,, \tag{5.112}$$

where $k^2 = -\omega^2 + q^2$. For timelike momenta, the solution satisfying the incoming wave boundary condition at $z = \infty$ (the horizon in the zero temperature limit) can be written in terms of the Hankel function of the first kind,

$$\Phi = z H^{(1)}_{\ell+1}(|k|z)\,, \tag{5.113}$$

assuming $\omega > 0$ [123]. The spectral function then becomes

$$\mathfrak{K}_s = \frac{N_{\rm f}N_{\rm c}}{2\pi^2}\,\mathrm{Im}\left[\lim_{\epsilon\to 0}\frac{\Phi'(\epsilon)}{\epsilon^{2\ell+1}\Phi(\epsilon)}\right]. \tag{5.114}$$

For $\ell = 0$, this is

$$\mathfrak{K}_s = \frac{N_{\rm f}N_{\rm c}}{4\pi}\,(\omega^2 - q^2)\theta(\omega^2-q^2)\,\mathrm{sgn}\,\omega \tag{5.115}$$

which for vanishing three-momentum $q = 0$ reduces to

$$\mathfrak{K}_s = \frac{N_{\rm f}N_{\rm c}\omega^2}{4\pi} \tag{5.116}$$

which coincides with the high frequency asymptotics which we found for all three $\ell = 0$ spectral functions in section 5.3. Of course, this asymptotic behaviour precisely matches

that of the analytic solution (5.64) with $\ell = 0$ found for the vector modes in the massless quark limit.

For $\ell = 1$ and vanishing three-momentum q, the spectral function is

$$\mathfrak{R}_s^{\ell=1} = \frac{N_{\rm f} N_{\rm c} \omega^4}{16\pi} \,. \tag{5.117}$$

Again, this matches the asymptotic behaviour of the analytic vector solution (5.64) for $M_{\rm q} = 0$ with $\ell = 1$. In fact, given that these asymptotics are independent of $M_{\rm q}$ and that we have found a common expression for all three channels, we can use eq. (5.64) to write the general asymptotic behaviour with $q = 0$ as

$$\mathfrak{R}_s^{\ell}(\omega, q=0) = \frac{N_{\rm f} N_{\rm c}}{2^{2\ell+2}\pi(\ell!)^2}\omega^{2\ell+2} \,. \tag{5.118}$$

Hence we have produced the expected asymptotic behaviour (5.14) for an operator of scaling dimension $\Delta = \ell + 3$. Of course, the behaviour for general q is in principle given by combining the expressions (5.113) and (5.114).

5.6.3 Effective potentials and quasinormal modes

In this section, we rewrite the equations of motion for the pseudoscalar and scalar fluctuations of the D7-brane in the form of the Schroedinger equation. This can be considered a first step towards calculating the spectrum of quasinormal modes for these fields – see, *e.g.,* [155]. The effective potential in each of these effective Schroedinger problems allows us to infer certain aspects of the quasinormal spectra. In particular, we argue that tachyonic modes appear in the scalar spectrum sufficiently close to the critical solution. The same analysis for the vector modes gives results that are essentially identical to those found for the pseudoscalar.

Pseudoscalar

Considering fluctuations of the pseudoscalar, we take the general ansatz

$$\delta\phi \sim e^{ikx}\, \mathcal{P}(\rho)\, \mathcal{Y}^{\ell}(S^3) \,, \tag{5.119}$$

where $\mathcal{Y}_\ell(S^3)$ are spherical harmonics on the S^3 and $k_\mu = (-\omega, q, 0, 0)$. Then the pseudoscalar's wave equation (5.71) can be written as

$$-\frac{H_0}{H_1}\,\partial_\rho\big[H_1\,\partial_\rho \mathcal{P}\big] + \big[\mathfrak{q}^2\, H_2 + L^2\, H_3\big]\,\mathcal{P} = \mathfrak{w}^2\,\mathcal{P} \ , \tag{5.120}$$

with:

$$H_0 \equiv \frac{\rho^4 f^2}{8\tilde{f}} \frac{(1-\chi^2)}{1-\chi^2+\rho^2\dot{\chi}^2}\,, \qquad H_1 \equiv \frac{\rho^5 f \tilde{f} \chi^2 (1-\chi^2)^2}{\sqrt{1-\chi^2+\rho^2\dot{\chi}^2}}\,,$$
$$H_2 \equiv \frac{f^2}{\tilde{f}^2}\,, \qquad H_3 \equiv \frac{\rho^2 f^2}{8\tilde{f}(1-\chi^2)}\,, \qquad L^2 \equiv \ell(\ell+2)\,. \tag{5.121}$$

With the substitution $\mathcal{P} = h\psi$, eq. (5.120) becomes

$$-H_0\,\ddot{\psi} - H_0\left(2\frac{\dot{h}}{h} + \frac{\dot{H}_1}{H_1}\right)\dot{\psi} + \left[\mathfrak{q}^2\,H_2 + L^2\,H_3 - H_0\left(\frac{\ddot{h}}{h} + \frac{\dot{H}_1}{H_1}\frac{\dot{h}}{h}\right)\right]\psi = \mathfrak{w}^2\,\psi\,, \tag{5.122}$$

where, as usual, the dot denotes a derivative with respect to ρ. The first term above can be rewritten as

$$-H_0\,\ddot{\psi} = -\sqrt{H_0}\partial_\rho\left(\sqrt{H_0}\partial_\rho\psi\right) + \frac{1}{2}\dot{H}_0\dot{\psi} = -\partial^2_{R^*}\psi + \frac{1}{2}\dot{H}_0\,\dot{\psi}\,, \tag{5.123}$$

where

$$R^* = \int_\rho^\infty \frac{d\tilde{\rho}}{\sqrt{H_0(\tilde{\rho})}}\,. \tag{5.124}$$

In terms of this new radial coordinate, the second derivative term takes the simple form found in a one-dimensional Schroedinger equation. Combining eqs. (5.122) and (5.123), all of the terms involving $\dot{\psi}$ are eliminated if we choose h as

$$h = \frac{H_0^{1/4}}{H_1^{1/2}}\,. \tag{5.125}$$

Hence the radial equation reduces to

$$-\partial^2_{R^*}\psi + V_{eff}\,\psi = \mathcal{E}\,\psi\,, \tag{5.126}$$

where the effective energy and potential are given by

$$\mathcal{E} = \mathfrak{w}^2\,, \qquad V_{eff} = \mathfrak{q}^2\,H_2 + L^2\,H_3 - H_0\left[\frac{\ddot{h}}{h} + \frac{\dot{H}_1}{H_1}\frac{\dot{h}}{h}\right]\,. \tag{5.127}$$

Let us comment on the new radial coordinate. In some sense, this coordinate is like the 'tortoise' radial coordinate introduced in the analysis of physics in the Schwarzschild geometry [278]. Approaching the event horizon, *i.e.,* as $\rho \to 1$, $H_0 \simeq (\rho-1)^2$ and so

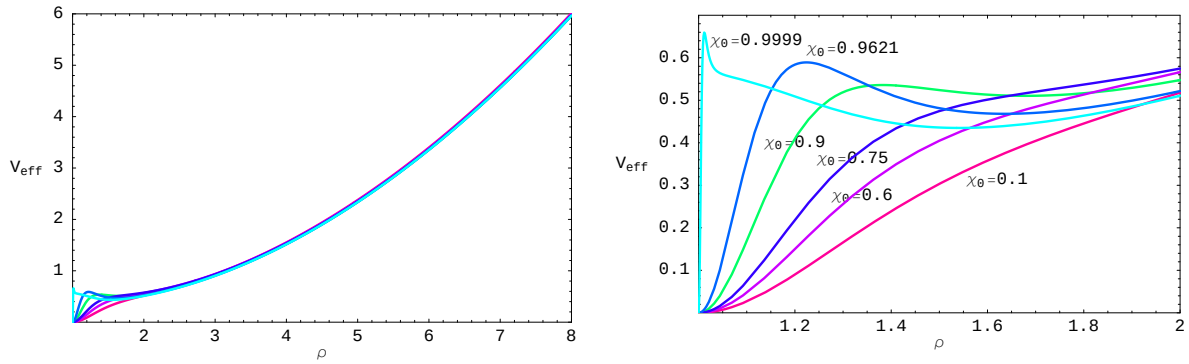

Figure 5.14: The effective potential (for $\delta\phi$ fluctuations) versus ρ for various χ_0 with $\ell = 0$ and $q = 0$.

$R^* \propto -\log(\rho - 1) \to +\infty$. For large ρ, $H_0 \simeq \rho^4$ and so $R^* \simeq 1/\rho \to 0$. Note that given the definition in eq. (5.121), H_0 is positive everywhere on the range $\rho \in (1, \infty)$. Hence we are assured that R^* is a monotonic function of ρ.

Although R^* is the appropriate coordinate to analyse the effective Schroedinger equation (5.126), we can still gain some intuition for the problem by plotting the effective potential (5.127) as a function of ρ for various different D7-brane embeddings. A summary of results (with $q, \ell = 0$) is given in fig. 5.14. Note that for all embeddings, the effective potential exhibits a large barrier in the asymptotic region, as expected for an asymptotically AdS geometry. Further, in all cases, the effective potential vanishes at the horizon. For small χ_0, the potential is monotonically increasing with ρ. For larger χ_0, a small potential barrier develops at intermediate values of the radius. Intuitively, the latter might give rise to metastable states in the effective Schroedinger problem.

For $\ell > 0$ nonzero and $q \neq 0$ the results are qualitatively similar to those depicted in fig. 5.14: The effective potential vanishes at the horizon and grows as $\rho \to \infty$. The potential barrier grows most quickly for $\ell \neq 0$, due to the term proportional to L^2 in (5.127) which is roughly $\ell(\ell+2)\rho^2/8$ for large ρ. For values of χ_0 near 1, a small potential barrier develops for intermediate values of the radius. Note that while a small potential barrier is already evident for $\chi_0 = 0.9$ (with $\ell = 0$ and $q = 0$) in fig. 5.14, the potential barrier only develops for larger values of χ_0, *e.g.*, $\chi_0 > 0.99$ for $\ell > 0$ and/or $q \neq 0$.

The quasinormal modes of the pseudoscalar can be found by solving the Schroedinger

problem constructed above, with the appropriate boundary conditions. One of the boundary conditions is that the pseudoscalar should have only an incoming wave component at the horizon, *i.e.,* $\rho \to 1$ or $R^* \to \infty$. Given the ansatz (5.119), we are thus looking for solutions with[15] $\psi \propto \exp(i\mathfrak{w}\, R^*)$. For large ρ or small R^* where the effective potential diverges, we demand that the wavefunction vanish. Generically, these boundary conditions lead to complex eigenvalues for the effective energy $\mathcal{E}$, which is in accord with our expectation that the quasinormal frequencies have the form [182, 279–283]

$$\mathfrak{w} = \pm\Omega - i\,\Gamma\,, \tag{5.128}$$

with $\Omega, \Gamma > 0$. Note that $\Gamma > 0$ ensures that the quasinormal excitations decay in time, as can be seen from the ansatz (5.119). However, given that

$$\mathcal{E} = \mathfrak{w}^2 = (\Omega^2 - \Gamma^2) \mp 2i\,\Omega\,\Gamma\,, \tag{5.129}$$

some translation is required to use our intuition for the Schroedinger problem to infer general characteristics of the quasinormal spectrum. Note that as the sign of $Im(\mathcal{E})$ is not fixed, we are implicitly admitting energy eigenvalues which would correspond to both decaying and growing wavefunctions in the effective Schroedinger problem. However, this Schroedinger problem is purely an auxiliary tool and so one should not ascribe any physical significance to this observation.

Above, we observed that for small χ_0, the effective potential rises monotonically from zero as we move away from the horizon towards larger ρ. Hence we would infer that $Re(\mathcal{E}) > 0$ or $\Omega > \Gamma$. Further we should not expect any suppression of $Im(\mathcal{E})$, *i.e.,* $Im(\mathcal{E}) \sim Re(\mathcal{E})$, which means that we should still expect to be Ω and Γ to be the same order of magnitude in this regime. This intuition would then suggest the absence of any interesting structure in the corresponding spectral functions, as the quasinormal frequencies should be far from the real axis. However, as noted above, a small potential barrier appears at intermediate values of R^* (or ρ) as χ_0 approaches one. Intuitively, one might expect to find long-lived states with $Re(\mathcal{E}) \gg Im(\mathcal{E})$ and $Re(\mathcal{E}) \sim V_{eff}$(well), *i.e., $Re(\mathcal{E})$* would be roughly given by the height of the potential in this intermediate potential well. From eq. (5.129), this requires $\Omega \gg \Gamma$ with Ω finite and so would correspond to quasinormal

[15]Note that taking the limit $\rho \to 1$ in eq. (5.125) yields a simple constant for h and so we have $\mathcal{P} \propto \psi$ as we approach the horizon.

frequencies approaching the real axis. Hence we would expect the formation of peaks in the spectral function in this regime, as discussed in section 5.1. Of course, this intuitive picture developed from the effective potential matches the behaviour of the spectral functions found in section 5.3.2. We emphasise, however, that this intuition only gives a very rough picture of the quasinormal spectrum and it would be interesting to develop a more detailed picture with a full calculation.

As mentioned above, the results for the effective potential for the vector fluctuations are essentially the same as for the pseudoscalar and hence the quasinormal spectrum should also be similar. We saw in section 5.3.1 that the behaviour of the vector spectral functions is very similar to those for the pseudoscalar.

Scalar

With the ansatz $\delta\theta \sim e^{ikx}\,\mathcal{R}(\rho)\,\mathcal{Y}^{\ell}(S^3)$, the scalar wave equation (5.72) can be written as

$$-\frac{H_0}{H_1}\,\partial_\rho\Big[H_1\,\partial_\rho\mathcal{R}\Big] + \big[\mathfrak{q}^2\,H_2 + (\ell+3)(\ell-1)\,H_3\big]\,\mathcal{R} = \mathfrak{w}^2\,\mathcal{R}\ , \tag{5.130}$$

where H_0, H_2 and H_3 are the same as defined in eq. (5.121), while we must redefine the following:

$$H_1 \equiv \frac{\rho^5 f\tilde{f}(1-\chi^2)^3}{(1-\chi^2+\rho^2\dot{\chi}^2)^{3/2}}\,, \quad L^2 \equiv (\ell+3)(\ell-1)\,. \tag{5.131}$$

Since eq. (5.130) has the same form as eq. (5.120), we can use precisely the same steps as above to cast this equation for the scalar fluctuations in the form of a Schroedinger equation. That is, taking $\mathcal{R} = h\,\psi$ with $h = H_0^{1/4}/H_1^{1/2}$ and defining the radial coordinate (5.124), eq. (5.130) takes the form of the Schroedinger equation (5.126) with the effective energy and potential given by (5.127). Examining the effective potential to gain some intuition for the physics, we find: For all embeddings, there is a large potential barrier in the asymptotic region and the effective potential vanishes at the horizon. For embeddings of the D7-branes with $0 \le \chi_0 < 0.7$, fig. 5.15 shows that the effective potential is a monotonically increasing function of ρ. For $\ell = 0$ and $q = 0$, once $\chi_0 \gtrsim 0.7$, the potential develops a negative well near the horizon. As χ_0 increases towards 1, this well near $\rho \simeq 1$ becomes deeper and wider. Note that $\chi_0 \simeq 0.9621$ and $\chi_0 \simeq 0.99973885$ correspond to the first and second kinks, respectively, in a plot of the free energy versus temperature – see fig. 5.3. For any modes with $\ell > 0$, one finds that there is never a region where

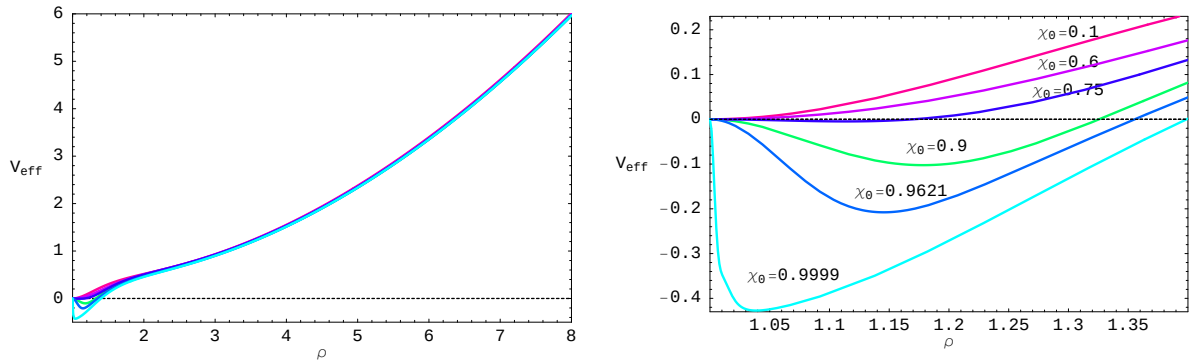

Figure 5.15: The effective potential for the scalar field ($\delta\theta$) versus ρ for various χ_0 with $\ell = 0$ and $k = 0$.

the effective potential becomes negative, however, for χ_0 near 1 the potential develops a small barrier near the horizon. For nonvanishing spatial momentum ($q \neq 0$), the effective potential exhibits a negative well near the horizon for values of χ_0 near 1. However, the well is neither as deep nor as wide as that for $q = 0$.

Certainly, the most interesting feature of the effective potential for the scalar is the negative potential well which develops and grows as $\chi_0 \to 1$. One would expect that if this negative well grows large enough, it will be able to support a 'bound' state with $\mathcal{E} < 0$. Actually, since such a state would still see a finite potential barrier between the centre of the well and the horizon, it would still be a long-lived state. Using a WKB approximation, we can estimate that a (zero-energy) bound state will appear for [187,187,284,284,285,285]

$$\left(n - \frac{1}{2}\right)\pi = \int_{R_0}^{\infty} dR^* \sqrt{-V_{eff}(R^*)} \tag{5.132}$$

$$= \int_{1}^{\rho_0} \frac{d\rho}{\sqrt{H_0}} \sqrt{-V_{eff}(\rho)} \equiv \bar{n} \tag{5.133}$$

where n is a positive integer and the integration is over the values of ρ for which the potential is negative. A plot of $\bar{n}/\pi + 1/2$ is given in figure 5.16 (for $\ell, q = 0$). This quantity reaches 1 for $\chi_0 \simeq 0.98297$ and 2 for $\chi_0 \simeq 0.99986$, and so we expect that the first two bound states form at roughly these values of χ_0. Below we will argue that the appearance of these bound states can be associated with the dramatic spikes observed in the scalar spectral functions in section 5.3.2. Note then that our results here do not (quite) match the values of χ_0 corresponding to the first two kinks (on the black hole branch) of the

free energy – recall that the latter correspond to $\chi_0 = 0.9621$ and 0.99973885, respectively. However, we expect this discrepancy is likely due to the approximations inherent in the WKB calculation.

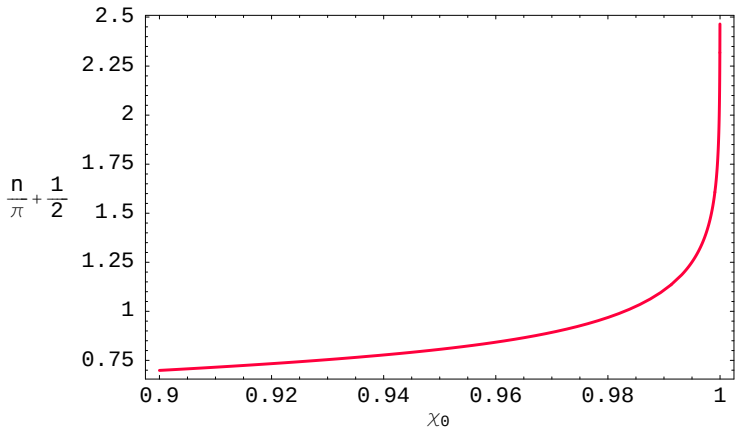

Figure 5.16: Plot of $\bar{n}/\pi + 1/2$ versus χ_0 for $\ell, q = 0$.

As the effective potential is positive and monotonically increasing in the small χ_0 regime, we expect the eigenfrequencies (5.128) in quasinormal spectrum will again have Ω and Γ with the same order of magnitude. Of course, the regime with large χ_0 is more interesting because of the appearance of bound states. These modes with $Re(\mathcal{E}) < 0$ are distinguished since $\Gamma^2 > \Omega^2$, as seen in eq. (5.129). Further, as alluded to above, the corresponding wavefunctions are below a potential barrier as $R^* \to \infty$ and so must have the form $\psi \sim \exp(-|\Gamma|\, R^*)$ to avoid a divergence at the horizon. Given the boundary condition there, *i.e.*, $\psi \propto \exp(i\mathfrak{w}\, R^*)$, this requires that $\Gamma < 0$ for these modes. Further then, it follows that these exceptional modes grow rather than decay in time and so these bound states really represent an instability of the system.

The above discussion indicates that these bound states appear when a quasinormal frequency crosses the real axis and so their appearance should be signalled by a pole appearing in the scalar spectral function calculated in section 5.3.2. Further, however, we argued that as the eigenfrequency crosses the real axis, it moves from a regime where $\Omega^2 > \Gamma^2$ for $\Gamma > 0$ to $\Omega^2 < \Gamma^2$ for $\Gamma < 0$. Hence at the point that $\Gamma = 0$, we must also

have $\Omega = 0$.[16] Hence we see that the quasinormal frequencies must cross the real axis by passing through the origin. This is, of course, precisely what was observed in section 5.3.2, where the poles in the spectral function appeared at precisely $\omega = 0$. Further, the lack of much structure in the spectral function aside from these poles would indicate that the quasinormal frequencies approach the origin uniformly so that we never find eigenfreqencies with $\Omega \gg \Gamma$. We reiterate that this discussion only gives a schematic picture of the quasinormal spectrum and it would be interesting to develop a more detailed picture with a full calculation [155].

5.6.4 Diffusion constants for Dp/Dq systems

This section extends the computation of the diffusion constant using the membrane paradigm [125] described in section 5.4.1 to that for the gauge theory dual to the supergravity configuration of a Dq-brane probe in the near-horizon black Dp-brane geometry.

The background geometry (5.15) is generalised to the near-horizon black Dp-brane metric (in the string-frame) [58] given in eq. (2.1) with the Hawking temperature related to the horizon position via eq. (2.6). As discussed in section 2.1, the gauge/gravity correspondence states that string theory on this background is dual to a supersymmetric $(p+1)$-dimensional gauge theory at temperature T.

In analogy with section 2.2, we consider placing a probe Dq-brane in the above geometry such that the probe has d spatial directions parallel and $n+1$ transverse to the background Dp-branes, so that $q = d + n + 2$ and such that it intersects the horizon at $u = u_0$. We introduce the coordinate ρ, defined in eq. (2.24), so that the horizon is at $\rho = 1$. Implicitly, we will assume in the following that the Dp/Dq system under consideration is T-dual to the D3/D7 one described by the array (2.34). This choice ensures that the brane configuration is supersymmetric at zero temperature and the probe brane embeddings should be stable in the finite temperature background (2.1) [112].

[16] Essentially we are just saying that $Re(\mathcal{E}) = 0$ just as the bound states form.

With the coordinate (2.24), the metric and the dilaton may be written as:

$$\begin{aligned} ds^2 &= \frac{1}{2}\left(\frac{u_0\rho}{L}\right)^{(7-p)/2}\left[-\frac{f^2}{\tilde{f}}dt^2+\tilde{f}dx_p^2\right] \\ &\qquad +\tilde{h}(\rho)\,\left[d\rho^2+\rho^2\left(d\theta^2+\sin^2\theta d\Omega_n+\cos^2\theta d\Omega_{7-p-n}\right)\right] \\ e^{\phi} &= \left(\frac{\tilde{f}}{2}\right)^{(p-3)/2}\left(\frac{u_0\rho}{L}\right)^{(7-p)(p-3)/4}, \end{aligned}$$

where

$$f(\rho)=1-1/\rho^{7-p},\quad \tilde{f}(\rho)=1/\rho^{7-p},\quad \tilde{h}(\rho)=u_0^2\,(L/u_0\rho)^{(7-p)/2}\left(\tilde{f}/2\right)^{(p-3)/(7-p)}.$$

Describing the probe brane profile using $\chi(\rho)=\cos\theta(\rho)$, the induced metric on the Dq-brane may be written as $ds^2(g)=ds^2(\tilde{g})+Z(\rho)d\Omega_n^2$, where

$$\begin{aligned} ds^2(\tilde{g}) &= \frac{1}{2}\left(\frac{u_0\rho}{L}\right)^{(7-p)/2}\left[-\frac{f^2}{\tilde{f}}dt^2+\tilde{f}dx_d^2\right]+\tilde{h}(\rho)\,\frac{1-\chi^2+\rho^2\dot{\chi}^2}{1-\chi^2}d\rho^2\,, \\ Z(\rho) &= \tilde{h}(\rho)\,\rho^2(1-\chi^2)\,. \end{aligned}$$

We assume that the gauge fields are s-waves on the S^3 and take $A_{t,x,y,z}$ to be nonvanishing while $A_\rho=A_{S^3}=0$. Using the DBI action and expanding the gauge fields to quadratic order, the relevant portion of the action for the gauge fields is

$$I_{q,F}=-T_q(\pi\ell_{\rm s}^2)^2\Omega_n\int dt\,d^dx\,d\rho\,\frac{\sqrt{-\tilde{g}}}{g_{eff}^2}F^2,\quad g_{eff}^2=e^{\phi}Z^{-n/2}\,. \tag{5.134}$$

We are now in a position to evaluate the diffusion constant using eq. (2.27) from [125]:

$$\begin{aligned} D &= \left.\frac{\sqrt{-\tilde{g}}}{\tilde{g}_{xx}\,g_{eff}^2\,\sqrt{-\tilde{g}_{tt}\,\tilde{g}_{\rho\rho}}}\right|_{\rho=1}\int_1^\infty d\rho\frac{-\tilde{g}_{tt}\,\tilde{g}_{\rho\rho}\,g_{eff}^2}{\sqrt{-\tilde{g}}} & (5.135)\\ &= \frac{(7-p)}{2\pi T}2^{\alpha}(1-\chi_0^2)^{n/2}\int_1^\infty d\rho\frac{f\,\rho^{\beta}}{\tilde{f}^{\gamma}}\frac{\sqrt{1-\chi^2+\rho^2\dot{\chi}^2}}{(1-\chi^2)^{(n+1)/2}}\,, & (5.136)\end{aligned}$$

where

$$\begin{aligned} \alpha &= \frac{d-p}{2}+\frac{(n-1)(p-3)}{2(7-p)}\,, \\ \beta &= \frac{(7-p)(p+n-3-d)}{4}-n\,, \\ \gamma &= \frac{(n-1)(p-3)}{2(7-p)}+\frac{d+4-p}{2}. \end{aligned}$$

One may check that for $p = 3 = n = d$ this result reduces to that for the D3/D7 case given in eq. (5.89).

We also evaluated DT numerically for the D4/D6 case ($p = 4,\ n = 2,\ d = 3$) and the results are plotted in figure 5.17. The horizontal axis is labelled by the ratio of the temperature to the natural mass scale of the problem, $\bar{M}$, defined in eq. (2.103). Asymptotically, DT approaches $3/4\pi$ for large temperatures. As the temperature is reduced, DT decreases dramatically near the phase transition. The value at the phase transition is $DT = 0.125 \simeq 0.785/2\pi$. If we continue following the black hole embeddings beyond the phase transition, DT continues to fall and it also becomes a multi-valued function of temperature, as was seen in fig. 5.12 for the D3/D7 system. Again, this simply reflects the fact that multiple embeddings can be found for a single temperature in the vicinity of the critical solution.

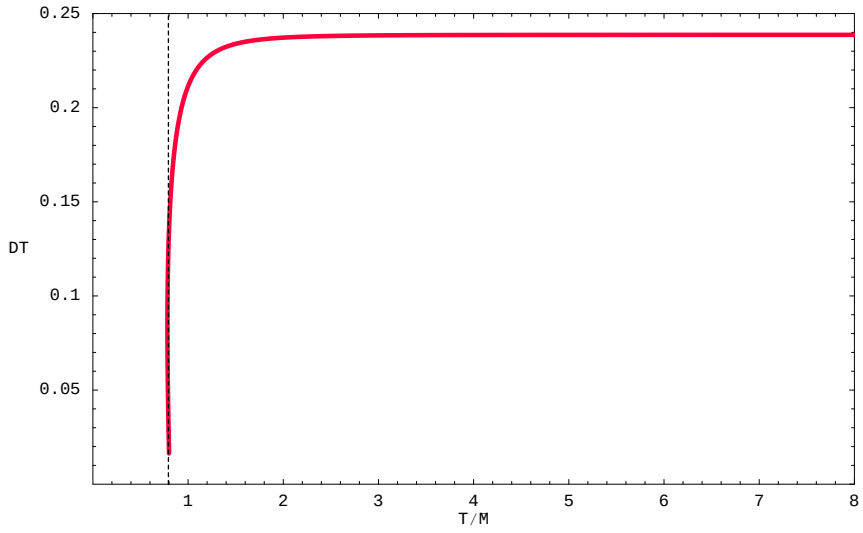

Figure 5.17: The diffusion constant D times the temperature T versus temperature $T/\bar{M}$ for a D6-brane probe in the black D4-brane geometry. For large T we have $DT \simeq 3/4\pi$.

Note that the asymptotic value for DT does not match that for the R-charge diffusion constant calculated for a near-extremal D4-brane result: $3/8\pi$ [125]. However, there is no reason that these two quantities should be equal since the D6-brane does not fill the entire D4-brane throat, *i.e.,* one of the D4-brane worldvolume directions is transverse to the D6 probe.

The D4/D6-brane system considered above is the basis for the construction of one holographic model which mimics QCD at large N_c [62]. Another interesting holographic model of a QCD-like theory comes from introducing D8 and anti-D8 probe branes in a D4-brane background [63, 64]. This system displays an interesting phase transition related to chiral symmetry breaking [107, 108].[17] One can again calculate the diffusion constant for the quark charge in the high temperature phase along the lines described above. In this case, the D8-brane wraps the entire S^4 of the D4 background but otherwise fills the same directions as the D6-branes above. After the phase transition the embeddings are much simpler since there is no non-trivial radial profile to be considered and, further, the embedding is temperature independent. The diffusion constant may be determined from eq. (5.136) setting $\chi = 0 = \chi_0$, $p = 4 = n$ and $d = 3$. The result for the calculation is $DT = 1/2\pi$.

[17] These models generalise to a broad family of models displaying a similar pattern of chiral symmetry breaking [110, 222, 254].

Chapter 6

Conclusion

The gauge/gravity duality has provided new approaches for studying the physics of strongly coupled systems. Through this duality, it is possible to explore a large class of strongly coupled gauge theories, obtaining intuitive geometric (gravity) pictures and alternate tangible descriptions of phenomena. From a theoretical perspective, the duality provides a valuable calculational tool and access to otherwise elusive regimes of physics. Though QCD is not yet in the class of gauge theories with a known gravity dual, it is hoped that some insights into QCD may be achieved through holographic studies.

This thesis presents studies of the properties of a class of thermal gauge theories dual to systems of $N_{\rm f}$ Dq-branes in the black Dp-brane geometry, namely $SU(N_{\rm c})$ SYM coupled to $N_{\rm f} \ll N_{\rm c}$ flavours of fundamental matter. These holographic studies were performed in the limit of large 't Hooft coupling and large-$N_{\rm c}$, in which case the dual gravity theory reduces to a classical theory. The focus was often on the D3/D7 brane system, for which the holographic dual is a four-dimensional field theory.

We studied the thermodynamics of these Dp/Dq brane systems, focussing on the thermal properties of the fundamental matter (chapter 2, [111, 112]). As depicted in fig. 2.1, there are two types of embeddings of Dq-branes in the near horizon geometry of black Dp-branes: The low temperature phase is characterised by 'Minkowski' embeddings, in which the branes close off above the horizon, and for which the meson spectrum is discrete and possesses a mass gap. In the high temperature phase, the Dq-branes intersect the horizon ('black hole' embeddings), and the meson spectrum is continuous and there is no mass gap.

In between the two different types of embeddings, there is a limiting, critical solution

in which the Dq-branes just 'touch' the horizon at a point. We showed that the phase diagram in the vicinity of this solution exhibits a self-similar structure, *e.g.,* the quark condensate is not a single-valued function of m (see, *e.g.,* figs. 2.4, 2.12), the dimensionless constant related to the temperature T and mass scale $\bar{M}$ (see eq. (2.32)) through $m^{(5-p)/2} = \bar{M}/T$. Hence, several different brane embeddings were possible for a given value of m, or equivalently, for a given temperature T in the dual field theory. Of course, the physically preferred configuration is the one which minimises the free energy density of the Dq-branes. Computing the free energy, one finds that as the temperature is increased, a first order phase transition occurs by discontinuously jumping from a Minkowski embedding to a black hole embedding – see, *e.g.,* figs. 2.5, 2.13. This first order phase transition is a direct consequence of the multi-valued nature of physical quantities, such as the quark condensate, and is universal in the Dp/Dq brane systems.

Though it may be possible to access the self-similar region through supercooling, some of the solutions in this region are dynamically unstable. The qualitative behaviour of the specific heat $c_{\rm V} = \partial E/\partial T$ may be seen from figs. 2.5 and 2.13. As the free energy spirals about the critical solution, the slope and hence $c_{\rm V}$ become negative, indicating that these embeddings are thermodynamically unstable. Interestingly, the scalar meson spectrum in the Minkowski phase (section 2.3.3) becomes tachyonic at precisely the point where the first turn-around occurs in the spiral (with T). The scalar spectral function (section 5.3.2) also suggests the existence of a tachyonic mode at the analogous point for black hole embeddings. Hence, dynamical instabilities are manifested in tachyonic modes for near-critical embeddings in both phases.

In these Dp/Dq brane models, the gluons and other adjoint fields were already in a deconfined phase at $T_{\rm fun}$, so the phase transition is not a confinement/deconfinement phase transition. In theories with a confining phase and sufficiently heavy quarks, two distinct phase transitions occur: At $T_{\rm deconf}$ the gluons and adjoint matter become deconfined and the dual gravitational background develops a black hole [59]. For sufficiently heavy quarks, the Dq-branes remain outside the horizon until temperature $T_{\rm fun}$ when the first order phase transition for fundamental matter occurs. This physics is in qualitative agreement with that observed in QCD for heavy-quark mesonic bound states.

The first order phase transition persists for small baryon number density $n_{\rm b}$, which may be introduced into the theory via a nonvanishing background gauge (electric) field on the Dq-branes (chapter 3, [151]). However, unlike the $n_{\rm b} = 0$ case, the phase transition

occurs between two black hole embeddings. Minkowski emebeddings are unphysical for $n_{\rm b} \neq 0$ because the radial electric field lines have nowhere to end if the probe branes close off above the horizon. Focussing on the D3/D7 system, the phase diagram (fig. 3.1) shows that a line of first order phase transitions ends with a critical point at $(T^*_{\rm fun}, n^*_{\rm b})$. To the left of the line there is a small region which is electrically unstable, indicating that black hole embeddings are not the true ground state there.

The gravity duals of gauge theories containing fundamental matter may also be used to study the hydrodynamics of strongly coupled plasmas. To compute the shear viscosity to leading order in $N_{\rm f}/N_{\rm c}$, one must begin to account for the backreaction of the D-branes on the black hole geometry. Focussing on the D3/D7 system, in chapter 4 we demonstrated that the ratio of shear viscosity to entropy density saturates the conjectured universal bound $\eta/S \geq 1/4\pi$. The contribution of the fundamental matter is therefore enhanced at strong 't Hooft coupling λ with $\eta_{\rm fun} \sim \lambda N_{\rm f} N_{\rm c} T^3$. The D3/D7 results extend straightforwardly to Dp/Dq and Dp/Dq/D$\bar{\rm q}$ systems, as well as to systems with a non-zero baryon number chemical potential, with the ratio of shear viscosity to entropy density saturating the bound.

In chapter 5 we computed mesonic spectral functions in the high temperature phase of the theory dual to the D3/D7 system, corresponding to black hole embeddings of the D7-branes. We calculated spectral functions for three operators, all bilinears of fundamental fields, corresponding to vector, pseudoscalar, and scalar channels. The vector (figs. 5.4, 5.6) and pseudoscalar (fig. 5.7) spectral functions are very similar: At high temperature, these show little structure and closely resemble the spectral function for a vector in $\mathcal{N} = 4$ SYM. As the temperature decreases, peaks form in the spectral function, and, at temperatures just above the phase transition, there are vector and pseudoscalar quasiparticles. The scalar spectral function also shows no distinguished structure at high temperatures (fig. 5.8). However, as the temperature decreases, a small peak develops near the origin (fig. 5.9). This peak is not well-developed at the phase transition, but continuing along the black hole branch past the phase transition, it grows, becoming sharply peaked and centred at $\omega = 0$ at precisely the first kink in the free energy. Beyond this point, the peak decays and moves away from $\omega = 0$. We interpret this behaviour as the lowest pair of quasinormal modes approaching the origin and crossing the real axis to the upper complex plane. Once in the upper half plane, these modes have a negative effective energy, indicating that they correspond to instabilities of the D7-branes, in accord with the tachyons found in the meson

spectrum on the Minkowski branch.

We computed the diffusion constant for the quark charge in section 5.4 via the membrane paradigm, the Green-Kubo formula, and the lowest quasinormal frequency, thereby demonstrating the internal consistency of the holographic framework – see fig. 5.12. At high temperatures, the diffusion constant approached $D = 1/(2\pi T)$, matching the result for $\mathcal{N} = 4$ SYM [125]. As $T/\bar{M}$ decreases, DT decreases, which can be understood as the rate of diffusion decreasing at a fixed temperature as the quark mass is increased. The calculation of the diffusion constant for the high temperature phase of other Dp/Dq brane systems appeared in section 5.6.4.

These studies illustrate the power of the gauge/gravity duality: Holographic studies can provide simple, intuitive pictures of strong coupling physics. For example, the meson meltdown phase transition is simply realised in the gravity theory as a discontinuous jump between different brane embeddings. Further, the duality provides a means of performing otherwise intractable calculations. There are currently no other reliable calculational methods to compute dynamical quantities such as transport coefficients *e.g.,* η, D. The success at applying the value of η/S computed in gravity duals to RHIC results suggests that insights into QCD may be gleaned from holographic studies. Though nature only provides one example of a strongly coupled gauge theory, QCD, a large class of gauge theories are theoretically accessible through holographic studies. Through studying many models, it may be possible to determine which properties are universal and which are unique to a particular theory. These have experimental application in the dynamics of the quark gluon plasma (*e.g.,* at RHIC or, in the future, at the Large Hadron Collider (LHC)), which cannot be studied reliably (at present) via lattice techniques.

There are many possible directions suggested by the work in this thesis. One might investigate the dynamics of the melting transition, uncovered in chapter 2, by constructing localised brane configurations in which only part of the probe branes has fallen through the horizon. The localised bubbles of melted fundamental matter would be analogous to the plasma balls uncovered in [219] corresonding to localised lumps of deconfined gluon plasma.

The discussion of brane systems with nonvanishing chemical potential $\mu_{\rm b}$ or baryon number density $n_{\rm b}$ in chapter 3 was formulated in terms of the canonical ensemble, with the phase diagram presented in the $(T, n_{\rm b})$ plane. Rephrasing the discussion in terms of the grand canonical ensemble would allow a direct comparison of the $(T, \mu_{\rm b})$ phase

diagram with that for QCD. The true ground state in the region of instability in the phase diagram 3.1 remains unknown, suggesting that the possibility of Minkowski-type embeddings carrying a gas of baryons should be explored. Spectral functions for bilinears of fundamental operators could be computed in this theory.

In analogy with calculations of the shear viscosity, spectral functions, and diffusion constants of chapters 4 and 5, one might further explore the dynamics of strongly coupled plasmas. The idea of emulating the quark gluon plasma through gravity models appeared in [286–289]. Studies of the drag on a quark moving through the plasma [133–136, 290, 291] and the rate of photon emission from the QGP [268, 271] are all relevant for current and future experimental studies. All the calculations of transport coefficients described above apply to theories in a deconfined phase. It would be interesting to compute transport coefficients using the holographic dual of a confining theory.

Holographic models might also be improved in a number of ways. With fully back-reacted geometries one would no longer need to depend on the probe approximation and would be able to study models with $N_{\rm f}/N_{\rm c}$ finite [83, 209–218]. Incorporating more features of QCD into a single gravity dual would allow for better comparisons with QCD. Work along these lines has occured in relation to the Dp/Dq/D$\bar{\rm q}$ [63,64,107–110,222,234,254–256] system which has a confining phase as well as a geometric realisation of chiral symmetry breaking and restoration. Recently, an attempt was made to allow for nonzero quark mass in the D4/D8/D$\bar{8}$ model [292].

Though a holographic dual to QCD is not yet on the horizon, perhaps these and future holographic studies will yield new insights into the physics of strongly coupled plasmas and QCD. It would certainly be exciting if these might help understand future experimental results, such as those from the LHC.

Appendix A

Holographic dictionary for fundamental fields in an $\mathcal{N} = 2$ four-dimensional gauge theory

Throughout this thesis we focus on three probe brane worldvolume fields: the gauge field A_μ and the embedding coordinates χ and ϕ. We made use of the fact that the asymptotic behaviour of these probe brane fields has a direct translation in terms of hypermultiplet operators in the gauge theory. In this appendix we elucidate this holographic dictionary in more detail for the holographic dual of the D3/D7 brane system, *i.e.,* four-dimensional $U(N_{\rm c})$ $\mathcal{N} = 4$ super-Yang-Mills coupled to $N_{\rm f}$ $\mathcal{N} = 2$ fundamental hypermultiplets.

Let us remind the reader that a hypermultiplet consists of two Weyl fermions $\psi, \tilde{\psi}$ and two complex scalars $q, \tilde{q}$. Of these, ψ and q transform in the fundamental of the $SU(N_{\rm c})$ gauge group, while $\tilde{\psi}$ and $\tilde{q}$ transform in the antifundamental. Further, with $N_{\rm f}$ flavours (of equal mass), the hypermultiplets transform under a global $U(N_{\rm f}) \simeq SU(N_{\rm f}) \times U(1)_{\rm q}$ symmetry. The charges of the fields under the diagonal $U(1)_{\rm q}$ are +1 for ψ and q and –1 for $\tilde{\psi}$ and $\tilde{q}$. Hence the $U(1)_{\rm q}$ charge naturally counts the net number of quarks in a given state. Here and below, we follow the notation of [293].

The operators dual to A_μ, χ and ϕ can be determined by considering the interactions of the open strings on the D3/D7 array (2.34) before the decoupling limit [44], in analogy

with the closed strings. Such an exercise leads to the following operators:

$$A_\mu \quad \leftrightarrow \quad J^\mu_{\rm q} = \bar\psi\bar\sigma^\mu\psi + \tilde\psi\sigma^\mu\tilde\psi^\dagger - i\left(q^\dagger\mathcal{D}^\mu q - (\mathcal{D}^\mu q)^\dagger q\right) - i\left(\tilde q\,(\mathcal{D}^\mu\tilde q)^\dagger - \mathcal{D}^\mu\tilde q\,\tilde q^\dagger\right)\,, \tag{A.1}$$

$$\chi \quad \leftrightarrow \quad \mathcal{O}_{\rm m} = i\tilde\psi\psi + \tilde q(M_{\rm q} + \sqrt{2}\Phi^1)\tilde q^\dagger + q^\dagger(M_{\rm q} + \sqrt{2}\Phi^1)q + h.c.\,, \tag{A.2}$$

$$\phi \quad \leftrightarrow \quad \mathcal{O}_\phi = \tilde\psi\psi + i\sqrt{2}\,\tilde q\,\Phi^1\,\tilde q^\dagger + i\sqrt{2}\,q^\dagger\,\Phi^1\,q + h.c.\,, \tag{A.3}$$

where $\mathcal{D}_\mu$ denote covariant derivatives in the $SU(N_{\rm c})$ gauge theory. Note that Φ^1, a complex scalar in the $\mathcal{N} = 4$ supermultiplet, as well as M_q, appear in the scalar terms after solving for the auxiliary field constraints within the full coupled theory. Note that all three operators have conformal dimension[1] $\Delta = 3$, which matches the standard prescription for the powers of ρ appearing in the asymptotic behaviour of the fields – see below.

The operator $\mathcal{O}_{\rm m}$ is the variation of the mass term in the microscopic Lagrangian, *i.e.,* $\mathcal{O}_{\rm m} = -\partial_{M_{\rm q}}\mathcal{L}$.

Let us comment on the derivation of $\mathcal{O}_\phi$. The mass term for the hypermultiplet fields originates from the following superpotential term

$$i\sqrt{2}\int d^2\theta\,\left(\tilde Q\,\Phi_{7,7}\,Q - h.c.\right) \tag{A.4}$$

where $\tilde Q$ and Q are chiral superfields containing $(\tilde q, \tilde\psi)$ and (q, ψ), respectively. These hypermultiplet fields appear as ground states of the 3-7 and 7-3 strings while, as the subscript indicates, the superfield $\Phi_{7,7}$ describes a particular set of massless modes in the 7-7 string sector. In particular, the lowest component of $\Phi_{7,7}$ is a complex scalar describing the transverse fluctuations of the D7-brane position, *i.e.,*

$$\Phi_{7,7} = \frac{1}{\sqrt{2}}\left(\frac{X^8 + i\,X^9}{2\pi\ell_s^2}\right) + \cdots\,, \tag{A.5}$$

for the orientation in array (2.34). After the decoupling limit, this is no longer a dynamical field in the gauge theory but its expectation value sets the mass of the hypermultiplets, *i.e.,* $\langle\Phi_{7,7}\rangle = M_{\rm q}/\sqrt{2}$. One sees from eq. (A.5) that the geometric angle ϕ appearing in our construction of the D7-brane embeddings in section 2.3.1 corresponds precisely to the phase of the complex field $\Phi_{7,7}$. Hence in deriving $\mathcal{O}_\phi$, we consider a phase rotation with the given expectation value for $\Phi_{7,7}$ in the Lagrangian (A.4). The resulting variation yields

[1] This dimension applies in the UV where the effects of quark mass are negligible and the theory becomes conformal.

$\delta\mathcal{L} = \delta\phi\, M_{\rm q}\, \mathcal{O}_\phi$ and so we have divided by the factor of $M_{\rm q}$ in defining the operator given in eq. (A.3).

Recall that the full flavour symmetry is $U(N_{\rm f})$, which of course matches the worldvolume gauge symmetry of the D7-branes. The current $J^\mu_{\rm q}$ is the conserved current corresponding to the diagonal $U(1)_{\rm q}$ of this global symmetry, *i.e.,* $J^t_{\rm q}$ is the quark charge density. Our discussion can easily extended to the $SU(N_{\rm f})$ symmetry by considering the nonAbelian gauge fields on the D7-brane. The corresponding flavour currents would be

$$A^a_\mu \quad\leftrightarrow\quad (J^a)^\mu = (T^a)_i{}^j \Big[\bar\psi^i\bar\sigma^\mu\psi_j + \tilde\psi^i\sigma^\mu\tilde\psi^\dagger_j - i\left(q^{\dagger i}\mathcal{D}^\mu q_j - (\mathcal{D}^\mu q)^{\dagger i} q_j\right) \\ -i\left(\tilde q^{\,i}\,(\mathcal{D}^\mu\tilde q)^\dagger_j - \mathcal{D}^\mu\tilde q^{\,i}\,\tilde q^\dagger_j\right)\Big]\,, \tag{A.6}$$

where T^a are (Hermitian) generators of $SU(N_{\rm f})$ and we have restored explicit flavour indices on the fields. With the operators $\mathcal{O}_{\rm m}$ and $\mathcal{O}_\phi$, we have also focussed on the $SU(N_{\rm f})$ neutral terms but it would be straightforward to extend these to a more general discussion. For example, in general $\Phi_{7,7}$ transforms in the adjoint of $U(N_{\rm f})$ and so one can easily chose a more elaborate mass matrix rather than one proportional to the identity as above.

A.1 Scalar

We can make the dictionary between the asymptotic coefficients and the dual gauge theory parameters precise by realising that the hypermultiplet states are the ground states of the 3-7 and 7-3 strings. Hence in the decoupling limit, these become precisely strings stretching between the D7-branes and the horizon of the D3-branes. For example, the quark mass is trivially derived for the brane array (2.34) in asymptotically flat space. As this brane configuration is supersymmetric at $T = 0$, this mass persists in the decoupling limit, where it is again the energy of a string stretching between the D3- and D7-branes. This gives a relation between $M_{\rm q}$ and the parameter m appearing in the asymptotic expansions (2.45) and (3.13):

$$M_{\rm q} = \frac{u_0}{2^{3/2}\pi\ell_{\rm s}^2}\, m = \frac{1}{2}\sqrt{\lambda}\, T\, m\,. \tag{A.7}$$

Further, this relation is inherited by the theory at finite temperature, since setting $T \neq 0$ does not alter the asymptotic properties that determine the gauge theory parameters.[2]

[2]Note that here we are referring to the bare or current quark mass. The constituent quark mass is certainly modified by thermal effects, as calculated in section 2.6.4 [112, 133].

Using this result, following [62] we can formulate a variational argument to relate the second coefficient in the asymptotic expansion of χ to the field theory condensate $\langle \mathcal{O}_m \rangle$. The Hamiltonian density of the gauge theory can be written (parametrically) as

$$\mathcal{H} = \mathcal{H}_0 + M_{\rm q} \int d^2\theta \tilde{Q} Q \,, \tag{A.8}$$

where $\mathcal{H}_0$ is independent of the quark mass $M_{\rm q}$ and $\tilde{Q}$, Q are the hypermultiplet superfields in $\mathcal{N} = 1$ language. With $\mathcal{E} = \langle \mathcal{H} \rangle$, the condensate is

$$\frac{\partial \mathcal{E}}{\partial M_{\rm q}} = \langle \int d^2\theta \tilde{Q} Q \, \rangle = \langle \mathcal{O}_m \rangle \,. \tag{A.9}$$

As discussed above, in the string description the quark mass is given by the asymptotic position of the D7-branes. Hence, in order to compute the condensate, we need to find the change in energy associated with a change in boundary condition m, recalling that asymptotically the D7-branes' position is given in (2.50) as $R_v(r) = m + c/r^2$. With the Lorentzian D7-brane action $S_{\rm D7} = \int d^8\sigma \mathcal{L}_0$ where the Lagrangian density $\mathcal{L}_0$ is given in eq. (2.72), we have

$$\delta\mathcal{E} = -\int dr d\Omega_3 \delta\mathcal{L}_0 = -2\pi^2 \left[\delta R_v \frac{\partial}{\partial \dot{R}_v} \frac{\mathcal{L}_0}{\sqrt{h}} \right]_{r=0}^{r=\infty} = -\pi^2 T_{\rm D7}\, u_0^4\, c\, \delta m \,, \tag{A.10}$$

where h is the determinant of the metric on the S^3 of unit radius. Then, in view of (A.7), the condensate is

$$\langle \mathcal{O}_m \rangle = -2^{3/2}\pi^3 \ell_{\rm s}^2 N_{\rm f} T_{\rm D7} u_0^3\, c = -\frac{1}{8}\sqrt{\lambda}\, N_{\rm f}\, N_{\rm c} T^3\, c \,. \tag{A.11}$$

As presented here, this dictionary was established for a constant coefficient (*i.e.,* the mass) and uniform expectation value of the operator $\mathcal{O}_{\rm m}$. However, the same relationships also apply in considering correlators where $M_{\rm q}$ is shifted with a general space- and time-dependent coefficient or source $\mu(x)$. In section 5.3.2, we express the relevant correlators in terms of variations $\delta\theta(x,\rho)$ (or its Fourier transform along the x^μ directions). Given that $\chi \equiv \cos\theta$, we have $\delta\theta \simeq -\delta\chi$ asymptotically where χ approaches zero. Hence, as confirmed from eq. (5.72), $\delta\theta$ has the following the asymptotic behaviour:

$$\delta\theta(x,\rho) = \frac{\delta\theta_0(x)}{\rho} + \frac{\Theta(x)}{\rho^3} + \cdots \,. \tag{A.12}$$

The source term is related to the first coefficient above as in eq. (A.7) (up to a sign): $\mu(x) = -\frac{1}{2}\sqrt{\lambda} T\, \delta\theta_0(x)$. Similarly the induced expectation value and $\Theta(x)$ are related as in eq. (A.11), again up to an overall sign.

A.2 Vector

In chapter 3 [151], we considered the gauge theory dual to the D3/D7 brane system at finite baryon density and chemical potential. The baryon density or chemical potential was introduced by allowing for a nonzero time component of the gauge field on the probe D7-branes. As noted above, the holographic dictionary relates A_t to the quark charge density $J^t_{\rm q} = \mathcal{O}_{\rm q}$. The asymptotic value of the potential $A_t(\infty)$ is proportional to the coefficient with which the charge density $\mathcal{O}_{\rm q}$ enters the microscopic Lagrangian. This operator is normalised so that acting on a particular state it yields exactly the net quark density, and therefore the corresponding coefficient is precisely the chemical potential μ for the quarks. Similarly the relevant expectation value is the quark density $n_{\rm q} = \langle \mathcal{O}_{\rm q} \rangle$.

We can provide a precise definition of the particle density on the string side of the duality. First, recall that the electric field on the worldvolume can be thought of as arising from fundamental strings 'dissolved' into the D7-brane [237]. The density of these strings can be determined from the local charge density for the two-form B-field. The standard convention is that the fundamental string couples to the NS two-form through the worldsheet interaction $T_{\rm f} \int d^2\sigma\, B$. Hence a string pointing along the x^i-axis sources B_{ti} with the charge being just the string tension $T_{\rm f} = 1/(2\pi\ell_{\rm s}^2)$. Further, the one-form gauge invariance of B requires that the D7-brane action only involves the combination $B + 2\pi\ell_{\rm s}^2 F$. Hence we have

$$\frac{\delta I_{\rm D7}}{\delta B_{ti}} = \frac{1}{2\pi\ell_{\rm s}^2} \frac{\delta I_{\rm D7}}{\delta F_{ti}} \,. \tag{A.13}$$

Combining these observations, we first conclude that since the D7-brane carries an electric field in the ϱ direction, the worldvolume effectively contains strings stretching along the radial direction with a density precisely determined by the electric displacement $d = -\delta I_{\rm D7}/\delta F_{t\varrho}$. The minus sign in the last expression means that for positive d the strings are oriented to be inward pointing towards the horizon at $\varrho = 1$. Since the number of strings corresponds precisely to the number of quarks in the field theory, the density of quarks is given by integrating the string density on the D7-branes over the internal three-sphere:

$$n_{\rm q} = \int d\Omega_3\, d = 2\pi^2\, d \,. \tag{A.14}$$

While d is not precisely the coefficient of the normalisable mode in eq. (3.7), the two satisfy the simple relation given in eq. (3.9).

As noted above, the non-normalisable mode $A_t(\infty)$ indicates that the charge density operator $\mathcal{O}_{\rm q}$ enters the microscopic Lagrangian. As we wish to relate this bulk mode to the chemical potential μ for the quarks in the microscopic theory, it is natural to frame the discussion in terms of the grand canonical ensemble. There the chemical potential enters the partition function as

$$\exp\left[-\beta\int d^3x\, W(\beta,\mu)\right] \equiv \sum \exp\left[-\beta\int d^3x\, \left(\mathcal{H}-\mu\,\mathcal{O}_{\rm q}\right)\right], \tag{A.15}$$

where a sum over all states is denoted on the right hand side. Of course, $W(\beta,\mu)$ and $\mathcal{H}$ are the Gibbs free energy and Hamiltonian densities, respectively. We know that $\mu \propto A_t(\infty)$ but we would like to determine the exact constant of proportionality. Towards this end, we note that, as can be seen from eq. (A.15),

$$\frac{\delta W}{\delta\mu} = -\langle\, \mathcal{O}_{\rm q}\,\rangle = -\,n_{\rm q}\,. \tag{A.16}$$

To compare to the string description, we turn to the semiclassical analysis of the Euclidean supergravity path integral, as described in section 3.2. The grand canonical ensemble is represented by the usual path integral with fixed $A_t(\infty)$ and the on-shell action gives the leading contribution to the Gibbs free energy, *i.e.,* $I_{\rm E} = \beta\, W$. Hence to compare to eq. (A.16), we need to evaluate the change of the on-shell D7-brane action induced by a change of the boundary value $A_t(\infty)$. Given the worldvolume action (3.5), the desired variation is

$$\delta W = \int d\varrho\, d\Omega_3\, \delta\mathcal{L}_{\rm E} = 2\pi^2\int_1^\infty d\varrho\, \frac{\delta\mathcal{L}_{\rm E}}{\delta\partial_\varrho A_t}\,\partial_\varrho\delta A_t\,, \tag{A.17}$$

where $\mathcal{L}_E$ is the D7-brane Lagrangian density. In eq. (A.17), we have only integrated over the internal three-sphere and the radial direction to produce the free energy density in the gauge theory directions. Once again we recognise the first factor as $d = \delta\mathcal{L}/\delta\partial_\varrho A_t = -\delta\mathcal{L}_{\rm E}/\delta\partial_\varrho A_t$ (in the current notation – note that we need to distinguish between the 'Lagrangian' densities appearing in the Minkowski (3.5) and Euclidean (3.39) actions), which is a constant on-shell. Hence eq. (A.17) reduces to

$$\delta W = -2\pi^2\, d\, \left(\delta A_t(\infty) - \delta A_t(1)\right) = -\,n_{\rm q}\,\delta A_t(\infty)\,, \tag{A.18}$$

where we used (A.14) and the fact that A_t always vanishes on the horizon so that we must have $\delta A_t(1) = 0$. Finally, comparing eqs. (A.16) and (A.18), we find

$$A_t(\infty) = \mu\,, \tag{A.19}$$

and so, as anticipated in the main text, the constant part of the asymptotic gauge potential is precisely the chemical potential for the quarks. If we wish to express results in terms of a baryon chemical potential, we would convert $\mu_{\rm b} = N_{\rm c}\,\mu$.

Let us also recall the formulae for the dimensionless quantities defined in eqs. (3.11) and (3.14) and which appear in our calculations:

$$\tilde{\mu} \;=\; \frac{2\pi\ell_{\rm s}^2\mu}{u_0} = \sqrt{\frac{2}{\lambda}}\,\frac{\mu}{T}\,, \tag{A.20}$$

$$\tilde{d} \;=\; \frac{d}{2\pi\ell_{\rm s}^2 u_0^3 N_{\rm f} T_{\rm D7}} = \frac{2^{5/2}}{N_{\rm f}N_{\rm c}\lambda^{1/2}}\,\frac{n_{\rm q}}{T^3} = \frac{2^{5/2}}{N_{\rm f}\lambda^{1/2}}\,\frac{n_{\rm b}}{T^3}\,. \tag{A.21}$$

Hence as with the previous definitions, the temperature T provides the scale to make these quantities dimensionless but implicitly we have also introduced interesting factors of the 't Hooft coupling, as well as of $N_{\rm f}$ and $N_{\rm c}$. In particular, we see that $\tilde{d}$ is naturally related to the expectation value of the baryon number $n_{\rm b}$ in (A.21).

The relationships (A.20) and (A.21) were established for constant chemical potential and uniform quark density, however, they still apply for more general configurations. In particular, for the correlators of section 5.3.1, we consider more general gauge field configurations with asymptotic behaviour

$$A_\mu = \Sigma_\mu(x) + \frac{\sigma_\mu(x)}{\rho} + \cdots\,. \tag{A.22}$$

In this case, Σ_μ corresponds to the (space- and time-dependent) coefficient of the current operator J_q^μ and the induced expectation values are given by

$$\langle J_q^\mu(x)\rangle = \frac{1}{4}N_{\rm f}N_{\rm c}\,T^2\,\sigma^\mu(x)\,. \tag{A.23}$$

Note that here the index on σ^μ is raised with $\eta^{\mu\nu}$, the inverse metric in the field theory.[3]

A.3 Pseudoscalar

Now we would like to turn to the holographic dictionary for the $\delta\phi$ modes. From the equation of motion (5.71) and the asymptotic behaviour of χ given in eq. (2.45), we can

[3]Note that while the calculation of the spectral function in section 5.3.1 is presented in terms of the gauge-invariant field strengths $F_{\mu\nu}$, this was simply choice of convenience and the final spectral function corresponds to that for current in eq. (A.1).

determine that $\delta\phi$ has the following asymptotic behaviour

$$\delta\phi(x,\rho) = \delta\phi_0(x) + \frac{\Phi(x)}{\rho^2} + \cdots \,. \tag{A.24}$$

From eq. (A.5), we saw that the geometric angle ϕ appearing in the D7-brane embeddings corresponds precisely to the phase of the complex field $\Phi_{7,7}$. Hence $\delta\phi_0$ corresponds to a fluctuation in the phase of the hypermultiplet mass term. As usual, the dimensionless constant Φ is proportional to the induced expectation value of $\mathcal{O}_\phi$ but we would still need establish the precise constant of proportionality.

To establish the latter relationship, it is natural to frame the discussion in terms of the thermal partition function – see [151], for example.[4] The source potential $\delta\phi_0$ enters the partition function as

$$\exp\left[-\beta\, F(\beta,\delta\phi_0)\right] \equiv \sum \exp\left[-\beta \int d^3x\, \left(\mathcal{H} - \delta\phi_0\, M_{\rm q}\, \mathcal{O}_\phi\right)\right] , \tag{A.25}$$

where a sum over all states is denoted on the right hand side and β denotes the inverse temperature. Of course, $F(\beta,\delta\phi_0)$ and $\mathcal{H}$ are the free energy and Hamiltonian densities, respectively. To begin, we note that, as can be seen from eq. (A.25),

$$\frac{\delta F}{\delta(\delta\phi_0)} = -M_{\rm q}\, \langle\, \mathcal{O}_\phi \,\rangle \,. \tag{A.26}$$

To compare to the string description, we turn to the semiclassical analysis of the Euclidean supergravity path integral – see [112, 151], for example. Here the on-shell action gives the leading contribution to the free energy, *i.e.,* $I_{\rm E} = \beta\, F$. Hence to compare to eq. (A.26), we need to evaluate the change of the on-shell D7-brane action induced by a variation $\delta\phi_0$. The background solution for this field is simply $\phi = 0$ and so to linear order the action is invariant. Hence we can focus on the appropriate Euclidean version of the quadratic action (5.73) and the variation yields a boundary term, as in eq. (5.75),

$$\begin{aligned} \delta F &= \frac{\pi^2}{4} N_{\rm f} T_7 {u_0}^4 \int d^3x\, \delta\phi_0 \left[\frac{\rho^5 f \tilde{f} (1-\chi^2)^2 \chi^2}{\sqrt{1-\chi^2+\rho^2\dot{\chi}^2}}\, \partial_\rho \delta\phi\right]_{\rho\to\infty} \\ &= -\frac{\pi^2}{2} N_{\rm f} T_7 {u_0}^4 m^2 \int d^3x\, \Phi(x)\, \delta\phi_0 \,, \end{aligned} \tag{A.27}$$

[4] In principle then this discussion only concerns space- but not time-dependent sources. However, the following results apply for the general case including time dependence.

where the last expression uses the asymptotic behaviour of both χ and $\delta\phi$ from eqs. (2.45) and (A.24), respectively. Comparing eqs. (A.26) and (A.27), we find

$$\langle\, \mathcal{O}_\phi \,\rangle = \frac{\pi^2}{2M_{\rm q}} N_{\rm f} T_7 {u_0}^4 m^2\, \Phi(x) = \frac{1}{8} N_{\rm f} N_{\rm c}\, M_{\rm q} T^2\, \Phi(x)\,, \tag{A.28}$$

which completes the holographic dictionary for the $\delta\phi$ modes.

A.4 Operators with $\ell > 0$

In the above, we've identified the $\ell = 0$ modes of the worldvolume fields with operators in the dual field theory. A similar dictionary relates the higher-ℓ modes to dimension $\ell + 3$ operators $\mathcal{O}^\ell$ in the gauge theory. Qualitatively, we may say that the latter are constructed out of products of ℓ adjoint scalar fields 'sandwiched' between two fundamental operators – see *e.g.,* [61, 294]. For example, the expression (A.4) for $\mathcal{O}_\phi$ would be generalised to

$$\mathcal{O}^\ell_\phi \sim \int d^2\theta\, \tilde{Q}\ \Phi_{7,7}\ \left(\Phi_{3,3}\right)^\ell\ Q \tag{A.29}$$

where $\left(\Phi_{3,3}\right)^\ell$ represents a traceless combination of scalar superfields in the adjoint hypermultiplet.[5] As is often the case in the AdS/CFT correspondence and its generalisations, determining the precise matchings between normalisations in the field theory and string theory is difficult, mainly due to the fact that one would need the full D3/D7 brane action before taking the decoupling limit to find the couplings of the bulk fields to field theory operators.

To study the spectral functions, overall numerical constants need not concern us. We simply choose a normalisation which is consistent with holography and ensure that the spectral function has the proper scaling dimension (5.14). The three equations of motion, (5.51) for the vector, (5.81) for the pseudoscalar, and (5.87) for the scalar, imply the asymptotic behaviour

$$\Psi_\ell = A_\ell\, \rho^\ell + B_\ell\, \rho^{-\ell-2}\,, \tag{A.30}$$

for some constants A_ℓ, B_ℓ where $\Psi_\ell = E^\ell_x$, $\delta\phi_\ell$, $\rho\delta\theta_\ell$. In order to obtain the correct scaling of the spectral function, we change to the standard dimensionful coordinates $z = L^2/u$

[5] Hence in this expression (A.29), the fundamental fields have an implicit sum of over the global $U(N_{\rm f})$ indices with $\Phi_{7,7}$ and the gauge $U(N_{\rm c})$ indices with $\left(\Phi_{3,3}\right)^\ell$.

(asymptotically, $z = \sqrt{2}/\pi T\rho$) used in the usual AdS/CFT prescriptions for computing correlation functions (see, *e.g.,* [53]). In these coordinates, (A.30) becomes

$$\delta\Psi_\ell = \tilde{A}_\ell\, z^{-\ell} + \tilde{B}_\ell\, z^{\ell+2}\,. \tag{A.31}$$

Hence, for $z \to 0$ (the boundary), we expect the leading behaviour $\Psi \sim z^{-\ell}$. Taking a cutoff at small $z = \epsilon$, this implies that we should take

$$\Psi_\ell = \Psi^0_\ell(k)\epsilon^{-\ell}\frac{\Phi_\ell(z)}{\Phi_\ell(\epsilon)} = \Psi^0_\ell(k)\frac{(\pi T)^\ell}{2^{\ell/2}}\rho^\ell_{\max}\frac{\Phi_\ell(\rho)}{\Phi_\ell(\rho_{\max})}\,, \tag{A.32}$$

where Φ_ℓ represents $E_{\ell,k}$ for the vector, $\mathcal{P}_{\ell,k}$ for the pseudoscalar, and $\rho\mathcal{R}_{\ell,k}$ for the scalar. As seen in section 5.6.2, using (A.32) the spectral functions have the correct scaling (5.14) for an operator of dimension $\Delta = \ell + 3$.

Bibliography

[1] D. J. Gross and F. Wilczek, Phys. Rev. Lett. **30**, 1343 (1973).

[2] H. D. Politzer, Phys. Rev. Lett. **30**, 1346 (1973).

[3] A. R. Bodmer, Phys. Rev. **D4**, 1601 (1971).

[4] T. D. Lee and G. C. Wick, Phys. Rev. **D9**, 2291 (1974).

[5] J. C. Collins and M. J. Perry, Phys. Rev. Lett. **34**, 1353 (1975).

[6] G. Baym and S. A. Chin, Phys. Lett. **B62**, 241 (1976).

[7] B. A. Freedman and L. D. McLerran, Phys. Rev. **D16**, 1169 (1977).

[8] G. Chapline and M. Nauenberg, Phys. Rev. **D16**, 450 (1977).

[9] E. V. Shuryak, Sov. Phys. JETP **47**, 212 (1978).

[10] E. V. Shuryak, Phys. Lett. **B78**, 150 (1978).

[11] O. K. Kalashnikov and V. V. Klimov, Phys. Lett. **B88**, 328 (1979).

[12] J. I. Kapusta, Nucl. Phys. **B148**, 461 (1979).

[13] J. D. Bjorken, Phys. Rev. **D27**, 140 (1983).

[14] T. A. DeGrand and K. Kajantie, Phys. Lett. **B147**, 273 (1984).

[15] D. J. Schwarz, Annalen Phys. **12**, 220 (2003), astro-ph/0303574.

[16] E. Witten, Phys. Rev. **D30**, 272 (1984).

[17] D. J. Schwarz, Mod. Phys. Lett. **A13**, 2771 (1998), gr-qc/9709027.

[18] J. W. Harris and B. Muller, Ann. Rev. Nucl. Part. Sci. **46**, 71 (1996), hep-ph/9602235.

[19] M. Gyulassy and L. McLerran, Nucl. Phys. **A750**, 30 (2005), nucl-th/0405013.

[20] B. Muller and J. L. Nagle, Ann. Rev. Nucl. Part. Sci. **56**, 93 (2006), nucl-th/0602029.

[21] BRAHMS, I. Arsene *et al.*, Nucl. Phys. **A757**, 1 (2005), nucl-ex/0410020.

[22] PHENIX, K. Adcox *et al.*, Nucl. Phys. **A757**, 184 (2005), nucl-ex/0410003.

[23] B. B. Back *et al.*, Nucl. Phys. **A757**, 28 (2005), nucl-ex/0410022.

[24] STAR, J. Adams *et al.*, Nucl. Phys. **A757**, 102 (2005), nucl-ex/0501009.

[25] L. Susskind, Nuovo Cim. **A69**, 457 (1970).

[26] N. B. Bielsen, An almost physical interpretation of the integrand of the n-point veneziano model, in *15th International Conference on High Energy Physics (Kiev)*, 1970.

[27] Y. Nambu, Quark model and factorization of the veneziano amplitude, in *Symmetries and Quark Models*, edited by Chand, Gordon, and Breach, 1970.

[28] E598, J. J. Aubert *et al.*, Phys. Rev. Lett. **33**, 1404 (1974).

[29] SLAC-SP-017, J. E. Augustin *et al.*, Phys. Rev. Lett. **33**, 1406 (1974).

[30] E. G. Cazzoli *et al.*, Phys. Rev. Lett. **34**, 1125 (1975).

[31] G. Goldhaber *et al.*, Phys. Rev. Lett. **37**, 255 (1976).

[32] I. Peruzzi *et al.*, Phys. Rev. Lett. **37**, 569 (1976).

[33] DASP, R. Brandelik *et al.*, Phys. Lett. **B70**, 132 (1977).

[34] J. Scherk and J. H. Schwarz, Nucl. Phys. **B81**, 118 (1974).

[35] M. B. Green and J. H. Schwarz, Phys. Lett. **B109**, 444 (1982).

[36] M. B. Green and J. H. Schwarz, Nucl. Phys. **B198**, 441 (1982).

[37] M. B. Green and J. H. Schwarz, Nucl. Phys. **B198**, 252 (1982).

[38] M. B. Green and J. H. Schwarz, Nucl. Phys. **B181**, 502 (1981).

[39] M. B. Green, J. H. Schwarz, and E. Witten, *Superstring theory. Vol. 1: Introduction* (Cambridge University Press, Cambridge, 1987).

[40] J. Dai, R. G. Leigh, and J. Polchinski, Mod. Phys. Lett. **A4**, 2073 (1989).

[41] P. Horava, Phys. Lett. **B231**, 251 (1989).

[42] J. Polchinski, Phys. Rev. Lett. **75**, 4724 (1995), hep-th/9510017.

[43] J. Polchinski, *String theory. Vol. 1: An introduction to the bosonic string* (Cambridge University Press, Cambridge, 1998).

[44] J. Polchinski, *String theory. Vol. 2: Superstring theory and beyond* (Cambridge University Press, Cambridge, 1998).

[45] C. V. Johnson, *D-branes* (Cambridge University Press, Cambridge, 2003).

[46] E. Witten, Nucl. Phys. **B443**, 85 (1995), hep-th/9503124.

[47] A. Strominger, Nucl. Phys. **B451**, 96 (1995), hep-th/9504090.

[48] C. M. Hull and P. K. Townsend, Nucl. Phys. **B438**, 109 (1995), hep-th/9410167.

[49] G. T. Horowitz and A. Strominger, Nucl. Phys. **B360**, 197 (1991).

[50] A. Strominger and C. Vafa, Phys. Lett. **B379**, 99 (1996), hep-th/9601029.

[51] P. K. Townsend, Phys. Lett. **B350**, 184 (1995), hep-th/9501068.

[52] J. M. Maldacena, Adv. Theor. Math. Phys. **2**, 231 (1998), hep-th/9711200.

[53] O. Aharony, S. S. Gubser, J. M. Maldacena, H. Ooguri, and Y. Oz, Phys. Rept. **323**, 183 (2000), hep-th/9905111.

[54] E. D'Hoker and D. Z. Freedman, (2002), hep-th/0201253.

[55] G. 't Hooft, Nucl. Phys. **B72**, 461 (1974).

[56] S. S. Gubser, I. R. Klebanov, and A. M. Polyakov, Phys. Lett. **B428**, 105 (1998), hep-th/9802109.

[57] E. Witten, Adv. Theor. Math. Phys. **2**, 253 (1998), hep-th/9802150.

[58] N. Itzhaki, J. M. Maldacena, J. Sonnenschein, and S. Yankielowicz, Phys. Rev. **D58**, 046004 (1998), hep-th/9802042.

[59] E. Witten, Adv. Theor. Math. Phys. **2**, 505 (1998), hep-th/9803131.

[60] A. Karch and E. Katz, JHEP **06**, 043 (2002), hep-th/0205236.

[61] M. Kruczenski, D. Mateos, R. C. Myers, and D. J. Winters, JHEP **07**, 049 (2003), hep-th/0304032.

[62] M. Kruczenski, D. Mateos, R. C. Myers, and D. J. Winters, JHEP **05**, 041 (2004), hep-th/0311270.

[63] T. Sakai and S. Sugimoto, Prog. Theor. Phys. **113**, 843 (2005), hep-th/0412141.

[64] T. Sakai and S. Sugimoto, Prog. Theor. Phys. **114**, 1083 (2006), hep-th/0507073.

[65] A. Fayyazuddin and M. Spalinski, Nucl. Phys. **B535**, 219 (1998), hep-th/9805096.

[66] O. Aharony, A. Fayyazuddin, and J. M. Maldacena, JHEP **07**, 013 (1998), hep-th/9806159.

[67] M. Grana and J. Polchinski, Phys. Rev. **D65**, 126005 (2002), hep-th/0106014.

[68] M. Bertolini, P. Di Vecchia, M. Frau, A. Lerda, and R. Marotta, Nucl. Phys. **B621**, 157 (2002), hep-th/0107057.

[69] M. Bertolini, P. Di Vecchia, G. Ferretti, and R. Marotta, Nucl. Phys. **B630**, 222 (2002), hep-th/0112187.

[70] X.-J. Wang and S. Hu, JHEP **09**, 017 (2003), hep-th/0307218.

[71] P. Ouyang, Nucl. Phys. **B699**, 207 (2004), hep-th/0311084.

[72] L. A. Pando Zayas, J. Sonnenschein, and D. Vaman, Nucl. Phys. **B682**, 3 (2004), hep-th/0311190.

[73] E. Schreiber, (2004), hep-th/0403226.

[74] N. J. Evans and J. P. Shock, Phys. Rev. **D70**, 046002 (2004), hep-th/0403279.

[75] J. L. F. Barbon, C. Hoyos, D. Mateos, and R. C. Myers, JHEP **10**, 029 (2004), hep-th/0404260.

[76] A. Armoni, JHEP **06**, 019 (2004), hep-th/0404248.

[77] K. Ghoroku and M. Yahiro, Phys. Lett. **B604**, 235 (2004), hep-th/0408040.

[78] D. Arean, D. E. Crooks, and A. V. Ramallo, JHEP **11**, 035 (2004), hep-th/0408210.

[79] M. Kruczenski, L. A. P. Zayas, J. Sonnenschein, and D. Vaman, JHEP **06**, 046 (2005), hep-th/0410035.

[80] D. Bak and H.-U. Yee, Phys. Rev. **D71**, 046003 (2005), hep-th/0412170.

[81] K. Ghoroku, T. Sakaguchi, N. Uekusa, and M. Yahiro, Phys. Rev. **D71**, 106002 (2005), hep-th/0502088.

[82] N. Evans, J. P. Shock, and T. Waterson, JHEP **03**, 005 (2005), hep-th/0502091.

[83] F. Bigazzi, R. Casero, A. L. Cotrone, E. Kiritsis, and A. Paredes, JHEP **10**, 012 (2005), hep-th/0505140.

[84] R. Apreda, J. Erdmenger, and N. Evans, JHEP **05**, 011 (2006), hep-th/0509219.

[85] R. Casero, A. Paredes, and J. Sonnenschein, JHEP **01**, 127 (2006), hep-th/0510110.

[86] K. Peeters, J. Sonnenschein, and M. Zamaklar, JHEP **02**, 009 (2006), hep-th/0511044.

[87] A. L. Cotrone, L. Martucci, and W. Troost, Phys. Rev. Lett. **96**, 141601 (2006), hep-th/0511045.

[88] F. Canoura, J. D. Edelstein, L. A. P. Zayas, A. V. Ramallo, and D. Vaman, JHEP **03**, 101 (2006), hep-th/0512087.

[89] R. Apreda, J. Erdmenger, N. Evans, J. Grosse, and Z. Guralnik, Fortsch. Phys. **54**, 266 (2006), hep-th/0601130.

[90] N. Evans and T. Waterson, JHEP **01**, 058 (2007), hep-ph/0603249.

[91] A. Karch, E. Katz, and N. Weiner, Phys. Rev. Lett. **90**, 091601 (2003), hep-th/0211107.

[92] T. Sakai and J. Sonnenschein, JHEP **09**, 047 (2003), hep-th/0305049.

[93] J. Babington, J. Erdmenger, N. J. Evans, Z. Guralnik, and I. Kirsch, Phys. Rev. **D69**, 066007 (2004), hep-th/0306018.

[94] C. Nunez, A. Paredes, and A. V. Ramallo, JHEP **12**, 024 (2003), hep-th/0311201.

[95] S. Kuperstein, JHEP **03**, 014 (2005), hep-th/0411097.

[96] I. Brevik, K. Ghoroku, and A. Nakamura, Int. J. Mod. Phys. **D15**, 57 (2006), hep-th/0505057.

[97] D. Arean, A. Paredes, and A. V. Ramallo, JHEP **08**, 017 (2005), hep-th/0505181.

[98] T. S. Levi and P. Ouyang, (2005), hep-th/0506021.

[99] M. J. Rodriguez and P. Talavera, (2005), hep-th/0508058.

[100] J. P. Shock, JHEP **10**, 043 (2006), hep-th/0601025.

[101] R. C. Myers and R. M. Thomson, JHEP **09**, 066 (2006), hep-th/0605017.

[102] D. Arean and A. V. Ramallo, JHEP **04**, 037 (2006), hep-th/0602174.

[103] A. Brandhuber, N. Itzhaki, J. Sonnenschein, and S. Yankielowicz, JHEP **06**, 001 (1998), hep-th/9803263.

[104] D. J. Gross and H. Ooguri, Phys. Rev. **D58**, 106002 (1998), hep-th/9805129.

[105] J. Sonnenschein, Class. Quant. Grav. **17**, 1257 (2000), hep-th/9910089.

[106] I. Kirsch, Fortsch. Phys. **52**, 727 (2004), hep-th/0406274.

[107] O. Aharony, J. Sonnenschein, and S. Yankielowicz, (2006), hep-th/0604161.

[108] A. Parnachev and D. A. Sahakyan, Phys. Rev. Lett. **97**, 111601 (2006), hep-th/0604173.

[109] Y.-h. Gao, W.-s. Xu, and D.-f. Zeng, JHEP **08**, 018 (2006), hep-th/0605138.

[110] E. Antonyan, J. A. Harvey, and D. Kutasov, (2006), hep-th/0608149.

[111] D. Mateos, R. C. Myers, and R. M. Thomson, Phys. Rev. Lett. **97**, 091601 (2006), hep-th/0605046.

[112] D. Mateos, R. C. Myers, and R. M. Thomson, JHEP **05**, 067 (2007), hep-th/0701132.

[113] T. Albash, V. Filev, C. V. Johnson, and A. Kundu, (2006), hep-th/0605088.

[114] T. Albash, V. Filev, C. V. Johnson, and A. Kundu, (2006), hep-th/0605175.

[115] V. G. Filev, C. V. Johnson, R. C. Rashkov, and K. S. Viswanathan, (2007), hep-th/0701001.

[116] A. Karch and A. O'Bannon, Phys. Rev. **D74**, 085033 (2006), hep-th/0605120.

[117] D. Forster, *Hydrodynamic Fluctuations, Broken Symmetry, and Correlation Functions* (Benjamin, Reading, 1975).

[118] D. T. Son and A. O. Starinets, (2007), arXiv:0704.0240 [hep-th].

[119] G. Policastro, D. T. Son, and A. O. Starinets, JHEP **09**, 042 (2002), hep-th/0205052.

[120] G. Policastro, D. T. Son, and A. O. Starinets, JHEP **12**, 054 (2002), hep-th/0210220.

[121] C. P. Herzog, JHEP **12**, 026 (2002), hep-th/0210126.

[122] C. P. Herzog, Phys. Rev. **D68**, 024013 (2003), hep-th/0302086.

[123] D. T. Son and A. O. Starinets, JHEP **09**, 042 (2002), hep-th/0205051.

[124] C. P. Herzog and D. T. Son, JHEP **03**, 046 (2003), hep-th/0212072.

[125] P. Kovtun, D. T. Son, and A. O. Starinets, JHEP **10**, 064 (2003), hep-th/0309213.

[126] R. C. Myers, A. O. Starinets, and R. M. Thomson, (2007), arXiv:0706.0162 [hep-th].

[127] P. Benincasa and A. Buchel, JHEP **01**, 103 (2006), hep-th/0510041.

[128] P. Benincasa and A. Buchel, Phys. Lett. **B640**, 108 (2006), hep-th/0605076.

[129] A. Buchel, Phys. Rev. **D72**, 106002 (2005), hep-th/0509083.

[130] P. Benincasa, A. Buchel, and A. O. Starinets, Nucl. Phys. **B733**, 160 (2006), hep-th/0507026.

[131] A. Buchel, Nucl. Phys. **B731**, 109 (2005), hep-th/0507275.

[132] A. Parnachev and A. Starinets, JHEP **10**, 027 (2005), hep-th/0506144.

[133] C. P. Herzog, A. Karch, P. Kovtun, C. Kozcaz, and L. G. Yaffe, JHEP **07**, 013 (2006), hep-th/0605158.

[134] H. Liu, K. Rajagopal, and U. A. Wiedemann, Phys. Rev. Lett. **97**, 182301 (2006), hep-ph/0605178.

[135] J. Casalderrey-Solana and D. Teaney, Phys. Rev. **D74**, 085012 (2006), hep-ph/0605199.

[136] S. S. Gubser, Phys. Rev. **D74**, 126005 (2006), hep-th/0605182.

[137] G. Policastro, D. T. Son, and A. O. Starinets, Phys. Rev. Lett. **87**, 081601 (2001), hep-th/0104066.

[138] A. Buchel and J. T. Liu, Phys. Rev. Lett. **93**, 090602 (2004), hep-th/0311175.

[139] A. Buchel, Phys. Lett. **B609**, 392 (2005), hep-th/0408095.

[140] P. Kovtun, D. T. Son, and A. O. Starinets, Phys. Rev. Lett. **94**, 111601 (2005), hep-th/0405231.

[141] A. Buchel, Nucl. Phys. **B708**, 451 (2005), hep-th/0406200.

[142] D. T. Son and A. O. Starinets, JHEP **03**, 052 (2006), hep-th/0601157.

[143] J. Mas, JHEP **03**, 016 (2006), hep-th/0601144.

[144] K. Maeda, M. Natsuume, and T. Okamura, Phys. Rev. **D73**, 066013 (2006), hep-th/0602010.

[145] O. Saremi, JHEP **10**, 083 (2006), hep-th/0601159.

[146] P. Benincasa, A. Buchel, and R. Naryshkin, Phys. Lett. **B645**, 309 (2007), hep-th/0610145.

[147] D. Mateos, R. C. Myers, and R. M. Thomson, Phys. Rev. Lett. **98**, 101601 (2007), hep-th/0610184.

[148] A. Buchel, J. T. Liu, and A. O. Starinets, Nucl. Phys. **B707**, 56 (2005), hep-th/0406264.

[149] E. Shuryak, Prog. Part. Nucl. Phys. **53**, 273 (2004), hep-ph/0312227.

[150] D. Teaney, Phys. Rev. **C68**, 034913 (2003), nucl-th/0301099.

[151] S. Kobayashi, D. Mateos, S. Matsuura, R. C. Myers, and R. M. Thomson, JHEP **02**, 016 (2007), hep-th/0611099.

[152] S. Matsuura, unpublished.

[153] A. Karch and L. Randall, JHEP **06**, 063 (2001), hep-th/0105132.

[154] A. V. Ramallo, Mod. Phys. Lett. **A21**, 1481 (2006), hep-th/0605261.

[155] C. Hoyos, K. Landsteiner, and S. Montero, JHEP **04**, 031 (2007), hep-th/0612169.

[156] M. Asakawa and T. Hatsuda, Phys. Rev. Lett. **92**, 012001 (2004), hep-lat/0308034.

[157] S. Datta, F. Karsch, P. Petreczky, and I. Wetzorke, Phys. Rev. **D69**, 094507 (2004), hep-lat/0312037.

[158] T. Hatsuda, Int. J. Mod. Phys. **A21**, 688 (2006), hep-ph/0509306.

[159] F. Karsch, D. Kharzeev, and H. Satz, Phys. Lett. **B637**, 75 (2006), hep-ph/0512239.

[160] H. Satz, Nucl. Phys. **A783**, 249 (2007), hep-ph/0609197.

[161] M. Cheng *et al.*, Phys. Rev. **D74**, 054507 (2006), hep-lat/0608013.

[162] Y. Aoki, Z. Fodor, S. D. Katz, and K. K. Szabo, Phys. Lett. **B643**, 46 (2006), hep-lat/0609068.

[163] MILC, C. Bernard *et al.*, Phys. Rev. **D71**, 034504 (2005), hep-lat/0405029.

[164] S. W. Hawking, *"The path-integral approach to quantum gravity" in General Relativity: An Einstein centenary survey, eds. S.W. Hawking and W. Isreal* (Cambridge University Press, Cambridge, 1979).

[165] M. Henningson and K. Skenderis, JHEP **07**, 023 (1998), hep-th/9806087.

[166] M. Henningson and K. Skenderis, Fortsch. Phys. **48**, 125 (2000), hep-th/9812032.

[167] V. Balasubramanian and P. Kraus, Commun. Math. Phys. **208**, 413 (1999), hep-th/9902121.

[168] C. R. Graham, (1999), math.dg/9909042.

[169] R. Emparan, C. V. Johnson, and R. C. Myers, Phys. Rev. **D60**, 104001 (1999), hep-th/9903238.

[170] R. B. Mann, Phys. Rev. **D60**, 104047 (1999), hep-th/9903229.

[171] A. W. Peet and J. Polchinski, Phys. Rev. **D59**, 065011 (1999), hep-th/9809022.

[172] S. S. Gubser, I. R. Klebanov, and A. W. Peet, Phys. Rev. **D54**, 3915 (1996), hep-th/9602135.

[173] V. P. Frolov, Phys. Rev. **D74**, 044006 (2006), gr-qc/0604114.

[174] V. P. Frolov, A. L. Larsen, and M. Christensen, Phys. Rev. **D59**, 125008 (1999), hep-th/9811148.

[175] M. Christensen, V. P. Frolov, and A. L. Larsen, Phys. Rev. **D58**, 085008 (1998), hep-th/9803158.

[176] A. Hanany and E. Witten, Nucl. Phys. **B492**, 152 (1997), hep-th/9611230.

[177] U. Danielsson, G. Ferretti, and I. R. Klebanov, Phys. Rev. Lett. **79**, 1984 (1997), hep-th/9705084.

[178] A. Karch, A. O'Bannon, and K. Skenderis, JHEP **04**, 015 (2006), hep-th/0512125.

[179] S. de Haro, S. N. Solodukhin, and K. Skenderis, Commun. Math. Phys. **217**, 595 (2001), hep-th/0002230.

[180] K. Skenderis, Class. Quant. Grav. **19**, 5849 (2002), hep-th/0209067.

[181] N. P. Landsman and C. G. van Weert, Phys. Rept. **145**, 141 (1987).

[182] G. T. Horowitz and V. E. Hubeny, Phys. Rev. **D62**, 024027 (2000), hep-th/9909056.

[183] A. Nunez and A. O. Starinets, Phys. Rev. **D67**, 124013 (2003), hep-th/0302026.

[184] P. K. Kovtun and A. O. Starinets, Phys. Rev. **D72**, 086009 (2005), hep-th/0506184.

[185] R. C. Myers, JHEP **12**, 022 (1999), hep-th/9910053.

[186] C. Csaki, H. Ooguri, Y. Oz, and J. Terning, JHEP **01**, 017 (1999), hep-th/9806021.

[187] N. R. Constable and R. C. Myers, JHEP **10**, 037 (1999), hep-th/9908175.

[188] K. Peeters, J. Sonnenschein, and M. Zamaklar, Phys. Rev. **D74**, 106008 (2006), hep-th/0606195.

[189] M. Chernicoff, J. A. Garcia, and A. Guijosa, JHEP **09**, 068 (2006), hep-th/0607089.

[190] H. Liu, K. Rajagopal, and U. A. Wiedemann, (2006), hep-ph/0607062.

[191] P. C. Argyres, M. Edalati, and J. F. Vazquez-Poritz, JHEP **01**, 105 (2007), hep-th/0608118.

[192] P. C. Argyres, M. Edalati, and J. F. Vazquez-Poritz, (2006), hep-th/0612157.

[193] J. J. Friess, S. S. Gubser, G. Michalogiorgakis, and S. S. Pufu, (2006), hep-th/0609137.

[194] P. Talavera, JHEP **01**, 086 (2007), hep-th/0610179.

[195] H. Liu, K. Rajagopal, and U. A. Wiedemann, JHEP **03**, 066 (2007), hep-ph/0612168.

[196] J. J. Friess, S. S. Gubser, and G. Michalogiorgakis, JHEP **09**, 072 (2006), hep-th/0605292.

[197] A. Buchel, Phys. Rev. **D74**, 046006 (2006), hep-th/0605178.

[198] S. Hong, S. Yoon, and M. J. Strassler, JHEP **04**, 046 (2004), hep-th/0312071.

[199] Y. Aoki, G. Endrodi, Z. Fodor, S. D. Katz, and K. K. Szabo, Nature **443**, 675 (2006), hep-lat/0611014.

[200] M. Asakawa, T. Hatsuda, and Y. Nakahara, Nucl. Phys. **A715**, 863 (2003), hep-lat/0208059.

[201] T. Matsui and H. Satz, Phys. Lett. **B178**, 416 (1986).

[202] O. Kaczmarek, F. Karsch, F. Zantow, and P. Petreczky, Phys. Rev. **D70**, 074505 (2004), hep-lat/0406036.

[203] O. Kaczmarek and F. Zantow, Phys. Rev. **D71**, 114510 (2005), hep-lat/0503017.

[204] S.-J. Rey, S. Theisen, and J.-T. Yee, Nucl. Phys. **B527**, 171 (1998), hep-th/9803135.

[205] J. S. A. Brandhuber, N. Itzhaki and S. Yankielowicz, Phys. Lett. B **434**, 36 (1998), hep-th/9803137.

[206] J. P. Blaizot, E. Iancu, U. Kraemmer, and A. Rebhan, (2006), hep-ph/0611393.

[207] S. S. Gubser, I. R. Klebanov, and A. A. Tseytlin, Nucl. Phys. **B534**, 202 (1998), hep-th/9805156.

[208] G. Veneziano, Nucl. Phys. **B117**, 519 (1976).

[209] F. Benini, F. Canoura, S. Cremonesi, C. Nunez, and A. V. Ramallo, JHEP **02**, 090 (2007), hep-th/0612118.

[210] A. Paredes, JHEP **12**, 032 (2006), hep-th/0610270.

[211] V. N. A. Fotopoulos and N. Prezas, JHEP **10**, 081 (2005), hep-th/0504010.

[212] R. Casero, C. Nunez, and A. Paredes, Phys. Rev. **D73**, 086005 (2006), hep-th/0602027.

[213] S. Murthy and J. Troost, JHEP **10**, 019 (2006), hep-th/0606203.

[214] I. Kirsch and D. Vaman, Phys. Rev. **D72**, 026007 (2005), hep-th/0505164.

[215] B. A. Burrington, J. T. Liu, L. A. Pando Zayas, and D. Vaman, JHEP **02**, 022 (2005), hep-th/0406207.

[216] S. A. Cherkis and A. Hashimoto, JHEP **11**, 036 (2002), hep-th/0210105.

[217] M. Gomez-Reino, S. Naculich, and H. Schnitzer, Nucl. Phys. **B713**, 263 (2005), hep-th/0412015.

[218] J. Erdmenger and I. Kirsch, JHEP **12**, 025 (2004), hep-th/0408113.

[219] O. Aharony, S. Minwalla, and T. Wiseman, Class. Quant. Grav. **23**, 2171 (2006), hep-th/0507219.

[220] R. Apreda, J. Erdmenger, N. Evans, and Z. Guralnik, Phys. Rev. **D71**, 126002 (2005), hep-th/0504151.

[221] D. Arean, A. V. Ramallo, and D. Rodriguez-Gomez, JHEP **05**, 044 (2007), hep-th/0703094.

[222] E. Antonyan, J. A. Harvey, S. Jensen, and D. Kutasov, (2006), hep-th/0604017.

[223] O. Aharony, A. Buchel, and A. Yarom, Phys. Rev. **D72**, 066003 (2005), hep-th/0506002.

[224] O. Aharony, A. Buchel, and A. Yarom, JHEP **11**, 069 (2006), hep-th/0608209.

[225] M. Berg, M. Haack, and W. Muck, Nucl. Phys. **B736**, 82 (2006), hep-th/0507285.

[226] M. Krasnitz, JHEP **12**, 048 (2002), hep-th/0209163.

[227] M. Krasnitz, (2000), hep-th/0011179.

[228] K. Skenderis and M. Taylor, JHEP **05**, 057 (2006), hep-th/0603016.

[229] A. Chamblin, R. Emparan, C. V. Johnson, and R. C. Myers, Phys. Rev. **D60**, 104026 (1999), hep-th/9904197.

[230] A. Chamblin, R. Emparan, C. V. Johnson, and R. C. Myers, Phys. Rev. **D60**, 064018 (1999), hep-th/9902170.

[231] S. S. Gubser, Nucl. Phys. **B551**, 667 (1999), hep-th/9810225.

[232] R.-G. Cai and K.-S. Soh, Mod. Phys. Lett. **A14**, 1895 (1999), hep-th/9812121.

[233] K.-Y. Kim, S.-J. Sin, and I. Zahed, (2006), hep-th/0608046.

[234] N. Horigome and Y. Tanii, JHEP **01**, 072 (2007), hep-th/0608198.

[235] A. Parnachev and D. A. Sahakyan, Nucl. Phys. **B768**, 177 (2007), hep-th/0610247.

[236] I. Racz and R. M. Wald, Class. Quant. Grav. **9**, 2643 (1992).

[237] E. Witten, Nucl. Phys. **B460**, 335 (1996), hep-th/9510135.

[238] J. Callan, Curtis G. and J. M. Maldacena, Nucl. Phys. **B513**, 198 (1998), hep-th/9708147.

[239] G. W. Gibbons, Nucl. Phys. **B514**, 603 (1998), hep-th/9709027.

[240] E. Witten, JHEP **07**, 006 (1998), hep-th/9805112.

[241] Y. Imamura, Nucl. Phys. **B537**, 184 (1999), hep-th/9807179.

[242] J. Callan, Curtis G., A. Guijosa, and K. G. Savvidy, Nucl. Phys. **B547**, 127 (1999), hep-th/9810092.

[243] B. Craps, J. Gomis, D. Mateos, and A. Van Proeyen, JHEP **04**, 004 (1999), hep-th/9901060.

[244] J. Callan, Curtis G., A. Guijosa, K. G. Savvidy, and O. Tafjord, Nucl. Phys. **B555**, 183 (1999), hep-th/9902197.

[245] J. P. Gauntlett, C. Koehl, D. Mateos, P. K. Townsend, and M. Zamaklar, Phys. Rev. **D60**, 045004 (1999), hep-th/9903156.

[246] A. Hashimoto, Phys. Rev. **D57**, 6441 (1998), hep-th/9711097.

[247] J. M. Maldacena, Phys. Rev. Lett. **80**, 4859 (1998), hep-th/9803002.

[248] S.-J. Rey and J.-T. Yee, Eur. Phys. J. **C22**, 379 (2001), hep-th/9803001.

[249] S.-M. Lee, A. W. Peet, and L. Thorlacius, Nucl. Phys. **B514**, 161 (1998), hep-th/9710097.

[250] E. Shuster and D. T. Son, Nucl. Phys. **B573**, 434 (2000), hep-ph/9905448.

[251] T. Schafer and E. V. Shuryak, Lect. Notes Phys. **578**, 203 (2001), nucl-th/0010049.

[252] S. Nakamura, Y. Seo, S.-J. Sin, and K. P. Yogendran, (2006), hep-th/0611021.

[253] A. Buchel and J. T. Liu, Nucl. Phys. **B771**, 93 (2007), hep-th/0608002.

[254] E. Antonyan, J. A. Harvey, and D. Kutasov, (2006), hep-th/0608177.

[255] D. Gepner and S. Sekahr Pal, (2006), hep-th/0608229.

[256] A. Basu and A. Maharana, Phys. Rev. **D75**, 065005 (2007), hep-th/0610087.

[257] D. Arean, A. V. Ramallo, and D. Rodriguez-Gomez, Phys. Lett. **B641**, 393 (2006), hep-th/0609010.

[258] D. Birmingham, I. Sachs, and S. N. Solodukhin, Phys. Rev. Lett. **88**, 151301 (2002), hep-th/0112055.

[259] P. Kovtun and A. Starinets, Phys. Rev. Lett. **96**, 131601 (2006), hep-th/0602059.

[260] T. Umeda, K. Nomura, and H. Matsufuru, Eur. Phys. J. **C39S1**, 9 (2005), hep-lat/0211003.

[261] A. Jakovac, P. Petreczky, K. Petrov, and A. Velytsky, (2006), hep-lat/0603005.

[262] G. Aarts *et al.*, PoS **LAT2006**, 126 (2006), hep-lat/0610065.

[263] G. Aarts, C. Allton, J. Foley, S. Hands, and S. Kim, (2006), hep-lat/0610061.

[264] P. Petreczky, Nucl. Phys. **A785**, 10 (2007), hep-lat/0609040.

[265] G. Aarts, C. Allton, J. Foley, S. Hands, and S. Kim, (2007), hep-lat/0703008.

[266] H. B. Meyer, (2007), arXiv:0704.1801 [hep-lat].

[267] D. Teaney, Phys. Rev. **D74**, 045025 (2006), hep-ph/0602044.

[268] S. Caron-Huot, P. Kovtun, G. D. Moore, A. Starinets, and L. G. Yaffe, JHEP **12**, 015 (2006), hep-th/0607237.

[269] D. Z. Freedman, S. D. Mathur, A. Matusis, and L. Rastelli, Nucl. Phys. **B546**, 96 (1999), hep-th/9804058.

[270] G. Chalmers, H. Nastase, K. Schalm, and R. Siebelink, Nucl. Phys. **B540**, 247 (1999), hep-th/9805105.

[271] D. Mateos and L. Patino, to appear.

[272] S. S. Gubser, (2006), hep-th/0612143.

[273] P. M. Chesler and A. Vuorinen, JHEP **11**, 037 (2006), hep-ph/0607148.

[274] PHENIX, A. Adare *et al.*, (2006), nucl-ex/0611018.

[275] S. S. Gubser, (2006), hep-th/0611272.

[276] G. D. Moore and D. Teaney, Phys. Rev. **C71**, 064904 (2005), hep-ph/0412346.

[277] J. Erdmenger, M. Kaminski, and F. Rust, (2007), arXiv:0704.1290 [hep-th].

[278] R. M. Wald, *General Relativity* (University of Chicago Press, Chicago, 1984).

[279] J. S. F. Chan and R. B. Mann, Phys. Rev. **D55**, 7546 (1997), gr-qc/9612026.

[280] J. S. F. Chan and R. B. Mann, Phys. Rev. **D59**, 064025 (1999).

[281] K. D. Kokkotas and B. G. Schmidt, Living Rev. Rel. **2**, 2 (1999), gr-qc/9909058.

[282] H.-P. Nollert, Class. Quant. Grav. **16**, R159 (1999).

[283] I. Sachs, Fortsch. Phys. **52**, 667 (2004), hep-th/0312287.

[284] J. A. Minahan, JHEP **01**, 020 (1999), hep-th/9811156.

[285] J. G. Russo and K. Sfetsos, Adv. Theor. Math. Phys. **3**, 131 (1999), hep-th/9901056.

[286] H. Nastase, (2005), hep-th/0501068.

[287] E. Shuryak, S.-J. Sin, and I. Zahed, J. Korean Phys. Soc. **50**, 384 (2007), hep-th/0511199.

[288] H. Nastase, (2006), hep-th/0603176.

[289] J. J. Friess, S. S. Gubser, G. Michalogiorgakis, and S. S. Pufu, (2006), hep-th/0611005.

[290] J. J. Friess, S. S. Gubser, G. Michalogiorgakis, and S. S. Pufu, (2006), hep-th/0607022.

[291] Y. V. Kovchegov and A. Taliotis, (2007), arXiv:0705.1234 [hep-ph].

[292] K. Hashimoto, T. Hirayama, and A. Miwa, (2007), hep-th/0703024.

[293] L. Alvarez-Gaume and S. F. Hassan, Fortsch. Phys. **45**, 159 (1997), hep-th/9701069.

[294] O. DeWolfe, D. Z. Freedman, and H. Ooguri, Phys. Rev. **D66**, 025009 (2002), hep-th/0111135.